

**Radical Polymerization Kinetics of
Non-Ionized and Fully-Ionized Monomers
Studied by Pulsed-Laser EPR**

Dissertation

zur Erlangung des mathematisch-naturwissenschaftlichen Doktorgrades
“Doctor rerum naturalium”
der Georg-August-Universität Göttingen

im Promotionsprogramm Chemie
der Georg-August University School of Science
(GAUSS)

vorgelegt von
Hendrik Kattner
aus Duderstadt

Göttingen, 2016

Betreuungsausschuss

Prof. Dr. Michael Buback Institut für Physikalische Chemie
Georg-August-Universität Göttingen

Prof. Dr. Philipp Vana, MBA Institut für Physikalische Chemie
Georg-August-Universität Göttingen

Mitglieder der Prüfungskommission

Referent

Prof. Dr. Michael Buback Institut für Physikalische Chemie
Georg-August-Universität Göttingen

Korreferent

Prof. Dr. Philipp Vana, MBA Institut für Physikalische Chemie
Georg-August-Universität Göttingen

Weitere Mitglieder der Prüfungskommission

Prof. Dr. Burkhard Geil Institut für Physikalische Chemie
Georg-August-Universität Göttingen

Prof. Dr. Ricardo Mata Institut für Physikalische Chemie
Georg-August-Universität Göttingen

PD Dr. Thomas Zeuch Institut für Physikalische Chemie
Georg-August-Universität Göttingen

Dr. Florian Ehlers Institut für Physikalische Chemie
Georg-August-Universität Göttingen

Tag der mündlichen Prüfung: 06.06.2016

"In many cases it is true to say that the kinetics and chemistry of the reactions involved [in radical polymerization] have been as completely elucidated [...] and there is not much to be written or discovered about such processes"

Melville in *High Polymers Series on the Mechanism of Polymer Reactions*, 3th Edition, **1954**; cited from Ref.¹³

Summary

The radical polymerization kinetics of non-ionized and fully-ionized monomers in organic and aqueous solution was investigated by SP-PLP-EPR, i.e., highly time-resolved single-pulse-pulsed-laser-polymerization (SP-PLP) in conjunction with electron paramagnetic resonance (EPR) spectroscopy.

Dicumyl peroxide as the photoinitiator allowed for investigations into the chain-length dependence of the termination rate coefficient, k_t , of styrene bulk polymerization. The *Composite Model* perfectly represents the chain-length-dependence of k_t for styrene and for all other monomers studied within the present investigation. The temperature dependence of the termination rate coefficient of two monomeric radicals, $k_t(1,1)$, scales with inverse viscosity, η^{-1} , of the reaction mixture prior to polymerization. The product $k_t(1,1)\cdot\eta$ thus turns out to be a temperature-independent quantity for non-ionized radicals, which allows for estimates of $k_t(1,1)$ on the basis of easily accessible viscosity data.

The impact of monomer concentration and temperature on the termination kinetics of charged radicals, as studied for fully-ionized methacrylic acid (NaMAA) at 5 wt.% and 10 wt.% monomer, is distinctly different. The measured activation energy, $E_A(k_t(1,1))$, is far below $E_A(\eta^{-1})$ and $k_t(1,1)$ for the more viscous solution at 10 wt.% NaMAA is higher than at 5 wt.%. This effect is assigned to the action of counter ions which is also seen with quaternary ammonium trimethylaminoethyl acrylate chloride (TMAEA) radicals.

A novel SP–PLP–EPR method has been developed for investigation into the propagation kinetics of slowly terminating radicals. The integral over radical concentration measured after applying a single laser pulse is related to the separately measured monomer-to-polymer conversion per laser pulse thus providing the propagating rate coefficient, k_p . The technique is illustrated for the fully-ionized methacrylate trimethylaminoethyl methacrylate chloride (TMAEMA) and the reliability is checked by investigations into di(*n*-butyl) itaconate (DBI) bulk polymerization. For the acrylate-type TMAEA radicals, the remarkably low value of the pre-exponential factor, $A(k_p)$, demonstrates the large entropy penalty associated with the formation of the transition state for propagation due to the restricted internal mobility induced by the charged side group. The bulky side groups in DBI cause a similar mobility restriction.

First evidence for mid-chain radicals (MCRs) formed from end-chain radicals (SPRs) by the backbiting process was provided for TMAEA and acrylamide (AAM) polymerizations via the EPR spectra recorded during stationary polymerization. AAM exhibits a molar fraction of MCRs, x_{MCR} , which is significantly lower than with butyl acrylate polymerization. The analysis of MCR concentration vs time profiles reveals the relatively high activation energy for the rate coefficient of backbiting, k_{bb} , as the main reason behind the low value of x_{MCR} . The MCR propagation and the cross-termination kinetics of SPRs and MCRs of AAM are similar to the associated values for acrylates. Although k_{bb} is similarly low, significantly higher numbers for x_{MCR} are found in TMAEA polymerization, which is due to the small rate coefficients of MCR propagation, k_p^{t} , and of SPR-MCR cross-termination, $k_t^{\text{st}}(1,1)$, in the case of fully-ionized species. The comprehensive kinetic picture obtained for TMAEA and AAM homopolymerizations underlines the enormous potential of the SP–PLP–EPR technique.

Contents

Summary	i
1 Introduction and Motivation	1
2 Theoretical Background	5
2.1 Ideal Polymerization Kinetics	5
2.1.1 Initiator Decomposition and Initiation of Chain-growth	5
2.1.2 Propagation	6
2.1.3 Termination	7
2.1.4 Steady-state Polymerization Rate	7
2.2 Transfer Reactions	8
2.2.1 The Backbiting Reaction	8
2.2.2 The Impact of Backbiting on Polymerization Kinetics	10
2.3 Diffusion Dependence of Rate Coefficients in CRP	12
2.3.1 Diffusion Control of Propagation	13
2.3.2 Diffusion Control of Initiation	14
2.3.3 Diffusion Control of Termination	15
2.4 Chain-length Dependency of Rate Coefficients in CRP	18
2.4.1 Chain-length Dependency of Propagation	18
2.4.2 Chain-length Dependency of Termination	19
2.5 Resolving CLDT by the SP–PLP–EPR Technique	22
2.6 Photoinitiators for the SP–PLP–EPR Technique	24
3 Experimental	27
3.1 Chemicals	27
3.1.1 Monomer	27
3.1.2 Initiators	29
3.1.3 Stable Radical Species	29
3.1.4 Purification of Water	30
3.2 The SP–PLP–EPR Technique	30

3.2.1	The Setup	30
3.2.2	EPR Sample Tubes and Cells	32
3.2.3	Sample Preparation	33
3.2.4	Experimental Procedure	34
3.2.5	Calibration Procedure	36
3.2.6	Kinetic Simulations and Data Analysis	39
3.3	Determination of Monomer-to-Polymer Conversion	39
3.4	Density and Viscosity Measurement	41
3.5	Simulation and Fitting of the EPR Spectra	41
4	Termination Kinetics in Styrene Bulk Polymerization	43
4.1	The EPR Spectrum of Styryl Radicals	44
4.2	Chain-Length Dependent Termination of Styryl Radicals	46
4.3	Relevance of Chain-Length Dependent Termination	54
4.4	Radical Structure and Reactivity in Termination Processes	58
5	Termination and Transfer Kinetics of Acrylamide in Aqueous Solution	63
5.1	The EPR Spectrum in AAm Polymerization	65
5.1.1	Simulation of EPR Spectra in the Presence of MCRs	65
5.1.2	Fraction of Mid-chain Radicals under Stationary Conditions	68
5.2	Termination and Transfer Kinetics of AAm	71
5.2.1	Homo-termination Kinetics of End-chain Radicals	72
5.2.2	Transfer and Cross-termination Kinetics	77
6	Novel Access to the Rate Coefficient of Propagation	93
6.1	Proof of Principle: Propagation Kinetics of TMAEMA	95
6.1.1	The EPR Spectrum in TMAEMA Polymerization	96
6.1.2	SP-PLP-EPR Investigations into TMAEMA Kinetics	98
6.2	Validation: Propagation and Termination in DBI Bulk Polymerization	109
6.2.1	The EPR Spectrum in DBI Bulk Polymerization	109
6.2.2	Propagation Kinetics of DBI	110
6.2.3	Termination Kinetics of DBI	114
6.3	Closing Remarks	119
7	Termination Kinetics of Sodium Methacrylate	121
7.1	The EPR Spectrum in NaMAA Polymerization	121
7.2	SP-PLP-EPR Investigations into the Termination Kinetics	124

7.2.1	Time-resolved EPR Profiles	124
7.2.2	Analysis of Termination Kinetics	126
7.3	Diffusion-controlled Termination of Ionized Radicals	134
8	Propagation, Termination and Transfer Kinetics of TMAEA	137
8.1	The EPR Spectrum in TMAEA Polymerization	138
8.1.1	Simulation of EPR Spectra in the Presence of MCRs	139
8.1.2	Fraction of Mid-chain Radicals under Stationary Conditions	142
8.1.3	Band Assignment used with the SP–PLP–EPR Experiment	143
8.2	Basic Strategy and Data Analysis	144
8.3	Results from PREDICI Fitting	145
8.3.1	Termination and Transfer Kinetics of TMAEA Radicals	147
8.3.2	Interplay of Backbiting, MCR Propagation and Termination in TMAEA, AAm and BA Polymerizations	156
8.3.3	Propagation Kinetics of End-chain Radicals in TMAEA Polymerization	157
8.3.4	Simulation of Steady-state Polymerizations of TMAEA	160
9	Open Questions and Remaining Challenges	163
9.1	CLDT up to High Conversion	163
9.2	DP–PLP–EPR-Experiments	165
9.3	Polymerization Kinetics of Ionic Monomers	166
9.4	Termination Kinetics in Radical Copolymerization	167
9.5	Transient EPR Spectroscopy	168
	Appendices	171
	Appendix A: Density and Fluidity Data	172
	Appendix B: Simulation and Fitting of EPR Spectra	183
	Appendix C: Abbreviations	189
	Bibliography	193
	Acknowledgements	205
	About the Author	207

Introduction and Motivation

Every year, several hundred million tons of synthetic polymer are produced worldwide and this market continues to grow.¹ Since the pioneering studies of Baekeland and Staudinger,²⁻⁴ synthetic polymers are appreciated for their tuneable properties. Polymers such as polyethylene, polypropylene, poly(vinyl chloride) and polyurethane are mainly used for automotive parts, in textiles, as packaging, building and construction materials.¹ Beside these mass products, materials from polymerization of acrylamide, fully-ionized (meth)acrylic acid and from the quaternary ammonium salts trimethylaminoethyl (meth)acrylate chloride are employed in many special applications, e.g., as flocculants in water treatment and oil recovery, as film-forming agents, for coatings, emulsifiers, gels, superabsorbents and for chemical analysis.⁵⁻¹²

The homo- and copolymers are mainly produced by conventional radical polymerization on an industrial scale because of the high tolerance of this type of polymerization toward solvents, monomer functionality and impurity. In this context, the radical polymerization in aqueous solution is especially attractive due to the environmentally friendly and inexpensive solvent.

The polymer properties are largely determined by the microstructure of the macromolecules, i.e., monomer composition, topology, functionality, molecular mass distribution (MMD) and tacticity. The microstructure in turn depends on the kinetics of the individual reaction steps occurring during polymerization (*microstructure as "frozen" kinetics*). The accurate

knowledge of the kinetics of the elementary reaction steps is thus mandatory for the understanding of radical polymerization and for the simulation and optimization of technical processes and product properties. Detailed investigations into radical polymerization kinetics is of both fundamental academic and industrial interest. The accuracy of the obtained kinetic data was rather low for many years.¹³ The situation has however enormously improved by the advent of pulsed-laser-polymerization (PLP) techniques.¹⁴ Since the pioneering work of Olaj and colleagues in 1987,^{15,16} size-exclusion chromatography (SEC) has been used to analyse the structured MMD of polymer produced after applying a sequence of evenly spaced laser pulses applied to a monomer-photoinitiator solution. From the position of characteristic masses, at inflection points and maxima, respectively, the propagation rate coefficient, k_p , is obtained.^{17,18} A detailed kinetic picture of propagation in aqueous-solution polymerizations is so far only available for non-ionized monomers, e.g., for acrylic acid^{19–23}, methacrylic acid^{19,20,24–26}, acrylamide^{27–29}, *N*-isopropyl acrylamide³⁰, methylated acrylamides³¹, 1-vinylpyrrolidin-2-one³² and for *N*-vinyl formamide³³. Beside some sulfobetaines,³⁴ only a few reliable k_p values for ionic (salt-like) monomers have been reported for ionized methacrylic acid.³⁵ The difficulties in k_p determination of fully-ionized monomers are due to the loss of PLP-structured MMD because of a low termination rates between two subsequent laser pulses.³⁶

The instantaneous initiation by a single laser pulse (SP) enables the measurement of the lumped rate constant $k_p/\langle k_t \rangle$ by the online monitoring of monomer consumption via time-resolved near-infrared (NIR) spectroscopy (SP-PLP-NIR). With k_p being known from PLP-SEC, chain-length-averaged k_t , $\langle k_t \rangle$, can be deduced.^{14,19} However, the chain-length dependency (CLD) of k_t cannot be resolved by this technique and, in addition, no information about transfer reactions is obtained by this technique.

It is therefore desirable to observe the active species in radical polymerization, i.e., the radicals, directly by electron paramagnetic resonance (EPR) spectroscopy. This strategy is unrivalled for identification and monitoring of paramagnetic species, e.g., of radicals, in organic and aqueous solution. After applying the single laser pulse to a monomer-photoinitiator mixture (SP-PLP-EPR), the highly time-resolved EPR detection of radical concentration allows for the quantitative investigation of systems with more than one type of propagating radicals, as with acrylates.^{10,11} The secondary propagating radicals (SPR) and the tertiary midchain (MCR) radicals, which are formed from SPRs by intramolecular

transfer (backbiting), exhibit clearly different EPR spectra.^{10,11} For these systems, SP-PLP-EPR provides access to the rate coefficients of backbiting, k_{bb} , and of propagation from MCRs, k_p^t . Such rate coefficients are of enormous relevance for polymerization kinetics, since SPRs and MCRs differ significantly in k_p . The knowledge about the important backbiting reaction is however very limited and is essentially restricted to butyl acrylate polymerization in bulk and in toluene solution and to the aqueous-solution polymerization of acrylic acid.³⁷⁻³⁹

The SP-PLP-EPR technique allows for instantaneous initiation by a laser single pulse which guarantees a narrow MMD of propagating radicals. Since these narrowly distributed radicals grow linearly with the time after applying the laser pulse, termination occurs exclusively between radicals of more or less identical size making SP-PLP-EPR a unique tool for the investigation of chain-length dependent termination (CLDT). Depending on the photoinitiator – monomer system, common initiators,⁴⁰ may not always provide instantaneous initiation, as is the case with styrene. The CLD of k_t is not just of academic interest but also important for the control of radical polymerization processes on an industrial scale. Moreover, the reliable determination of transfer rate coefficients, e.g., k_{bb} and k_p^t , requires highly accurate termination rate coefficients, including the chain-length dependency of k_t . CLDT has been reported for polymerization in organic environments.⁴¹⁻⁴³ In aqueous solution only the termination of radicals of relatively small size was investigated with non-ionized methacrylic acid.⁴⁴ For non-ionized and fully-ionized acrylic acid in aqueous solution, the CLDT measured for acrylates in organic phase was adopted.^{38,39}

This thesis presents an in-depth investigation into the kinetics of radical polymerization in organic and aqueous solution by the SP-PLP-EPR technique. On the basis of careful selection of a photoinitiator, CLDT of styrene bulk polymerization could be measured.

In the area of aqueous-solution polymerization, the first detailed kinetic analysis of acrylamide polymerization is provided. EPR spectra recorded under stationary conditions allow for the unambiguous detection of mid-chain radicals formed by backbiting. The analysis of SPR and MCR concentration vs time profiles from SP-PLP-EPR provides access to a comprehensive set of rate coefficients, including chain-length dependent k_t , k_{bb} and k_p^t .

For the first time, the CLD termination kinetics of a charged monomer, i.e., of fully-ionized methacrylic acid, has been investigated as a function of temperature and monomer concentration. Investigations into the kinetics of further ionic monomers, e.g., of quaternary ammonium salts, suffer from the lack of reliable k_p data. A novel SP-PLP-EPR-based method is presented which allows for deducing both k_p and CLD k_t from a single (EPR) radical concentration vs time profile. The method is outlined for the methacrylate trimethylaminoethyl methacrylate chloride. The obtained insight into propagation and termination kinetics is used for the comprehensive kinetic study of the acrylate-type monomer trimethylaminoethyl acrylate chloride. As with acrylamide, also the intramolecular transfer is investigated. The results for fully-ionized and non-ionized monomers are compared, as are the effects of aqueous and organic solvent environments.

Theoretical Background

2.1 Ideal Polymerization Kinetics

The basic kinetic description of conventional radical polymerization (CRP) rests upon the scheme of "ideal" polymerization which comprises the following assumptions:

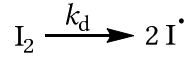
1. All reaction steps are irreversible.
2. Monomer is exclusively consumed by propagation.
3. All radicals exhibit identical reactivity irrespective of chain length and degree of monomer-to-polymer conversion.
4. Termination takes place by recombination and disproportionation.
5. All primary radicals are generated by initiator decomposition and are consumed by initiation.

Using these assumptions, the fundamental reaction steps of radical polymerization can be defined by the following trisection.

2.1.1 Initiator Decomposition and Initiation of Chain-growth

Radical polymerization requires the formation of primary radicals, R^{\cdot} , which are able to initiate chain growth by addition of a monomer molecule. They are usually formed by homolysis of thermolabile compounds, by photolysis of photoinitiators, by redox initiation or by self-

initiation as with styrene polymerization.⁴⁵ The related rate coefficient of decomposition is k_d .

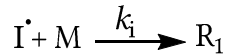


The rate of decomposition is given by

$$\frac{dc_i}{dt} = 2 \cdot k_d \cdot f \cdot c_{I_2}, \quad (2.1)$$

with c_i being the primary radical concentration and f the initiator efficiency which describes the fraction of initiator-derived radicals starting chain growth. The efficiency is assumed to be unity for ideal polymerization conditions but is usually smaller in real systems due to side reactions and to recombination of primary radicals (*cage effect*). A decrease of f is observed for bulk polymerizations when the fractional monomer-to-polymer conversion gets close to unity.⁴⁶

The subsequent addition of a monomer molecule, M, to primary radicals initiates the polymerization by the formation a monomeric radical, R_1 .

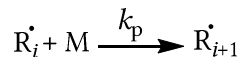


For suitable initiators, this reaction step is assumed to occur instantaneously and to be significantly faster than propagation. Initiation is therefore not considered for the overall kinetic description.⁴⁷

$$\frac{dc_{R_1}}{dt} = k_i \cdot c_M \cdot c_i \quad (2.2)$$

2.1.2 Propagation

The term chain propagation describes the addition of a monomer molecule to the growing chain, R_i .

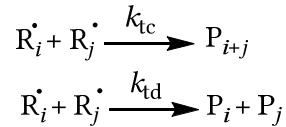


With k_p being the propagation rate coefficient the following rate law is obtained.

$$\frac{dc_M}{dt} = -k_p \cdot c_M \cdot c_R \quad (2.3)$$

2.1.3 Termination

Termination of chain growth proceeds either by combination which results in a head-head coupling, P_{i+j} , or by disproportionation which comprises the transfer of a β -H-atom and formation of a saturated and an unsaturated "dead" macromolecule, P_i and P_j .



Since combination and disproportionation are parallel reactions, the termination rate coefficient, k_t , is the sum of the rate coefficients for combination, k_{tc} , and disproportionation, k_{td} .

The associated termination rate,

$$\frac{dc_R}{dt} = -2 \cdot k_t \cdot c_R^2, \quad (2.4)$$

is second order in c_R and follows the IUPAC-recommendation with the factor 2 being included and applied throughout this thesis.^{17,48}

2.1.4 Steady-state Polymerization Rate

Under stationary conditions, i.e., $dc_R/dt = 0$, the rate of radical formation equals the termination rate:

$$f \cdot k_d \cdot c_i = 2 \cdot k_t \cdot c_R^2 \quad (2.5)$$

The combination of eqs (2.3) and (2.5) yields an expression for the overall polymerization rate, R_p ,

$$R_p = -\frac{dc_M}{dt} = k_p \cdot c_M \cdot \sqrt{\frac{f \cdot k_d \cdot c_I}{k_t}}, \quad (2.6)$$

which is first order in c_M and k_p but exhibits a fractional reaction order of 0.5 for k_t , k_d , f and c_I . The reaction order in c_M , often separately denoted with ω , was found to be $\omega > 1$ in polymerizations where intramolecular transfer reactions occur.⁴⁹

2.2 Transfer Reactions

Side reactions such as transfer steps are not included in the ideal polymerization scheme but are important for many polymerizations. The transfer reactions may be subdivided in intra- and intermolecular transfer reactions. In the latter case, the radical functionality is transferred to another species being a monomer, a solvent, an initiator molecule, to "dead" macromolecules or to an added chain-transfer agent (CTA). The accompanied stopping of chain growth is used for controlling the molar mass of macromolecules by adding CTAs. The intermolecular transfer is described in detail in the literature.⁴⁵

2.2.1 The Backbiting Reaction

Intramolecular transfer refers to the H-abstraction from the same macroradical which process, in contrast to intermolecular chain transfer, does not stop chain growth of the particular macroradical. However, the microstructure is altered in that short-chain branching is induced. The transfer step (called backbiting) proceeds via a six-membered ring structure with the radical functionality being transferred to the third side-group moiety counted from the chain end by a concerted [1,5]-H-shift reaction with the backbiting rate coefficient k_{bb} .

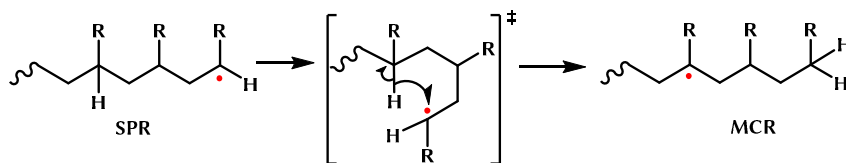


Figure 2.1: Backbiting reaction by a [1,5]-H-shift via a six-membered transition state (tagged by ‡) transferring a secondary propagating end-chain radical (SPR) into a tertiary mid-chain radical (MCR). The side group is denoted by R. The corresponding rate coefficient for backbiting is k_{bb} .

The secondary propagating end-chain radical (SPR) is hence converted into a tertiary mid-chain radical (MCR) which is accompanied by an increase in radical stability and makes backbiting an enthalpy-driven reaction (Figure 2.1).^{49,50} Some entropic contribution might be relevant since the radical functionality can be transferred subsequently to inner positions of the backbone by further backbiting steps.⁵¹ An indication for MCR formation is even given for highly mesomeric stabilized styryl macroradicals at high temperatures, i.e., from 260 to 343 °C.^{52,53} Simulations demonstrate that, since no gain in radical stability is obtained, the consecutive transfer, e.g., the [5,9]-shift, is hundred times slower than the [1,5]-shift which in turn is preferred over other theoretical backbiting steps, e.g., over the [1,3]-, [1,7]- and [1,11]-shift.⁵⁴

Although Kajiwara *et al.* have shown by EPR studies with radical precursors that backbiting is an irreversible reaction,^{55,56} SPRs can be regenerated, i.e., by the addition of a monomer to the MCR, (MCR propagation). Moreover, termination steps between SPRs and MCRs (SPR-MCR cross-termination) as well as between two MCRs, (MCR homotermination) may occur during polymerization. The underlying reaction scheme is given in Figure 5.7. As the MCR structure differs significantly from the one of the SPR, it is evident that the presence of MCRs affects the overall polymerization kinetics strongly.⁵⁷⁻⁵⁹ The conversion vs time profiles of acrylate polymerizations exhibit a monomer concentration dependency which is well above the ideal value of unity, i.e., $\omega \leq 1.8$,⁶⁰⁻⁶³ and the polymerization rates are retarded compared to simulations based exclusively upon end-chain radical kinetics. The reason behind this retardation is the reduced reactivity of MCRs compared to SPRs.

2.2.2 The Impact of Backbiting on Polymerization Kinetics

A detailed description of the mathematical framework for including the impact of backbiting into the steady-state polymerization kinetics can be found in Ref.⁶⁴⁻⁶⁸ A brief and intuitive presentation of the basic relationships is given here. In what follows, rate coefficients with the superscript "t" refer to MCRs with the radical functionality at the tertiary carbon atom while "s" denotes a radical functionality at the chain-end of SPRs. The MCR propagation rate coefficient, k_p^t , is several orders of magnitude lower than the one for SPRs, k_p^s .^{19,37} Thus, an increase of MCRs in radical polymerization is equivalent to a reduction of the effective rate coefficient of propagation, k_p^{eff} , according to eq (2.7),^{21,69}

$$k_p^{\text{eff}} = k_p^s \cdot (1 - x_{\text{MCR}}) + k_p^t \cdot x_{\text{MCR}}, \quad (2.7)$$

where x_{MCR} denotes the molar MCR fraction (eq (2.8)) given by the concentrations of MCRs, c_{MCR} , and of SPRs, c_{SPR} .^{21,69}

$$x_{\text{MCR}} = \frac{c_{\text{MCR}}}{c_{\text{MCR}} + c_{\text{SPR}}} \quad (2.8)$$

With $k_p^t \ll k_p^s$ and $x_{\text{MCR}} \ll 1$, the right-hand side term of eq (2.7) can be ignored and eq (2.9) is obtained.

$$k_p^{\text{eff}} = k_p^s \cdot (1 - x_{\text{MCR}}) \quad (2.9)$$

An analogous expression may be given for MCR termination kinetics when SPR-SPR, MCR-MCR and SPR-MCR termination are considered with k_t^{ss} , k_t^{tt} and k_t^{st} , respectively (eq (2.10)).

$$k_t^{\text{eff}} = k_t^{\text{ss}} \cdot (1 - x_{\text{MCR}})^2 + k_t^{\text{st}} \cdot (1 - x_{\text{MCR}}) \cdot x_{\text{MCR}} + k_t^{\text{tt}} \cdot (x_{\text{MCR}})^2 \quad (2.10)$$

For butyl acrylate polymerization in toluene, the termination rate coefficients differ only by approximately a factor of $k_t^{\text{ss}} / k_t^{\text{st}} \approx 3$ and $k_t^{\text{ss}} / k_t^{\text{tt}} \approx 7$ at 60 °C, respectively, being well below the ratio observed for k_p^s / k_p^t .^{37,70} Assuming stationary MCR concentration, i.e., $dc_{\text{MCR}}/dt = 0$, and

MCR degradation to occur exclusively by MCR propagation (long-chain-approximation), an intuitive expression for x_{MCR} is obtained (eq (2.11)). At high overall radical concentrations, as with EPR measurements, SPR-MCR cross-termination gets important and eq (2.11) has to be replaced by eq (2.12).

$$x_{\text{MCR}} = \frac{k_{\text{bb}}}{k_{\text{bb}} + k_{\text{p}}^{\text{t}} \cdot c_{\text{M}}} \quad (2.11)$$

$$x_{\text{MCR}} = \frac{k_{\text{bb}}}{k_{\text{bb}} + k_{\text{p}}^{\text{t}} \cdot c_{\text{M}} + k_{\text{t}}^{\text{st}} \cdot c_{\text{SPR}}} \quad (2.12)$$

According to these equations, x_{MCR} depends on monomer concentration and thus a conversion dependence for $k_{\text{p}}^{\text{eff}}$ and $k_{\text{t}}^{\text{eff}}$ is obvious. In addition, the conversion dependence of k_{p}^{s} (and maybe also of k_{p}^{t}) has to be considered which is especially true for aqueous-phase polymerizations.^{19,24,26,35,71-73} The degree of complexity is further increased when β -scission of MCRs comes into play at higher temperatures and macromonomers with terminal double bonds are formed.^{49,65,68,74}

Interpreting k_{p} and k_{t} as "effective" quantities, eq (2.5) may be written as

$$R_{\text{p}} = -\frac{dc_{\text{M}}}{dt} = k_{\text{p}}^{\text{eff}} \cdot c_{\text{M}} \cdot \sqrt{\frac{f \cdot k_{\text{d}} \cdot c_{\text{I}}}{k_{\text{t}}^{\text{eff}}}} \quad (2.13)$$

The origin behind $\omega > 1$ found with acrylate polymerizations can be illustrated by assuming that k_{t}^{st} is the geometric mean of k_{t}^{ss} and k_{t}^{tt} , i.e., $k_{\text{t}}^{\text{st}} = \sqrt{k_{\text{t}}^{\text{ss}} + k_{\text{t}}^{\text{tt}}}$, which yields eq (2.14).

$$\sqrt{k_{\text{t}}^{\text{eff}}} = \sqrt{k_{\text{t}}^{\text{ss}}} \cdot (1 - x_{\text{MCR}}) + \sqrt{k_{\text{t}}^{\text{tt}}} \cdot (x_{\text{MCR}}) \quad (2.14)$$

Implementing the eqs (2.8), (2.9) and (2.14) in eq (2.13), the following expression for the polymerization rate under stationary conditions is obtained.

$$R_p = -\frac{dc_M}{dt} = \frac{k_p^s}{\sqrt{k_t^{ss}}} \cdot c_M \cdot \sqrt{f \cdot k_d \cdot c_I} \cdot \left(\frac{c_M}{c_M + \frac{\sqrt{k_t^{tt}}}{\sqrt{k_t^{ss}}} \cdot \frac{k_{bb}}{k_p^t}} \right) \quad (2.15)$$

The upper limit of 2 is reached for ω , if $\sqrt{\frac{k_t^{tt}}{k_t^{ss}}} \cdot \frac{k_{bb}}{k_p^t} \gg c_M$.^{64,66} In other words, the addition of monomer to a polymerization in which MCRs are present causes a higher MCR propagation rate which reduces x_{MCR} and thus enhances k_p^{eff} . As a consequence, R_p increases disproportionately with c_M , i.e., $\omega > 1$.

2.3 Diffusion Dependence of Rate Coefficients in CRP

For each bimolecular reaction, the mutual approach of the reactants by diffusion is the basic step. During polymerization, small monomers are transformed into large macromolecules which goes along with a significant change in the properties of the reaction mixture. The increase in dynamic viscosity, η , perhaps the most obvious change, can amount to several orders of magnitude and may induce a conversion dependence for k_p , k_t and for the initiator efficiency, f . The individual self-diffusion coefficient, D^1 , may be approximated by the Stokes-Einstein equation (eq (2.16) with k_B as the Boltzmann constant, the hydrodynamic radius, r_1 , and the absolute temperature, T .

$$D^1 = \frac{k_B \cdot T}{6 \cdot \pi \cdot r_1 \cdot \eta} \quad (2.16)$$

According to this fundamental relationship, the increase in viscosity is accompanied by a decrease in molecular mobility. Reactions for which the diffusion of the reactants is the rate-determining step are called diffusion controlled and the associated rate coefficient can be expressed by the Smoluchowski equation (eq (2.17)).⁷⁵

$$k_{\text{D}} = 4 \cdot \pi \cdot N_{\text{A}} \cdot (D_{\text{A}}^{\text{l}} + D_{\text{B}}^{\text{l}}) \cdot R_{\text{c}} \quad (2.17)$$

Here, N_{A} is the Avogadro constant and R_{c} is the capture radius. Thus, the rate of diffusion-controlled reactions is reduced upon increasing monomer-to-polymer conversion, X , whereas so-called chemically controlled processes, such as propagation, may become diffusion controlled at higher X . The importance of diffusion control can be seen by the fact that many tags have been created which relate to the diffusion control of termination (*gel* or *Trommsdorf effect*), initiation (*cage effect*), and of propagation (*glass effect*).⁴⁶ A comprehensive review about diffusion control can be found in Ref.⁴⁶ It is important to mention that the viscosity of the reaction mixture, η , (macroscopic viscosity) and the effective microviscosity which applies to the macroradicals are identical only in the initial (polymer-free) period. At low conversion, k_{t} stays more or less constant, whereas η increases significantly with conversion.⁴⁴

2.3.1 Diffusion Control of Propagation

In principle, also the propagation reaction requires the mutual diffusion of monomer and macroradical. Because of the enormous concentration of monomer as compared to radicals, which is especially true for bulk polymerizations, monomer is ubiquitous and no center-of-mass diffusion is required. Only at very high conversions, above 80 %, a decrease in k_{p} (glass effect) may occur, in particular in cases where the polymerization is carried out at temperatures below the glass-transition temperature. In order to describe the change of η with X , $\eta(X)$, relative viscosity, η_{rel} , is defined with respect to the initial viscosity η^0 (eq (2.18)).

$$\eta_{\text{rel}}(X) = \frac{\eta(X)}{\eta^0} \quad (2.18)$$

The diffusive contribution to k_{p} may thus be expressed by

$$k_{\text{p},X} = \frac{k_{\text{p}}}{\eta_{\text{rel}}(X)}, \quad (2.19)$$

with k_p being the propagation rate coefficient deduced from PLP-SEC at low conversion. At high conversion, the decay of k_p is difficult to be observed since the decrease in initiator efficiency may occur simultaneously. The conversion dependence of k_p can be described by

$$\frac{1}{k_p} = \frac{1}{k_p} + \frac{1}{k_{p,x}}. \quad (2.20)$$

2.3.2 Diffusion Control of Initiation

After homolytic bond cleavage, the primary radicals from initiator decomposition have to leave the solvent cage. At high viscosity, the rate of this diffusion-controlled process is reduced and the recombination of primary radicals is favored over initiation. The decrease of initiator efficiency, f , is called the cage effect.

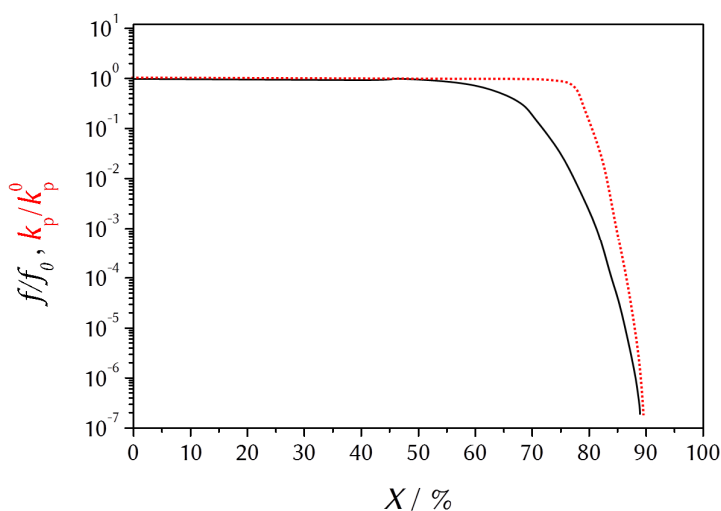


Figure 2.2: Qualitative comparison of the relative decrease of propagation rate coefficient, k_p , (glass effect) and of initiator efficiency, f , (cage effect) upon increasing monomer-to-polymer conversion, X , according to Ref.⁴⁶

2.3.3 Diffusion Control of Termination

Since the early days of polymerization reaction kinetics, the diffusion control of termination was obvious for the following grounds:⁴⁶

1. k_t was found to be inversely proportional to η .
2. The Smoluchowski equation (eq (2.17)) allows for an accurate description of the termination of small radicals.⁷⁶⁻⁷⁸
3. k_t decreases with increasing pressure.⁴⁶

The latter point implies a positive activation volume which is against the observation made with chemically controlled processes. The temperature and pressure dependences arise from the correlation with viscosity.

The Mechanism of Termination

A detailed kinetic scheme of the termination process was first described by Benson and North (Figure 2.3). They considered three individual steps.^{79,80} Direct contact of two macroradicals is provided by translational (center-of-mass) diffusion (TD) in a first step. Subsequently, the two radical functionalities on the entangled macroradicals have to approach each other by segmental diffusion (SD) forming a radical encounter pair. The final step is the actual chemical reaction (CR).

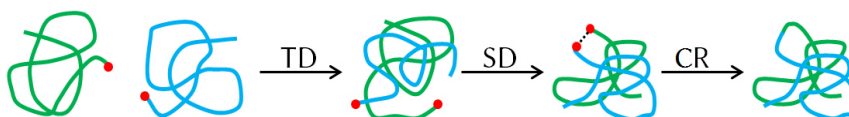


Figure 2.3: Illustration of the elementary reaction steps for termination of two macroradicals (see text).^{79,80}

Conversion Dependence of Termination

The three modes of termination control relate to different conversion regimes during a polymerization at low and moderate conversion (Figure 2.4). As the chemical reaction is extremely fast, CR is not rate controlling. It turns out that at moderate and high degrees of monomer conversion, reaction diffusion (RD) needs to be included as another termination mechanism. RD refers to the process of two radicals approaching each other by propagation steps. At very high conversion, RD may be delayed by diffusion control of propagation.

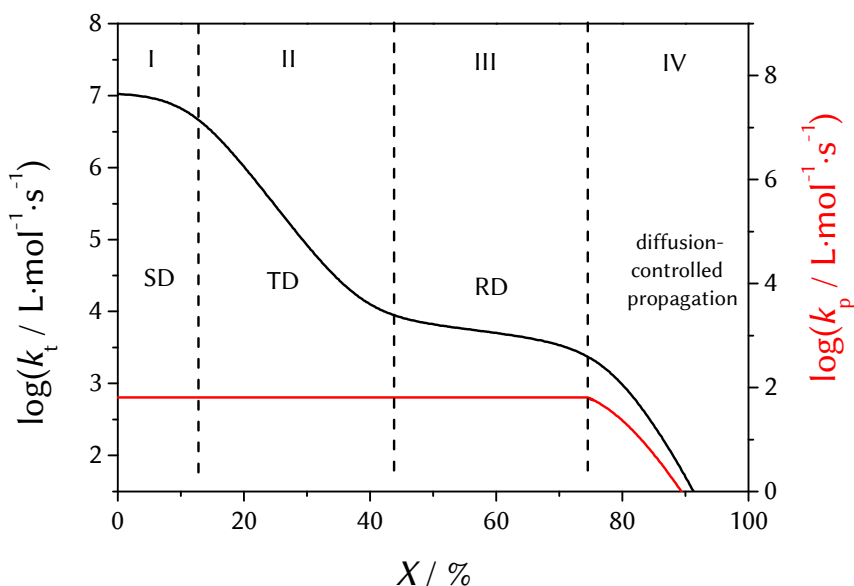


Figure 2.4: Qualitative illustration of conversion dependence of the propagation and termination rate coefficient, k_p and k_t , with respect to the four termination modes (I – IV) as described in the text. The sigmoid decay of k_t refers to a bulk polymerization of methyl methacrylate at 50 °C.⁴⁶

Starting from an SD- controlled plateau in region I, where k_t exhibits at best minor changes with X , a significant steep decrease occurs under TD control (II) (gel effect) until the reaction diffusion (RD) dominates (III). The decrease in k_t upon passing from region I to III is accompanied by a significant increase in radical concentration which in turn causes a massive acceleration of polymerization. At higher conversion but prior to the potential onset of the glass effect,⁸¹ the macroradical motion becomes very slow such that the radical chain end diffuses by propagation steps (RD).⁸² For highly cross-linked macromonomers, RD may even occur at lower conversion.⁸³ The decrease of k_t in region III is less pronounced than with region II since propagation becomes diffusion controlled only at very high conversion (IV) (glass effect).

According to this scheme, the termination rate coefficient may be expressed by a model introduced by Buback:⁸²

$$\frac{1}{k_t} = \frac{1}{k_{SD}} + \frac{1}{k_{TD}} + \frac{1}{k_{CR}} \quad (2.21)$$

Analogous to the description of the conversion dependence for k_p (eq (2.19)) the translational diffusion controlled rate coefficient, k_{TD} , is given by

$$k_{TD} = \frac{k_{TD}^0}{\eta_{rel}(X)}, \quad (2.22)$$

with k_{TD}^0 being the (hypothetical) TD rate coefficient at $X = 0$. Since propagation leads to termination in case of RD, k_{RD} is proportional to k_p (eq (2.23)).

$$k_{t,RD} = C_{RD} \cdot k_p \cdot \frac{c_M}{c_M^0} = C_{RD} \cdot k_p \cdot (1 - X). \quad (2.23)$$

Here, c_M^0 is the initial monomer concentration and C_{RD} is the reaction-diffusion constant describing the efficiency of termination by RD.

Thus

$$k_t = \frac{1}{\frac{1}{k_{SD}} + \frac{1}{k_{TD}} + \frac{1}{k_R}} + k_{t,RD}, \quad (2.24)$$

which leads to

$$k_t = \frac{1}{\frac{\eta_{rel}}{k_{TD}^0} + \frac{1}{k_{SD}}} + \frac{C_{RD} \cdot (1 - X)}{\frac{1}{k_p} + \frac{\eta_{rel}}{k_p^0}}. \quad (2.25)$$

Eq (2.25) allows for an accurate description of the conversion dependence of k_t for the systems studied so far. It should however be mentioned that, depending on the monomer under investigation, the relevance of the individual termination mechanisms may be quite different which affects the overall appearance of the k_t vs X correlations.

2.4 Chain-length Dependency of Rate Coefficients in CRP

In what follows, the impact of chain length, i , on k_p and k_t is discussed. As termination is diffusion-controlled, the impact of chain length is much larger on k_t than on k_p , which is chemically controlled.

Macroradicals of different size coexist during polymerization and are subjected to propagation and termination. The propagation and termination rate coefficients mentioned so far were chain-length averaged quantities, which should be correctly denoted as $\langle k_p \rangle$ and $\langle k_t \rangle$.

2.4.1 Chain-length Dependency of Propagation

As described in Section 2.3.1, propagation can be looked upon as a conversion-independent process up to very high conversion. The chain-length dependency of chemically controlled propagation may be interpreted in terms of the Transition State Theory (TST).^{84–88} A detailed discussion is given in Ref.⁸⁷ Simulations suggest that, due to the increase in chain length, the internal mobility in the transition state structure is restricted which leads to a decrease in the entropy-driven pre-exponential, $A(k_p)$, thus lowering k_p . The monomeric k_p , $k_p(1)$, may exceed the limiting value for long chains, k_p , as determined by PLP–SEC, by up to one order of magnitude. The decrease in $k_p(i)$ with increasing chain length is restricted to the very initial growth period up to about $i = 10$. As a consequence, propagation is adequately described by the long-chain value k_p and the notation $\langle k_p \rangle$ is omitted. On the basis of experimental studies,⁸⁷ the following expression is proposed for chain-length dependent propagation (CLDP).

$$k_p^i = k_p \left[1 + C_1 \exp \left(- \frac{\ln 2}{i_{1/2}} (i - 1) \right) \right], \quad (2.26)$$

whereby the extent of the k_p reduction is given by C_1 .

$$C_1 = \frac{(k_p^1 - k_p)}{k_p} \quad (2.27)$$

The characteristic chain length $i_{1/2}$ may be interpreted as a "half-life" quantity in terms of first-order kinetics. E.g., at $i_{1/2}+1$, $k_p^i - k_p$ has half the value of $k_p^1 - k_p$.⁸⁷ Thus $i_{1/2}$ is indicative of the chain-length range being effected by CLDP.

2.4.2 Chain-length Dependency of Termination

Since termination is a diffusion controlled process, it comes as no surprise that radicals diffuse and hence terminate slower upon increasing chain length. Consequently, the chain-length dependence (CLD) of k_t reflects the impact of i on the self-diffusion coefficient, D , i.e., $D \sim i^{-\alpha}$, which is indeed true for very short radicals where center-of-mass-diffusion is dominating.⁸⁹ The exponent α , which is above zero, reflects the extent of chain growth on D . The situation is however more complex in that long-chain radicals exhibit another chain-length dependence, i.e., another power-law exponent.

The Composite Model by Smith, Russell and Heuts

According to Figure 2.4, the SD is the rate determining step in the initial period of the polymerization. The statement is however only true for large radicals. For two radicals at very small size, the TD is the dominating diffusion mode since the entanglement of two radicals which is necessary for SD, requires larger chain lengths. The CLDT of small radicals in the initial polymerization period is therefore expressed by a power-law expression (eq (2.28)) which is based on a TD approach with α being identified as the exponent in $D \sim i^{-\alpha}$. The termination rate coefficient of two radicals of identical size is $k_t(i,i)$ with $k_t(1,1)$ referring to the termination of two monomeric radicals.

$$k_t(i,i) = k_t(1,1) i^{-\alpha} \quad (2.28)$$

Above a critical chain length, the two growing radicals may entangle upon the formation of an encounter-pair and the SD becomes dominant. The transition from TD (center-of-mass diffusion, short-chain regime) to CD (long-chain regime) was taken into account by the so-called *Composite Model* introduced by Smith, Russell and Heuts (eq (2.29)).⁹⁰ According to this fundamental expression, the two regimes are separated by the *crossover* chain length, i_c , and the CLDT is described by two exponents, α_s and α_l , for the short-chain and long-chain regime, respectively. The composite-model behavior is widely accepted and so far no exception from

this general type of composite-model behavior has been reported. A comprehensive description of CLDT can be found in Ref.⁸⁹

$$\begin{aligned} k_t(i,i) &= k_t(1,1) \cdot i^{-\alpha_s} && ; i \leq i_c \\ k_t(i,i) &= k_t(1,1) \cdot i_c^{-\alpha_s + \alpha_1} \cdot i^{-\alpha_1} = k_t^0 i^{-\alpha_1} && ; i > i_c \end{aligned} \quad (2.29)$$

The quantity k_t^0 is the rate coefficient for termination of two (hypothetical) coiled radicals of chain length unity. The range of experimentally determined numbers for i_c extends from above one hundred, i.e., for ethyl hexyl methacrylate, $i_c(\text{EHMA}) = (270 \pm 30)$,⁹¹ methyl methacrylate, $i_c(\text{MMA}) = 100$,⁹² and vinyl pivalate, $i_c(\text{VPi}) = 110 \pm 30$,⁴² over the medium i_c values for butyl acrylate, $i_c(\text{BA}) = 65 \pm 20$,⁴¹ to relatively small values as reported for vinyl acetate, $i_c(\text{VAc}) = 20 \pm 10$,⁴² and methyl acrylate polymerization, $i_c(\text{MA}) = 35 \pm 10$. Only for methacrylates, a temperature dependency of i_c has been observed which might be due to the strong hindrance toward internal rotation of the macroradicals induced by the α -methyl group (see Appendices).⁹¹

In the short-chain regime, $k_t(1,1)$ may accurately be described by the Smoluchowski equation (eq (2.30)) with R_c being the chain-length independent capture radius and P_{spin} being the spin factor.

$$k_t(1,1) = 2 \cdot \pi \cdot P_{\text{spin}} \cdot N_A \cdot (D_A^{\dagger} + D_B^{\dagger}) \cdot R_c \quad (2.30)$$

Under the assumption that the Stokes-Einstein equation (eq (2.16)) holds for the self-diffusion coefficients of monomeric radicals and $D_A^{\dagger} = D_B^{\dagger}$, the following expression is obtained with $P_{\text{spin}} = 0.25$.^{78,93}

$$k_t(1,1) = \frac{R \cdot T}{6 \cdot \eta} \cdot \frac{R_c}{r_i} \quad (2.31)$$

For spherical radicals, R_c is the sum of the hydrodynamic radii, i.e., $R_c = 2 \cdot r_1$ which results in the so-called *diffusion limit* (eq (2.24)) determining the theoretical maximum of $k_t(1,1)$ at given temperature and viscosity.

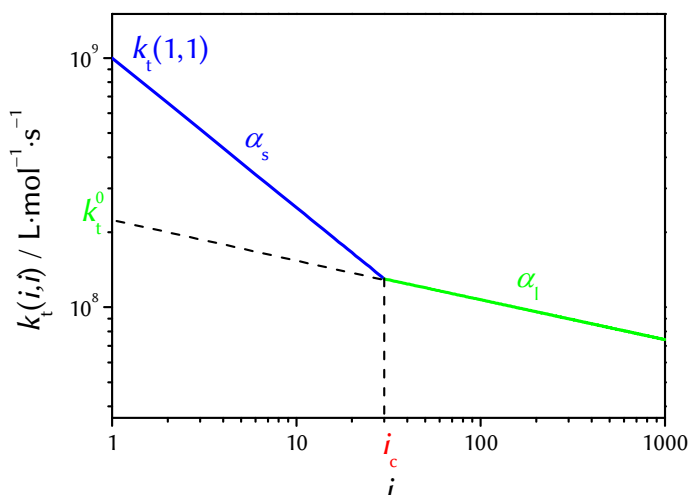


Figure 2.5: Chain-length dependency of k_t according to the Composite Model with $k_t(1,1) = 1.0 \cdot 10^9 \text{ L}\cdot\text{mol}^{-1}\cdot\text{s}^{-1}$, $\alpha_s = 0.60$, $i_c = 30$ and $\alpha_l = 0.16$.

$$k_t(1,1) = \frac{R \cdot T}{3 \cdot \eta} \quad (2.32)$$

This expression suggests a fundamental relationship between $k_t(1,1)$ and η , i.e., $k_t(1,1) \propto \eta^{-1}$, meaning that $k_t(1,1)$ scales with fluidity. As a consequence, the activation energies for both quantities should be similar.

Depending on the structure of the macroradicals (random coil vs rod-like coil), α_s values are expected to be in the range of 0.5 up to 1.0,^{41,90,94,95} whereas the theory of coil dynamics predicts an α_l for two large macroradicals with the radical functionality at the chain-end to be 0.16.^{96–98} In case that the radical functionalities of one or both species are located at a position along the backbone, numbers of α_l are predicted to be 0.27 and 0.43, respectively.⁹⁶ Thus, the CLDT in the long-chain regime will be different for SPR and MCR homo-termination. An increase in α_l from 0.16 to 0.27 for k_t^{st} (SPR-MCR cross-termination) as well as to 0.43 for k_t^{tt} (MCR homo-termination) is expected and was verified by investigations of Fröhlich *et al.*⁹⁹ The change in $k_t(i,i)$ is depicted in Figure 2.5 for typical composite-model parameters.¹⁰⁰

Termination of Radicals Differing in Size

The Composite Model refers to termination between radicals of identical i . Under stationary conditions, however, radicals with different chain lengths occur. Three models have been proposed to estimate $k_t(i,j)$ for the termination of two radicals of sizes i and j : the geometric mean model (gm), the diffusion mean model (dm) and the harmonic mean model (hm).^{89,101,102} The models differ in the weighting of the chain lengths. For example, the dm model rests on the Smoluchowski equation in that the self-diffusion coefficients of both species add to each other, $D(i,j) = D(i,i) + D(j,j)$.⁸⁹ Thus, the dm model might be seen as an arithmetic mean model.

$$k_t(i,j) = k_t(1,1) \cdot (\sqrt{i \cdot j})^{-\alpha_s} \quad (\text{gm}) \quad (2.33)$$

$$k_t(i,j) = \frac{1}{2} \cdot k_t(1,1) \cdot (i^{-\alpha_s} + j^{-\alpha_s}) \quad (\text{dm}) \quad (2.34)$$

$$k_t(i,j) = k_t(1,1) \cdot \left(\frac{2 \cdot i \cdot j}{i + j} \right)^{-\alpha_s} \quad (\text{hm}) \quad (2.35)$$

It is evident that for $i = j$, $k_t(i,i) = k_t(1,1) \cdot i^{-\alpha_s}$ is recovered for each model. The situation for termination between radicals of different size is unsatisfactory as is highlighted in Ref.⁸⁹ since the reported experimental data do not allow to distinguish between the three models. For $\alpha_s < 1$, the order $k_t(i,j)$ (GM) $>$ $k_t(i,j)$ (DM) $>$ $k_t(i,j)$ (HM) is obtained.

2.5 Resolving CLDT by the SP–PLP–EPR Technique

The SP–PLP–EPR method is perfectly suited for studying CLDT, as i of the radicals increases with time t after applying the laser pulse according to eq (2.36) where k_p is the propagation rate coefficient and c_M is the actual monomer concentration. The instantaneous initiation of chain growth ensures a narrow molar mass distribution (Poisson-type) and hence termination occurs exclusively between radicals of more or less identical size which yields $k_t(i,i)$.

$$i = k_p \cdot c_M \cdot t \quad (2.36)$$

In order to deduce the composite-model parameters from radical concentration vs time profiles, the time domain has to be transformed into the chain-length domain. The combination of eq (2.4) with the expressions for the Composite Model (eq (2.29)) and eq (2.36), after integration, yields eq (2.37) and eq (2.38) for the short-chain and long-chain regime, respectively, with c_R^0 being the primary radical concentration after applying the laser pulse.

$$\frac{c_R(t)}{c_R^0} = \left(\frac{2 \cdot k_t^{1.1} \cdot c_R^0 \cdot t^{\alpha_s}}{1 - \alpha_s} \cdot t^{(1-\alpha_s)} + 1 \right)^{-1} \quad (2.37)$$

$$\frac{c_R(t)}{c_R^0} = \left(\frac{2 \cdot k_t^0 \cdot c_R^0 \cdot t^{\alpha_l}}{1 - \alpha_l} \cdot t^{(1-\alpha_l)} + 1 \right)^{-1} \quad (2.38)$$

The propagation time, t_p , is given by $(c_M \cdot k_p)^{-1}$. The logarithmic forms of eqs (2.36) and (2.37) are eq (2.39) and eq (2.40), respectively. According to these two latter equations, the composite-model parameters α_s , i_c and α_l are deduced by plotting $\log(c_R^0/c_R(t)-1)$ vs $\log(t)$: Two linear sections with the slopes $(1-\alpha)$ are obtained, which intersect at i_c .

$$\log\left(\frac{c_R^0}{c_R(t)} - 1\right) = \log\left(\frac{2 \cdot k_t(1,1) \cdot c_R^0 \cdot t^{\alpha_s}}{1 - \alpha_s}\right) + (1 - \alpha_s) \cdot \log(t) \quad i \leq i_c \quad (2.39)$$

$$\log\left(\frac{c_R^0}{c_R(t)} - 1\right) = \log\left(\frac{2 \cdot k_t^0 \cdot c_R^0 \cdot t^{\alpha_l}}{1 - \alpha_l}\right) + (1 - \alpha_l) \cdot \log(t) \quad i \gg i_c \quad (2.40)$$

The chain length for $t \rightarrow 0$ is not adequately represented by eq (2.36) for single-pulsed experiments. Smith and Russell therefore proposed an alternative expression, based on eq (2.41).¹⁰³

$$i = k_p \cdot c_M \cdot t + 1 \quad (2.41)$$

According to eq (2.41) the EPR data should be analyzed by eq (2.42) and eq (2.43), respectively.

$$\frac{c_R(t)}{c_R^0} - 1 = \frac{2 \cdot k_t^{1.1} \cdot c_R^0 \cdot \left((k_p \cdot c_M \cdot t + 1)^{1-\alpha_s} - 1 \right)}{k_p \cdot c_M \cdot (1-\alpha_s)} \quad i \leq i_c \quad (2.42)$$

$$\frac{c_R(t)}{c_R^0} - 1 = \frac{2 \cdot k_t^{1.1} \cdot c_R^0 \cdot \left((i_c)^{1-\alpha_s} - 1 \right)}{k_p \cdot c_M \cdot (1-\alpha_s)} - \frac{2 \cdot k_t^{1.1} \cdot c_R^0 \cdot (i_c)^{1-\alpha_s}}{k_p \cdot c_M \cdot (1-\alpha_1)} + \frac{2 \cdot k_t^0 \cdot c_R^0 \cdot (k_p \cdot c_M \cdot t + 1)^{1-\alpha_1}}{k_p \cdot c_M \cdot (1-\alpha_1)} \quad i \gg i_c \quad (2.43)$$

Since the analysis of the EPR data for long radical chains via eq (2.43) is not very sensitive toward α_1 , application of eq (2.40) is recommended for deducing α_1 and i_c .¹⁰⁴ The required relative radical concentration, $c_R^0/c_R(t)$, is given by the relative EPR signal intensity, $I^0/I(t)$, which is directly obtained from the SP-PLP-EPR experiment without any calibration procedure being necessary. The detailed procedure of deducing the entire set of composite-model parameters is illustrated for styrene bulk polymerization in Section 4.2.

2.6 Photoinitiators for the SP-PLP-EPR Technique

The central paradigm of laser-single-pulsed techniques is the linearity between delay time and chain length according to eq (2.36) and (2.41), respectively. The criterion of narrowly distributed molar masses of the growing radicals leads to the following requirements for a "suitable" photoinitiator.

1. The UV absorption of the photoinitiator should be high at 351 nm, which is the laser wavelength.
2. The thermal stability should be high at the applied temperature.
3. The initiator efficiency should be close to unity.
4. The initiation of the initiator-derived primary radicals should be fast compared to propagation..
5. The photoinitiator-derived radicals should exhibit more or less identical reactivity.

Investigations by Buback and Külpmann indicate that α -methyl-4-(methylmercapto)- α -morpholinopropiophenone (MMMP) is perfectly suited for acrylates.⁴⁰ Vana *et al.* extended the application of MMMP to itaconates. MMMP is the major initiator for electrophilic monomers in organic systems.¹⁰⁵ For aqueous solutions, Darocur[®] is used. With more nucleophilic monomers such as vinyl esters, the reactivity of the MMMP-derived primary radicals (Figure 2.6) is too low.

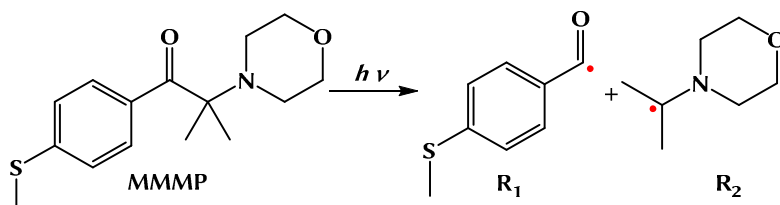


Figure 2.6: Photolysis of MMMP releasing the primary radicals R_1 and R_2 .

As a consequence, the typical quartet-structured hyperfine coupling patterns as expected for vinylic end-chain radicals could not be observed with vinyl acetate (VAc). Instead, the formation of a radical-adduct has been observed as illustrated in Figure 2.7.^{42,106}

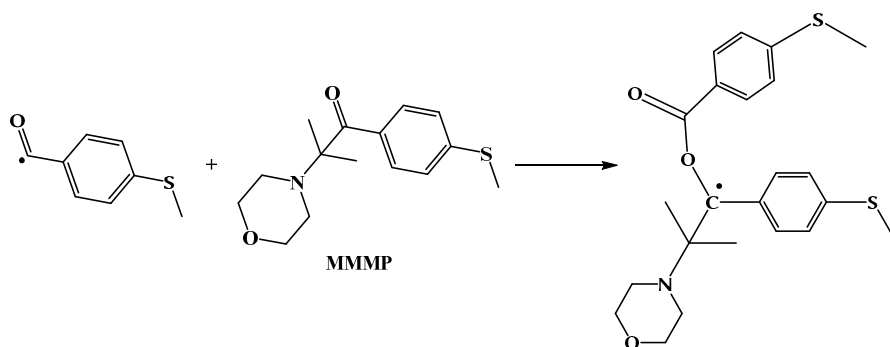


Figure 2.7: Radical adduct formation for MMMP as proposed in VAc polymerization.^{42,106} Reproduced with permission from Kattner, H.; Buback, M. *Macromol. Chem. Phys.* **2014**, *215*, 1180–1191. Copyright 2016, Wiley-VCH.

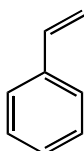
After careful testing of several photoinitiators, dicumyl peroxide (DCP) has been identified as the best option for SP-PLP-EPR experiments on vinyl acetate and similar monomers.¹⁰⁶ In addition to the favorable symmetric structure, the high reactivity of the oxygen-centered primary radicals constitutes the important signature of this photoinitiator. The half-life is sufficiently large to allow for measurements at temperatures as high as 120 °C.^{42,106} Since the vinyl moiety in both vinyl esters and in styrene is non-activated, the poor success of investigations into the CLDT of styrene polymerization by SP-PLP-EPR, is obviously due to MMMP being no perfect initiator for this monomer for which DCP should be better suited.

Experimental

3.1 Chemicals

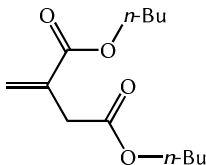
3.1.1 Monomer

Styrene

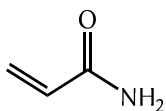


Non-deuterated styrene (Sty-H8, $M = 104.15 \text{ g}\cdot\text{mol}^{-1}$, purum, $\geq 99\%$, Aldrich) and per-deuterated styrene (Sty-d8, $M = 112.20$, 99.5 atom % D, over molecular sieve 3 Å, ABCR) were purified by passing through a column filled with aluminum oxide (Brockmann Number 1, grade 507-C-I, neutral).

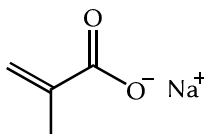
Di (*n*-butyl) itaconate



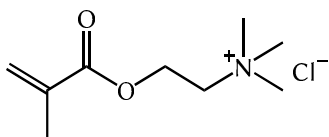
Di (*n*-butyl) itaconate (DBI, IUPAC: dibutyl 2-methylidenebutanedioate, $M = 242.31 \text{ g}\cdot\text{mol}^{-1}$, purum, $\geq 99\%$ Sigma Aldrich) was cleaned by passing through a column filled with inhibitor remover (Sigma).

Acrylamide

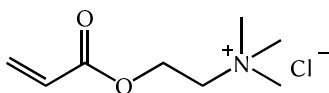
Acrylamide (AAM, IUPAC: prop-2-enamide, Fluka, purum, $\geq 98.0\%$, stabilized with Cu^{2+} , $M = 71.08 \text{ g}\cdot\text{mol}^{-1}$) was recrystallized from acetone dried under reduced pressure and stored at $-21 \text{ }^\circ\text{C}$.

Sodium methacrylate

Sodium methacrylate (NaMAA, IUPAC: sodium 2-methylprop-2-enoate, 99%, $M = 108.07 \text{ g}\cdot\text{mol}^{-1}$, Sigma Aldrich) was used as received.

Trimethylaminoethyl methacrylate chloride

Trimethylaminoethyl methacrylate chloride (TMAEMA, IUPAC: 2-(methacryloyloxy)-*N,N,N*-trimethylethan-1-aminium chloride, $M = 207.69 \text{ g}\cdot\text{mol}^{-1}$, 80 wt.% in H_2O , 600 ppm monomethyl ether hydroquinone as inhibitor, Sigma-Aldrich, Sigma Aldrich) was used as received.

Trimethylaminoethyl acrylate chloride

Trimethylaminoethyl acrylate chloride (TMAEA, IUPAC: 2-(acryloyloxy)-*N,N,N*-trimethylethan-1-aminium chloride, $M = 193.67 \text{ g}\cdot\text{mol}^{-1}$, 80 wt.% in H_2O , 600 ppm monomethyl ether hydroquinone as inhibitor, Sigma Aldrich) was used as received.

3.1.2 Initiators

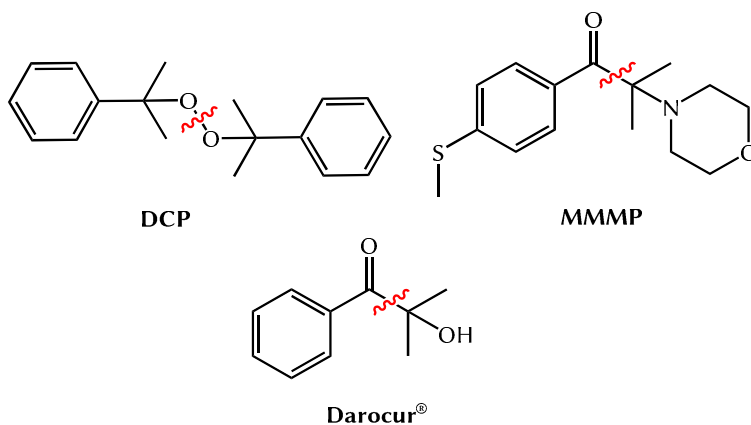


Figure 3.1: UV initiators used for SP-PLP-EPR measurements. For the abbreviations see text. The position of primary homolytic bond cleavage is indicated by the red line.

The initiators used for the time-resolved EPR measurements are presented in Figure 3.1. The position of primary homolytic bond cleavage is indicated by the red line. All initiators were used as received. For polymerizations in organic phase, i.e., with styrene and DBI, dicumyl peroxide (DCP, IUPAC: 2-(2-phenylpropan-2-ylperoxy)propan-2-ylbenzene, $M = 207.37 \text{ g}\cdot\text{mol}^{-1}$, 98 %, Aldrich) and MMMP (IUPAC: α -methyl-4(methylmercapto)- α -morpholinopropiophenone, $M = 279.40 \text{ g}\cdot\text{mol}^{-1}$, 98 %, Aldrich) were used, respectively, while Darocur[®] (IUPAC: 2-hydroxy-2-methyl-1-phenylpropan-1-one, $M = 164.20 \text{ g}\cdot\text{mol}^{-1}$, 97%, Aldrich) was chosen for the aqueous-solution polymerizations.

For chemically-initiated polymerizations, which were performed by Patrick Drawe, the thermal initiator VA-86 (2,2'-Azobis[2-methyl-*N*-(2-hydroxyethyl)propionamide], > 98 %, $M = 288.35 \text{ g}\cdot\text{mol}^{-1}$, Wako) was used as received.¹⁰⁷

3.1.3 Stable Radical Species

The stable radical species 2,2,6,6-tetramethyl-1-piperidinyloxy (TEMPO, $M = 156.26 \text{ g}\cdot\text{mol}^{-1}$, 99 %, Aldrich,) and 4-hydroxy-2,2,6,6-tetramethylpiperidine 1-oxyl (TEMPOL, $M = 172.24 \text{ g}\cdot\text{mol}^{-1}$, 97 %, Aldrich,) were used for EPR calibration of the setup for organic and aqueous solution, respectively.

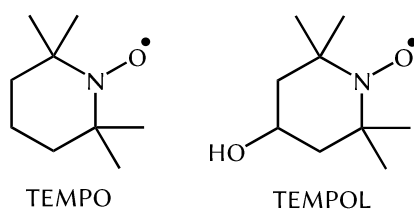


Figure 3.2: Stable radical species used for EPR calibration of the setup used for organic (TEMPO) and aqueous (TEMPOL) solution.

3.1.4 Purification of Water

Experiments in aqueous solution were performed with ultra-pure water (type 1, *Milli-Q*[®]) by purifying demineralized water with the Millipore Simplicity[®] UV (Merck Millipore) operating at a resistance of 18.2 M Ω -cm at 25 °C with a Millipore SimpliPak[®] 2, a Millipore final particle filter (0.05 μ m) and a Millipore UV lamp (185 nm).

3.2 The SP–PLP–EPR Technique

3.2.1 The Setup

Most of the experimental features have already been published in Ref.^{43,108,109}

The EPR measurements were performed on a Bruker EPR CW/transient spectrometer system Elexsys-II 500T operating in the X-band region (~9.85 GHz) equipped with an ER 41122SHQE-LC cavity with cooling plates (Bruker) and synchronized with a XeF laser (LPX 210 iCC, Lambda Physik) by a Quantum Composers 9314 pulse generator (Scientific Instruments) (Figure 3.3). In case of stationary measurements a mercury-arc lamp (LAX 1450/SH2/5,500W, Müller) was used. The cavity has a grid through which the sample is irradiated (Figure 3.4). The spectrometer consists of a microwave bridge containing a microwave source and a detector, a console for electronic data processing and two tunable magnets. The magnets, the console and the cavity are cooled by an internal cooling circuit. The theoretical operating temperature range extends from 100 K to 600 K using the cavity mentioned above. A temperature control of ± 0.05 K was provided by an ER 4131VT control unit (Bruker) by purging the cavity with nitrogen.

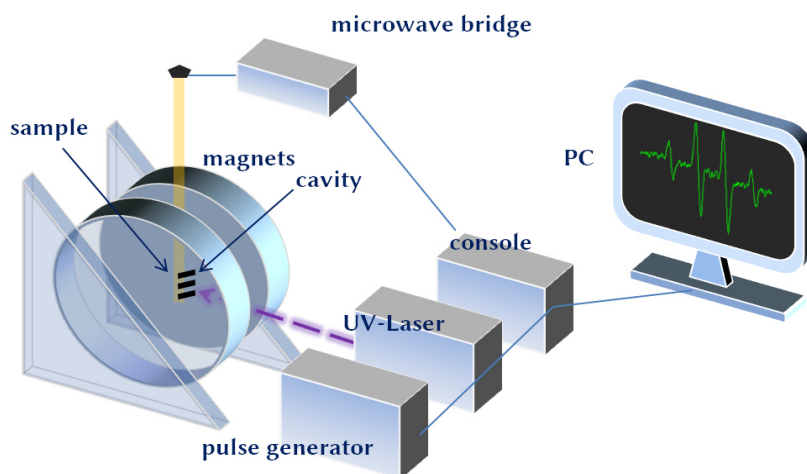


Figure 3.3: Schematic view of the experimental SP-PLP-EPR setup consisting of spectrometer, laser, console and the cavity which is shown in Figure 3.4. For the more detailed description see text. Reproduced with permission from Buback, M.; Schroeder, H.; Kattner, H. *Macromolecules* **2016**, 49, 3193–3213, Copyright 2016, American Chemical Society.

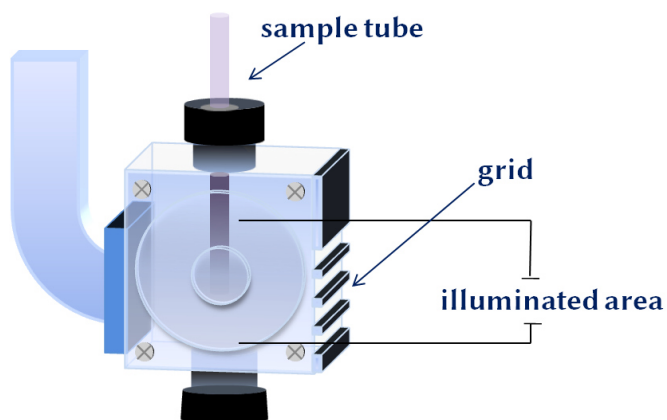


Figure 3.4: Schematic illustration of the cavity used within the presented studies. For a more detailed description see text. Reproduced with permission from Buback, M.; Schroeder, H.; Kattner, H. *Macromolecules* **2016**, 49, 3193–3213, Copyright 2016, American Chemical Society.

3.2.2 EPR Sample Tubes and Cells

The EPR tubes and flat cells consisted of synthetic quartz (Suprasil®) characterized by high purity, optical homogeneity and high UV transmission in the range between 200 and 100 nm with high resistance against discoloration.¹¹⁰ The choice of the sample tubes and cells depends strongly on the polarity of the system due to dielectric loss and is particularly critical for EPR measurements in aqueous solution for which flat cells have been chosen.

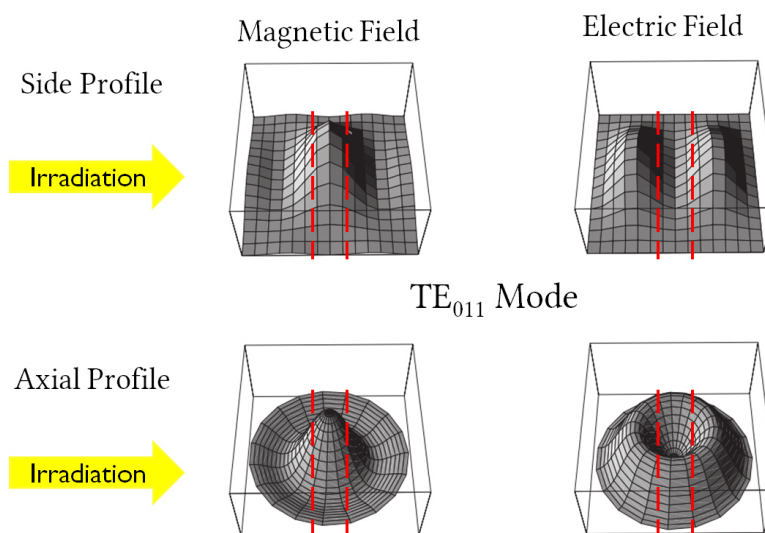


Figure 3.5: Field distribution in a TE_{011} cylindrical cavity as used for the experiments. The ideal orientation of the flat cell for enhanced S/N quality is indicated by the red hashed lines. Figure was partially adopted with permission from Ref.¹¹⁰

The geometry of the flat cell has to be suitable for the shape of the stationary mode formed inside the cavity (see Figure 3.5) in order to ensure a maximum interaction of the sample with the magnetic field component while minimizing the interaction with the electric field component.¹¹⁰ The ideal orientation of the flat cell is illustrated by the

dashed lines in Figure 3.5. The cell is placed perpendicularly with respect to the grid which guarantees homogeneous irradiation of the sample. The orientation must be taken into account even with measurements for which no irradiation is intended. For a so-called TE_{011} mode formed with the used ER 41122SHQE-LC cavity shown in Figure 3.5, a flat cell (Suprasil TE_{102} Aqueous Cell, sample volume 100 μL , Rototec-Spintec) is recommended and was used.^{110–112} Measurements in organic solution were performed using of cylindrical EPR tubes (Wilmad) with either an outer diameter (o.d.) of 3 mm and an inner diameter (i.d.) of 2 mm (for styrene) or with 5 mm o.d. and 4 mm i.d. (for DBI).

3.2.3 Sample Preparation

Solvents, cleaned liquid monomers and Darocur[®] were degassed by several pump–freeze–thaw cycles under the exclusion of visible light with aluminum foil. Solid components, e.g., solid monomer and photoinitiator, were added under an argon atmosphere in a glove box. The samples were filled into the EPR tubes and flat cells, respectively, which were closed with a cap, sealed with Parafilm[®] and used immediately after preparation.

Measurements for styrene and DBI refer to bulk polymerizations while investigations into aqueous-solution polymerizations were performed with the monomer contents listed in Table 3.1.

Table 3.1: Monomer contents in weight percent, wt.%, and molar concentration, c , at 25 °C used for SP–PLP–EPR investigations. The weight percent refers to the monomer-solvent mixture.

	AAm		TMAEMA	TMAEA		NaMAA	
wt.%	10	20	20	10	20	5	10
$c / \text{mol}\cdot\text{L}^{-1}$ (25 °C)	1.42	2.85	0.98	0.52	1.06	0.49	0.98

Organic Solution

Organic samples (0.35 mL), i.e., styrene and DBI in bulk, were filled into the EPR tubes by using an Eppendorf pipette (100/1000 μL , VMR).

Aqueous Solution

Volumes of 100 μL were filled into the EPR flat cells in case of aqueous solutions by using a MicroliterTM syringe (50 μL , Hamilton) after inserting the lower Teflon[®] plug.

Samples of TMAEA and TMAEMA

The huge amounts of monomethyl ether hydroquinone acting as inhibitor may be considered as a factor of uncertainty in SP-PLP-EPR investigations into aqueous-solution polymerization of TMAEA and TMAEMA. The inhibitor is usually consumed within the first laser pulse. The monomer-to-polymer conversion related to this first pulse was less than 2 % for aqueous-solution polymerization of TMAEA (20 wt.%) at 80 °C.

3.2.4 Experimental Procedure

The samples were placed into the cavity as described above. Since the EPR spectrometer is a reflection spectrometer, the setup parameters, e.g., resonance frequency, signal phase, etc., have to be adjusted so that prior to the experiment no microwave energy is reflected to the microwave bridge containing the detector diode (*critical coupling*).¹¹¹ The quality of the *critical coupling* is quantified by the Q -factor which is defined as the ratio of stored and dissipated energy in the cavity (eq (3.1)).

$$Q = \frac{\text{stored Energy}}{\text{dissipated Energy}} = \frac{\nu_{\text{res}}}{\Delta\nu} \quad (3.1)$$

The Q -factor can easily be derived from the shape of the *resonance dip* which is the absolute minimum in a diagram of detector diode current, I , vs microwave frequency, ν , as illustrated in Figure 3.6. According to eq (3.1), the Q -factor is the ratio of the width at half height, $\Delta\nu$, and ν_{res} being the resonance frequency. The Q -factor should not be below 800 (lower limit) for receiving EPR signals intensity in good quality. Quantitative measurements should be performed with Q -values above 1200 as is the case for the studies presented in this thesis.

The experimental EPR parameters were chosen carefully in order to ensure a good signal-to-noise (S/N) quality. The modulation amplitude was set to 3 G with a modulation frequency of 100 kHz. For measurements in aqueous solution a receiver gain of 84 and an attenuation of 13 dB were selected.

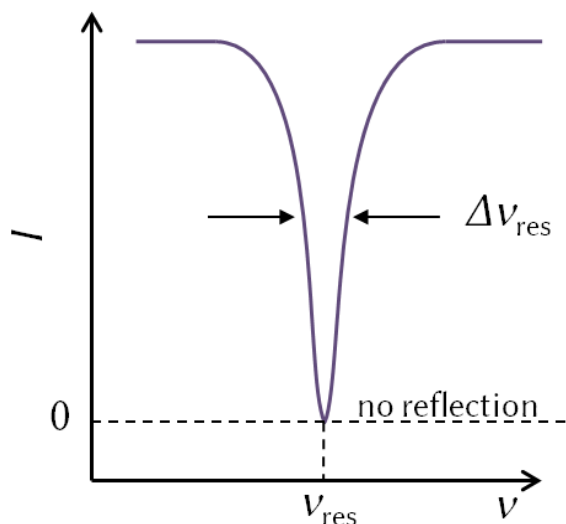


Figure 3.6: Schematic view of resonance dip, i.e., the absolute minimum in a diagram of diode current, I , vs microwave frequency, ν . The resonance frequency, ν_{res} , and the width at half height, $\Delta\nu$, allow for an easy deduction of the Q -factor according to eq (3.1).¹¹¹

The microwave power was close to 10 mW. In organic solution, the receiver gain and the attenuation were reduced to 60 and 26 dB, respectively, with a microwave power at approximately 3.2 mW.

Prior to the actual SP-PLP-EPR experiment, a spectrum under stationary or pseudo-stationary conditions was recorded. For measuring the stationary spectra the UV mercury-arc lamp was used whereas pulsed-laser initiation with a constant pulse-repetition rate (p.r.r.) was applied for pseudo-stationary measurements. The spectra were recorded under conditions as close as possible to the time-resolved experiments. The typical sweep time was 5.12 s with a conversion time of 5.24 ms at 1024 data points. Depending on monomer and temperature, the monomer-to-polymer conversion changes slightly during measurements of the spectra which may affect polarity and changes the diode current. In this particular case, the diode current was readjusted manually to the initial value of 200 μA during the experiment. The variation in diode current is proportional to the monomer-to-polymer conversion and is more pronounced for highly polar monomers. In order to enhance the S/N ratio, several individual EPR spectra were co-added.

Mostly, enhanced EPR signal quality is achieved at low temperatures, e.g., up to -65°C for vinyl ester polymerization,⁴² due to the Boltzmann distribution. Such low temperatures are not accessible with aqueous monomer solutions. The melting points for aqueous solutions used within this work are about -5°C . The S/N quality usually decreases with aqueous solutions toward temperatures from 20°C to 40°C ("valley of tears") but increases again at higher temperatures. The reason behind this effect is the significant decrease in dielectric constant of water with increasing temperature which allows for a higher signal intensity due to the reduction of dielectric loss.¹¹³

The single-pulsed EPR measurements were usually run at magnetic field positions related to the highest signal intensity. It was carefully checked whether the radical concentration vs time profiles are affected by the monomer-to-polymer conversion, i.e., during the application of an increasing number of laser pulses.

3.2.5 Calibration Procedure

During SP-PLP-EPR experiments, signal intensity is recorded which has to be "converted" into absolute radical concentration. To do so, a two step procedure has been applied. The principle is illustrated in Figure 3.7.

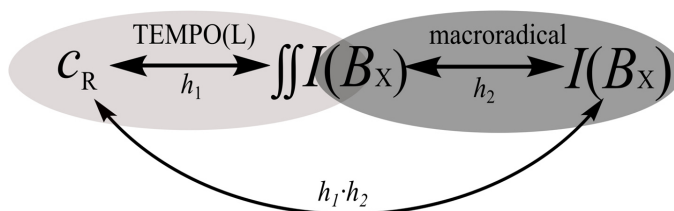


Figure 3.7: Illustration of the two-step procedure used for EPR signal calibration along with the corresponding calibration constants h_1 and h_2 . Reproduced with permission from Kattner, H.; Buback, M. *Macromol. Symp.* **2013**, 333, 11-23, Copyright 2013 Wiley-VCH.

The EPR spectra show the first derivative of the absorption signal. Thus the double integral, in what follows denoted as $\iint I(B_x)$, is proportional to the absolute stationary radical concentration, $c_R(t)$, according to eq (3.2) with h_1 being the proportionality coefficient related to the experimental conditions of the experiment, e.g., temperature, concentration and EPR parameters.

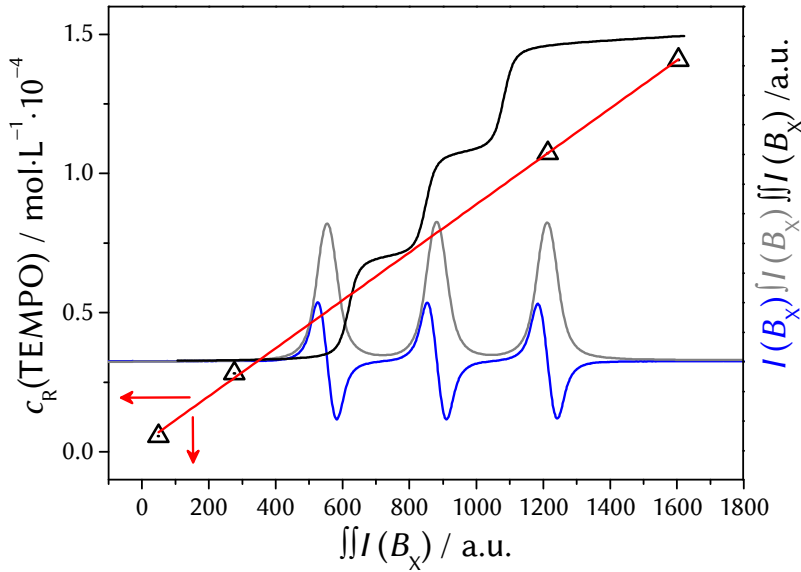


Figure 3.8: Correlation between the spectral double integral, $\iint I(B_x)$, and absolute radical concentration for a dilution series of stable radical species (black triangles). The associated linear fit (red) provides h_1 as the slope according to eq (3.2). The spectrum (blue) as well as the corresponding first integral $\int I(B_x)$ (grey) and $\iint I(B_x)$ (black) relate to the $1.4 \text{ mol}\cdot\text{L}^{-1}$ solution of TEMPO as radical species in bulk DBI at 303 K.

The value of h_1 may also change with small structural deviations of the handmade flat cells which make an individual calibration for each flat cell necessary.

$$c_R(t) = h_1 \cdot \iint I(B_x) \quad (3.2)$$

The EPR spectra for a dilution series of a stable radical species are recorded under experimental conditions being as close as possible to the polymerization conditions. The double integration is exemplarily shown in Figure 3.8. The determined $\iint I(B_x)$ is correlated with $c_R(t)$ (black triangles) yielding a linear relationship with h_1 being the slope of the related linear fit (red line).

In a second step, $\iint I(B_x)$ of the EPR spectrum for the investigated radical species is correlated with the corresponding maximum in band intensity, $I(B_x)$, at which the intensity is monitored during the SP-PLP-EPR experiment.

According to eq (3.3), the proportional coefficient h_2 is deduced as slope from the related linear fitting (see Figure 3.9).

$$\iint I(B_x) = h_2 \cdot I(B_x) \quad (3.3)$$

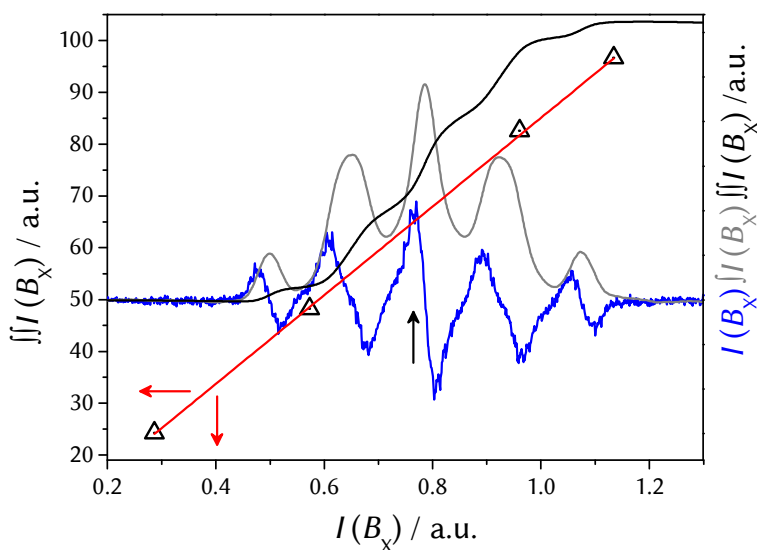


Figure 3.9: Correlation between the intensity at the band maximum, $I(B_x)$, indicated by the arrow and the related double integral, $\iint I(B_x)$, with respect to the EPR spectrum of the species under investigation, i.e., the propagating DBI radical in bulk polymerization (black triangles) in this case. The linear fit (red) provides h_2 as the slope according to eq (3.3). The underlying EPR spectrum, the first integral $\int I(B_x)$ and $\iint I(B_x)$ are shown as blue, grey and black line, respectively. The spectrum was recorded under identical condition as with the TEMPO spectrum shown in Figure 3.8.

The combination of eq (3.2) and eq (3.3) yields eq (3.4) which correlates signal intensity $I(B_x)$ at the peak maximum to absolute radical concentration.

$$c_R(t) = h_1 \cdot h_2 \cdot I(B_x) \quad (3.4)$$

3.2.6 Kinetic Simulations and Data Analysis

The so-obtained radical concentration vs time profiles were either analyzed in the light of analytic expressions as stated in related parts of the main text or by the numerical simulation package PREDICI[®]. It should be noted that the IUPAC-recommended form of the termination rate law, $dc_R/dt = -2 k_t \cdot c_R^2$, has been used throughout this thesis.^{17,48}

3.3 Determination of Monomer-to-Polymer Conversion

The monomer-to-polymer conversion was either determined by Fourier-transform near-infrared (FT-NIR) spectroscopy or gravimetrically as outlined in Ref.^{108,114}

Parts of this section have already been published in Ref.^{108,114}

Aqueous Solution

For aqueous-solutions polymerizations, i.e., for TMAEMA and TMAEA polymerization in D₂O, the monomer-to-polymer conversion was determined by a (FT)-NIR spectrometer (Bruker Optik, IFS 88) equipped with a tungsten halogen lamp (Gilway Technical Lamp, L7417A, 12 V, 50 W), a silicon-coated calcium difluoride beam splitter (model T8401) and a liquid-nitrogen-cooled InSb detector (InfraRed Associates, model D413). The flat cell was placed into a sample holder and a zero-conversion spectrum was recorded at ambient temperature (22 °C) shown for TMAEMA in Figure 3.10. After pulsing, the FT-NIR measurements were repeated to measure the degree of monomer-to-polymer conversion by integration, between 6250 and 6100 cm⁻¹, i.e., of the first overtone of the antisymmetric C-H stretching mode of the methyldene group with band maximum at 6183 cm⁻¹. For integration, the software OPUS (Version 6.0.72, method B) was used.

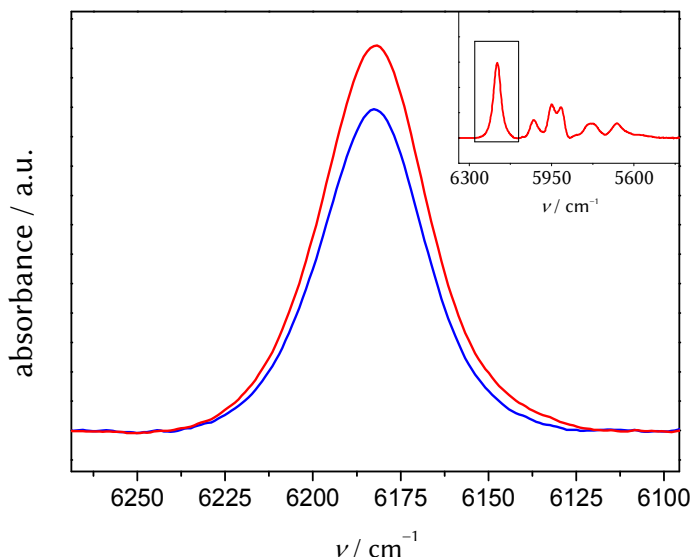


Figure 3.10: FT-NIR absorbance spectrum of TMAEMA (20 wt.% in D₂O) recorded prior (red) and after (blue) applying a sequence of 10 laser pulses. Integration of the absorbance band around between 6100 cm⁻¹ and 6250 cm⁻¹, which is assigned to the first overtone of the antisymmetric C-H stretching mode of the methyldene group, yields the monomer-to-polymer conversion, i.e., 0.207 in this case. The inset shows the entire spectrum with the region of interest being framed.

The impact of NIR band overlap is minimized by subtraction of a reference spectra and by using D₂O rather than H₂O as the solvent. It is not to be expected that the kinetics of polymerization in D₂O differs significantly from the one in H₂O solution under otherwise identical experimental conditions.^{108,115} The procedure is in principle identical for determination of conversion vs time profiles under stationary conditions provided by Patrick Drawe. The experimental aspects are described in detail elsewhere.¹⁰⁷

Organic Solution

Polymerizations in organic solution, i.e., during styrene and DBI bulk polymerization, allow for a gravimetric determination of monomer-to-polymer conversion (Satorius Balance CPA3245) due to the high vapor pressure. After a series of laser pulses the contents of the EPR tube were filled in a previously weighed aluminum shell and the monomer

evaporated under ambient pressure in the dark followed by reweighting the shell including the residual polymer. In order to enhance the accuracy of the gravimetric analysis, polymer produced within three experiments carried out under identical conditions has been combined.

3.4 Density and Viscosity Measurement

The density and the dynamic viscosity measurements were performed on a density meter system DPR 2000 (Anton Paar) and a viscosity meter AMVn (Anton Paar, 1569), respectively.

3.5 Simulation and Fitting of the EPR Spectra

The recorded EPR Spectra were simulated and fitted using MATLAB[®] in conjunction with the software package Easyspin[®]. The basic script, which has to be adapted for the individual spectrum, is part of the Appendices section and allows for detailed and precise determination of the hyperfine coupling constants (hfcc) and the relative molar fraction of coexisting radical species and conformers, respectively. The script also provides different fitting algorithms, e.g., genetic algorithm, Monte Carlo, Levenberg-Marquardt and Nelder/Mead simplex, and different scaling methods of experimental and simulated spectra. The strategies applied for complex spectra in which different types of radicals and conformers coexist, are described in the main text for each system.

Termination Kinetics in Styrene Bulk Polymerizationⁱ

During the last decade, the SP–PLP–EPR technique has successfully be applied to investigations into termination and transfer kinetics of itaconate¹¹⁶ acrylate-type^{37–39,41,70} and methacrylate-type^{117–119} radicals under different experimental conditions. However, styrene, the archetype monomer, evaded investigation by this technique so far. No reliable EPR spectra could be observed with pulsed-laser initiation. EPR investigations into vinyl acetate and vinyl pivalate revealed that the photoinitiator MMMP which has been recommended for the monomer classes mentioned above^{40,105} is unsuitable for relatively nucleophilic monomers such as styrene. By comparative studies with different types of initiators DCP could be identifies as initiator of choice.⁴² It appears to be a matter of priority to accurately determine the composite-model parameters for styrene. In view of the importance of styrene radical polymerization, the knowledge about the termination kinetics of this monomer is scarce. The Russell group¹²⁰ has provided the most recent report on styrene termination, in which the existing literature has been reviewed. When

ⁱ Reproduced with permission from Kattner, H.; Buback, M. *Macromolecules* **2015**, *48*, 309–315, Copyright 2015, American Chemical Society.

applied to styrene, even the SP–PLP–EPR technique runs into problems, which are associated with the unfavorable combination of low propagation and high termination rate. It goes without saying that investigations into CLDT require substantial propagation. With styrene, studies into CLDT become difficult, as the laser-pulse-induced radical concentration decays to a low level before larger chain lengths have been reached. At 25 °C, the propagation rate coefficient of styrene is below the k_p of methyl acrylate, vinyl acetate, and methyl methacrylate by a factor of 154, 40, and 3.8, respectively. In order to reach a reasonable chain size within the time window of 0.01 s, which has to be selected for time-resolved EPR detection of the rapidly terminating radicals, SP–PLP–EPR experiments on bulk styrene have been carried at temperatures up to 135 °C, where a maximum chain length of $i_{\max} \approx 236$ may be reached. Measurements at further enhanced temperature run into difficulties because of significant styrene self-initiation. Because of the rapid consumption of radicals, high S/N quality of the EPR analysis is of key importance. Thus, the favorable effect already used in our preceding study into vinyl acetate⁴² has been applied, and the fully deuterated monomer, Sty-d8, has been subjected to EPR analysis, which allows for reaching radical chain lengths beyond i_c under acceptable signal quality for quantitative EPR analysis.

Beside the kinetic investigation into the termination kinetics of styrene, this section also serves the purpose of exemplarily illustrating the deduction of composite-model parameters by analytic expressions which have been introduced in Section 2.1. Furthermore, the importance of CLDT for understanding termination kinetics under different experimental conditions is shortly underlined by a general analysis of radical structure and its impact on diffusion controlled processes.

4.1 The EPR Spectrum of Styryl Radicals

In contrast to chain-end radicals of vinylic monomers, such as acrylates,^{37,121} vinyl esters^{42,122–124}, and itaconates,¹¹⁶ styryl-H8 radicals exhibit a relatively complicated but characteristic hyperfine coupling (hfc) pattern due to the delocalization of radical functionality over the aromatic ring (Figure 4.1). The measured spectrum is in close agreement with literature and is adequately fitted via the hyperfine coupling constants (hfcc), a , listed in Table 4.1, which are insensitive toward temperature in the region under investigation, i.e., between 73 and 135 °C.^{125,126} The quality of the single-pulsed measurements is impaired, as overall EPR intensity is spread over a multitude of peaks with Sty-H8.

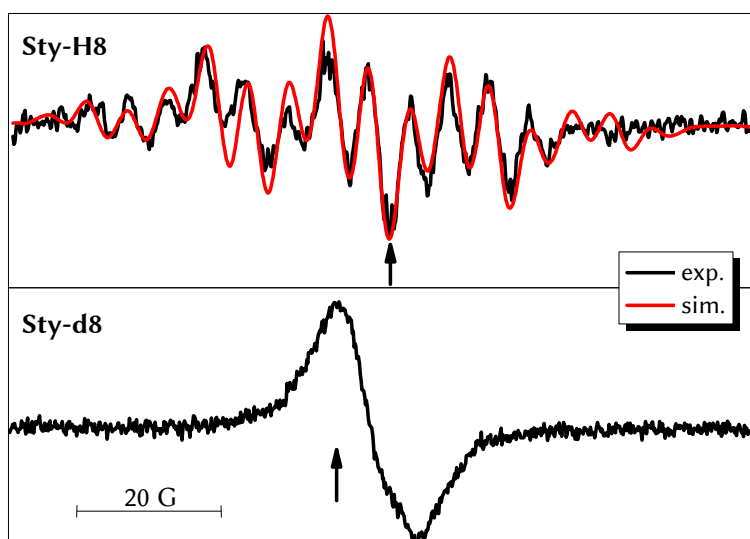


Figure 4.1: EPR spectra of Sty-H8 and of Sty-d8 at 85 °C with DCP ($9.0 \cdot 10^{-2} \text{ mol L}^{-1}$) acting as the photoinitiator under continuous irradiation with a mercury-arc lamp. The simulation (—) of the Sty-H8 spectrum was achieved under the assumption of a delocalized unpaired electron. Radical concentration was close to $3 \cdot 10^{-7} \text{ mol} \cdot \text{L}^{-1}$ in both cases. The magnetic field positions used within the time-resolved SP-PLP-EPR experiments are indicated by the arrows.

Table 4.1: Hyperfine coupling constants a for Sty-H8 radicals in styrene bulk homopolymerization as obtained from fitting of the experimental spectra, e.g., of the one in Figure 4.1.

nuclei	a / G
1H_α	17.6
2H_β	16.3
2H_{ortho}	5.2
2H_{meta}	1.7
1H_{para}	5.3

Therefore, fully deuterated styrene, Sty-d8, has been studied, where the EPR intensity of the styryl radical is more or less condensed into a singlet band (Figure 4.1). The reason behind this simplification is the lower, by a factor of 0.154, gyromagnetic ratio, γ , of deuterium compared to hydrogen.^{42,127} With respect to the termination kinetics, Sty-d8 is expected to behave as does Sty-H8, because the impact of deuteration on diffusion-controlled termination should be negligible.¹²⁸ Although no clear dynamic isotope effect has been observed for MMA and VAc bulk homopolymerizations,^{42,117} the assumption of a negligible isotope effect on termination will be experimentally verified for styrene (see below).

4.2 Chain-Length Dependent Termination of Styryl Radicals

Single-pulse measurements were performed at the magnetic field positions indicated by the arrows in Figure 4.1. To enhance the signal-to-noise ratio of the radical concentration vs time traces, about 10 individual traces were co-added. Monomer-to-polymer conversion was checked gravimetrically to ensure that polymerization occurs in the initial range up to 9 per cent monomer conversion. The radical concentration vs time traces at the lowest and highest experimental temperature are close to each other (Figure 4.2). This surprising result is due to some compensation of the effect of temperature on k_p and k_t : The decay of radical concentration by termination should be enhanced toward higher temperature, but is partially reduced at the same time, due to the prediction of the Composite Model, as the terminating radicals are of larger size within an identical time interval because of higher k_p . The activation energy of k_p , i.e., $E_A = 32.5 \text{ kJ}\cdot\text{mol}^{-1}$,^{19,129,130} is significantly higher than with acrylates¹³¹⁻¹³³, methacrylates^{134,135} and vinyl esters^{124,136,137} for which no such compensation has been observed.^{41,42,117,118} The similarity of radical concentration vs time profiles of different temperatures appears to be indicative of CLDT and highlights the necessity of analyzing termination kinetics in detail. The similarity of radical concentration vs time profiles is however also affected by $k_t(1,1)$, k_p , α_s , α_t , i_c .

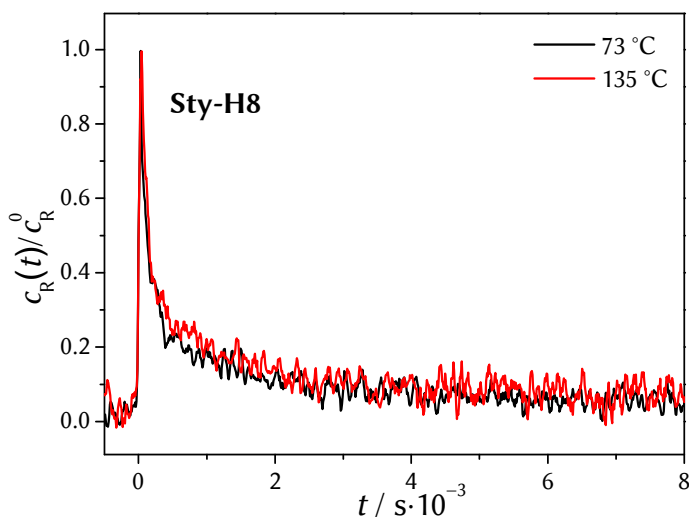


Figure 4.2: Normalized EPR intensity vs time traces measured for non-deuterated styrene, Sty-H8, at the lowest (—) and the highest temperature of the present study (—) with DCP ($9.0 \cdot 10^{-2} \text{ mol L}^{-1}$) being used as the photoinitiator. About 10 individual traces were co-added to enhance the SP-PLP-EPR signal-to-noise ratio. EPR intensity vs time traces were recorded at the magnetic field position indicated in Figure 4.1. The initial radical concentrations were $6.7 \cdot 10^{-6} \text{ mol} \cdot \text{L}^{-1}$ in both cases.

In order to determine the composite-model parameters from SP-PLP-EPR data on the basis of analytic expressions, a two-step procedure has been used. In a first step, the parameters i_c and α_1 were deduced from the linear correlation according to eq (2.40) where c_R^0 refers to the initial radical concentration at $t = 0$. The time required for a single propagation step to occur is referred to as $t_p = (k_p \cdot c_M)^{-1}$. Eq (2.40) is derived on the basis of assuming i to be given by $i = k_p \cdot c_M \cdot t$ (eq (2.36)).

$$\log\left(\frac{c_R^0}{c_R(t)} - 1\right) = \log\left(\frac{2 \cdot k_t^0 \cdot c_R^0 \cdot t_p^{\alpha_1}}{1 - \alpha_1}\right) + (1 - \alpha_1) \cdot \log(t) \quad i \gg i_c \quad (2.40)$$

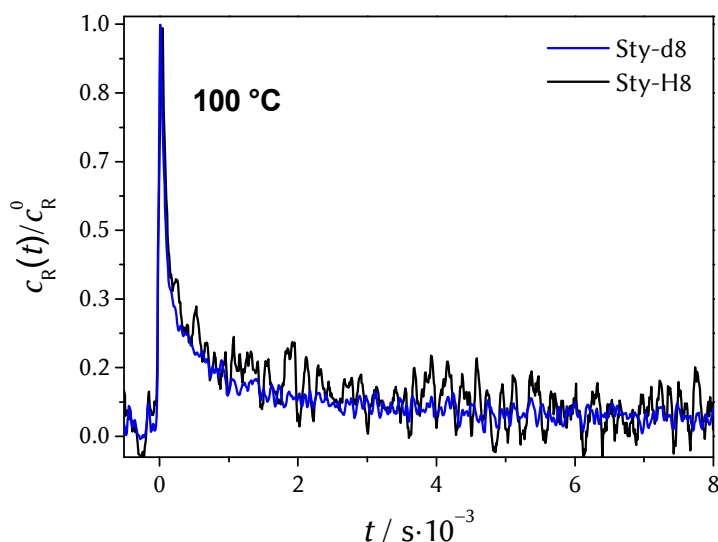


Figure 4.3: Relative radical concentration vs time traces for Sty-H8 (—) and Sty-d8 (—) at 100 °C with DCP ($9.0 \cdot 10^{-2} \text{ mol L}^{-1}$) acting as the photoinitiator. Both traces have been deduced from co-adding the same number of (19) pulses. Initial radical concentration was close to $3.5 \cdot 10^{-4} \text{ mol} \cdot \text{L}^{-1}$ in both cases.

The slope of the straight line fitted to the experimental data for large chain lengths, i.e., large times t after pulsing, yields $(1-\alpha_1)$ and the intersection point of the straight line fits for small and large radicals determines the size of i_c . It should be noted that the composite-model parameters α_1 , i_c (and also α_s) are deduced from relative radical concentrations, $c_R^0/c_R(t)$, which may be directly taken from the measured EPR single-pulsed signal without requiring any calibration for absolute radical concentration at this point. Bulk monomer concentration, c_M , and k_p at the experimental temperature are available from literature.^{19,120,138,139} Due to the enhanced S/N ratio (Figure 4.3) i_c has exclusively been deduced from Sty-d8 experiments. According to Clouet and Chaffanjon,¹⁴⁰ the propagation rate coefficient of fully deuterated styrene is by a factor of 1.2 above $k_p(\text{Sty-H8})$. The bulk density of Sty-d8 at 100 °C is by 7 per cent above the one of Sty-H8. Both effects were included into the analysis.

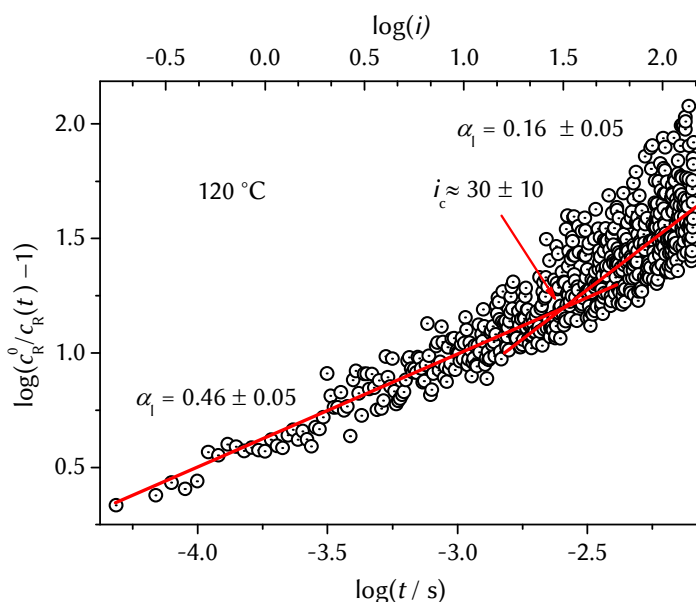


Figure 4.4: Double-log plot of the SP-PLP-EPR data measured for Sty-d8 at 120 °C according to eq (2.40). Analysis of the long-chain regime at high t yields α_1 . i_c is obtained from the intersection of the straight lines fitted to the data at low and high radical chain length.

The resulting impact on the composite-model parameters of styrene is however small and occurs within the limits of experimental accuracy, as is indicated by the close agreement of the relative radical concentration vs time profiles in Figure 4.3. The interception of the two straight-lines in Figure 4.4 occurs at $i_c(\text{Sty-d8}) = 30 \pm 10$ for 120 and 135 °C. This value slightly exceeds $i_c \approx 18$, as reported by Johnston-Hall and Monteiro,¹⁴¹ but is in perfect agreement with the value of $i_c \approx 30$ subsequently published by the same authors.⁹⁵ These two literature values were determined by the RAFT-CLDT-technique which takes advantage of chain-growth control by reversible addition-fragmentation chain transfer (RAFT) polymerization. This approach requires stationary conditions (thermal initiation) and the accurate knowledge of initiation and transfer (RAFT) kinetics as well as the precise measurement of overall polymerization rate. The crossover chain length of styrene is significantly below the ones of methyl methacrylate, $i_c(\text{MMA}) = 100$,⁹² and vinyl pivalate, $i_c(\text{VPi}) = 110 \pm 30$,⁴², but is close to the numbers for vinyl acetate,⁴²

$i_c(\text{VAc}) = 20 \pm 10$ and methyl acrylate,⁴¹ $i_c(\text{MA}) = 35 \pm 10$) and is not too far off the number for butyl acrylate,⁴¹ $i_c(\text{BA}) = 65 \pm 20$. No detailed understanding of the dependence of crossover chain length on monomer structure has emerged so far. Chain-flexibility might be one important factor controlling i_c as higher flexibility should favor the entanglement of two macroradical chains, which is considered to be the initializing step for the transition from center-of-mass to segmental diffusion as this glass-transition temperature, however, should not be stressed in this respect as this quantity refers to solid polymer. Interestingly, the size of the alkyl side chain has an opposite effect on i_c in the acrylate and methacrylate families. Toward larger size of the alkyl side chain, the crossover chain length increases for acrylates⁴¹ and vinyl esters⁴², but decreases (from a higher i_c level) for methacrylates.^{104,117} A tentative explanation of this finding may be that long alkyl side chains solubilize the stiffer methacrylate backbone structure and thus lower i_c , whereas they reduce the mobility of the flexible acrylate structure and thus enhance i_c . Unless a mechanistic understanding and thus a prediction of i_c has been reached, i_c needs to be experimentally determined and should be treated as an empirical quantity.^{37,41,117,118}

The power-law exponent associated with the straight-line fit (Figure 4.4) for long-chain radicals, $\alpha_l = 0.16 \pm 0.05$, is in perfect agreement with the experimental values reported for other monomers^{95,141} and with the exponent which theory predicts for termination of two long chain-end radicals.^{96-98,142} The insensitivity of i_c and α_l toward temperature, which is evidenced by the experiments, has also been found for other monomers.^{42,104,117}

As described earlier, the correlation eq (2.36) underlying eq (2.40), is not valid in the very early time period after applying the laser pulse. As an adequate expression for the region $t \rightarrow 0$, Smith and Russell¹⁰³ introduced eq (2.41) which, results in eq (2.42).

$$\frac{c_R^0}{c_R(t)} - 1 = \frac{2 \cdot k_t(1,1) \cdot c_R^0 \cdot \left((k_p \cdot c_M \cdot t + 1)^{1-\alpha_s} - 1 \right)}{k_p \cdot c_M \cdot (1 - \alpha_s)} \quad 1 \leq i < i_c \quad (2.42)$$

Fitting the EPR data taken at $t < t(i_c)$ according to eq (2.42) yields the exponent α_s together with the product $k_t(1,1) \cdot c_R^0$. As the initial radical concentration, c_R^0 , is known from calibration, $k_t(1,1)$ is directly accessible from $k_t(1,1) \cdot c_R^0$.

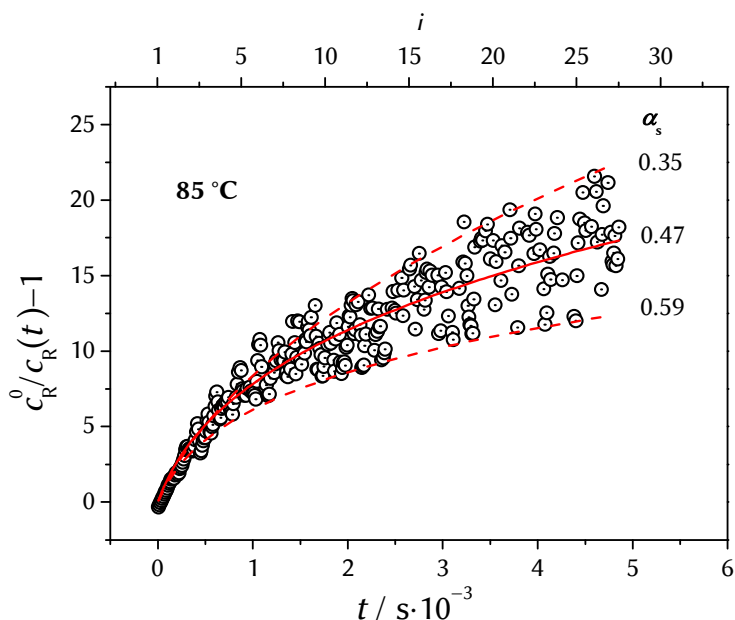


Figure 4.5: Fitting of the SP-PLP-EPR data for deducing α_s and $k_t(1,1)$ for Sty-d8 homopolymerization at 85 °C. The underlying data set is identical to the one shown in Figure 4.4 but has been restricted to the short chain regime, i.e., $i < i_c$. The solid line represents the best fit according to eq (2.42) with $\alpha_s = 0.47$ and $k_t(1,1) = 9.0 \cdot 10^8 \text{ L} \cdot \text{mol}^{-1} \text{ s}^{-1}$. The dashed lines, which were estimated for identical $k_t(1,1)$ but different α_s , may be considered as lower and upper bounds for α_s .

Shown in Figure 4.5 are the results for the fitting of the time-resolved EPR traces for Sty-d8 at 85 °C according to eq (2.42). The analysis was restricted to EPR data taken at chain lengths below i_c . Neither for Sty-H8 nor for Sty-d8, individual α_s exhibits any systematic variation with temperature. Moreover, the arithmetic mean values: $\alpha_s = 0.53 \pm 0.05$ for Sty-H8 and $\alpha_s = 0.49 \pm 0.05$ for Sty-d8 agree within the limits of experimental accuracy. The mean value of $\alpha_s = 0.51 \pm 0.05$, represented by the dashed line in Figure 4.6, is deduced as the temperature-independent power-law exponent for termination of short-chain radicals, $i < i_c$, in styrene homopolymerization. The α_s value is not affected by deuteration.

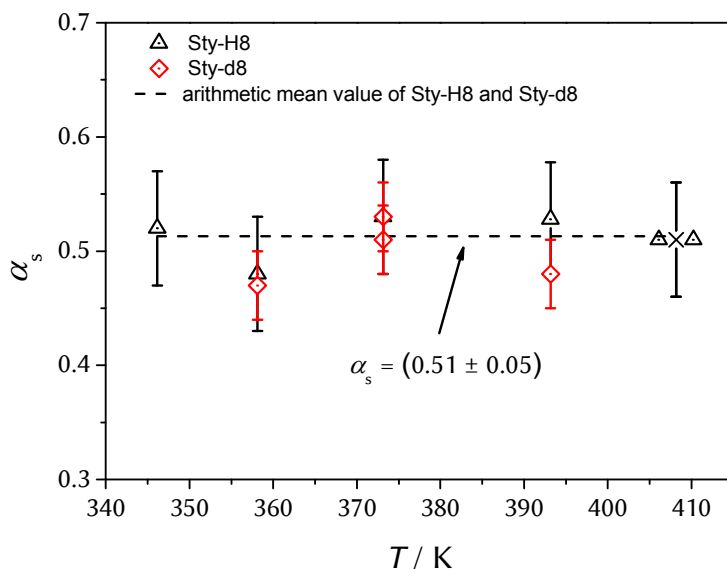


Figure 4.6: Individual values (symbols) deduced for the short-chain exponent, α_s , according to eq (2.42) for Sty-H8 and Sty-d8 at polymerization temperatures from 73 to 135 °C. The symbol X indicates that two data points are sitting exactly on top of each other.

The insensitivity of α_s toward both deuteration and temperature has also been found for MMA (between 5 °C and 50 °C) and VAc (between -65 °C and 5 °C).^{42,117} Figure 4.6 is not indicative of any need for using deuterated styrene, however, as Figure 4.3 tells, deuteration is required to reach high signal-to-noise quality at large t , which corresponds to long radical chain lengths. The α_s value for styrene is in close agreement with the number from RAFT-CLDT investigations, i.e., $\alpha_s = 0.53$,¹⁴¹ and agrees with the power-law exponent measured for the chain-length dependency of the styrene self-diffusion coefficient D^i , $\alpha^D = 0.51 \pm 0.13$.¹⁴³ The power-law exponent for short-chain styryl radicals is below the associated numbers for MMA, $\alpha_s = 0.65$,¹¹⁷ for VPi, $\alpha_s = 0.67$,⁴² and for MA, $\alpha_s = 0.80$,⁴¹ but agrees within experimental accuracy with the α_s values reported for VAc, $\alpha_s = 0.57$,⁴² and for di-(*n*-butyl) itaconate, $\alpha_s = 0.50$.¹¹⁶ This finding is consistent with literature,^{89,141} in which styrene is listed among the monomers with lowest α_s .

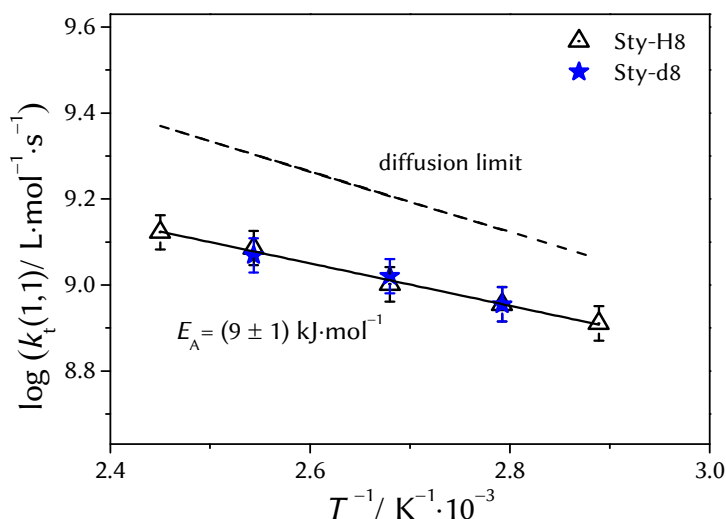


Figure 4.7: Arrhenius-type plot of the rate coefficient for termination of two monomeric radicals, $k_t(1,1)$, for Sty-H8 and Sty-d8 homopolymerizations at low degrees of monomer conversion. The dashed line represents the diffusion limit of $k_t(1,1)$ for styrene as estimated via the separately measured value of $E_A(\eta^{-1}) = 10.4 \pm 0.1 \text{ kJ} \cdot \text{mol}^{-1}$.

As described earlier, the rate coefficient for termination of two radicals both of chain length unity, $k_t(1,1)$, may be interpreted in terms of the Smoluchowski expression (eq (3.4)) assuming termination of short chains ($i < i_c$) to be dominated by center-of-mass diffusion. With the monomeric self-diffusion coefficient, D^1 , obeying the Stokes-Einstein equation (eq (2.16)) and r_1 being the hydrodynamic radius of the monomer, $k_t(1,1)$ scales with fluidity, η^{-1} , i.e., the inverse viscosity, $k_t(1,1) \propto \eta^{-1}$. The activation energy for termination of two monomeric radicals, $E_A(k_t(1,1))$, should thus be essentially given by the activation energy of fluidity, $E_A(\eta^{-1})$, as seen from eq (4.1) with R_c as the capture radius.

$$k_t(1,1) = \text{const.} \cdot \frac{1}{\eta} \cdot \frac{R_c}{r_1} \quad (4.1)$$

Molecular mobility is reduced by deuteration, as the associated increase in viscosity results in a lower diffusion coefficient. Holz *et al.*¹²⁸

showed that this dynamic isotope effect is small for molecules of relatively high molar mass, such as benzene and dimethyl formamide. From the molar mass ratio of $M(\text{Sty-H8})/M(\text{Sty-d8})$, the lowering of $k_t(1,1)$ is estimated to be below 6 %, i.e., occurs within the limits of accuracy of our $k_t(1,1)$ measurement. The results of corresponding estimates for fully deuterated and non-deuterated VAc and VPi are in line with the results from the associated SP-PLP-EPR experiments.⁴² From the experimental $k_t(1,1)(\text{Sty-d8})$ and $k_t(1,1)(\text{Sty-H8})$ values, which are in close agreement (Figure 4.7), the following Arrhenius relation is obtained:

$$\ln(k_t(1,1)(\text{Sty})/\text{L}\cdot\text{mol}^{-1}\cdot\text{s}^{-1}) = 23.7 - 1117/(T/\text{K}).$$

Depending on temperature, experimental $k_t(1,1)$ is between 20 and 50 per cent below the diffusion limited value estimated under the assumption that each encounter of two monomeric radicals results in a termination event. Mathematically, the estimation requires $R_c = 2\cdot r_1$, $P_{\text{Spin}} = 0.25$, and the Stokes-Einstein equation (eq (2.16)) to hold for D^1 . The activation energy, $E_A(k_t(1,1)) = 9 \pm 1 \text{ kJ}\cdot\text{mol}^{-1}$, is close to $E_A(\eta^{-1}) = 10.4 \pm 0.1 \text{ kJ}\cdot\text{mol}^{-1}$, which value has been determined from independent viscosity measurements on styrene containing DCP of the concentration as used in the SP-PLP-EPR experiments (see Appendices).

4.3 Relevance of Chain-Length Dependent Termination

The relevance of taking chain-length dependent termination into account may be illustrated by a comparison of the SP-PLP-EPR results with data from both chemically initiated polymerization and from SP-PLP experiments carried out in conjunction with the time-resolved measurement of monomer consumption by near-infrared spectroscopy (SP-PLP-NIR). Chain-length averaged k_t values, $\langle k_t \rangle$, from SP-PLP-NIR yield $\langle k_t \rangle(\text{Sty})/\langle k_t \rangle(\text{MMA}) = 2.0$ for 90 °C and ambient pressure for an activation volume of $14.5 \text{ cm}^3\cdot\text{mol}^{-1}$ of both monomers.^{19,144,145} In contrast, the SP-PLP-EPR measurements result in $k_t(1,1)(\text{Sty})/k_t(1,1)(\text{MMA}) = 0.7$ for the same temperature. This seeming contradiction may be resolved by considering the average chain length associated with the SP-PLP-NIR data for the two monomers, deduced from the same time interval (0.15 s) after laser pulsing.

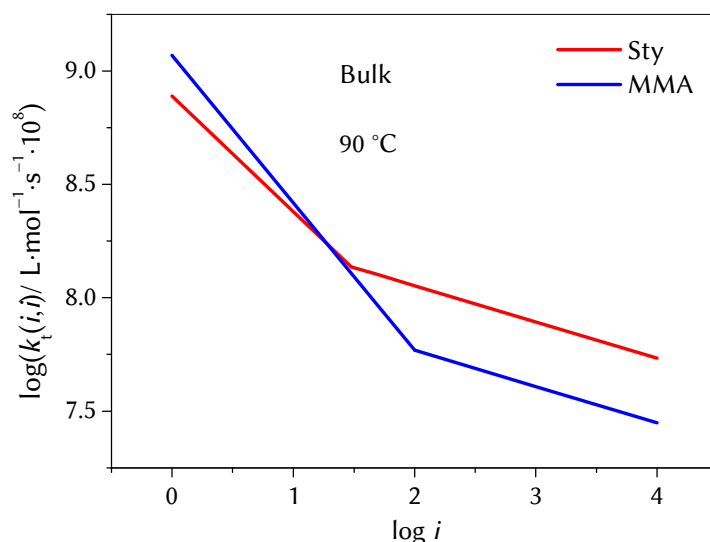


Figure 4.8: Decay of the rate coefficient for termination of two radicals at identical chain length i , $k_t(i,i)$ in styrene (Sty) and methyl methacrylate (MMA) bulk polymerization at 90 °C according to their composite-model parameters (see text). The figure serves the purpose of illustrating the seeming contradiction found for k_t ratios between MMA and Sty deduced from different types of experiments.

Within 0.15 s,^{19,144} chain growth at 90 °C occurs up to a maximum chain length of $i_{\max}(\text{Sty}) = 1092$ and of $i_{\max}(\text{MMA}) = 2120$, respectively. Based on estimated average chain lengths of $\langle i \rangle(\text{Sty}) = 500$ and $\langle i \rangle(\text{MMA}) = 1000$ and on the composite-model parameters for both monomers, with $\alpha_s = 0.65$, $i_c = 100$, $\alpha_1 = 0.16$ for MMA,^{95,117} an adjusted ratio of about $k_t(500,500)(\text{Sty})/k_t(1000,1000)(\text{MMA}) = 2.2$ is found, which number is in close agreement with the above-cited ratio of $\langle k_t \rangle(\text{Sty})/\langle k_t \rangle(\text{MMA})$ from SP-PLP-NIR experiments averaged over the same time period, i.e., of 0.15 s. The detailed analysis of termination behavior thus requires propagation rate and chain-length dependence of termination, as given by the composite-model parameters, to be properly taken into account. The higher k_p value of MMA results in larger radicals which in conjunction with higher i_c and α_s , reduce termination rate and contribute to the bulk polymerization rate of MMA being above the one of styrene under stationary conditions at 80 °C.¹²⁰ This effect on $k_t(i,i)$ is illustrated in Figure 4.8 and is also true for chemically initiated

polymerizations in which chain lengths far above i_c are expected. It appears to be a matter of principle that a direct comparison of $\langle k_t \rangle$ data for different monomers should as the consequence be restricted to monomers which are not that different in absolute k_p values and composite-model parameters.

The all invasive impact of CLDT on $\langle k_t \rangle$ from chemically initiated polymerizations might be further highlighted if the temperature dependence of $\langle k_t \rangle$, i.e., the Arrhenius activation energy $E_A(\langle k_t \rangle)$, is considered. Taylor *et al.* measured $\langle k_t^{\text{exp}} \rangle$ for chemically initiated bulk polymerization of styrene¹²⁰ under steady-state conditions, i.e., in the presence of a broad distribution of chain lengths, between 40 °C and 90 °C. Important kinetic quantities such as $\langle k_t \rangle$ and the number average degree of polymerization might be correlated with the power-law expression for chain-length dependent k_t by Mahabadi¹⁴⁶ and by Olaj and his group.^{147,148} On the basis of this early work, eq (4.2) has been proposed for deducing chain-length averaged $\langle k_t \rangle$ from chain-length dependent $k_t(i,i) = k_t^0 \cdot i^{-\alpha_1}$ with k_t^0 being defined in eq (2.29)^{89,90,120}. The equation in this form rests on the assumption that only the long-chain regime, i.e., $i > i_c$ has to be considered in chemically initiated polymerizations which might be true due to the larger i values of the terminating radicals under typical the experimental conditions.¹²⁰ The simultaneous impact of initiation, propagation and termination on chain length has been taken into account by this expression. The symbol Γ in eq (4.2) denotes the gamma function. The efficiency of initiation, f , the rate coefficient for decomposition of the thermal initiator, k_d , as well as the initiator concentration, c_i , are available from Ref.¹²⁰

$$\langle k_t^{\text{CLDT}} \rangle = k_t^0 \cdot \left[\Gamma \left(\frac{2}{2 - \alpha_1} \right) \right]^{-2} \cdot \left[\frac{\sqrt{4 \cdot f \cdot k_d \cdot c_i \cdot k_t^0}}{k_p \cdot c_M} \cdot \left(\frac{2}{2 - \alpha_1} \right) \right]^{\frac{2 - \alpha_1}{2 - \alpha_1}} \quad (4.2)$$

Figure 4.9 illustrates the remarkable agreement of $\langle k_t^{\text{CLDT}} \rangle$ with experimental $\langle k_t^{\text{exp}} \rangle$ from stationary polymerization. $\langle k_t^{\text{CLDT}} \rangle$ is only by about 18 per cent below $\langle k_t^{\text{exp}} \rangle$ in the temperature range 40 to 90 °C with the experiments covering the range up to 15 % monomer conversion. This minor discrepancy may in part be due to the calculation via eq (4.2) being entirely based on parameters for the long-chain regime, but neglect small radicals of $i < i_c$, for which $k_t(i,i)$ is higher than predicted by the specific power-law expression underlying eq (4.2). Thus $\langle k_t^{\text{CLDT}} \rangle$ may slightly underestimate $\langle k_t \rangle$.

Via PREDICI[®] simulation, the Composite Model may be used in a second approach with all four parameters: $k_t(1,1)$, α_s , i_c , and α_1 for an estimate of a Composite Model k_t average, $\langle k_t^{\text{PREDICI}} \rangle$, which turns out (Figure 4.9) to be very close to $\langle k_t^{\text{CLDT}} \rangle$. The $\langle k_t^{\text{exp}} \rangle$ is slightly above $\langle k_t^{\text{PREDICI}} \rangle$ as the impact of small radical termination is also ignored within the PREDICI[®] estimate. The PREDICI[®] procedure is specified in the Appendices section. It should be noted that the activation energy resulting from the estimate via eq (4.2), $E_A(\langle k_t^{\text{CLDT}} \rangle) = 15.3 \text{ kJ}\cdot\text{mol}^{-1}$, is significantly above $E_A(k_t(1,1))$, but is close to the experimental value: $E_A(\langle k_t^{\text{exp}} \rangle) = 14.3 \text{ kJ}\cdot\text{mol}^{-1}$. The activation energy associated with the PREDICI[®] based estimate, $E_A(\langle k_t^{\text{PREDICI}} \rangle) = 14.8 \text{ kJ}\cdot\text{mol}^{-1}$, is in very satisfying agreement with $E_A(\langle k_t^{\text{exp}} \rangle)$. The discrepancy between $E_A(\langle k_t \rangle)$ and $E_A(k_t(1,1))$ might be seen from eq (4.3) which is derived from eq (4.2) and correlates $E_A(\langle k_t \rangle)$ with $E_A(k_p)$, $E_A(k_t(1,1))$ and the activation energy of the effective initiator decay, $E_A(fk_d)$.¹²⁰ Since $E_A(fk_d)$ is usually far higher than $E_A(k_p)$, $E_A(\langle k_t \rangle)$ exceeds $E_A(k_t(1,1))$ for chemically initiated polymerizations. This relationship reflects that a faster initiator decay at higher temperature leads to higher radical concentrations and thus to shorter chains of terminating radicals being tantamount to a higher value of $\langle k_t \rangle$. Note that for $\alpha_1 = 0$, $E_A(\langle k_t \rangle)$ equals $E_A(k_t(1,1))$.¹²⁰

$$E_A(\langle k_t \rangle) = (1+a) \cdot E_A(k_t^{1,1}) + a \cdot E_A(fk_d) - 2 \cdot a \cdot E_A(k_p); \quad a = \frac{\alpha_1}{2 - \alpha_1} \quad (4.3)$$

The close agreement of $\langle k_t^{\text{CLDT}} \rangle$ and $\langle k_t^{\text{exp}} \rangle$ suggests that the data from the SP-PLP-EPR experiments and the ones from conventional steady-state polymerization are both reliable. It appears recommendable to use the $k_t(i,i)$ data from SP-PLP-EPR whenever CLDT needs to be explicitly taken into account, whereas $\langle k_t^{\text{exp}} \rangle$ provides an adequate description of conventional chain-length averaged termination kinetics. Obviously, $k_t(i,i)$ constitutes the suitable set of rate coefficients for representation of termination with reversible deactivation polymerization of styrene, where growing radicals of more or less identical size react with each other.

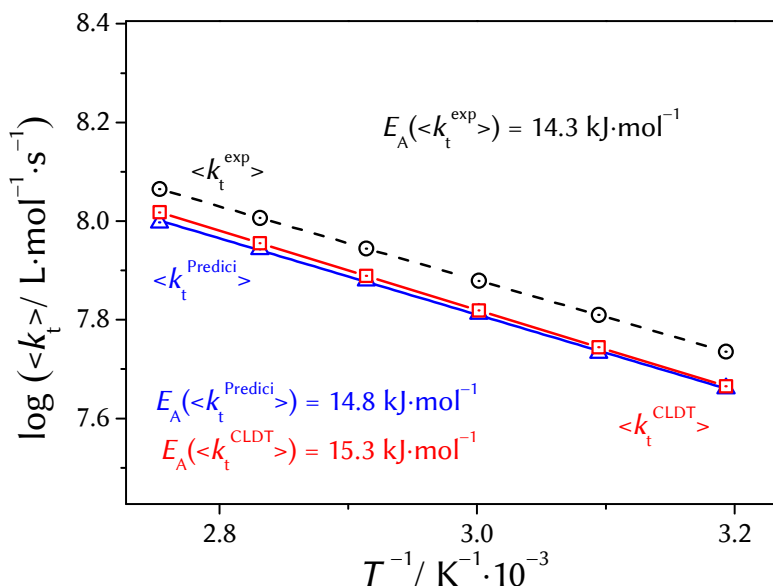


Figure 4.9: Arrhenius-type plot of experimental $\langle k_t^{\text{exp}} \rangle$ and calculated chain-length averaged $\langle k_t^{\text{CLDT}} \rangle$ for chemically initiated styrene homopolymerization at 90 °C; $\langle k_t^{\text{CLDT}} \rangle$ has been deduced from the EPR-derived composite-model parameters for long-chain radicals via eq (4.2), whereas the $\langle k_t^{\text{PREDICI}} \rangle$ data are from PREDICI simulation including the entire set of the four composite-model parameters. The experimental values, $\langle k_t^{\text{exp}} \rangle$, are from Ref.¹²⁰

4.4 Radical Structure and Reactivity in Termination Processes

In addition to describing temperature dependence of $k_t(1,1)$, eq (4.1) also allows for a systematic analysis of the structure-reactivity correlation since the absolute number of the product of $k_t(1,1)$ and η , $k_t(1,1) \cdot \eta$, depends on the ratio of R_c and r_1 (eq (4.4)).

$$k_t(1,1) \cdot \eta = \text{const} \cdot \frac{R_c}{r_1} \quad (4.4)$$

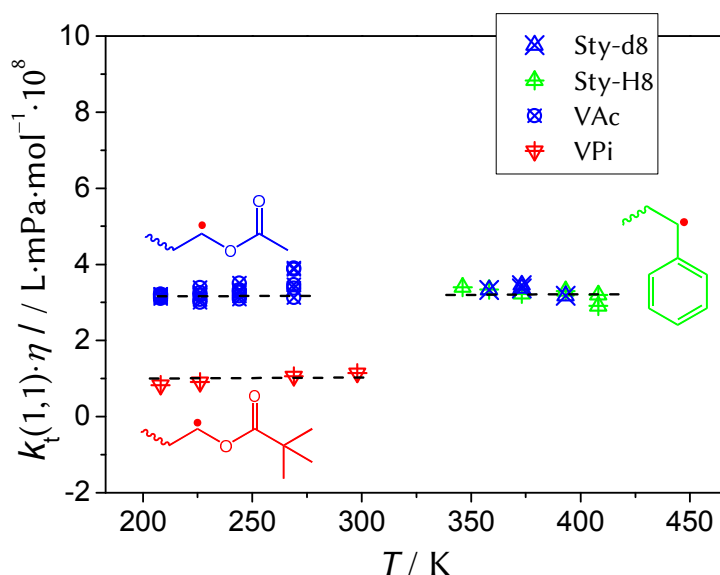


Figure 4.10: Product of $k_t(1,1)$ and η , $k_t(1,1) \cdot \eta$, according to eq (4.4) for deuterated (Sty-d8) and non-deuterated styrene (Sty-H8) as well as for vinyl acetate (VAc) and vinyl pivalate (VPi) at the experimental temperatures. The quantities refer to bulk polymerizations investigated by SP-PLP-EPR. Data for VAc and VPi were taken from Ref.⁴² The number of monomers is restricted to three due reasons of clarity but might be extended to further monomers as seen in Table 4.2. Mean values are indicated by dashed lines. The slight changes in $k_t(1,1) \cdot \eta$ as a function of temperature appear to be due to experimental uncertainty.

Analysis of $k_t(1,1)$ data in terms of eq (4.4) holds for different temperatures since $E_A(k_t(1,1)) \approx E_A(\eta)$, as is illustrated for several monomers in Figure 4.10. The values for $k_t(1,1) \cdot \eta$ are listed in Table 4.2 along with further monomers which allows for a general discussion. As is illustrated by the upper four entries in Table 4.2, almost the same value of $k_t(1,1) \cdot \eta$ is obtained for styrene, vinyl acetate and for the "first" (methyl ester) members of the acrylate and methacrylate families. The data refer to 80 °C and thus include extrapolations for some monomers, as the related SP-PLP-EPR measurements have not been carried out at that temperature. The close agreement of the four entries suggests that, with these small radicals, most of the diffusional encounters result in reaction. As the activation energies of $k_t(1,1)$ and of fluidity are close to each other, the product $k_t(1,1) \cdot \eta$ should not be sensitive toward temperature.

Table 4.2: Comparison of $k_t(1,1)\cdot\eta$ for bulk polymerizations of several monomers. The activation energies required for extrapolation to 80 °C were taken from the cited literature. The $k_t(1,1)$ values are exclusively from SP–PLP–EPR investigations. MMA = methyl methacrylate, VAc = vinyl acetate, MA = methyl acrylate, VPi = vinyl pivalate, Sty = styrene, BMA = butyl methacrylate, and DBI = dibutyl itaconate. The numbers given for DBI in italics indicate higher uncertainty.

	$k_t^{1,1}(80\text{ °C})$ / $\text{L}\cdot\text{mol}^{-1}\cdot\text{s}^{-1}\cdot 10^9$	$\eta(80\text{ °C})$ / $\text{mPa}\cdot\text{s}$	$k_t(1,1)\eta(80\text{ °C})$ / $\text{L}\cdot\text{mPa}\cdot\text{mol}^{-1}\cdot 10^8$	Ref.
1 VAc	(1.5 ± 0.3)	0.24	3.6	42
2 MMA	(1.1 ± 0.3)	0.34 ¹⁴⁹	3.7	117
3 MA	(1.2 ± 0.3)	0.31	3.7	41
4 Sty	(0.83 ± 0.05)	0.39	3.2	this work
5 VPi	(0.41 ± 0.05)	0.33	1.4	42
6 <i>tert</i> -BMA	(0.3 ± 0.1)	0.45 ^{118,150}	1.3	118
7 DBI	(0.09 ± 0.01) ^{a)}	1.32	0.12	116

^{a)}extrapolated from the reported k_t^0 value at 45 °C via $E_A(k_t^0) = 27.6\text{ kJ}\cdot\text{mol}^{-1}$ and estimated with $i_c = 100$, $\alpha_s = 0.5$, and $\alpha_l = 0.16$.

Toward larger side group of the radicals, $k_t(1,1)\cdot\eta$ should decrease due to an enhancement of both hydrodynamic radius and shielding of the radical site which appears to a reduction of the R_c/r_1 ratio. This is indeed what the entries 5 and 6 in Table 4.2 suggest. It is interesting to note that the replacement of a methyl group by a *tert*-butyl moiety, i.e., passing from vinyl acetate to vinyl pivalate (VPi) and from MMA to *tert*-butyl methacrylate (*tert*-BMA) results in almost the same decrease in $k_t(1,1)\cdot\eta$. It comes as no surprise that larger shielding as in the case of dibutyl itaconate (DBI) gives rise to an even stronger reduction of $k_t(1,1)\cdot\eta$. This can be seen from entry 7. The number for DBI rests on a rough extrapolation of reported data since the analysis introduced with styrene has not been performed with DBI so far.¹¹⁶ As will be shown in Section 6.2.3, the true number for $k_t(1,1)\cdot\eta$ is even smaller. It should be noted that similar values for $k_t(1,1)\cdot\eta$ are found for monomeric radicals in aqueous solution of acrylic acid and methacrylic acid. The scaling of $k_t(1,1)$

with viscosity can perhaps be used to estimate $k_t(1,1)$ for other temperatures and monomer contents and even for novel, unexplored systems with radicals of similar size

This finding plays a role for aqueous-solution polymerization of acrylamide in which investigations into the termination kinetics of end-chain radicals are impeded by intramolecular transfer process, i.e., backbiting.

Termination and Transfer Kinetics of Acrylamide in Aqueous Solutionⁱⁱ

Radical polymerization in aqueous solution is attractive because of the environmentally friendly and inexpensive solvent. The so-produced water-soluble polymers find widespread applications in water treatment, for paints, adhesives and cosmetics. Poly(acrylamide) has the ability of absorbing large amounts of water.^{6,8} Despite the importance, the level of kinetic knowledge about the polymerization of acrylamide (AAm) is limited. Investigations mainly focused on overall polymerization rates so far.^{151–157} Ishige and Hamielec reported a "non-classic" dependency of polymerization rate on monomer concentration in that the partial reaction order with respect to monomer concentration, ω , slightly exceeds unity and reaches values up to $\omega \leq 1.2$,¹⁵⁵ which might be indicative of side-reactions such as backbiting (see Section 2.2.1). However the number reported for AAm is significantly below the ones for acrylate

ⁱⁱ Reproduced with permission from Kattner, H.; Buback, M. *Macromolecules* **2015**, *48*, 7410–7419. Copyright 2015, American Chemical Society, and from Kattner, H.; Buback, M. *Macromol. Rapid Commun.* **2015**, *36*, 2186. Copyright 2015, Wiley-VCH.

polymerizations, $\omega \leq 1.8$,^{60–63} in which backbiting occurs. It should be noted that for vinyl acetate (VAc), where backbiting is absent,⁴² an ω value of (1.17 ± 0.05) has been found which has been assigned to the chain-length dependence of termination.¹⁵⁸ In 2005, Seabrook succeeded in the determination of chain-length averaged k_t data.¹⁵⁷ The propagation kinetics was investigated by several groups via PLP–SEC in the early 1990's.^{27,28,159} The latest data set on k_p was published in 2016 by Lacík *et al.*²⁹ However, simulations of monomer-to-polymer conversion vs time profiles for chemically initiated polymerization of AAm based on the reported values however failed.¹⁶⁰ The simulations neglected backbiting, since no indication for short-chain branching was found by NMR spectroscopy^{160,161} and no variation of k_p with laser pulse repetition rate was observed in PLP–SEC measurements as with acrylates.⁶⁹ It goes without saying that EPR provides an easy access to this field since SPRs and MCRs can be distinguished by their hyperfine coupling (hfc) pattern. No EPR spectra of AAm have been reported in literature so far due to the very challenging experimental conditions associated with the highly polar solvent water.

It is evident that, besides an impact on polymer structure (short-chain branching), the presence of MCRs strongly affects the overall polymerization kinetics.^{57–59} The prediction of backbiting for certain monomers is still challenging. In the past, even the IUPAC-recommended^{14,18,130} method for k_p^s determination, PLP–SEC, failed for acrylates at moderate temperatures due to lack of knowledge that backbiting occurs.^{132,162,163} The concept of backbiting was introduced in 1953 by Roedel⁵⁰ for ethylene polymerization and was in the beginning considered to be unimportant for acrylate-type polymerization due to the higher stability of acrylate SPRs.^{49,163} Decades passed until the importance of backbiting was widely accepted for acrylate polymerizations.⁴⁹ Until now, data for backbiting are restricted to acrylate-type monomers³⁷ including acrylic acid (AA)³⁸ and sodium acrylate (NaAA)³⁹. The argumentation in terms of radical stability for predicting backbiting is not generally valid as has been shown by the EPR investigations into the highly unstable VAc radicals.⁴² Answering the question if and to which extent backbiting occurs in radical polymerization is crucial for further kinetic investigations.

This Section deals with the first evidence for backbiting in aqueous-solution homopolymerization of a *N*-vinyl amide, i.e., AAm, for 10 wt.% and 20 wt.% monomer content relating at 25 °C to concentrations of 1.40 and 2.85 mol·L⁻¹, respectively. Because of the low signal-to-noise ratio, up to 600 individual SP–PLP–EPR traces and up to 300 individual spectra had

to be co-added for each temperature and monomer concentration to obtain a good signal quality. It is the goal of this Section to provide a comprehensive data set of termination and transfer kinetics for AAm.

In what follows, rate coefficients with the superscript "t" refer to MCRs with the radical functionality at the tertiary carbon atom while "s" denotes a radical functionality at the chain-end of SPRs.

5.1 The EPR Spectrum in AAm Polymerization

The EPR spectra were recorded with a sweep time of 5.12 s. Monomer-to-polymer conversion was kept rather low, i.e., up to 12 % at 0 °C and up to 20 % at 98 °C, to avoid conversion-related effects on the spectra.¹⁶⁴ Hence, the EPR spectra refer to the initial conversion regime of AAm homopolymerization. Monomer conversion was checked by the NIR spectra recorded immediately after applying a sequence of laser pulses. No significant changes in hfc pattern and in the fraction of radicals were observed in a small number of experiments carried out up to 80 % monomer conversion. Shown in Figure 5.1a is the 4-line EPR spectrum recorded at -5 °C which is assigned to the propagating AAm macroradical. The same type of hfc pattern for end-chain radicals was reported for acrylate and acrylate-derived chain-end radicals, e.g., for BA^{121,165,166}, ionized³⁹ (NaAA) and non-ionized³⁹ acrylic acid (AA) and vinyl acetate (VAc).^{42,122} This hfc pattern is characteristic of the coupling of the unpaired electron with one α -proton and two equivalent β -methylene protons. The hfc constants of the AAm macroradical, $a(\alpha\text{-H}) = 20.6$ G and $a(\beta\text{-H}) = 18.5$ G, are close to the ones reported for BA, AA, NaAA and VAc propagating radicals.^{38,39,42,122,165,166} In principle, the SPR spectrum should occur as a doublet of triplets, i.e., a 6-line spectrum, but is condensed to a phenotypical quartet (4-line spectrum) due to line broadening. Although SPRs are the by far dominant species, as will be shown further below, MCRs are present to about 3 % even at -5 °C.

5.1.1 Simulation of EPR Spectra in the Presence of MCRs

The occurrence of backbiting and hence the presence of MCRs becomes obvious upon increasing temperature (Figure 5.1b). The characteristic hfc pattern, which makes MCRs easily distinguishable from SPRs, arises from the difference in chemical environment of the radical functionality after the [1,5]-H-shift reaction. The unpaired electron at the tertiary carbon atom couples with two pairs of non-equivalent protons which results in a triplet of triplets (*tt*, 9-line spectrum).^{124,165-168}

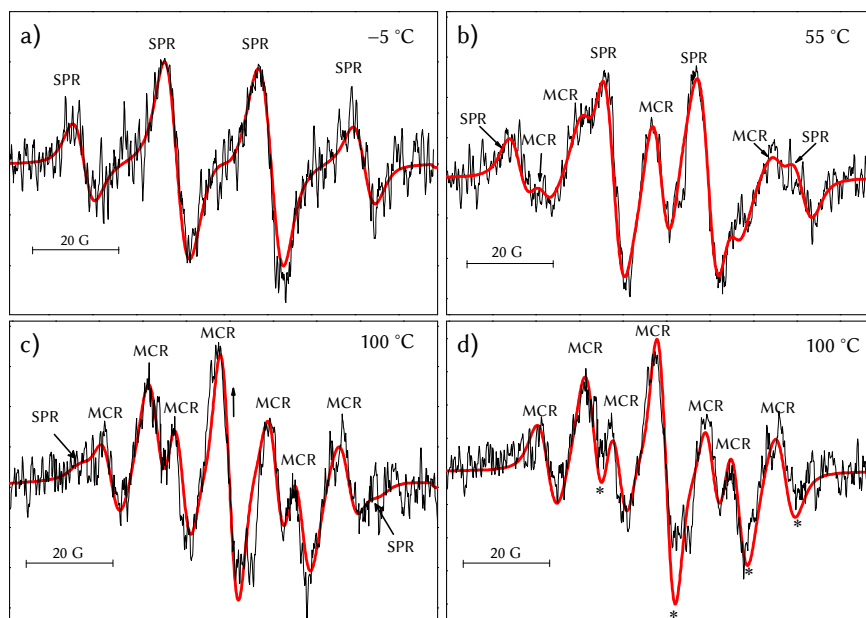


Figure 5.1: EPR spectra recorded during a homopolymerization of AAm (10 wt.% in aqueous solution) and associated fits (red) for different temperatures (a-c). Radicals were produced by stationary UV irradiation of the photoinitiator Darocur[®] ($2.2 \cdot 10^{-2} \text{ mol} \cdot \text{L}^{-1}$). Bands dominated by a specific radical species are labeled as SPR or MCR. Spectrum (d) illustrates the situation of neglecting SPR contributions in the simulation of the high-temperature EPR spectrum. EPR components showing major differences between simulated and measured bands are indicated by an asterisk (*).

Line broadening reduces the tt to a 7-line multiplet. The MCR hfc constants (see Table 5.1) derived from fitting the EPR spectra, $a(\beta - H_1) = 9.6 \text{ G}$ and $a(\beta - H_2) = 14.7 \text{ G}$, are again in close agreement with the associated literature data for acrylates.^{121,165,166} The inner peak of this multiplet is characteristic of MCRs and allows for the detection of these tertiary radicals even in minor concentrations, as is the case at low temperatures. At higher temperatures, MCRs are dominant (Figure 5.1c) and SPRs show up as weak shoulders on the outer peaks.

Table 5.1: Hyperfine coupling constants of SPRs and MCRs in AAm polymerization deduced from the experimental spectra taken in aqueous solution at the indicated temperatures.

radical	$\theta / ^\circ\text{C}$	$a(\text{H}) / \text{G}$	$a(\text{H}) / \text{G}$
SPR	-5	20.6 (1H, α -H)	18.5 (2H, β -H)
MCR	+100	9.6 (2H, β -H ₁)	14.7 (2H, β -H ₂)

Nevertheless, even for the highest experimental temperature, the intensity of the central MCR-dominated peaks could not be perfectly fitted without taking contributions from SPR bands into account (Figure 5.1d). In contrast to the EPR spectra reported for acrylates, e.g., BA^{165,167-169}, phenyl acrylate¹⁷⁰, cyclohexyl acrylate¹⁷¹, dodecyl acrylate¹⁶⁶ and ethylhexyl acrylate¹⁶⁹, no contribution from an additional 3-line MCR spectrum has to be considered for the simulation of the EPR spectra for AAm. MCR triplet components appear to be related to a conformer of reduced rotational freedom around the C _{α} -C _{β} bond, which is more likely to occur with monomers bearing sterically demanding^{121,165,167} or charged³⁹ side groups, and being contained in viscous media¹⁷¹ or at low temperature^{121,165}. The difference in the hfc constants of the two β -proton pairs in the 7-line MCR spectrum reported for BA at -40 °C, $a(\beta - \text{H}_1) = 7.0 \text{ G}$ and $a(\beta - \text{H}_2) = 20.0 \text{ G}$, is lowered toward increasing temperature and thus toward higher chain flexibility, resulting in $a(\beta - \text{H}_1) = 11.2 \text{ G}$ and $a(\beta - \text{H}_2) = 16.3 \text{ G}$ at +60 °C.¹²¹ Since the size of $a(\beta - \text{H})$ is related to the dihedral angle, Θ , between the single-occupied p-orbital and the σ -orbital of the C _{β} -H bond, according to the Heller-McConnel equation (eq (5.1)), the absence of any temperature dependence of $a(\beta - \text{H})$ with AAm macroradicals further suggests an essentially unhindered internal rotation around the C _{α} -C _{β} -H bond in the backbone.

$$a(\beta - \text{H}) = A(\text{H}) \cdot \cos^2(\Theta) \quad (5.1)$$

In eq (5.1), $A(\text{H})$ denotes a proportionality constant with the highest value of a for $\Theta = 0^\circ$. Because of the symmetry of the p-orbital, only angles between 0° and 90° are relevant.¹⁷² Assuming an ideal bond angle of 120° between the two β -methylene protons in the Newman projection of the MCR, dihedral angles of, $\Theta_{\beta_1} = 63.4^\circ$ and $\Theta_{\beta_2} = 56.6^\circ$ are obtained with $A(\text{H}) = 48.2 \text{ G}$.

5.1.2 Fraction of Mid-chain Radicals under Stationary Conditions

For fitting the overall EPR spectrum, a two-step procedure was applied. First, the hfc constants of SPRs and MCRs were deduced from the experimental spectra taken at the highest and at the lowest temperature where either MCRs or SPRs are dominant (see Table 5.1). Within the second step, the molar fraction of MCRs, x_{MCR} , according to eq (5.2), was determined for each temperature from the deconvoluted SPR and MCR spectra deduced from fitting the overall EPR spectrum via the Levenberg–Marquardt algorithm. The double integrals of the so-obtained individual components are proportional to the associated SPR and MCR concentrations, respectively, and thus yield the molar fraction of MCRs, x_{MCR} :

$$x_{\text{MCR}} = \frac{\iint I_{\text{MCR}}}{\iint I_{\text{SPR}} + \iint I_{\text{MCR}}} \quad (5.2)$$

During the fitting procedure, higher weight was imposed on the inner EPR peaks to enhance the accuracy of x_{MCR} determination. Different algorithms, i.e., the Genetic Algorithm, the Nelder-Mead Algorithm, Monte Carlo, and a slight variation of the hfc constants and of the Landé factor were applied to estimate the uncertainty of x_{MCR} , which is mainly due to noise and increases toward lower relative concentration. The numbers for x_{MCR} of AAm (circles in Figure 5.2) are accurate within $\pm 2\%$ between 25 and 75 °C and within $\pm 4\%$ toward lower and higher temperatures.

Also plotted in Figure 5.2 are reported literature data of x_{MCR} for BA polymerized in a 1.5 M solution of toluene (triangles).¹²¹ At identical temperature, the MCR content of an AAm polymerization in aqueous solution is far below the values reported for BA. At -5 °C , the concentration of MCRs is almost negligible with AAm, whereas 40 percent of the total radical concentration is MCRs in BA solution polymerization at the same temperature. The differences in x_{MCR} between AAm and BA are largest at around 20 °C and become smaller toward higher temperature where x_{MCR} of both monomers approach values above 0.8. The data in Figure 5.2 demonstrates that significant and even dominant amounts of MCRs occur even in AAm polymerization once the reaction temperature is sufficiently high.

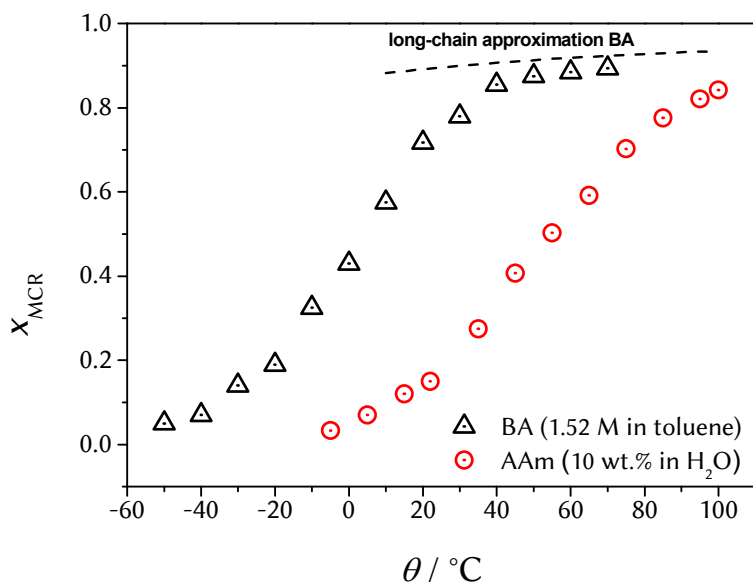


Figure 5.2: Molar fraction of mid-chain radicals, x_{MCR} , deduced from fitting the experimental EPR spectra (circles) recorded during polymerization of AAm (10 wt.%) in aqueous solution between -5 and $+100$ °C. The values of x_{MCR} are identical for 20 wt.%. For comparison, reported experimental values of x_{MCR} for BA polymerization (1.52 M in toluene)¹²¹ are included (triangles). The dashed line illustrates x_{MCR} of BA calculated assuming the long-chain approximation, i.e., eq (2.11), to be valid. The rate coefficients required for this estimate were taken from Ref.³⁷

A sigmoidal dependence of x_{MCR} on temperature is seen with both AAm and BA. At least for BA, the strong increase of x_{MCR} at intermediate temperatures is not easily understood on the basis of eq (2.11), as the activation energies of backbiting and of MCR propagation differ only by $6.4 \text{ kJ}\cdot\text{mol}^{-1}$.³⁷

$$x_{\text{MCR}} = \frac{k_{\text{bb}}}{k_{\text{bb}} + k_{\text{p}}^{\text{t}} \cdot c_{\text{M}}} \quad (2.11)$$

Eq (2.11) which assumes that MCRs react exclusively by propagation, yields the dashed line in Figure 5.2 for the temperature dependence of x_{MCR} in BA polymerization. The large discrepancy between estimated and measured x_{MCR} tells that termination plays an increasingly important role in BA polymerization toward lower temperatures. As a consequence, eq (2.11) has to be replaced by eq (2.12), which considers SPR-MCR cross-termination with the rate coefficient $\langle k_t^{\text{st}} \rangle$. The brackets indicate that $\langle k_t^{\text{st}} \rangle$ is implemented as chain-length averaged quantity.

$$x_{\text{MCR}} = \frac{k_{\text{bb}}}{k_{\text{bb}} + k_{\text{p}}^{\text{t}} \cdot c_{\text{M}} + \langle k_t^{\text{st}} \rangle \cdot c_{\text{SPR}}} \quad (2.12)$$

The essential reason behind the important role of SPR-MCR termination in BA polymerization is the low activation energy of cross-termination, $E_{\text{A}}(k_t^{\text{st}}) = 6.6 \text{ kJ}\cdot\text{mol}^{-1}$, which is much smaller than the activation energy of MCR propagation: $E_{\text{A}}(k_{\text{p}}^{\text{t}}) = 28.3 \text{ kJ}\cdot\text{mol}^{-1}$. Whereas the rates of these two reactions are close to each other at the highest experimental temperature of $100 \text{ }^{\circ}\text{C}$, SPR-MCR cross-termination rate exceeds the one of propagation from MCRs by about one order of magnitude at $0 \text{ }^{\circ}\text{C}$ as is seen from extrapolation of the individual reaction rates for SPR-MCR termination and MCR propagation for these two limiting temperatures.^{37,173}

Using the large body of kinetic information available for BA, it has been shown¹⁷³ that eq (2.12) allows for an excellent representation of the dependence of x_{MCR} on polymerization temperature for BA in toluene solution with $\langle k_t^{\text{st}} \rangle$ as the chain-length averaged k_t values for SPR-MCR cross-termination. The pronounced sigmoidal shape of x_{MCR} vs T correlation suggests that eq (2.12) needs to be applied also toward AAm polymerization in aqueous solution. It appears to be a matter of priority to carry out SP-PLP-EPR experiments for obtaining a comprehensive kinetic picture of AAm radical polymerization.

5.2 Termination and Transfer Kinetics of AAm

To improve signal-to-noise quality in SP-PLP-EPR experiments, up to 600 individual EPR signals of radical concentration vs time were co-added. Monomer-to-polymer conversion was checked by NIR spectroscopy after each series of laser pulses. The conversion was below 12% at the higher temperatures, of 75 and 95 °C, and was below 8% at -5 °C. No variation of concentration vs time profiles toward higher conversion could be observed.

Time-resolved EPR detection of SPR and MCR concentration requires separate band positions for each of the two types of radicals. It is known from the shown EPR spectra under stationary AAm polymerization conditions that the spectrum of SPRs is heavily overlapped by MCR bands. The resulting problem may be overcome by a two-step procedure. First, SP-PLP-EPR measurements were performed at around the lowest temperature where the system is still in the liquid state, i.e., at -5 °C, and almost all radicals are SPRs. An EPR spectrum recorded at -5 °C on an aqueous solution containing 10 wt.% AAm is shown on the left-hand side of Figure 5.3. Time-resolved studies at the magnetic field position indicated by the arrow allow for measuring CLD termination of SPRs. The so-obtained composite-model parameters for SPR termination were implemented into PREDICI[®] and used within a second step for the analysis of the MCR concentration vs time profiles recorded at higher polymerization temperatures, between 75 and 95 °C. The MCR concentration may be accurately determined by EPR in the presence of SPRs, as the central EPR component is exclusively due to MCRs.¹⁷⁴ This situation is illustrated on the r.h.s. of Figure 5.3 by an EPR spectrum of an aqueous solution with 10 wt.% AAm at 75 °C. The (simulated) EPR contribution of SPRs is represented by the red line. At the central magnetic field position, indicated by the arrow, SPRs do not contribute to the EPR spectrum. Time-resolved studies into MCR kinetics at temperatures below 75 °C have not been carried out, as the concentration of MCRs becomes too low to afford good S/N quality.

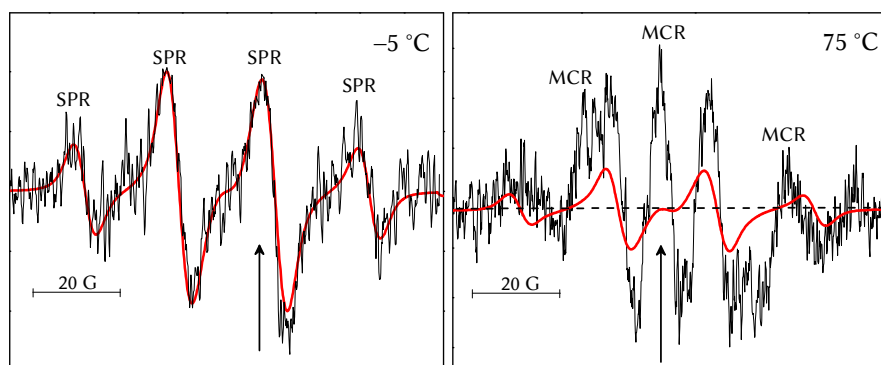


Figure 5.3: EPR spectra recorded during radical polymerizations of AAm (10 wt.%) in aqueous solution under stationary UV irradiation at -5 and 75 °C with Darocur[®] ($2.2 \cdot 10^{-2} \text{ mol}\cdot\text{L}^{-1}$) as the photoinitiator. The magnetic field positions used for SP-PLP-EPR investigations into time-resolved SPR and MCR concentrations are indicated by the arrows. The dashed line illustrates the baseline. The EPR signal for SPRs (red) has been estimated from the hyperfine coupling constants in Table 5.1 which turned out to be insensitive toward temperature.

5.2.1 Homo-termination Kinetics of End-chain Radicals

Illustrated in Figure 5.4 is the time-resolved SPR concentration after applying a laser pulse at $t = 0$ for an AAm polymerization at 10 wt.% and -5 °C. The trace results from co-addition of 600 individual SP-PLP-EPR measurements up to a monomer-to-polymer conversion of 8%. The decay of SPR concentration is due to SPR-SPR termination. The time t after laser pulsing is linearly related to the chain length i according to eq (2.41) which allows for an analysis of SPR homo-termination in the light of a CLDT. The related composite-model parameters are derived from the trace in Figure 5.3 by the same procedure as demonstrated with the styryl radicals in homopolymerization of styrene (see Section 4), i.e., by plotting of relative radical concentration as shown in Figure 5.5 and Figure 5.6. The so-obtained numbers for α_s , α_1 and i_c are listed in Table 5.2 together with $k_t^{ss}(1,1)$ for the two AAm concentrations under investigation.

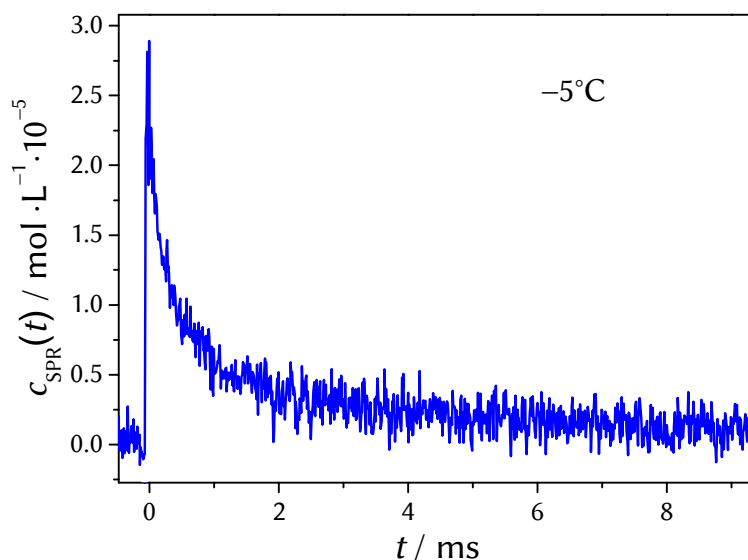


Figure 5.4: Time-resolved concentration of SPRs in AAm homopolymerization, 10 wt.% in aqueous solution, as obtained from the SP-PLP-EPR experiments at -5°C . At this relatively low temperature, SPRs are more or less exclusively present. The laser pulse was applied at $t=0$ to generate an initial SPR concentration, c_{SPR}^0 , close to $2.7 \cdot 10^{-5} \text{ mol} \cdot \text{L}^{-1}$.

Because of the structural similarities, it comes as no surprise that the values of $i_c(\text{AAm}, 10 \text{ wt.}\%) = 30 \pm 10$ and of $i_c(\text{AAm}, 20 \text{ wt.}\%) = 35 \pm 10$ are close to the associated numbers reported for methyl acrylate, $i_c(\text{MA}) = 35 \pm 10$, and vinyl acetate, $i_c(\text{VAc}) = 20 \pm 10$, bulk polymerizations.^{41,42,95} The value for styrene bulk polymerization is of similar size, $i_c(\text{Sty}) = 30 \pm 10$. The exponents $\alpha_s = 0.53 \pm 0.05$ and $a_1 = 0.15 \pm 0.03$ for 10 wt.% AAm and $\alpha_s = 0.50 \pm 0.05$ and $a_1 = 0.17 \pm 0.03$ for 20 wt.% AAm, respectively, meet the expectations from theory.^{90,94,96,98,143,175} These numbers are close to the ones reported for acrylates,⁴¹ methacrylates,^{117,118} vinyl acetate⁴² and styrene. That the composite-model parameters α_s , a_1 and i_c are insensitive toward temperature has been found for several monomers in organic^{41,42,95,100,117} as well as in aqueous solution.⁴⁴ Moreover, this finding has been successfully adopted within SP-PLP-EPR investigations into radical polymerizations of non-ionized acrylic acid.^{38,176}

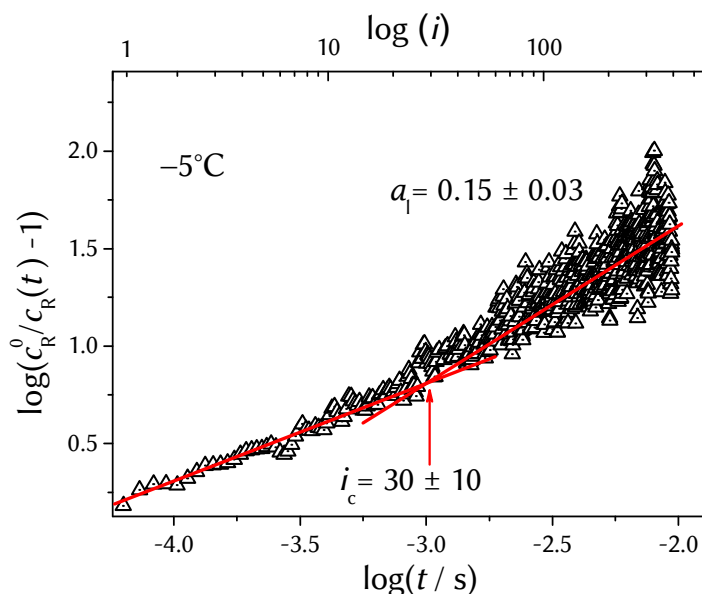


Figure 5.5: Double-log plot according to eq (2.40) for 10 wt.% AAm polymerized in aqueous solution at $-5\text{ }^{\circ}\text{C}$. This plot serves the purpose of estimating i_c and α_1 (see text) listed in Table 5.2.

Hence, α_s , α_1 and i_c of AAm were used for modeling SPR-SPR termination in AAm polymerizations at higher temperatures, where MCRs are additionally present. The fourth composite-model parameter, $k_t^{ss}(1,1)$, varies with monomer concentration (Table 5.2) and, according to the concept of diffusion-controlled termination,^{46,95,177,178} also with temperature. Changes in $k_t^{ss}(1,1)$ may be correlated via the Smoluchowski and Stokes-Einstein equations and scaled by the initial fluidity, η^{-1} , of the reaction medium, i.e., at zero conversion prior to polymerization.^{41,42,46,100,118} Upon passing from 20wt.% to 10 wt.% AAm in aqueous solution at $-5\text{ }^{\circ}\text{C}$, experimental $k_t^{ss}(1,1)$ increases by a factor of 1.4 (Table 5.2) and initial fluidity is enhanced by a factor of 1.3.

The correlation between $k_t^{ss}(1,1)$ and η^{-1} allows for predictions of $k_t^{ss}(1,1)$ at other temperatures via $E_A(\eta^{-1})$, the experimentally accessible activation energy of inverse viscosity (fluidity).^{8-10,14,16,23,24,28} The fluidities of reaction mixtures were determined between $20\text{ }^{\circ}\text{C}$ and $60\text{ }^{\circ}\text{C}$ for aqueous solutions containing 10 wt.% and 20 wt.% AAm (see Appendices).

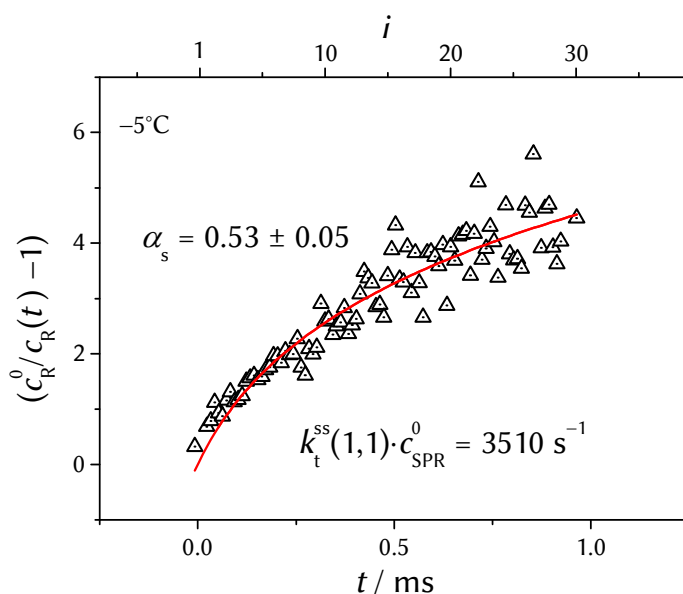


Figure 5.6: Plot of time-resolved SPR data at $-5\text{ }^{\circ}\text{C}$ for 10 wt.% AAm in aqueous solution in order to derive α_s and $k_t^{ss}(1,1)$ according to eq (2.42). The fitting parameters were α_s as well as the product of $k_t^{ss}(1,1)$ and the initial SPR concentration, c_{SPR}^0 , which is known via the calibration procedure (see Figure 5.4).

Table 5.2: Composite-model parameters derived from SP-PLP-EPR measurements at $-5\text{ }^{\circ}\text{C}$ for 10 and 20 wt.% AAm in aqueous solution.

	AAm (10 wt.%/H ₂ O)	AAm (20 wt.%/H ₂ O)
α_s	0.53 ± 0.05	0.50 ± 0.05
α_1	0.15 ± 0.03	0.17 ± 0.03
i_c	30 ± 10	35 ± 10
$k_t^{ss}(1,1)/10^7\text{ L}\cdot\text{mol}^{-1}\cdot\text{s}^{-1}$	13.0 ± 0.8	9.8 ± 0.5

The measured viscosities yield: $E_A(\eta^{-1}) = (17.8 \pm 0.1) \text{ kJ}\cdot\text{mol}^{-1}$ for 10 wt.% AAm as well as $E_A(\eta^{-1}) = (19.0 \pm 0.1) \text{ kJ}\cdot\text{mol}^{-1}$ for 20 wt.% AAm. The accuracy of the viscosity measurements is far higher than the one of $k_t^{ss}(1,1)$ determination. On the basis of absolute $k_t^{ss}(1,1)$ from SP-PLP-EPR experiments at -5°C , the following Arrhenius expressions result from identifying $E_A(\eta^{-1})$ with $E_A(k_t^{ss}(1,1))$.

$$k_t^{ss}(1,1) / (\text{L}\cdot\text{mol}^{-1}\cdot\text{s}^{-1}) = 3.9\cdot 10^{11} \cdot \exp(-2138/T(\text{K}))$$

for 10 wt.% AAm in aqueous solution

$$k_t^{ss}(1,1) / (\text{L}\cdot\text{mol}^{-1}\cdot\text{s}^{-1}) = 5.0\cdot 10^{11} \cdot \exp(-2289/T(\text{K}))$$

for 20 wt.% AAm in aqueous solution

Table 5.3: Comparison of $k_t(1,1)\cdot\eta$ for bulk polymerizations of several monomers. Table 4.2 was extended by AAm but restricted to the third column with $k_t(1,1)(80^\circ\text{C})\cdot\eta(80^\circ\text{C})$ due to reasons of clarity. The activation energies required for extrapolation to 80°C were taken from the cited literature. MMA = methyl methacrylate, VAc = vinyl acetate, MA = methyl acrylate, VPi = vinyl pivalate, Sty = styrene, BMA = butyl methacrylate, and DBI = dibutyl itaconate. Unless otherwise state, values refer to bulk polymerization. For more details, see Table 4.2.

	Monomer System	$k_t(1,1)(80^\circ\text{C})\cdot\eta(80^\circ\text{C})$ / $\text{L}\cdot\text{mPa}\cdot\text{mol}^{-1}\cdot 10^8$	Ref.
1	AAm (10 wt.%/H ₂ O)	3.3	this work
2	AAm (20 wt.%/H ₂ O)	3.2	this work
4	Sty	3.2	this work
5	VAc	3.6	42
6	MMA	3.7	117
7	MA	3.7	41
8	VPi	1.4	42
9	<i>tert</i> -BMA	1.3	118
10	DBI	0.12	116

According to these expressions, $k_t^{ss}(1,1)$ for 10 wt.% AAm is by 15% and $k_t^{ss}(1,1)$ for 20 wt.% AAm is by 21% below the so-called diffusion limiting values which refer to the maximum termination rate coefficient according to the Smoluchowski model.^{46,100} The analysis of $k_t(1,1)$ in terms of the Smoluchowski and Stokes-Einstein equations as introduced in Section 4 allows for an extension of Table 4.2 (see Table 5.3). The comparison shows that AAm fits perfectly into the line of monomers bearing the "smallest" side groups within the homologous series of small radicals. The finding underlines the diffusion control character of termination in AAm homopolymerization.

5.2.2 Transfer and Cross-termination Kinetics

The midchain radical kinetics was studied by SP-PLP-EPR between 75 and 95 °C, where MCRs are the dominant radical species. The measured MCR concentration vs time profiles were fitted by PREDICI[®] on the basis of the reaction steps listed in Figure 5.7.

Figure 5.7: Reaction steps implemented into the PREDICI[®] model for fitting MCR concentration vs time profiles deduced from SP-PLP-EPR experiments between 75 and 95 °C. The composite-model parameters for SPR homo-termination, α_s , α_i , and i_c , were adopted for cross-termination from the low-temperature experiments described above.

Reaction Step	Reaction	Ref.
laser induced initiation	$I_2 \xrightarrow{h\nu} 2I^\bullet$	see text
	$I^\bullet + \text{monomer} \xrightarrow{k_i} \text{SPR}$	
SPR propagation	$\text{SPR}_n + \text{monomer} \xrightarrow{k_p^s} \text{SPR}_{n+1}$	Lacík <i>et al.</i> ²⁹
SPR-SPR homo-termination	$\text{SPR} + \text{SPR} \xrightarrow[\alpha_s, \alpha_i, i_c]{k_t^{ss}(1,1)} \text{dead}$	this work
backbiting	$\text{SPR} \xrightarrow{k_{bb}} \text{MCR}$	this work
MCR propagation	$\text{MCR} + \text{monomer} \xrightarrow{k_p^t} \text{SPR}$	this work
SPR-MCR (cross-) termination	$\text{SPR} + \text{MCR} \xrightarrow[\alpha_s, \alpha_i, i_c]{k_t^{st}(1,1)} \text{dead}$	this work

The laser-induced decomposition of Darocur[®] was assumed to be much faster than a single SPR propagation step.⁴⁷ The rate coefficient for addition of a monomer molecule to the photoinitiator-derived primary radical, k_i , was estimated from $k_i = 10^4 \cdot k_p^s$, to ensure rapid initiation and to exclude an impact of initiation on the monomer concentration vs t profile.^{47,179,180} The propagation rate coefficient, k_p^s , including its dependence on AAm concentration in aqueous solution, was taken from literature.²⁹ SPR termination was estimated via the composite-model parameters deduced from the experiments at -5°C with only $k_t^{ss}(1,1)$ being adjusted, by the correlation through fluidity, to the actual polymerization temperature. Backbiting was treated as independent of chain length with the restriction of at least three monomer units being required for MCR formation by a [1,5]-H-shift reaction. Even at high temperatures, no indication for β -scission was found. MCR propagation kinetics was assumed to exhibit the same dependency on monomer concentration as k_p^s , but to differ in absolute value. The associated rate coefficient, k_p^t , was expressed by $k_p^t = a \cdot k_p^s$, with a being a fit parameter for each temperature. As reported by Fröhlich *et al.*, the composite-model parameters may differ for SPRs and MCRs.⁹⁹ PREDICI[®] simulations using different values for α_s , α_1 and i_c of MCRs, however, showed no significant impact on the fitting result. Thus the MCR-SPR cross-termination rate coefficient, k_t^{st} , was implemented by $k_t^{st}(1,1) = b \cdot k_t^{ss}(1,1)$ with the chain-length dependence being entirely contained in $k_t^{ss}(1,1)$. Note that $k_t^{st}(1,1)$ and $k_t^{tt}(1,1)$, the MCR homo-termination rate coefficient, are hypothetical quantities introduced for applying the Composite Model. PREDICI[®] simulations revealed that even extensive variation of the $k_t^{tt}(1,1)$ has only a negligible impact on the MCR concentration vs time traces within the range of polymerization conditions under investigation (see Appendices). The situation is different for chemically initiated polymerizations at temperatures at which the molar fraction of MCRs is very high. A similar conclusion had been reached for AA homopolymerizations.³⁸ Hence, the experimental MCR concentration vs time traces were fitted only for the rate coefficients k_{bb} , k_p^t , and $k_t^{st}(1,1)$. Within a first step, the measured maximum MCR concentration after applying the laser pulse, $c_{\text{MCR}}^{\text{max}}$, was fitted for k_{bb} . Within the second step, a , i.e., k_p^t , and b , i.e., k_t^{st} , were fitted to the measured decay in MCR concentration after passing the maximum MCR concentration. Finally, all three rate coefficients were simultaneously fitted. Note that a "typical" MCR concentration vs time profile exhibits specific regions which are sensitive toward one out of the rate coefficients mentioned above.

Sensitivity of MCR Concentration vs Time Profiles toward Transfer- and Termination Kinetics

It goes without saying that MCR formation by backbiting, and degradation by MCR propagation and cross-termination, can easily be separated by fitting the experimental MCR concentration vs time profiles. It comes as no surprise that the rate of backbiting, i.e., $dc_{\text{MCR}}/dt = k_{\text{bb}} \cdot c_{\text{SPR}}$, determines $c_{\text{MCR}}^{\text{max}}$, i.e., the maximum MCR concentration after applying the laser pulse. Since $k_{\text{t}}^{\text{ss}}(1,1)$ and thus c_{SPR} are usually known from prior experiments, i.e., for AAm and BA, k_{bb} is easily accessible by fitting $c_{\text{MCR}}^{\text{max}}$.

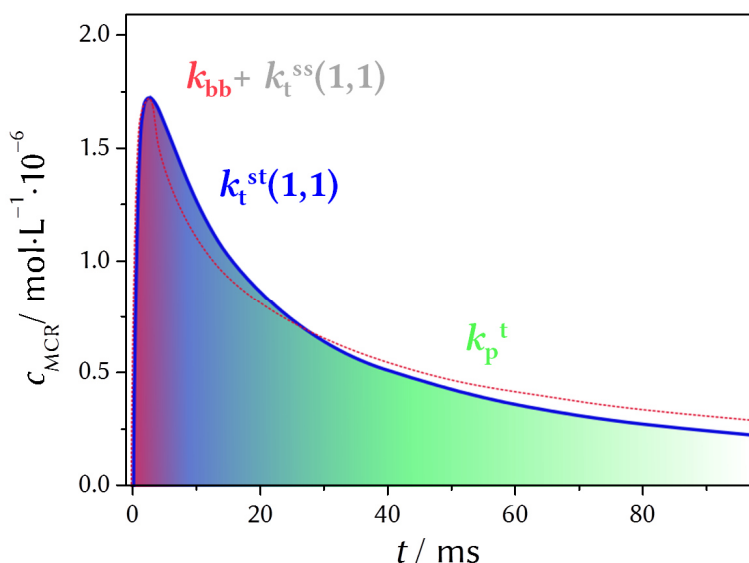


Figure 5.8: The simulated MCR concentration vs time profile for AAm polymerization (10 wt.% / H₂O) at 95 °C (blue line) is identical to the one shown in Figure 5.9. The figure serves the purpose of illustrating the sensitivity of MCR concentration vs time profiles toward backbiting, MCR propagation and SPR-MCR cross-termination. The corresponding rate coefficients, i.e., k_{bb} , k_{p}^{t} and $k_{\text{t}}^{\text{st}}(1,1)$, are depicted. $k_{\text{t}}^{\text{ss}}(1,1)$ might be known from prior investigations. The regions dominated by one out of these three steps are colored. The dashed red line represents the fitting upon increasing $k_{\text{t}}^{\text{st}}(1,1)$ and k_{bb} but constant k_{p}^{t} such that the MCR maximum is correctly reproduced. The resulting fit is of poorer quality.

The decay of MCR concentration, on the other side, is given by the competition between MCR propagation and SPR-MCR cross-termination. The latter one is more pronounced at high radical concentrations while k_p^t usually becomes apparent at higher delay times at which MCR-SPR cross-termination may be neglected due to the low SPR concentration. Thus, SP-PLP-EPR allows for distinction between these processes and hence for a precise determination of k_p^t and $k_t^{st(1,1)}$ as illustrated exemplarily for AAm (10 wt.% / H₂O) at 95 °C in Figure 5.8. It is obvious that the formation and degradation of MCRs occur simultaneously during the whole reaction time. The colored regions in Figure 5.8 are related to the ones in which one process might be dominant. The simultaneousness of MCR formation and degradation results in a slight interdependency of the determined rate coefficients induced by the fitting procedure, e.g., a higher value for $k_t^{st(1,1)}$ would lead to a higher number of k_{bb} in order to compensate the faster degradation process. However, a higher $k_t^{st(1,1)}$ would also change the shape of the MCR concentration vs time profile yielding a poorer fit of the experimental profile as demonstrated by the dashed red line in Figure 5.8. In case of both SPR and MCR concentration vs time profiles can be measured, the uncertainty in the rate coefficients may be further reduced.

Results from PREDICI® fitting

Shown in Figure 5.9 are time-resolved MCR concentrations measured after applying a laser pulse at 75 and 95 °C. The two profiles differ in c_{MCR}^{max} , and in the time required for reaching this maximum. That MCRs are not produced instantaneously, but by a consecutive reaction, as visualized by adding the simulated SPR concentration profile to the measured and fitted MCR traces for 95 °C (Figure 5.10). Shown in Figure 5.11 are the Arrhenius plots of k_{bb} for temperatures between 75 and 95 °C at both AAm concentrations, 10 and 20 wt.%. The uncertainty of the k_{bb} data has been estimated by varying, during PREDICI fitting, the pulse-induced primary radical concentration within the reasonable range of ± 20 percent in order to taking the noise into account.

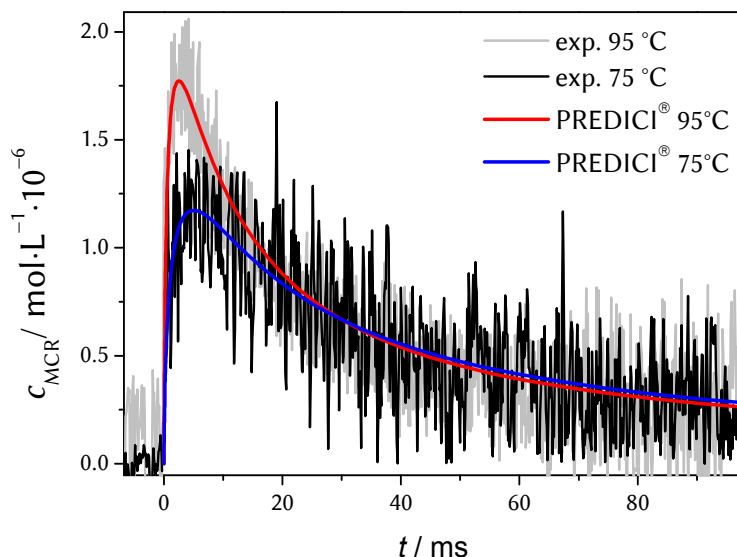


Figure 5.9: Measured and simulated MCR concentration vs time profiles after applying a laser pulse at $t = 0$ during an AAm polymerizations (10 wt.%) in aqueous solution at 75 and 95 °C. Included into the figure are the associated PREDICI® fits.

The individual Arrhenius-line in Figure 5.11 fits for each concentration are represented by the dashed lines corresponding to activation energies and pre-exponentials of: $E_A(k_{bb}, 10 \text{ wt.}\%) = (48.8 \pm 0.7) \text{ kJ}\cdot\text{mol}^{-1}$ with $A(k_{bb}, 10 \text{ wt.}\%) = (3.4 \pm 0.6) \cdot 10^9 \text{ s}^{-1}$ for the lower as well as $E_A(k_{bb}, 20 \text{ wt.}\%) = (49.6 \pm 0.8) \text{ kJ}\cdot\text{mol}^{-1}$ along with $A(k_{bb}, 20 \text{ wt.}\%) = (3.9 \pm 0.8) \cdot 10^9 \cdot \text{s}^{-1}$ for the highest AAm content, respectively. As both Arrhenius parameters agree within the limits of experimental accuracy, k_{bb} was treated as being independent of AAm concentration in the 10 wt.% to 20 wt.% AAm range and adequately represented by:

$$k_{bb} / \text{s}^{-1} = 3.7 \cdot 10^9 \cdot \exp(-5893/T(\text{K}))$$

(red line (Figure 5.11) for 10 to 20 wt.% AAm)

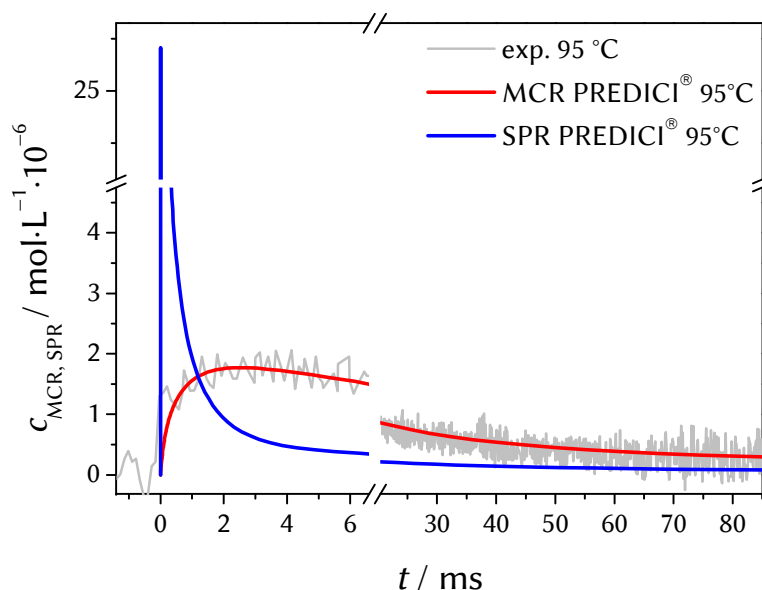


Figure 5.10: Simulated SPR concentration vs t profile together with the experimental and fitted MCR profile for 10 wt.% AAm in aqueous solution at 95 °C. The simulation of SPR concentration is based on both the composite-model parameters determined at -5 °C and the rate coefficients from PREDICI® fitting of the MCR trace (see text). The MCR trace is identical to the one for 95 °C in Figure 5.9.

AAm exhibits a remarkably high activation energy of backbiting as compared to non-ionized AA, NaAA and to BA (1.5M in toluene), but a higher pre-exponential which however only partially compensates the impact of the higher activation energy ending up in a lower absolute $k_{bb}(\text{AAm})$ (see Table 5.4). As can be seen from k_{bb} for the reference temperature of 50 °C, absolute k_{bb} is by about one order of magnitude below the associated values for AA in dilute aqueous solution and for butyl acrylate (BA) in toluene solution and is lower than k_{bb} in fully ionized AA (NaAA) polymerization. This low k_{bb} is responsible for the relatively small fraction of MCRs observed in stationary EPR experiments into AAm as compared to BA and AA polymerization. The reason behind the different Arrhenius parameters is not yet fully understood. The higher pre-exponential for AAm is entropic in origin and might result from the weaker restriction to intramolecular mobility in AAm (see Simulation of EPR Spectra in the Presence of MCRs, p. 67).

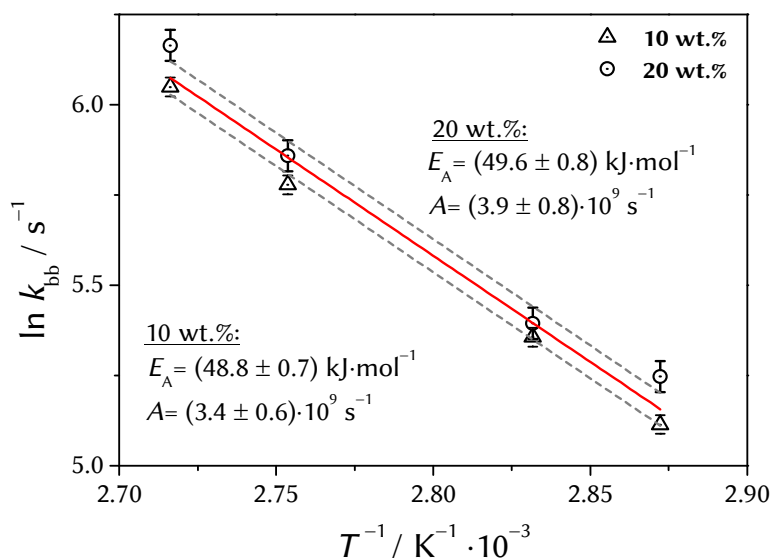


Figure 5.11: Arrhenius plot of the backbiting rate coefficient, k_{bb} , for 10 and 20 wt.% AAm between 75 and 95 °C. The rate coefficients were determined by PREDICI[®] fitting of c_{MCR} vs t traces. The individual linear regressions for the two AAm concentrations are indicated by the dashed lines. The red line represents the joined fit.

Table 5.4: Comparison of the rate coefficients for backbiting of various monomers in aqueous or in organic solution.

k_{bb}	$E_A(k_{bb})/$ $\text{kJ}\cdot\text{mol}^{-1}$	$A(k_{bb})/ 10^8$ s^{-1}	$k_{bb}(50\text{ }^\circ\text{C})$ $/ \text{s}^{-1}$	Ref.
AAm (10 wt.%, 20 wt.% / H₂O)	(49 ± 2)	(37 ± 7)	44	this work
AA (20 wt.% / H₂O)	(38 ± 3)	(10 ± 2)	705 ^{a)}	176
NaAA (20 wt.% / H₂O)	(26 ± 2)	(0.22 ± 0.09)	160	39
BA (1.5 M / toluene)	(35 ± 2)	(0.48 ± 0.07)	393	37

a) determined by ¹³C-NMR technique. Italicized numbers indicate a higher uncertainty.

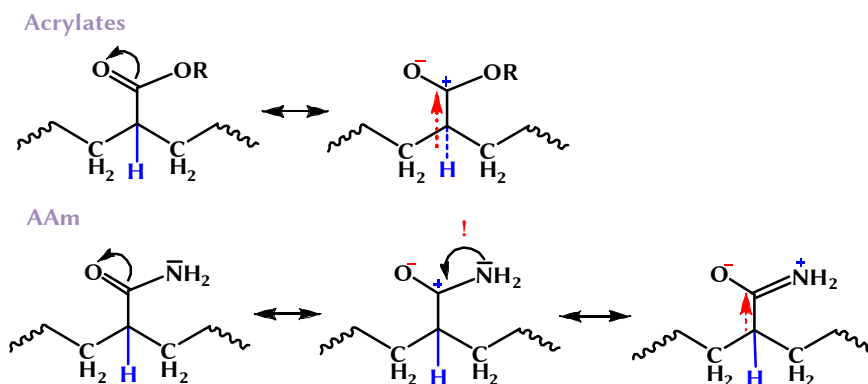


Figure 5.12: Resonance structures of acrylates and AAm at mid-chain position which may be relevant for the backbiting reaction. The dashed arrows indicate the inductive effects of side-group moieties which are less pronounced for AAm than with acrylates.

As mentioned earlier, the MCR spectra of AAm could *only* be fitted by neglecting contributions from a triplet species related to a hindered conformer which supports the assumption of a weaker entropy penalty accompanying the formation of the cyclic transition state (TS) structure for backbiting yielding a higher $A(k_{bb})$ than with acrylates.

The situation is more complex for the enthalpy-driven $E_A(k_{bb})$. Beside the ring-strain of the six-membered structure and interactions with the solvent also electronic effects on the TS may occur. Amides differ from acrylates in terms of internal stabilization effects within their side-groups (Figure 5.12).

The higher internal resonance stabilization within the nitrogen-containing amide moiety leads to a higher electron density of the C_{α} -H bond in AAm than in the acrylates which goes along with a higher bond dissociation energy and hence a higher activation energy of C_{α} -H bond scission. This argument may also hold for the "non-activated" vinyl acetate (VAc) radical for which the effect of higher bond dissociation energy, suppressing backbiting, should be even stronger. Indeed, no MCRs could be detected in VAc bulk polymerization by EPR investigation in a broad temperature range,⁴² although the VAc radicals exhibit a remarkably high chain flexibility which should facilitate the formation of six-membered ring structures.¹⁸¹

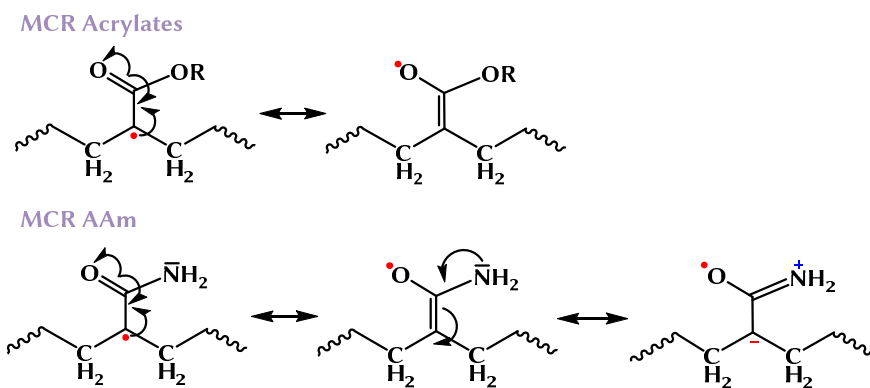


Figure 5.13: Resonance MCR structures of acrylates and AAm.

In addition to the different $E_A(k_{bb})$ values, the resonance structures of MCRs for acrylates and AAm may explain the differences in $A(k_{bb})$. As illustrated in Figure 5.13, the associated MCR structures exhibit some double-bond character which is more pronounced with the acrylate radical. Assuming that the resonance structures in Figure 5.13 permit conclusions about the TS structures, the stronger double-bond character with acrylate MCRs reduces the intramolecular mobility in the TS and thus lowers the corresponding entropy-driven $A(k_{bb})$ of acrylates. The effect may also account for the higher internal friction observed in the MCR EPR spectrum of BA as compared to AAm.¹²¹

Extrapolation of the Arrhenius expression to $-5\text{ }^\circ\text{C}$ results in $k_{bb} = 1.0\text{ s}^{-1}$, which corresponds to a half-life, $\ln 2/k_{bb}$, for SPRs of 0.7 s. This time interval is far above the half-life given by the rapid termination of SPRs (see Figure 5.4). This estimate provides further support for ignoring contributions of MCRs at this low temperature and for analyzing the experimental radical decay entirely in terms of SPR termination.

The second parameter deduced from fitting the SP-PLP-EPR experiments is the rate coefficient of MCR propagation, k_p^t . As can be seen from Figure 5.14, no clear effect of monomer concentration was detected. For several water-soluble monomers an increase of k_p^s toward higher dilution has been reported.^{22,24-26,33,182,183} This effect, which appears to be characteristic of an aqueous environment, is understood in terms of transition-state theory (TST) as being entropy-driven with water as the solvent providing less friction to internal rotational motions of the TS structure than provided by the highly dipolar environment in bulk polymerization.^{73,183,184}

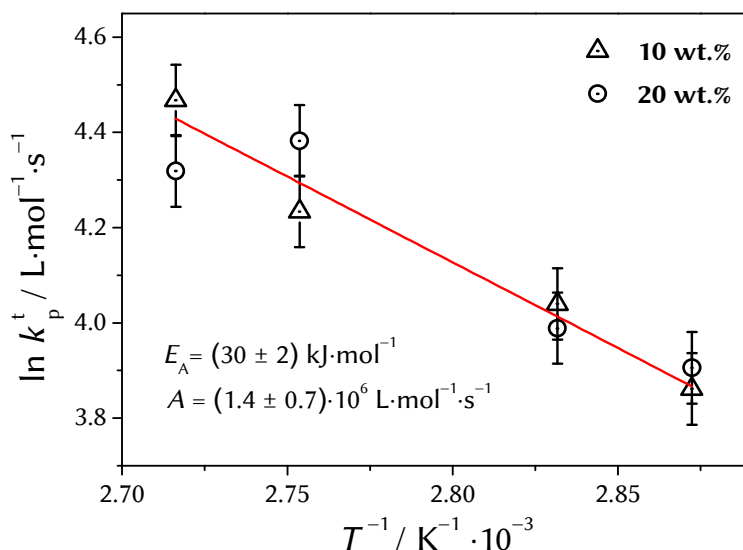


Figure 5.14: Arrhenius plot of the rate coefficients of MCR propagation, k_p^t , for 10 and 20 wt.% AAm in aqueous solution between 75 and 95 °C. The full red line represents the joint fit for both concentrations. The rate coefficients were determined by PREDICI[®] fitting of the c_{MCR} vs t traces from SP-PLP-EPR experiments.

With methacrylic acid (MAA), k_p^s at 25 °C increases by one order of magnitude from bulk to high dilution in an aqueous environment and by 50 % from 20 wt.% to 10 wt.% MAA.^{24,26,183} The effect is similar to *N*-vinylpyrrolidone,^{182,183} but less pronounced for other monomers, e.g., *N*-vinyl formamide.^{33,182} For methacrylamide, an increase in k_p^s by 32 percent has been observed in passing from 20 wt.% to 10 wt.% monomer content in aqueous solution.³¹ Since SPR and MCR propagation are subject to the same effects of molecular environment, k_p^t may reflect the same dependence on monomer concentration as does k_p^s . Lacík *et al.*²⁹ observed a weak dependence of k_p^s (AAm): At 75 °C, k_p^s for 10 wt.% AAm is by 8 % above k_p^s for 20 wt.%, which is within the limits of experimental accuracy.

Table 5.5: Comparison of the rate coefficients for MCR propagation, k_p^t , at 50 °C and of Arrhenius parameters for various monomers in aqueous and in organic phase.

k_p^t	$E_A(k_p^t)/$ $\text{kJ}\cdot\text{mol}^{-1}$	$A(k_p^t)/ 10^6\cdot\text{s}^{-1}$	$k_p^t(50\text{ }^\circ\text{C})/$ $\text{L}\cdot\text{mol}^{-1}\cdot\text{s}^{-1}$	Ref.
AAm (10 wt.%, 20 wt.% / H₂O)	(30 ± 2)	(1.4 ± 0.2)	20	this work
AA (20 wt.% / H₂O)	(33 ± 3)	(14 ± 4)	56	176
NaAA (20 wt.% / H₂O)	(23 ± 3)	(0.06 ± 0.01)	14	39
BA (1.5 M / toluene)	(28 ± 2)	(0.9 ± 0.2)	25	37

Italicized numbers indicate a higher uncertainty.

Thus, a single Arrhenius expression has been fitted to the k_p^t data for 10 and 20 wt.% AAm in aqueous solution:

$$k_p^t / (\text{L}\cdot\text{mol}^{-1}\cdot\text{s}^{-1}) = 1.4\cdot 10^6 \cdot \exp(-3608/T(\text{K}))$$

for 10 and 20 wt.% AAm

Table 5.5 shows that k_p^t of AAm polymerization is much closer to the associated numbers for AA and BA than are the backbiting rate coefficients of these monomers. The k_p^t/k_p^s ratio for AAm, e.g., at 50 °C is $3.5\cdot 10^{-4}$, which is not too dissimilar from BA in 1.5 M in toluene, $k_p^t/k_p^s = 9.1\cdot 10^{-4}$.^{19,22,29} The higher $A(k_p^t)$ for AAm compared to BA may reflect the higher internal mobility of AAm in the TS structure for propagation.²⁹ The finding is in line with the higher $A(k_p^s)$ found for AAm compared to $A(k_p^s)$ of BA and other acrylates.^{19,29,131} A mean ratio for 10 wt.% and 20 wt.% AAm of $A(k_p^t)/A(k_p^s) = 0.02$ is slightly smaller than the corresponding number for BA, i.e., $A(k_p^t)/A(k_p^s) = 0.05$, indicating that the relative reduction of internal mobility in the TS between SPRs and MCRs is higher for more flexible radicals. The kinetic data for AA in aqueous solution are of incomparable quality and thus are not compared to the rate coefficients for the other systems but are listed due to reasons of completeness. A comparison with NaAA suffers from the lack of reliable k_p^s data for this monomer.

In contrast to k_p^t and k_{bb} , AAm concentration has a clear effect on the rate coefficient of cross-termination, $k_t^{st}(1,1)$, as shown in Table 5.6. The activation energy, $E_A(k_t^{st}(1,1))$, obtained by fitting the experimental $k_t^{st}(1,1)$ data is slightly higher for 20 wt.% AAm than for 10 wt.%, which is in agreement with the trend of the measured viscosities, i.e.,

$E_A(\eta^{-1}) = 19.0 \pm 0.1 \text{ kJ}\cdot\text{mol}^{-1}$ and $E_A(\eta^{-1}) = 17.8 \pm 0.1 \text{ kJ}\cdot\text{mol}^{-1}$ for 20 wt.% and 10 wt.%, respectively. The mean ratio of $k_t^{\text{st}}(1,1)$ for the two AAm concentrations in the range of 75 to 95 °C is almost identical to the ratio of the associated fluidities,

$$\frac{k_t^{\text{st}}(1,1)(10 \text{ wt.}\%) }{k_t^{\text{st}}(1,1)(20 \text{ wt.}\%) } \approx \frac{\eta^{-1}(10 \text{ wt.}\%) }{\eta^{-1}(20 \text{ wt.}\%) } \approx 1.3 - 1.4 ,$$

which underlines the diffusion-controlled character of cross-termination in AAm homopolymerization and the applicability of the combined Smoluchowski and Stokes-Einstein modelling (eq (2.31)) for small radicals. The Arrhenius expressions associated with the lines for $k_t^{\text{st}}(1,1)$ in Figure 5.15 read:

$$\begin{aligned} k_t^{\text{st}}(1,1) / (\text{L}\cdot\text{mol}^{-1}\cdot\text{s}^{-1}) &= 1.2\cdot 10^{11} \cdot \exp(-2237/T(\text{K})) && \text{for 10 wt.\% AAm} \\ k_t^{\text{st}}(1,1) / (\text{L}\cdot\text{mol}^{-1}\cdot\text{s}^{-1}) &= 2.1\cdot 10^{11} \cdot \exp(-2550/T(\text{K})) && \text{for 20 wt.\% AAm} \end{aligned}$$

The Arrhenius parameters collected in Table 5.6 indicate that $k_t^{\text{st}}(1,1)$ and $k_t^{\text{ss}}(1,1)$ differ such that the activation energy for $k_t^{\text{st}}(1,1)$ is slightly higher than for $k_t^{\text{ss}}(1,1)$, whereas the pre-exponentials show the opposite trend. To summarize these results on the termination kinetics: The $k_t^{\text{st}}(1,1)$ data were obtained by PREDICI[®] fitting of the measured MCR concentration vs time traces with $k_t^{\text{ss}}(1,1)$ for 10 and 20 wt.% AAm as measured at -5 °C being introduced as an input parameter (extrapolated to the actual polymerization temperature via $E_A(\eta^{-1})$). Each MCR concentration vs t trace yields $k_t^{\text{st}}(1,1)$ for the specific temperature and AAm concentration. Within the temperature and concentration range under investigation, the ratio of SPR-MCR cross-termination to SPR homo-termination rate coefficients is found to be in the narrow range: $k_t^{\text{st}}(1,1)/k_t^{\text{ss}}(1,1) = 0.25 \pm 0.05$, which appears to be an important and useful result. This difference by a factor of about four is assigned to enhanced shielding of the radical functionality in case of termination with a tertiary radical being involved.

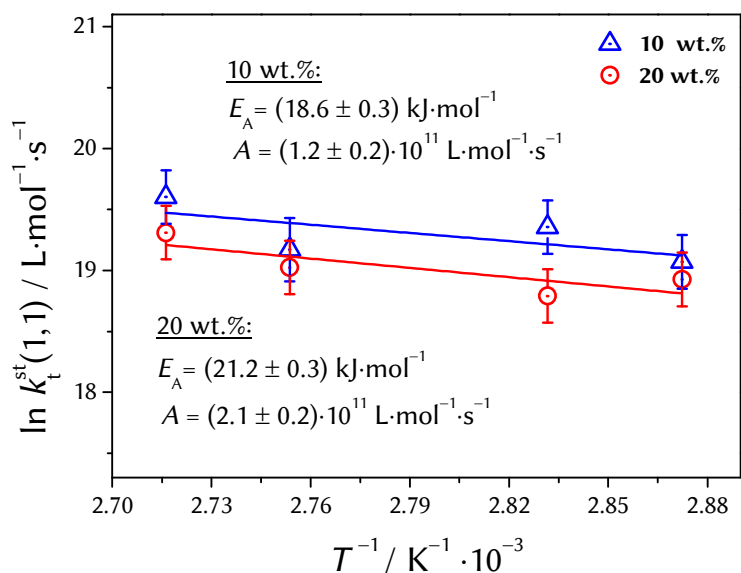


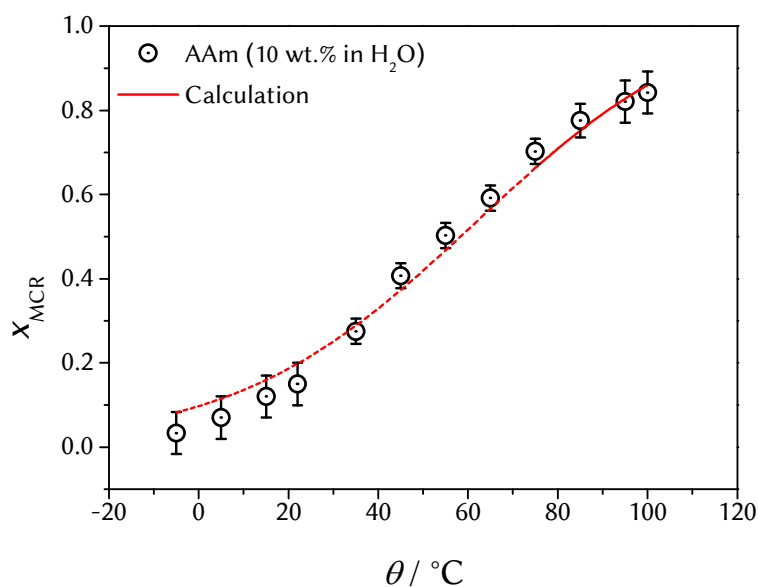
Figure 5.15: Arrhenius plot of the rate coefficient for MCR-SPR cross-termination, $k_t^{\text{st}}(1,1)$, at 10 and 20 wt.% AAm in aqueous solution between 75 and 95 °C. The rate coefficients were determined by PREDICI[®] fitting of the c_{MCR} vs t traces from SP-PLP-EPR experiments.

Table 5.6: Comparison of Arrhenius parameters for the rate coefficients of homo-termination, $k_t^{\text{ss}}(1,1)$, and cross-termination, $k_t^{\text{st}}(1,1)$, in the aqueous-solution polymerization of 10 and 20 wt.% AAm.

	$E_A / \text{kJ}\cdot\text{mol}^{-1}$	$A / 10^{11} \cdot \text{L}\cdot\text{mol}^{-1}\cdot\text{s}^{-1}$
10 wt.%		
$k_t^{\text{ss}}(1,1)$	17.8 ± 0.1	3.9 ± 0.3
$k_t^{\text{st}}(1,1)$	18.6 ± 0.3	1.2 ± 0.2
20 wt.%		
$k_t^{\text{ss}}(1,1)$	19.0 ± 0.1	5.0 ± 0.3
$k_t^{\text{st}}(1,1)$	21.2 ± 0.3	2.1 ± 0.2

Table 5.7: Cross-termination rate coefficients, $k_t^{\text{st}}(1,1)$, for several monomers at 50 °C.

$k_t^{\text{st}}(1,1)$	$k_t^{\text{st}}(1,1)$ (50 °C)/ $10^8 \text{ L}\cdot\text{mol}^{-1}\cdot\text{s}^{-1}$	Ref.
AAm (10 wt.% / H₂O)	1.2	this work
AAm (20 wt.% / H₂O)	0.8	this work
BA (1.5 M / toluene)	3.6	37

**Figure 5.16:** MCR fraction, x_{MCR} , of total radical concentration derived from the EPR spectra recorded during stationary UV irradiation of AAm (10 wt.% in aqueous solution). The full line is estimated from eq (2.12) using the entire set of rate coefficients determined in the present study. The dashed part of the line indicates that these x_{MCR} values below 75 °C are based on k_{bb} , k_p^{t} and $\langle k_t^{\text{st}} \rangle$ values extrapolated along the Arrhenius expressions presented above.

As seen for k_p^t , AAm also does not differ significantly from BA in cross-termination rate coefficient. Listed in Table 5.7 are the $k_t^{st}(1,1)$ values for 50 °C. The modest differences in both k_p^t and in $k_t^{st}(1,1)$ indicate that the far lower MCR fraction previously reported for AAm in aqueous solution under stationary polymerization conditions is essentially due to the lower backbiting rate coefficient, k_{bb} . The relatively small fraction of MCRs with AAm is plotted as a function of temperature in Figure 5.16. The full line is estimated from eq (2.12) using the entire set of rate coefficients determined in the present study with $\langle k_t^{st} \rangle$ as chain-length averaged quantity of cross-termination estimated from $k_t^{st}(1,1)$ via eq (2.29) for an average chain length of 1000. Absolute c_{SPR} values at the polymerization conditions underlying the experiments in Figure 5.16 are listed as part of the Appendices section.

In view of the uncertainty associated with deducing individual rate coefficients from SP-PLP-EPR data, the agreement of estimated and measured x_{MCR} is a strong argument in favor of the quality of the MCR-related rate coefficients from SP-PLP-EPR studies. The Arrhenius expressions presented for k_{bb} , k_p^t , and $k_t^{st}(1,1)$ appear to afford reasonable estimates of these coefficients even beyond the temperature range in which the underlying SP-PLP-EPR experiments have been performed. The set of rate coefficients from SP-PLP-EPR together with k_p^s from the PLP-SEC experiments²⁹ allows for the modeling of AAm kinetics and product properties in an extended range of experimental conditions for chemically initiated polymerization, i.e., under stationary conditions, as have been performed by Calista Preusser.^{160,161} The (very) satisfactory agreement between experiment and simulation in her study might be seen as verification for the presented comprehensive description of termination and transfer kinetics of AAm polymerization provided by SP-PLP-EPR.

Novel Access to the Rate Coefficient of Propagationⁱⁱⁱ

Despite the increasing importance of radical polymerization in aqueous solution, the knowledge about the kinetics of (salt-like) ionic monomers is surprisingly limited which is particularly true for k_p . Studying polymerization kinetics of ionic species mainly suffered from the lack of reliable k_p data. While a reliable set of k_p values for several polymerizations of non-ionized water-soluble monomers was established within the last years, e.g., for acrylic acid^{19–23}, methacrylic acid^{19,20,24–26}, AAm^{27–29}, *N*-isopropyl acrylamide³⁰, methylated acrylamides³¹, 1-vinylpyrrolidin-2-one³² and for *N*-vinyl formamide³³, the investigations into k_p of fully-ionized monomers are scarce. Lacík *et al.* published k_p data for sodium acrylate⁷² and sodium methacrylate³⁵, i.e., for fully-ionized acrylic and methacrylic acid by using the pulsed laser polymerization – size-exclusion chromatography (PLP–SEC) technique which has been

ⁱⁱⁱ Reproduced with permission from Kattner, H.; Drawe, P.; Buback, M. *Macromol. Chem. Phys.* **2015**, *216*, 1737–1745. Copyright 2015, Wiley-VCH, and from Kattner, H.; Buback, M.; *Macromolecules* **2016**, *49*, 3716–3722. Copyright 2016, American Chemical Society. Simulations on PLP–SEC and chemically initiated polymerizations were performed by Patrick Drawe.¹⁰⁷

introduced by Olaj and colleagues^{15,16} and is known as the IUPAC-recommended method for accurate determination of individual k_p data.^{17,18} The studies into fully ionized monomers are difficult because of the reduced quality of PLP induced molar-mass distributions. The detailed discussion of the PLP-SEC characteristics is beyond the scope of this work and the reader is referred to the literature.^{18,19,36} Shortly spoken, PLP-SEC rests on the assumption that, by a sequence of evenly spaced laser pulses, the polymeric chain length is determined by the time between two subsequent UV laser pulses, t_0 . This principle implies a) the linearity between chain length and t_0 and b) that initiation and preferential termination occurs immediately after the laser pulse. It goes without saying that a moderate if not high rate coefficient of termination is indispensable for generation of PLP-structured molar-mass distributions and that transfer reactions, which scramble the linearity between t_0 and chain length, should be absent or unimportant.³⁶ Neutralization, i.e., ionization, of side groups of acrylic acid and methacrylic acid reduces k_t by several orders of magnitude^{38,44,119} which makes PLP-SEC with fully-ionized monomers challenging. It is the aim of this section to provide a novel technique for reliable k_p determination which is particularly suitable for slowly terminating radicals. The proposed method differs from the established procedure of k_p determination from stationary EPR measurements.^{122,185} These stationary experiments, which are performed over a wider conversion range, suffer from the disadvantage that the microwave energy stored in the cavity and thus signal intensity may vary due to changes in dielectricity of the sample which may in turn affect the accuracy of k_p determination. E.g., methyl methacrylate (MMA) homopolymerization up to high conversion is accompanied by an increase in EPR signal intensity by a factor of three.^{124,186,187} The presented novel instationary method may be applied in the initial polymerization period and thus under conditions, for which EPR calibration is more easily and accurately carried out.

The method is introduced for the aqueous-solution polymerization of the salt trimethylaminoethyl methacrylate chloride (TMAEMA)¹⁰⁸ at 60 °C (*proof of principle*) and will be validated by the investigations into bulk polymerization of non-ionized but slowly terminating di(*n*-butyl) itaconate for which k_p data are reported.

Since the novel k_p approach rests on the SP-PLP-EPR technique, both k_p and k_t will be derived simultaneously but independently from a single experiment.

6.1 Proof of Principle: Propagation Kinetics of TMAEMA

Shown in Figure 6.1 is the EPR spectrum of propagating TMAEMA radicals for 20 wt.% monomer in D₂O at 60 °C recorded under pulsed-laser irradiation with a pulse-repetition rate (p.r.r.) of 20 Hz. Usually and as seen with AAm polymerizations, EPR measurements in highly polar solvents such as D₂O suffer from poor S/N quality due to the dielectric loss of microwave energy.^{38,39,44} The signal quality for TMAEMA is however well above the one of radicals in organic solvents because of the high radical concentration of $2.63 \cdot 10^{-5} \text{ mol} \cdot \text{L}^{-1}$.^{37,42,100,118,121,124,185}

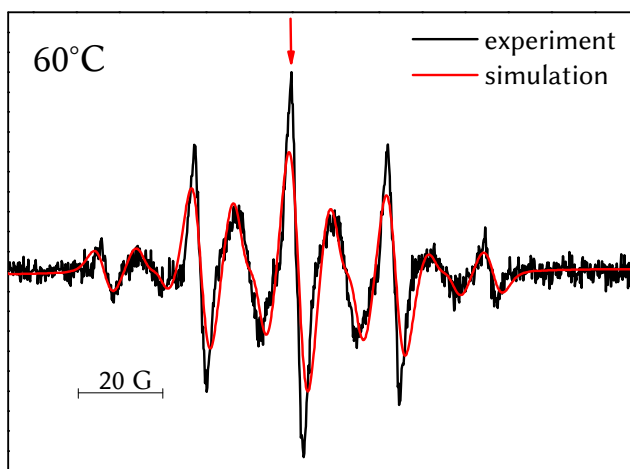


Figure 6.1: Comparison of experimental and simulated EPR spectra for TMAEMA (20 wt.% in D₂O) polymerization at 60 °C. The spectrum was recorded within 5.12 s under pulsed-laser initiation at a p.r.r. of 20 Hz. The quasi-stationary radical concentration was $2.63 \cdot 10^{-5} \text{ mol} \cdot \text{L}^{-1}$. The magnetic field position used for time-resolved single-pulsed experiments is indicated by the arrow. Simulation of the spectrum was carried out with the hyperfine coupling constants listed in Table 6.1. The initial Darocur[®] concentration was chosen to be $1.1 \cdot 10^{-2} \text{ mol} \cdot \text{L}^{-1}$.

6.1.1 The EPR Spectrum in TMAEMA Polymerization

The simulation (red line in Figure 6.1) was obtained by assuming, as a characteristic feature of methacrylate (end-chain) radicals, the hindered rotation around the C_{α} - C_{β} bond.^{55,164,188-193} This phenomenon rests on the same principles as already introduced for MCRs in AAm polymerization for which the rotation around the C_{β} - C_{β} bond is hindered. According to the Heller-McConnel equation (eq (5.1)),¹⁷² non-equivalent hfcc, of the two β -protons, $a(\beta\text{-H})$, are associated with preferred dihedral angles θ and θ' of the conformers with the lowest potential energy (Table 6.1).¹⁶⁴ Interestingly, the entire spectrum can be simulated under the assumption of a single conformer at any temperature with constant hfcc as illustrated in Figure 6.2.

Table 6.1: Hyperfine coupling constants, a , for TMAEMA radicals as deduced from fitting the EPR spectrum in Figure 6.1.

nuclei	a / G
3H (α -CH ₃)	19.6
1H (β -H ₁)	11.7
1H (β -H ₂)	8.1

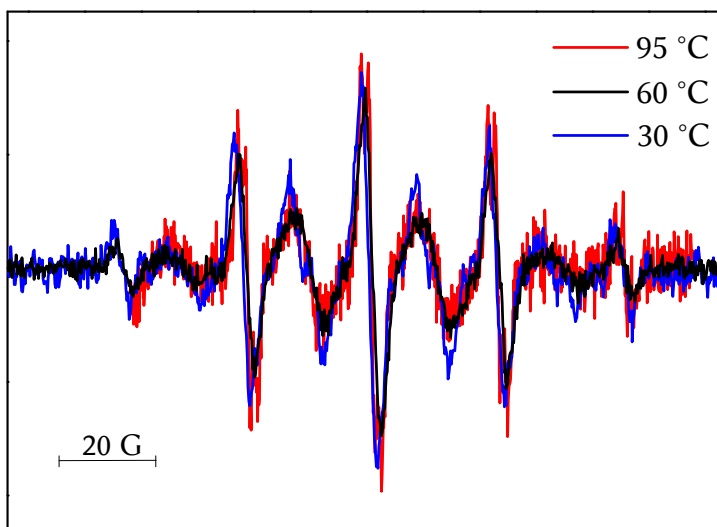


Figure 6.2: Comparison of EPR spectra of TMAEMA (20 wt.% in D_2O) for different temperatures under otherwise identical experimental conditions. The spectrum for 60 °C is identical to the one presented in Figure 6.1. The figure serves the purpose of illustrating the invariance of TMAEMA spectra toward temperature between 30 °C and 95 °C.

The invariance in hfc and hfc pattern along with the apparent existence of a single conformer might be explained with a symmetric potential energy diagram with two conformations yielding an identical hfc pattern as illustrated schematically in Figure 6.3. The conformers are shown with their dihedral angles in Newman projections for different internal rotational angles τ . Such a diagram as proposed for MMA radicals in bulk polymerization adequately describes the hfc pattern of the TMAEMA radicals.¹⁶⁴

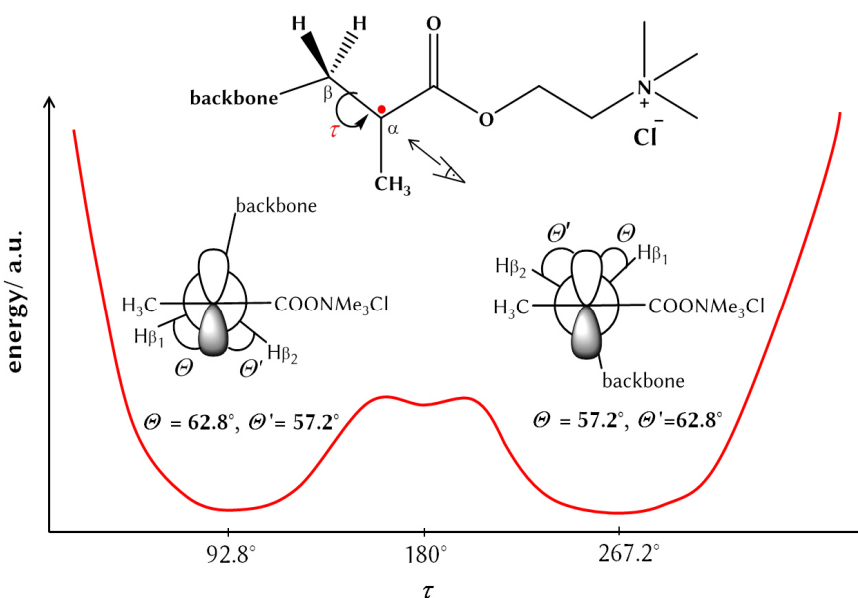


Figure 6.3: Potential energy diagram for TMAEMA radicals as proposed for MMA in the literature.¹⁶⁴ The schematic diagram rests on plausibility arguments (see text). The internal rotational angle, τ , as well as the dihedral angles θ and θ' were adapted for TMAEMA according to the Heller-McConnel equation. The two stable conformers are included in their Newman projections. The corresponding viewpoint is indicated in the chemical structure exposed above.

Under the assumption of a bond angle between the two β -methylene protons of 120° in their Newman projection, dihedral angles of $\theta = 62.8^\circ$ and $\theta' = 57.2^\circ$ are obtained with $A = 39.8$ G. The conformer assignment is not absolutely necessary for the application of the SP-PLP-EPR method. Nevertheless, it is considered as relevant to understand the origin of the hfc pattern.

6.1.2 SP-PLP-EPR Investigations into TMAEMA Kinetics

The time-resolved single-pulsed experiments were performed at the magnetic field position with the highest intensity indicated by the arrow in Figure 6.1. The resulting radical concentration vs time profile essentially reflects termination, as side reactions, e.g., the backbiting step, can be ignored for TMAEMA being a methacrylate.

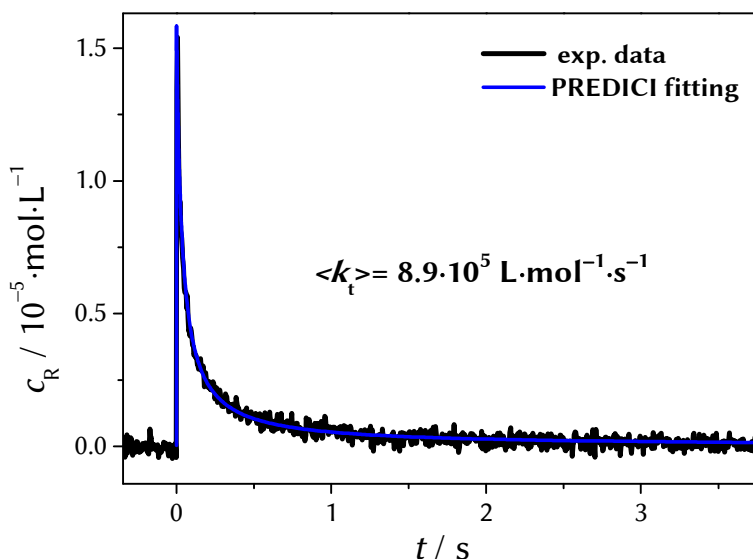


Figure 6.4: Time-resolved absolute radical concentration of TMAEMA radicals after applying a single laser pulse at $t = 0$ on the monomer solution in D_2O at $60\text{ }^\circ\text{C}$; the trace was measured at the magnetic field position indicated by the arrow in Figure 6.1. The chain-length averaged termination rate coefficient, $\langle k_t \rangle$, was obtained by PREDICI[®] fitting. The initial Darocur[®] concentration was chosen to be $1.1 \cdot 10^{-2} \text{ mol} \cdot \text{L}^{-1}$.

PREDICI[®] fitting of the trace in Figure 6.4 yields the chain-length-averaged termination rate coefficient, $\langle k_t \rangle$. The so-obtained mean value of $\langle k_t \rangle = 8.9 \cdot 10^5 \text{ L} \cdot \text{mol}^{-1} \cdot \text{s}^{-1}$ is significantly below $\langle k_t \rangle$ reported for other monomers (see Table 6.2). These reference $\langle k_t \rangle$ values in Table 6.2 were obtained from the experimental composite-model parameters using the Mahabadi-Olaj equation (eq (4.2)),¹⁴⁶⁻¹⁴⁸ which allows to estimate $\langle k_t \rangle$ for a distribution of radical sizes on the basis of CLDT.^{100,120}

Table 6.2: Comparison of chain-length averaged termination rate coefficients, $\langle k_t \rangle$, for selected monomers in organic and in aqueous solution at 60 °C. The numbers were obtained by the Mahabadi-Olaj equation (eq (4.2)).¹⁴⁶⁻¹⁴⁸ The other parameters required for this estimate, i.e., the k_p values and composite-model parameters are known; the initial initiator concentration of $5.5 \cdot 10^{-4} \text{ mol} \cdot \text{L}^{-1}$ and the decomposition rate coefficient, $k_d = 6.12 \cdot 10^{-6} \text{ s}^{-1}$, were selected to be the same for all studies; k_p of sodium acrylate (NaAA) at 60 °C needed according to eq (4.2) was estimated from the value for non-ionized acrylic acid divided by a factor of 8, which difference has been found experimentally at 6 °C.⁷² The rate coefficients exclusively refer to chain-end radicals. MAA = methacrylic acid.

60 °C	$\langle k_t \rangle / 10^5 \cdot \text{L} \cdot \text{mol}^{-1} \cdot \text{s}^{-1}$	Ref.
TMAEMA (20 wt.% in D₂O)	(8.9 ± 0.4)	this work
Sty (bulk)	635	100
VAc (bulk)	638	19,42,194,195
MMA (bulk)	219	19,117
NaAA (20 wt.% in H₂O)	76	39,72
AAM (10 wt.% in H₂O)	207	this work and 29
AA (10 wt.% in H₂O)	<i>1012</i>	23,38
MAA (10 wt.% in H₂O)	520	26,35,44

The italic number for AA indicates a higher uncertainty.

The low $\langle k_t \rangle$ value of TMAEMA should be primarily due to the (positive) charge sitting close to the reactive site of the two radicals. Also with fully ionized sodium acrylate (NaAA) (Table 6.2), $\langle k_t \rangle$ is relatively low.³⁹ Under such slow-termination conditions, the PLP-SEC experiment runs into difficulties.³⁶ They may be overcome by the novel EPR-based strategy which will now be illustrated.

Propagation Kinetics of TMAEMA Polymerization

The propagation rate coefficient, k_p , is derived from the same concentration vs time profile as used for $\langle k_t \rangle$ determination. The only piece of required additional information is the knowledge of monomer-to-polymer conversion, X , induced by the single pulse.

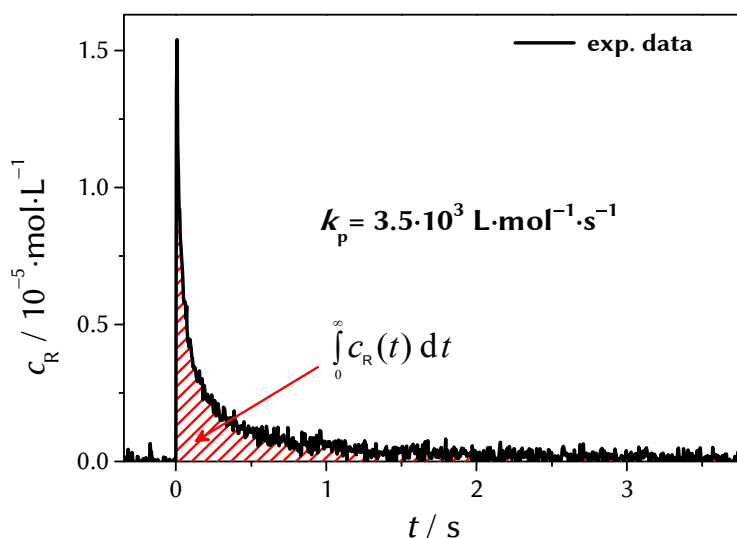


Figure 6.5: Integration of the time-resolved radical concentration of TMAEMA radicals (20 wt.% in D₂O) at 60 °C with Darocur[®] (1.1 · 10⁻² mol · L⁻¹) acting as the photoinitiator. The hatched area below the curve corresponds to the integral in eq (6.1). The radical concentration vs time profile is identical to the one presented in Figure 6.4.

The integrated rate law for polymerization relates X to the integral of radical concentration, c_R , over time t (eq (6.1)).

$$\ln\left(\frac{1}{1-X}\right) = k_p \cdot \int_0^{\infty} c_R(t) dt \quad (6.1)$$

The integral $\int_0^{\infty} c_R(t) dt$ is given by the area under the radical concentration vs time profile as illustrated in Figure 6.5. Assuming chain-length independent k_p , this area yields k_p upon knowing the conversion X . The analysis for k_p via eq (6.1) needs no assumptions other than the chain-length dependency of k_p does not take effect, i.e., k_p is independent of time after the laser pulse, the propagation process is irreversible and the measured monomer conversion being entirely due to the growth of the observed type of radical. This latter requirement is fulfilled in the case of

methacrylate-type and styrene-type^{100,122} radicals as well as for vinyl esters⁴², where backbiting does not take place and only one type of radicals will be present.^{21,49,196-198} With monomers that undergo backbiting, the method may be restricted to cases where the time-resolved concentration of chain-end radicals may be accurately monitored and the contribution to monomer conversion of mid-chain radicals is negligible in good approximation.^{37,38} This might be the case with NaAA polymerization.³⁹ If the contribution of MCR propagation to the overall monomer conversion gets important, e.g., if the MCR fraction is high, PREDICI[®] fitting procedures need to be used. Here, the value for X has to be reproduced on the basis of a model which includes all relevant reactions with k_p^s as the only fitting parameter (see Section 8.2).

Table 6.3: Determination of the propagation rate coefficient, k_p , for TMAEMA (20 wt.% in D₂O) at 60 °C via eq (6.1). For each sample, monomer-to-polymer conversion, X , after single-pulse initiation was measured four times upon minor variation of the vertical position of the sample in the sample holder. This variation does not affect X .

Sample	conversion X after 10 pulses	$X /$ pulse	$\int c_R(t) dt /$ $\text{mol}\cdot\text{L}^{-1}\cdot\text{s} \cdot 10^{-6}$	$k_p /$ $\text{L}\cdot\text{mol}^{-1}\cdot\text{s}^{-1}\cdot 10^3$
1	0.184	0.0184	5.26	3.54
	0.184	0.0184	5.26	3.54
	0.184	0.0184	5.26	3.54
	0.184	0.0184	5.26	3.54
2	0.207	0.0207	5.96	3.52
	0.207	0.0207	5.96	3.53
	0.208	0.0208	5.96	3.51
	0.206	0.0206	5.96	3.51
3	0.179	0.0179	5.23	3.46
	0.179	0.0179	5.23	3.45
	0.177	0.0177	5.23	3.41
	0.177	0.0177	5.23	3.41
				3.50

Table 6.4: Comparison of measured rate coefficients of propagation, k_p , for selected monomers in an organic and in an aqueous environment at 60 °C. The rate coefficients exclusively refer to chain-end radicals. NaMAA = sodium methacrylate

60 °C	$k_p / 10^3 \cdot \text{L} \cdot \text{mol}^{-1} \cdot \text{s}^{-1}$	Ref.
TMAEMA (20 wt.% in D₂O)	(3.5 ± 0.3)	this work
Sty (bulk)	0.3	19
VAc (bulk)	8.3	19
MMA (bulk)	0.8	9
AA (10 wt.% in H₂O)	160	23
MAA (10 wt.% in H₂O)	9.0	26,35
NaMAA (10 wt.% in H₂O)	1.6	26,35

As described in Section 3.3, monomer conversion, X , may be determined by FT-NIR spectroscopy via the first overtone of the antisymmetric C-H stretching mode of the methyldene group. The so-obtained conversions per laser pulse are listed in Table 6.3 for three SP-PLP-EPR experiments carried out on TMAEMA (20 wt.% in D₂O) at 60 °C.

In very close agreement, the three experiments at 60 °C (Table 6.3) result in $k_p = (3.5 \pm 0.3) 10^3 \text{ L} \cdot \text{mol}^{-1} \cdot \text{s}^{-1}$ for 20 wt.% TMAEMA in solution of D₂O. This number is compared to a selection of literature k_p values in Table 6.4. Interestingly, k_p for 20 wt.% TMAEMA in aqueous solution is in between the corresponding numbers for styrene, methyl methacrylate and vinyl acetate bulk radical homopolymerizations. Comparison with k_p of other monomers in aqueous solution shows that the TMAEMA value is close to k_p of fully ionized sodium methacrylate (10 wt.% in H₂O). This sodium methacrylate k_p is almost a factor of six below the associated k_p of non-ionized MAA and by two orders of magnitude below the k_p value of non-ionized acrylic acid (10 wt.% in H₂O). The effects seen with the aqueous solutions are understood by the significant lowering of k_p upon full ionization and by the lowering in passing from an acrylate to a methacrylate monomer.

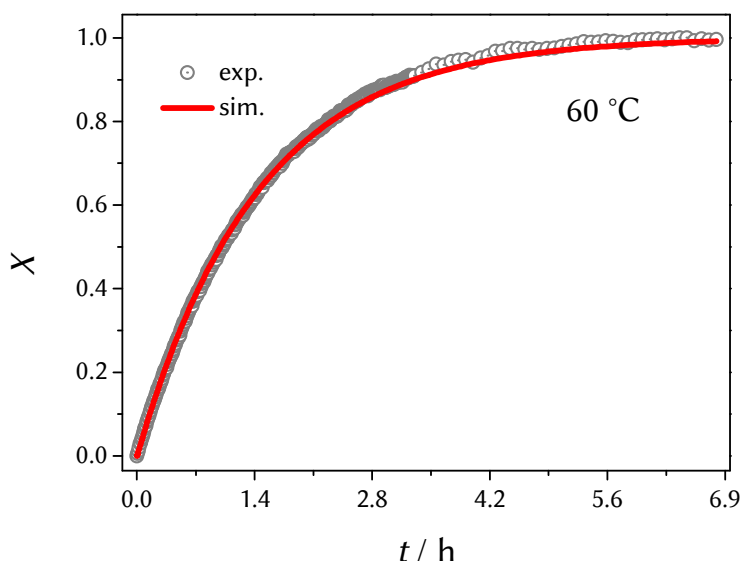


Figure 6.6: Comparison of experimental and simulated conversion, X , vs time traces for chemically initiated TMAEMA (20 wt.% in D_2O) polymerization at 60 °C with VA-086, $c_{VA-86} = 9.57 \text{ mmol}\cdot\text{L}^{-1}$, acting as the thermal initiator. The simulation is based on ideal polymerization kinetics with the k_p and $\langle k_t \rangle$ data being taken from the SP-PLP-EPR experiment presented above. The experiment was performed by Patrick Drawe.^{107,108}

Both changes largely enhance the friction to internal rotational motion in the transition state for propagation and thus reduce the pre-exponential for entropic reasons.^{19,26,35,71,73,199} An additional effect of ionization on the activation energy may not be excluded.

Reliability of Deduced k_p and $\langle k_t \rangle$ Value

As no k_p value for TMAEMA has been published so far, the reliability of the number from SP-PLP-EPR has been checked by carrying out a chemically initiated polymerization for 20 wt.% TMAEMA in D_2O at 60 °C with VA-086 acting as the thermal initiator at an initial concentration of $9.57 \text{ mmol}\cdot\text{L}^{-1}$. These experiments were performed by Patrick Drawe and the experimental details are described elsewhere.¹⁰⁷

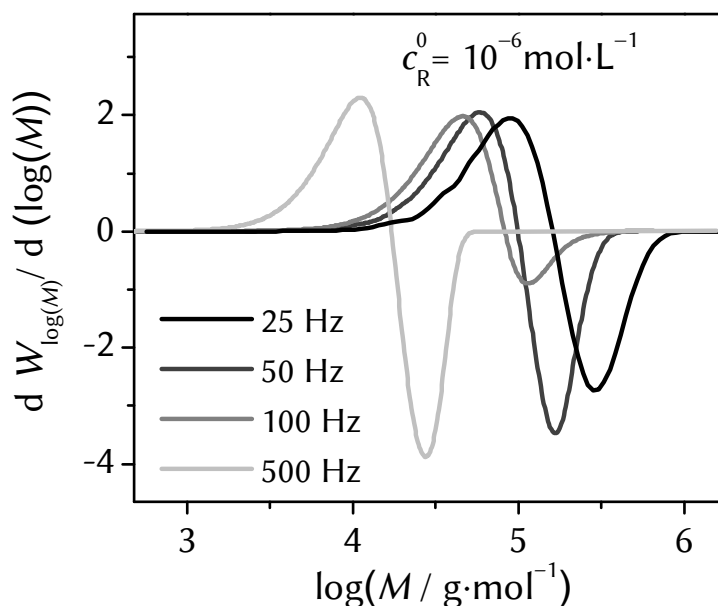


Figure 6.7: Simulated first-derivative curves of MMDs for samples from PLP-SEC experiments on 20 wt.% TMAEMA in D₂O at 60 °C carried out at different laser pulse repetition rates. The radical concentration induced by the first pulse, c_R^0 , was chosen to be $c_R^0 = 1.0 \cdot 10^{-6} \text{ mol} \cdot \text{L}^{-1}$. The rate coefficients k_p and $\langle k_t \rangle$ were taken from the SP-PLP-EPR experiment of this study. Simulation provided by Patrick Drawe.^{107,108}

The measured conversion vs time trace is compared with the data simulated by the PREDICI[®] program on the basis of the above k_p and $\langle k_t \rangle$ values from SP-PLP-EPR. For this simulation, ideal polymerization kinetics was assumed to apply.

The effective rate coefficient of initiator decomposition was taken from literature:^{200,201} $k_d f(60^\circ\text{C}) = 2.6 \cdot 10^{-7} \text{ s}^{-1}$, where f is the initiator efficiency and k_d the decomposition rate coefficient. The almost perfect agreement between experiment and simulation over the entire range of monomer conversion (Figure 6.6) is indicative of the quality of the rate coefficients from SP-PLP-EPR measurements. The close comparison further suggests that, for TMAEMA (20 wt.%) polymerization in D₂O at 60 °C, the coefficients k_p and $\langle k_t \rangle$ do not significantly depend on monomer conversion. Moreover, the reported numbers for k_p and k_t have been verified by independent SP-PLP-NIR experiments.¹⁰⁸ In contrast to SP-

PLP–EPR technique, within SP–PLP–EPR k_p and $\langle k_t \rangle$ are determined independently from each other.

With k_p and $\langle k_t \rangle$ being known, the MMD of PLP–SEC samples may be simulated via PREDICI[®]. These estimates have been carried out for p.r.r. of 25, 50, 100 and 500 Hz, using a pulse-induced primary radical concentration of $c_R^0 = 1.0 \cdot 10^{-6} \text{ mol} \cdot \text{L}^{-1}$. Hydrodynamic SEC broadening due to the SEC columns was included into the simulation by a broadening function that is described in detail elsewhere²⁰² with the broadening parameters: $\sigma = 0.172 \text{ mL}$ and $\tau = 0.279 \text{ mL}$. The results in Figure 6.7 demonstrate that even at 25 Hz the PLP-induced structure on the MMD is too poor as to allow for accurate k_p measurements. Toward higher p.r.r. this situation becomes even worse. The data thus indicates that p.r.r. far below 25 Hz are required for reliable k_p determination via PLP–SEC. According to eq (2.36) and eq (2.41), k_p correlates the time t after pulsing to radical chain length.

Resolving CLDT for TMAEMA at 60 °C

As a consequence, by analysis of the radical concentration vs time data in Figure 6.4, the k_p value from SP–PLP–EPR also provides chain-length dependent k_t values. Because of the relatively low $\langle k_t \rangle / k_p$ ratio only a few data points can be assigned to the short-chain regime as is seen from the double logarithmic plotting according to eq (2.40) (Figure 6.8). The small number of data points related to $i < i_c$ with the small number for α_1 may explain the adequate fitting of concentration vs time profile with chain-length averaged k_t in Figure 6.4. Thus, the composite-model parameters $\alpha_s = 0.65 \pm 0.09$, $\alpha_1 = 0.18 \pm 0.03$, and $i_c = 45 \pm 25$ are deduced, however, with a higher uncertainty for α_s and i_c than usually seen for this data. The number for $k_t(1,1)$ is easily accessible by fitting the concentration vs time profile shown in Figure 6.4 using PREDICI[®]. Because of the small number of data points for low i , the analysis according to eq (2.42) for determination of $k_t(1,1) \cdot c_R^0$ cannot be applied. Therefore, the Composite Model with α_s , α_1 , and i_c has been implemented into the PREDICI[®] model with $k_t(1,1)$ being the only fitting parameter (see Figure 6.9).

The so-obtained value being $k_t(1,1) = (1.2 \pm 0.2) \cdot 10^7 \text{ L} \cdot \text{mol} \cdot \text{s}^{-1}$ for 60 °C is again well below the reported ones for the tabulated monomers (see Table 6.5). The quality of the PREDICI[®] fitting is identical to the one from Figure 6.4 providing an equivalent and consistent description of TMAEMA by the Composite Model.

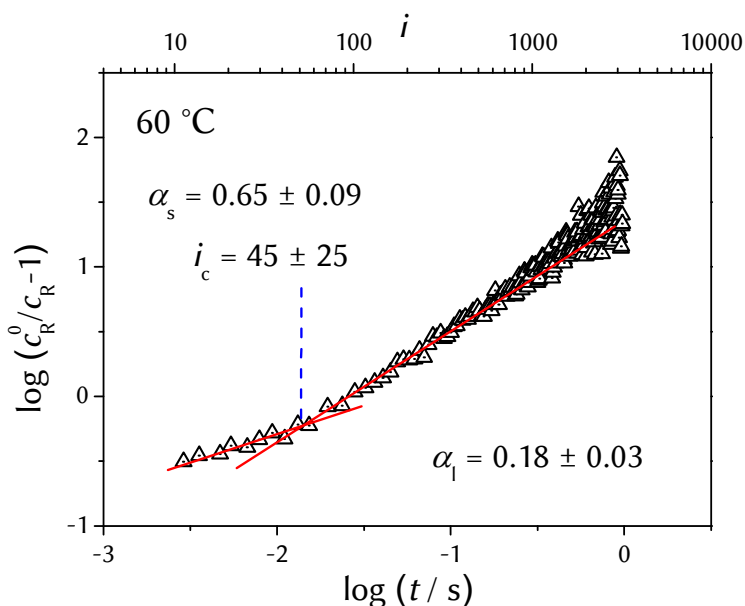


Figure 6.8: Double-log plot of relative radical concentration for TMAEMA polymerization (20wt.% in D₂O) at 60 °C in order to derive the composite-model parameters α_s , α_1 and i_c .

Variation of α_s and i_c within the range of reported uncertainty produces minor changes in the determined $k_t(1,1)$, i.e., $\pm 13\%$, which is already included in $k_t(1,1)$ being accurate within $\pm 20\%$. Note that the quality of the fit is reduced by changing α_s and i_c . The obtained power-law exponents are in good agreement with theory and with the reported numbers for other monomers.^{90,94,96,98,143,175} The crossover chain length is well below the number for methyl methacrylate, i.e., $i_c = 100$, but is in the region found for *n*-butyl methacrylate,¹¹⁸ acrylates,⁴¹ styrene,¹⁰⁰ vinyl acetate⁴² and AAm¹⁰⁹. Hence, one may conclude that beside the very low value for $k_t(1,1)$ at least for TMAEMA (20 wt.% in D₂O) at 60 °C no further impact of ionization on CLDT is observed.

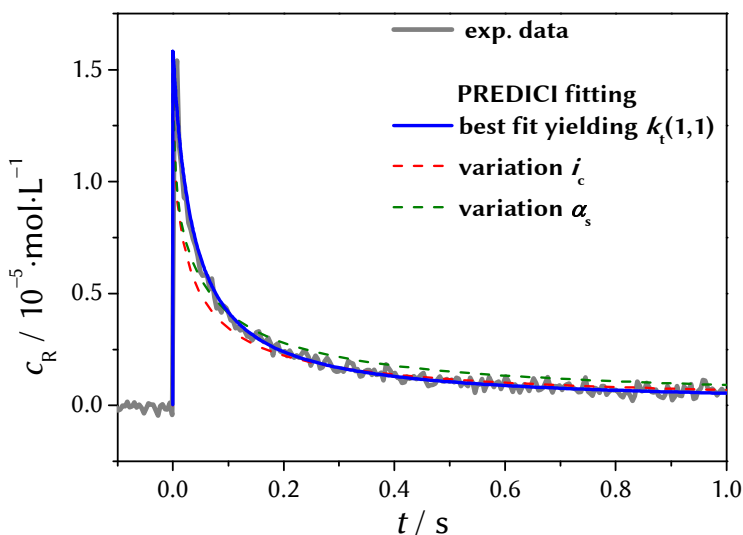


Figure 6.9: PREDICI[®] fitting of radical concentration of TMAEMA radicals at 60 °C with k_p as the only fitting parameters. The residual composite-model parameters were taken as deduced from Figure 6.8. The best fit which provides $k_t(1,1)$ is presented as blue line. The accuracy of the determined composite-model parameters is exemplarily illustrated by changing i_c (red line) and α_s (green line) from $i_c = 45$ to $i_c = 70$ and from $\alpha_s = 0.65$ to $\alpha_s = 0.56$ respectively (see text).

Table 6.5: Comparison of the termination rate coefficients $k_t(1,1)$ for selected monomers in organic and in aqueous solution at 60 °C. The rate coefficients exclusively refer to chain-end radicals.

60 °C	$k_t(1,1) / 10^7 \cdot \text{L} \cdot \text{mol}^{-1} \cdot \text{s}^{-1}$	Ref.
TMAEMA (20 wt.% in D₂O)	(1.2 ± 0.2)	this work
Sty (bulk)	69	this work
VAc (bulk)	123	42
MMA (bulk)	90	117
AAm (10 wt.% in H₂O)	63	this work
MAA (10 wt.% in H₂O)	118	41

6.2 Validation: Propagation and Termination in DBI Bulk Polymerization

As illustrated with TMAEMA, the time-resolved SP-PLP-EPR technique constitutes a valuable tool for simultaneous determination of polymerization rate coefficients, i.e., from a single radical concentration vs time profile. For validation of the novel k_p approach, a system with slowly terminating radicals has been chosen for which reliable k_p data is already available: the bulk polymerization of di-(*n*-butyl) itaconate (DBI).

6.2.1 The EPR Spectrum in DBI Bulk Polymerization

The black line in Figure 6.10 represents the experimental spectrum of radicals occurring during DBI bulk polymerization at 45 °C under laser-pulse-periodic initiation using a p.r.r. of 20 Hz. The spectrum is in perfect agreement with the reported one.^{185,203} The red line represents the associated fit obtained with the hfcc for two equivalent pairs of β -methylene protons: $a(2H, H-\beta_1) = 20.5$ G and $a(2H, H-\beta_2) = 16.8$ G. As with other monomers bearing bulky side groups, e.g., methacrylates or mid-chain radicals, internal rotation around the C-C σ -bond of the backbone is hindered with the two methylene protons being symmetrically fixed with respect to the singly occupied p-orbital, while the two methylene protons of the side chain rotate freely yielding an averaged hfcc. This situation results in a characteristic EPR spectrum according to the Heller-McConnell equation (eq (5.1)).^{122,164,172} The assignment of the hfcc to the two types of methylene groups is however not fully clear.²⁰³ Other than with methacrylate radicals and mid-chain-radicals in acrylate polymerizations, the EPR spectrum of DBI radicals in bulk polymerization refers to a single conformer in the investigated temperature range with the hfcc being insensitive toward temperature which is similar to what is known from polymerization of TMAEMA in aqueous solution and suggests an comparable potential energy diagram as with TMAEMA radicals.

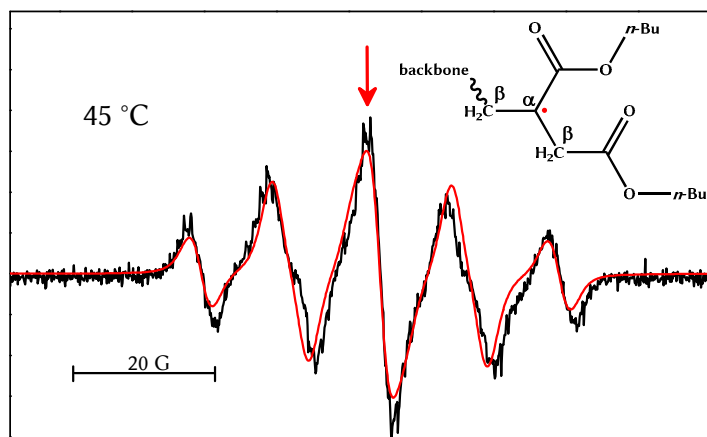


Figure 6.10: Experimental (black) and fitted (red) EPR spectrum for bulk polymerization of DBI at 45 °C under pseudo-stationary PLP conditions applying a repetition rate of 20 Hz. The arrow indicates the magnetic field position used for the SP–PLP–EPR experiments. The structural formula illustrates the two pairs of equivalent CH₂ groups, one pair on the backbone and the other pair in the side chain.

6.2.2 Propagation Kinetics of DBI

The SP–PLP–EPR measurements were run at the magnetic field position indicated by the arrow in Figure 6.10. Illustrated in Figure 6.11 is the decay in absolute radical concentration of DBI radicals at 30 °C after applying a laser pulse at $t = 0$. As with TMAEMA the decay is exclusively due to termination which allows for determination of k_p according to eq (5.1) by determining the monomer-to-polymer conversion, X , and the integral over radical concentration (hatched red area). X may be accurately determined after laser pulsing by gravimetry. Because of low k_p and hence low conversion induced by a single laser pulse, several pulses were applied and the individual radical concentration vs time profiles were co-added. It was checked that the decay in radical concentration with time does not depend on the number of applied pulses. In order to enhance the accuracy of the gravimetric analysis, polymer produced within three experiments carried out under identical conditions has been combined.

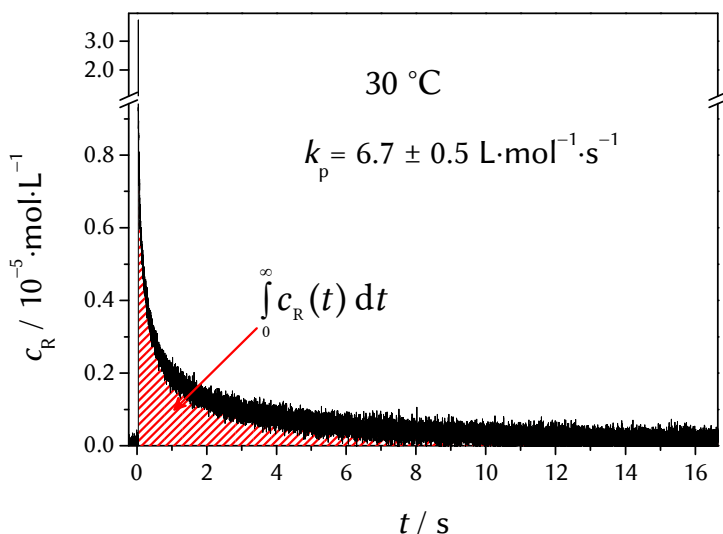


Figure 6.11: Decay of absolute radical concentration after applying a laser pulse at $t=0$ during a DBI bulk polymerization at 30 °C with MMMP ($4.1 \cdot 10^{-2}\text{ mol}\cdot\text{L}^{-1}$) acting as the photoinitiator. The red hatched area corresponds to the integral in eq (6.1). The radical concentration vs time profile results from the co-addition of 81 laser single pulses, which were recorded at a time resolution of $10\text{ }\mu\text{s}$ with a delay of 30 s between successive laser pulses.

Overall monomer conversion, X_{ov} , measured after applying several pulses, divided by the number of pulses, yields X_{SP} , the monomer conversion per (single) pulse. Because of the slow chain growth and the associated small conversion, the monomer consumption induced by the initiation step, i.e., the addition of the primary photoinitiator-derived radical to a DBI molecule, needs to be taken into account. As the initial concentration of DBI radicals at time zero, c_{R}^0 , is known by EPR calibration, an equimolar amount of DBI monomer has been subtracted from X_{SP} to yield the relevant number for X , which refers to the decay in DBI radical concentration per laser pulse according to eq (6.1). The experimental parameters, the primary results and the obtained k_{p} values are summarized in Table 6.6.

Table 6.6: Rate coefficients of propagation, k_p , from SP–PLP–EPR experiments on the bulk polymerization of DBI at several temperatures, θ . Tabulated is the measured overall monomer-to-polymer conversion, X_{ov} , the associated conversion per laser single pulse, X_{SP} , and the monomer-to-polymer conversion X obtained from X_{SP} under consideration of the amount of DBI required for the production of the initial DBI radical. The number for X together with the measured integral $\int_0^{\infty} c_R(t) dt$ yields the propagation rate coefficient, k_p , (see text).

$\theta / ^\circ\text{C}$	$X_{ov} / 10^{-3}$	no. of pulses	$X_{SP} / 10^{-5}$	$X / 10^{-5}$	$\int c_R(t) dt / 10^{-6} \text{ mol}\cdot\text{L}^{-1}\cdot\text{s}$	$k_p / \text{L}\cdot\text{mol}^{-1}\cdot\text{s}^{-1}$
30	1.72	14	12.32	11.38	16.3	6.98
	3.45	81	4.26	3.73	5.5	6.79
	5.66	73	7.75	6.96	10.1	6.86
	5.88	76	7.74	7.10	10.2	6.94
40	8.14	55	14.80	13.87	15.3	9.06
	3.07	43	7.13	6.60	7.3	9.05
	6.74	46	14.66	13.57	13.7	9.93
45	4.04	52	7.77	7.30	7.2	10.07
	6.33	49	12.93	12.42	11.5	10.79
	3.33	43	7.75	7.28	6.6	10.96
50	5.81	41	14.18	14.08	10.1	13.99
	6.33	56	11.30	10.19	8.7	11.70
	8.61	49	17.57	16.49	13.8	11.93
	4.82	56	8.61	7.54	7.2	10.48
	2.93	35	8.36	7.90	4.9	15.97
60	1.36	33	4.12	3.78	2.5	14.87
	1.70	55	3.09	2.80	1.9	14.42
	5.19	29	17.91	16.80	10.0	16.79

The individual experiments for each temperature yield k_p data which scatter by less than 10 percent around the arithmetic mean value, with the exception of the data for 50 °C, where the scatter approaches 17 percent.

The mean values of k_p are plotted in Figure 6.12 with the error bars estimated from the maximum deviation of k_p from the associated mean value. The activation energy and the pre-exponential deduced from the Arrhenius line are: $E_A(k_p) = (22.6 \pm 0.5) \text{ kJ}\cdot\text{mol}^{-1}$ and $A(k_p) = (5.4 \pm 1.1)\cdot 10^4 \text{ L}\cdot\text{mol}^{-1}\cdot\text{s}^{-1}$, respectively. This data is close to the numbers reported by Szablan *et al.* from multi-pulse PLP-SEC experiments,²⁰⁴ resulting in the almost perfect agreement in Figure 6.12 of the Arrhenius lines from the two investigations, thus providing strong evidence for the reliability of the two fully independent strategies for k_p measurement. The Arrhenius expression deduced from the SP-PLP-EPR experiments reads

$$\ln(k_p / (\text{L}\cdot\text{mol}^{-1}\cdot\text{s}^{-1})) = 10.9 - 2726 (T^{-1}/\text{K}^{-1}),$$

and holds for the experimental range up to 60 °C. Toward higher temperature, depropagation may lead to lower apparent k_p .²⁰⁴ Extrapolation to 0 °C yields $k_p = 2.5 \text{ L}\cdot\text{mol}^{-1}\cdot\text{s}^{-1}$ which is in almost perfect agreement with an earlier reported experimental value of $2.4 \text{ L}\cdot\text{mol}^{-1}\cdot\text{s}^{-1}$.¹¹⁶ The activation energy is in the typical region of methacrylates which is due to the structural similarities of the propagating radicals.¹⁹ The pre-exponential, $A(k_p)$, of DBI is by several orders of magnitude below the numbers for acrylates,¹⁹ vinyl esters^{124,137,194} and styrene^{129,130} which, e.g., are $A(k_p) = 1.66\cdot 10^7 \text{ L}\cdot\text{mol}^{-1}\cdot\text{s}^{-1}$ for methyl acrylate, $A(k_p) = 1.47\cdot 10^7 \text{ L}\cdot\text{mol}^{-1}\cdot\text{s}^{-1}$ for vinyl acetate, and $A(k_p) = 4.27\cdot 10^7 \text{ L}\cdot\text{mol}^{-1}\cdot\text{s}^{-1}$ for styrene bulk polymerization. The low $A(k_p)$ of DBI demonstrates the large entropy penalty of the transition state structure for propagation due to restricted internal rotational mobility around the radical-monomer bond because of the bulky side groups.¹⁹

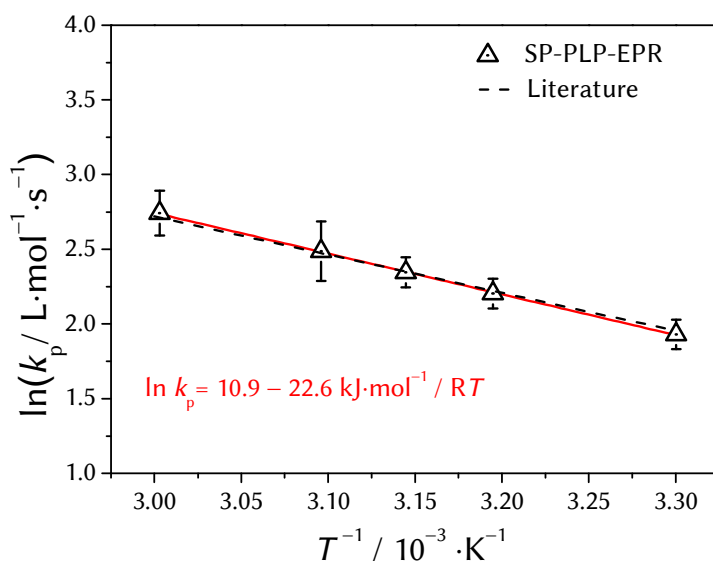


Figure 6.12: Arrhenius plot for k_p of DBI bulk polymerizations between 30 and 60 °C. The mean values of k_p deduced from several independent SP-PLP-EPR experiments at each polymerization temperature are fitted by the full red Arrhenius line. The associated literature data reported by Szablan *et al.*²⁰⁴ are represented by the dashed line.

The k_p values from the novel SP-PLP-EPR experiment are estimated to be accurate within $\pm 15\%$. This uncertainty includes the effect of small radicals, up to about $i = 5 - 10$, which may propagate faster than long-chain radicals. As the maximum chain lengths within our studies are 384 and 528 for 30 and 60 °C, respectively, the impact of the higher k_p for very small radicals,⁸⁷ does not significantly affect the measured k_p values. They may be looked upon as typical long-chain k_p data. The maximum chain lengths were calculated according to eq (2.41) at the time the radical concentration reaches the baseline.

6.2.3 Termination Kinetics of DBI

Within the time range covered by the SP-PLP-EPR experiment, chain lengths above $i = 300$ are reached, which are considered to be sufficiently long to allow for the analysis of CLDT. The early SP-PLP-EPR work into CLDT of DBI was on the basis of the simplified expression, i.e., eq (2.36).¹¹⁶

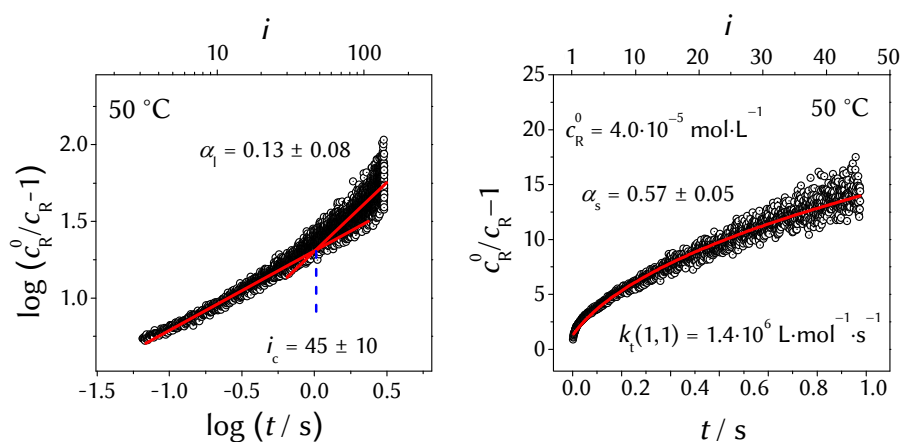


Figure 6.13: Determination of composite-model parameters for a DBI bulk polymerization at 50 °C according to eq (2.40) (l.h.s.) and eq (2.42) (r.h.s.). The analysis provides α_s , α_l , i_c and $k_t(1,1) \cdot c_R^0$. With the initial radical concentration, c_R^0 , being known from calibration, $k_t(1,1)$ is directly accessible. The underlying radical concentration vs time data is identical to the ones used for k_p determination, but is restricted to the range $i < i_c$ for the linear plot (r.h.s.).

The composite-model parameters for the temperature range 30 to 60 °C were determined by the introduced two-step procedure illustrated for 50 °C in Figure 6.13. The so-obtained quantities α_s , i_c and α_l are plotted in Figure 6.14. No temperature dependence is seen for α_s and α_l . The temperature-averaged values $\alpha_s = (0.57 \pm 0.05)$ and $\alpha_l = (0.17 \pm 0.08)$ are as expected from theory.^{90,94,96,98,143,175} The crossover chain length $i_c = (45 \pm 10)$ is identical with $i_c(\text{TMAEMA})$ and hence well below the one found for methyl methacrylate, $i_c(\text{MMA}) = 100$,¹¹⁷ as well as for vinyl pivalate, $i_c(\text{VPi}) = 110 \pm 30$.⁴² It is close to the numbers for vinyl acetate, $i_c(\text{VAc}) = 20 \pm 10$,⁴² methyl acrylate, $i_c(\text{MA}) = 35 \pm 10$,⁴¹ and for styrene, $i_c(\text{Sty}) = 30 \pm 10$,¹⁰⁰ and is slightly below the butyl acrylate value of $i_c(\text{BA}) = 65 \pm 20$.³⁷ During our earlier EPR investigations into CLD k_t , an i_c value of about 45 has been found,¹¹⁶ which is in perfect agreement with the number from the present study, underlining the reliability of data obtained from SP-PLP-EPR.

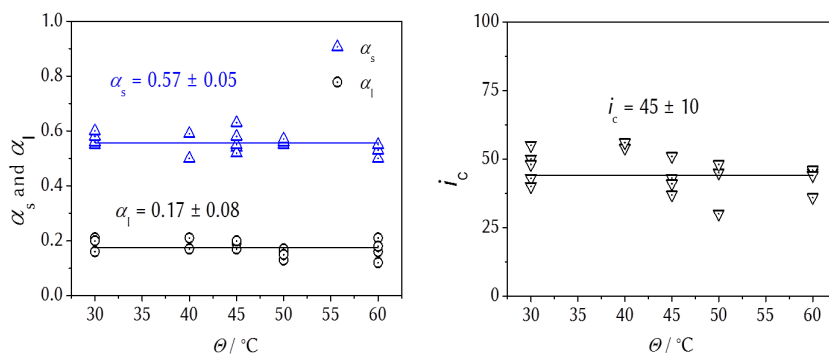


Figure 6.14: Composite-model parameters α_s , α_l and i_c for DBI bulk polymerization between 30 and 50 °C derived from SP-PLP-EPR data via eq (2.40) and to eq (2.42) (see Figure 6.13).

The activation energy for $k_t(1,1)$ deduced from the DBI data presented in Figure 6.15, $E_A(k_t(1,1)) = 19.8 \text{ kJ}\cdot\text{mol}^{-1}$, is close to the activation energy of the fluidity of DBI: $E_A(\eta^{-1}) = 20.5 \pm 0.3 \text{ kJ}\cdot\text{mol}^{-1}$. The experimental $k_t(1,1)$ values which obey the relationship

$$\ln(k_t(1,1)/\text{L}\cdot\text{mol}^{-1}\cdot\text{s}^{-1}) = 21.6 - 2381\cdot(T^{-1}/\text{K}^{-1})$$

are however far below the numbers estimated for the diffusion limit, i.e., from eq (2.32). This lower values for $k_t(1,1)$ points at the strong steric impact, which makes a high fraction of encounters between radicals inefficient for termination.

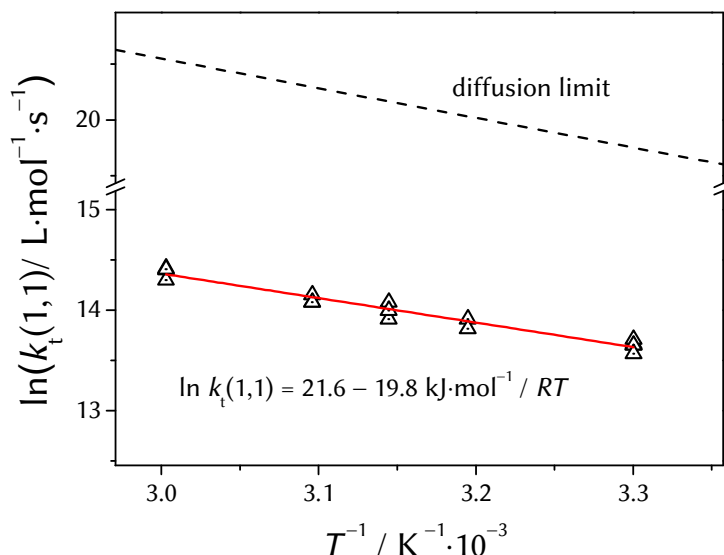


Figure 6.15: Arrhenius-type plots of the rate coefficient for termination of two monomeric radicals, $k_t(1,1)$, in DBI homopolymerization. The dashed line represents the diffusion-controlled limiting value of $k_t(1,1)$ estimated from $k_t(1,1) = 1/3 \cdot RT/(\eta(T))$ (eq (2.31)) via the separately measured value of $E_A(\eta^{-1}) = 20.5 \pm 0.3 \text{ kJ mol}^{-1}$.

As detailed in Sections 4 and 5, the combined quantity $k_t(1,1) \cdot \eta$ allows for an analysis of termination kinetics in terms of structural properties of the monomeric radical. The experimental $k_t(1,1) \cdot \eta$ values, with $k_t(1,1)$ from SP-PLP-EPR and η from viscosity measurements, are summarized for a series of monomers at 80 °C in Table 6.7. Because of the similarity of the activation energies of $k_t(1,1)$ and of fluidity, the numbers should, to a good approximation, also apply to other polymerization temperatures. For the smallest members of the acrylate and methacrylate families, i.e., for methyl acrylate and methyl methacrylate, as well as for vinyl acetate, acrylamide, methacrylic acid and styrene, this product is in the range of $k_t(1,1)(80 \text{ °C}) \cdot \eta(80 \text{ °C}) = (3.4 \pm 0.3) \cdot 10^8 \text{ L}\cdot\text{mPa}\cdot\text{mol}^{-1}$ and is by less than a factor of approximately 2 below the diffusion-controlled value. This value holds irrespective of termination taking place in bulk or in aqueous solution at different weight percentages. This remarkable agreement of $k_t^{1,1} \cdot \eta$ values is indicative of diffusion-controlled termination in the initial polymerization period in case of similar ratios of R_c to r_1 of these small

monomeric radicals. Upon increasing bulkiness, e.g., in passing to vinyl pivalate and to *tert*-butyl methacrylate, $k_t^{1,1} \cdot \eta$ is reduced by about a factor of three to $k_t(1,1)(80\text{ °C}) \cdot \eta(80\text{ °C}) = (1.35 \pm 0.30) \cdot 10^8 \text{ L}\cdot\text{mPa}\cdot\text{mol}^{-1}$, which indicates an enhanced shielding of the radical functionality that may be expressed in terms of a lower value for the ratio R_c/r_1 .¹⁰⁹ With the results from this work, the product for DBI is further reduced, to $k_t(1,1)(80\text{ °C}) \cdot \eta(80\text{ °C}) = (0.04 \pm 0.01) \cdot 10^8 \text{ L}\cdot\text{mPa}\cdot\text{mol}^{-1}$ thus pointing at the enormous shielding effect in case of termination of two DBI radicals.

Table 6.7: Comparison of $k_t(1,1)\cdot\eta$ values for bulk polymerizations of several monomers. Compared to Table 5.3 and Table 4.2 the line for DBI has been updated and numbers for SPRs and MCRs of butyl acrylate (BA, entry 5 and 12) have been included. Unless otherwise state, the values refer to bulk polymerization and homo-termination of end-chain radicals, i.e., $k_t^{ss}(1,1)$, respectively. For more details, see text and Table 4.2.

	Monomer System	$k_t(1,1)(80\text{ °C})\cdot\eta(80\text{ °C})$ / $\text{L}\cdot\text{mPa}\cdot\text{mol}^{-1}\cdot 10^8$	Ref.
1	AAm (10 wt.%/H ₂ O)	3.3	this work
2	AAm (20 wt.%/H ₂ O)	3.2	this work
3	Sty	3.2	this work
4	BA	3.3	41
5	VAc	3.6	42
6	MMA	3.7	117
7	MA	3.7	41
8	VPi	1.4	42
9	<i>tert</i> -BMA	1.3	118
10	DBI	0.04	this work
11	BA ($k_t^{tt}(1,1)$) ^{a)}	0.07	70

a) Homo-termination of mid-chain radicals

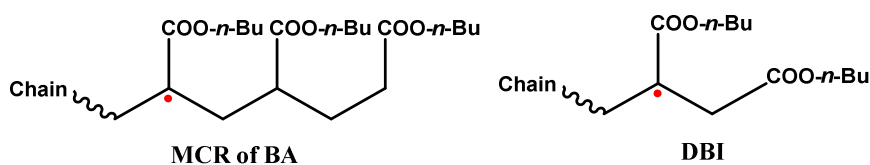


Figure 6.16: Comparison of the structures of mid-chain radicals in *n*-butyl acrylate polymerization and of DBI radicals, which illustrates the structural similarities of these two radical species.

Midchain radicals (MCRs), as are occurring in acrylate and acrylamide polymerization due to intramolecular [1,5]-H-transfer (backbiting) processes of secondary chain-end radicals, also exhibit a significant steric crowding close to the site of the tertiary radical functionality. The structure of the BA MCR is given in Figure 6.16 together with the one for the DBI radical. The termination rate coefficient for such MCRs, k_t^{tt} , has been measured for the polymerization of butyl acrylate in toluene (1.5 M).⁷⁰ For the BA midchain radical $k_t^{tt}(1,1) \cdot \eta$ has been found to be around $0.07 \cdot 10^8 \text{ L} \cdot \text{mPa} \cdot \text{mol}^{-1}$ at 80°C (entry 12 in Table 6.7). It goes without saying that the coefficient $k_t^{tt}(1,1)$ refers to a hypothetical MCR of chain length unity, which should be looked upon as a composite-model parameter. The term $k_t^{tt}(1,1) \cdot \eta$ turns out to be rather similar for both the DBI radical and for a butyl acrylate MCR and may allow for transferring kinetic data from DBI radicals to MCR-homo-termination in acrylate or even acrylamide polymerization, which are not easily obtained otherwise.

6.3 Closing Remarks

The novel SP–PLP–EPR-based method is suitable for investigating the propagation kinetics and is complementary to PLP–SEC for systems close the low-termination limit. The reliability of the deduced k_p values depends on the EPR signal quality and on the accuracy of conversion determination. If only one radical species is present in the system, the following aspects should be considered for reliable k_p data.

- 1.) The S/N quality of the final radical concentration vs time profile, i.e., after co-addition of several individual traces, should be as high as with DBI and TMAEMA.
- 2.) The illumination of the sample should be complete in order to avoid dilution effects in the cell which may result in an underestimation of k_p . This criterion is fulfilled with the used EPR setup.

- 3.) At an initial radical concentration of $10^{-5} \text{ mol}\cdot\text{L}^{-1}$, the conversion induced by the addition of primary radicals to monomer should be taken into account when the monomer-to-polymer conversion per pulse is below 1 %.

As stated earlier, the data analysis is more difficult if two propagating radicals coexist during the polymerization as with TMAEA polymerization (Section 8) for which high fractions of MCRs were observed. In this particular case, the assignment of conversion to one radical species is challenging. The EPR data and the conversion should be analysed by using a PREDICI[®] model which includes the entire set of relevant rate coefficients (Section 8).

Termination Kinetics of Sodium Methacrylate

The investigations into CLDT carried out so far refer to polymerizations of non-ionized radicals in organic phase or in aqueous solution. The previously presented studies into the aqueous-solution polymerization of trimethylaminoethyl methacrylate chloride (TMAEMA) suggested that termination rate of equally charged macroradicals should be by a few order of magnitude below the one of non-ionized radicals.¹⁰⁸

The present investigation aims at providing a comprehensive set of kinetic data for the CLDT of fully-ionized radicals. Sodium methacrylate (NaMAA) was chosen as the fully ionized monomer for this first study in concentrations of 5 wt.% and 10 wt.%. The propagation kinetics of NaMAA has already been reported by Lacík and coworkers.³⁵

7.1 The EPR Spectrum in NaMAA Polymerization

The experimental EPR spectrum for 10 wt.% of NaMAA in H₂O at 60 °C is given in Figure 7.1 along with the associated simulation. The spectrum is entirely due to propagating tertiary radicals^{205,206} and has to be interpreted in terms of the coexistence of conformers.¹⁹⁰ The presence of energetically favoured conformers stabilized by hindered internal rotation around the C_α-C_β single bond in the backbone is indicated by the simulation using the individual spectra of the two conformers (blue and green) shown in the

lower part of Figure 7.1. The overall simulation presented in red results from co-addition of the individual spectra with 61% of conformer A and 39% of conformer B. The two conformers differ in dihedral angle, θ , and in the hyperfine coupling constants (hfcc), $a(\text{H})$, of the β -methylene protons, $a(\beta\text{-H})$, according to the Heller-McConnel equation (eq (5.1)).^{172,190,191} The proportionality factor, A , i.e., the maximum value for $a(\beta\text{-H})$ at $\theta = 0^\circ$, may be estimated from the averaged hfcc for the equivalent α -methyl protons, i.e., $A(\beta\text{-H}) = 2 \cdot a(\alpha\text{-H})$.¹⁶⁴ The numbers for the three equivalent methyl protons and for the two non-equivalent β -methylene protons were determined by simulation and are listed in Table 7.1 for the highest and lowest temperature under investigation. No temperature dependence of $a(\text{H})$ is observed whereas the fraction of conformer A decreases slightly from 61 to 54 percent upon lowering the temperature from 60 to 5 °C which indicates a higher potential energy for conformer A compared to conformer B.¹⁹⁰ The decrease in the fraction of conformer A is equivalent to a decrease of relative intensity of the inner eight lines, indicated by asterisk symbols (*) in Figure 7.1, which are exclusively due to conformer A. The hfcc and the relative amounts of the two conformers do not vary significantly at monomer contents of 5 and 10 wt.%. The proportionality factor, $A(\beta\text{-H}) = 43.2 \text{ G}$, allows for an estimation of the dihedral angles for the two conformers, θ and θ' , which slightly deviate, by about 4° , from the ideal angle of 120° between the two β -methylene protons (Table 7.1). The occurrence of 16 overall lines along with 8 inner lines (16/8-system) has not been observed with methyl methacrylate radicals (13/9-system) but with the non-ionized methacrylic acid (MAA) and *tert*-butyl methacrylate.^{189,191} The reported hfcc for MAA, i.e., $a(3\text{H}, \alpha\text{-H}) = 22.3 \text{ G}$, $a(1\text{H}, \beta\text{-H}) = 17.9 \text{ G}$ and $a(1\text{H}, \beta\text{-H}) = 7.3 \text{ G}$, are in close agreement with the ones for conformer A (Table 7.1) indicating a more symmetric position of the β -methylene protons for MAA toward the single-occupied p-orbital.²⁰⁶

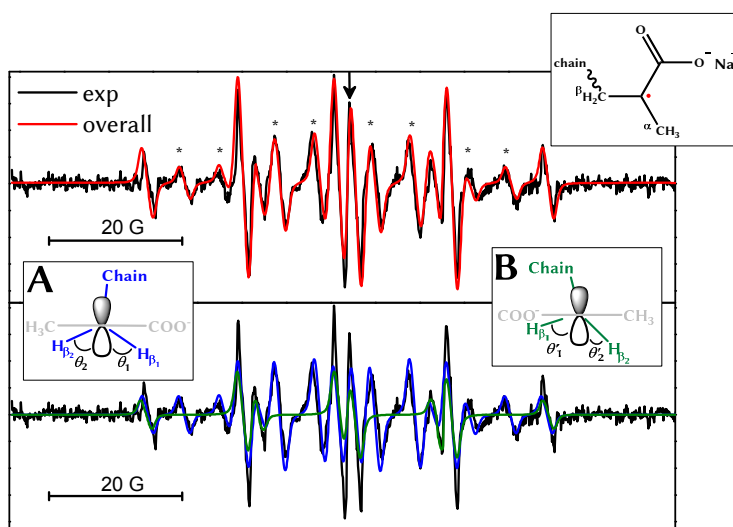


Figure 7.1: Experimental (black line) and simulated (red line) EPR spectra of propagating NaMAA radicals of 10 wt.% monomer in aqueous solution at 60 °C. The spectra were recorded under stationary UV irradiation with Darocur[®] (2.1 mmol·L⁻¹) as the initiator. The EPR spectrum is assigned to the two conformers A (blue) and B (green) contributing to the overall simulated spectrum (red) to 61 and 39 percent, respectively. The hfc used for the simulations of the overall spectrum are listed in Table 7.1. The magnetic field position used for the SP-PLP-EPR experiments is indicated by the arrow. The eight inner lines which are exclusively due to conformer A are indicated by the asterisk symbols (*).

Table 7.1: Hyperfine coupling constants $a(\text{H})$ deduced from the experimental EPR spectra of propagating NaMAA radicals (Figure 7.1) for the lowest and the highest temperature under investigation.

	Conformer A			Conformer B	
$a(\text{H}) / \text{G}$	21.6 (3H, H _α)	17.3 (1H, H _{β1})	6.8 (1H, H _{β2})	25.3 (1H, H _{β1})	0.2 (1H, H _{β2})
$\theta / ^\circ$	freely rotating	50.7	63.5	40.0	84.5

7.2 SP–PLP–EPR Investigations into the Termination Kinetics

7.2.1 Time-resolved EPR Profiles

The arrow in Figure 7.1 indicates the magnetic field position used for the SP–PLP–EPR study. The concentration vs time trace of NaMAA radicals as obtained by a SP–PLP–EPR experiment are shown in Figure 7.2 for three temperatures and initial monomer concentrations of 5 wt.% and 10 wt.%. The impact of monomer-to-polymer conversion was found to be negligible. Because of the low solubility of Darocur[®] in solution of NaMAA, the radical concentration after the laser pulse is lower by a factor of two compared with TMAEMA polymerization (Section 6.1.2) and thus the conversion after a sequence of laser pulse was too low to be accurately determined. Up to 30 individual profiles had to be co-added in order to enhance the signal quality. The so-obtained data reveals three remarkable trends which have not been reported for non-ionized monomers, at least not to a comparable extent. First, the radical life-time exceeds the one of non-ionized radicals, which is typically around a few milliseconds, by several orders of magnitudes.^{42,100,117} Similar observations have been made with TMAEMA radicals in aqueous solution. They were attributed to electrostatic repulsion during the termination process.¹⁰⁸ Second, no variation of termination rate with temperature is seen which, at first glance, appears to be counter-intuitive for diffusion-controlled termination. This similarity indicates the importance of CLD termination with NaMAA polymerization. The enhancement of diffusivity upon increasing temperature is, at least partially, compensated by the larger chain length associated with the higher propagation rate at increased temperature. Note that in Figure 7.2, the chain lengths of the radicals at a given time vary between the different profiles due to temperature.

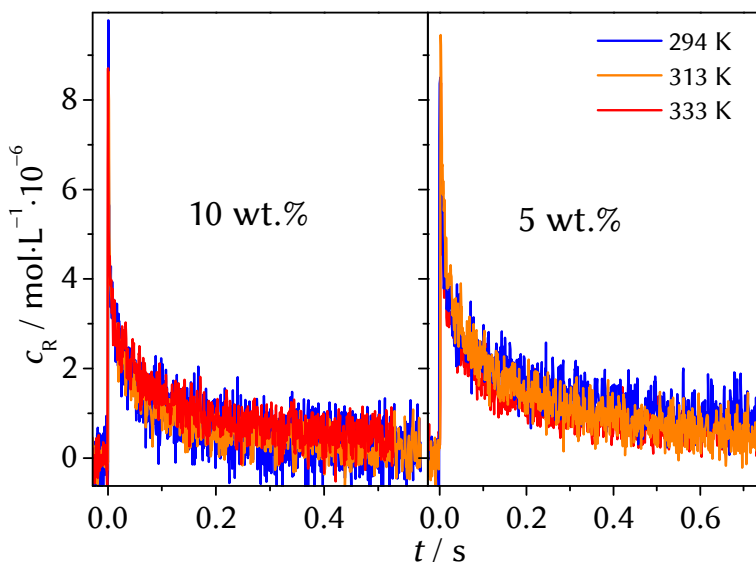


Figure 7.2: Absolute radical concentration vs time profiles for NaMAA radicals at three temperatures for 5 and 10 wt.% monomer. The data for 278 K were not included into the figure due to reasons of clarity.

Third, the direct comparison of primary data for 5 and 10 wt.% monomer (Figure 7.3) reveals a higher termination rate for the more viscous system which is in contrast to what has been reported for non-ionized radicals where $k_t(1,1)$ was observed to scale with fluidity, i.e., with inverse viscosity.¹⁰⁹ The viscosity of an aqueous solution containing 10 wt.% NaMAA exceeds the one of a solution with 5 wt.% NaMAA by 20 percent (see Appendices). Because of higher monomer concentration and enhanced k_p upon increasing NaMAA concentration, as reported by Lacík and coworkers for NaMAA concentrations below 20 wt.%, larger macroradicals are produced at 10 wt.% monomer. Thus CLD termination would offer no explanation for the higher k_t at higher NaMAA concentration.

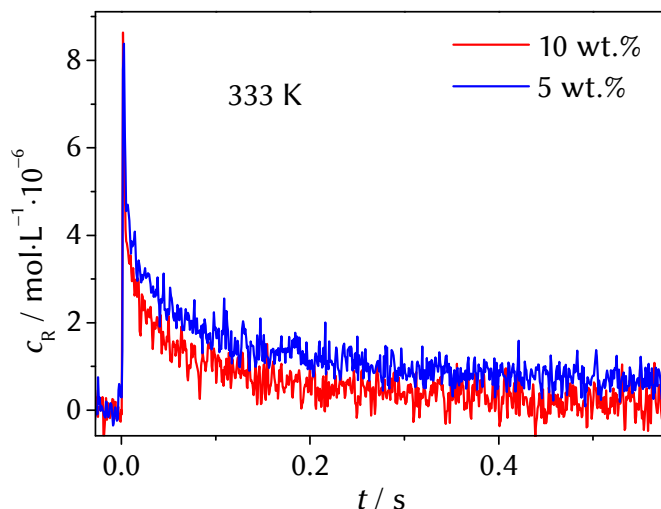


Figure 7.3: Comparison of absolute radical concentration vs time profiles measured during SP–PLP–EPR experiments on NaMAA at 5 and 10 wt.% monomer in aqueous solution at 333 K. The profiles are already contained among the ones shown in Figure 7.2. The purpose of this figure is to highlight the unexpected effect of monomer concentration on the termination kinetics of NaMAA in aqueous solution.

7.2.2 Analysis of Termination Kinetics

The linear correlation of time after laser pulsing with the chain length of propagating radicals (eq (2.36) and eq (2.41)) enables an analysis of the SP–PLP–EPR traces for CLD k_t on the basis of the Composite Model. The four parameters of this model are deduced by a two-step procedure as described for styryl radicals in Section 4.2. First, the crossover chain length i_c and the power-law exponent α_1 are determined from a double-log plot of the EPR-derived relative radical concentrations measured as a function of time t after pulsing, according to eq (2.40). This plot is shown in Figure 7.4. The slope of the straight-line fit at large t yields $(1-\alpha_1)$ and thus α_1 . The chain length at the intersection of the two straight directly provides the crossover chain length i_c .^{41,100,116}

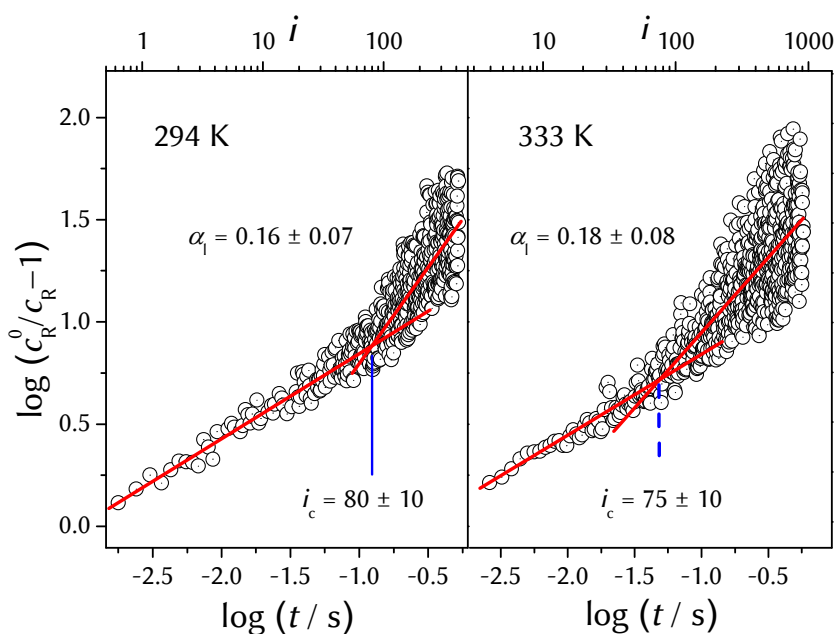


Figure 7.4: Double-log plot of relative radical concentration for NaMAA (10 wt.%) polymerization in aqueous solution at 21 °C and 60 °C. The intersection point of the two fitted lines and the slope to the straight line for large chain lengths yields the composite-model parameters i_c and α_1 , respectively.

This kind of data treatment yields no values for i_c and α_1 of 5 wt.% NaMAA solutions as is shown in Figure 7.5 for the highest temperature under investigation, i.e., 60 °C, and thus for the largest chain lengths. Only a single line may be fitted to the data for chain lengths up to 297 at 333 K which allows for no accurate measurement of i_c and α_s . The exponent deduced from the fit suggests that only the short-chain region has been investigated. The reason may be due to the fact that only a smaller chain-length region is observed at the lower monomer concentration compared to 10 wt.% which makes the determination of i_c more difficult. Moreover, the structure of the macroradicals at 5 wt.% might be more "rode-like" because of the lower counter-ion concentration in the solution. However, no indication for different degrees of internal mobility are observed in the EPR spectra for the lowest and the highest measurable monomer concentrations, i.e., 5 and 10 wt.%, between 5 and 60 °C. The addition of small amounts of sodium chloride, which might enhance chain flexibility, could not be tested because of a break-down of critical coupling.

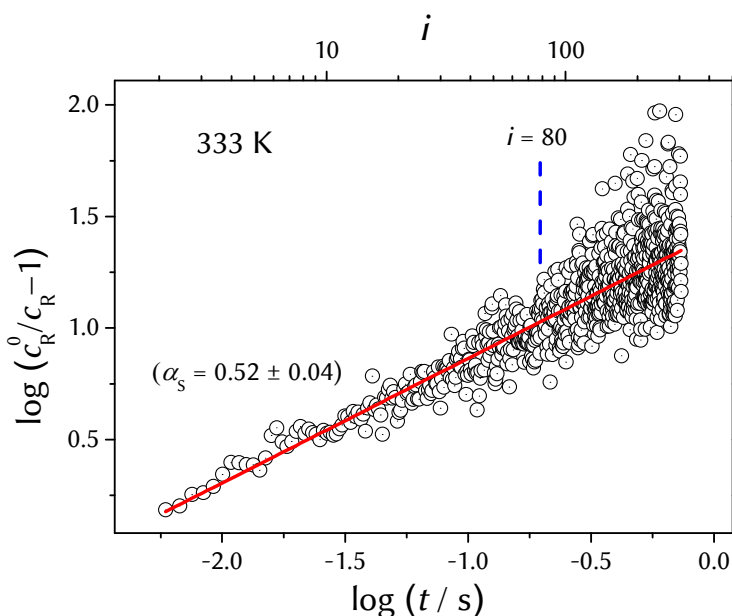


Figure 7.5: Double-log plot of relative radical concentration for NaMAA (5 wt.%) polymerization in aqueous solution at 60 °C. No intersection point and hence no values for i_c and α_1 are observed at this monomer content. The number of i_c found with 10 wt.% is denoted. The regime under investigation can be assigned to short chains, i.e., to $i < i_c$, as indicated by $i_c = 80$.

Within the early time regime at chain lengths below i_c , eq (2.41) provides a more adequate description than eq (2.36).¹⁰³ Thus eq (2.42) is the preferable option for deducing α_s and $k_{t(1,1)} \cdot c_R^0$.⁴¹ The fit of the experimental data for chain lengths below i_c is shown for 10 wt.% NaMAA at 60 °C in Figure 7.6.

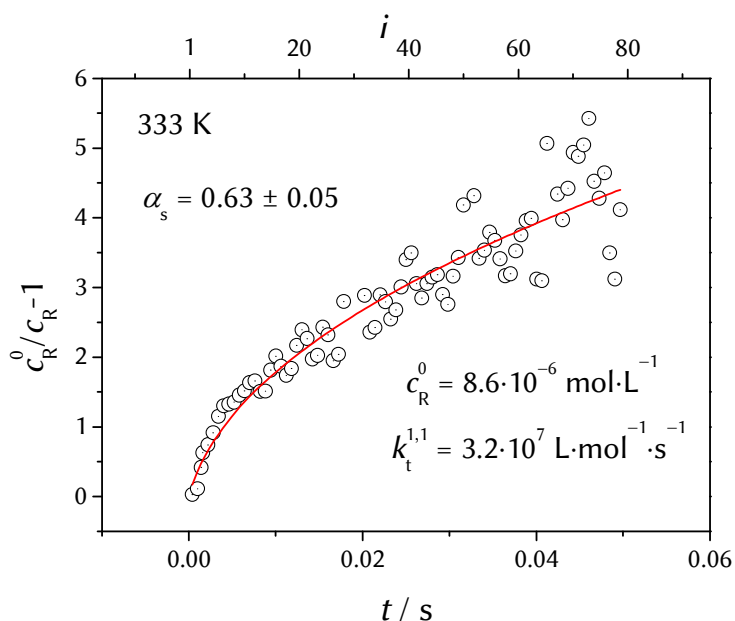


Figure 7.6: Plot of relative radical concentration for NaMAA (10 wt.%) polymerization in aqueous solution at 60 °C according to eq (2.42).

No calibration is required for the plots in Figure 7.4 to Figure 7.6 as EPR signal intensity is proportional to radical concentration. The initial radical concentration, c_R^0 , needs, however, to be known for deducing $k_t(1,1)$ from $k_t(1,1) \cdot c_R^0$.

Illustrated in Figure 7.7 are the composite-model exponents for the experimental temperature range. No variation with temperature is observed for either α_s or α_l . The arithmetic mean value is found to be: $\alpha_l = 0.18 \pm 0.05$ for 10 wt.% NaMAA. The power-law exponents for small chain lengths are: α_s (5 wt.%) = 0.62 ± 0.05 and α_s (10 wt.%) = 0.56 ± 0.05 . In view of the experimental uncertainty it appears justified to determine an overall power-law exponents for the two NaMAA concentrations under investigation: $\alpha_s = 0.59 \pm 0.08$ which together with α_l (10 wt.%) fully meet the expectations from theory and are both close to the numbers measured for non-ionized radicals with the radical functionality being located at the chain-end.^{41,95}

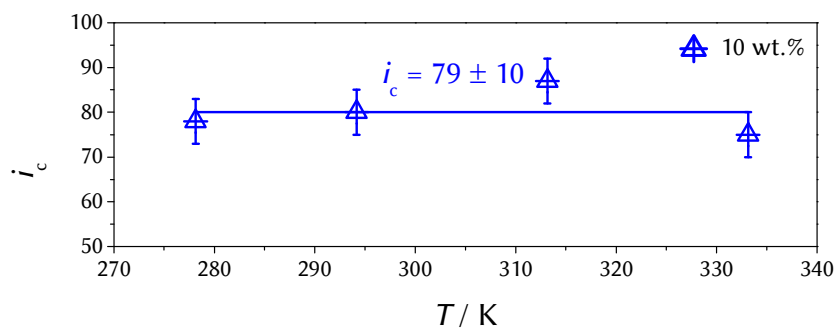


Figure 7.8: Individual and arithmetic mean values (full line) of i_c for 10 wt.% NaMAA determined for the polymerization temperatures under investigation.

NaMAA differs from MAA by a lower termination rate which allows for an accurate determination of i_c . Wittenberg *et al.* performed batch polymerizations with 30 wt.% MAA and estimated $i_c = 68$, which is not that dissimilar from the number for NaMAA, obtained under chain-length control by 2-mercaptoethanol.²⁰⁸

The obtained rate coefficients of termination for two monomeric radicals are illustrated by the Arrhenius plot in Figure 7.9. The associated Arrhenius expressions read

$$\ln(k_t(1,1)/\text{L}\cdot\text{mol}^{-1}\cdot\text{s}^{-1}) = 19.1 - 999 \cdot (T^{-1}/\text{K}^{-1})$$

for 5 wt.% NaMAA in aqueous solution

and

$$\ln(k_t(1,1)/\text{L}\cdot\text{mol}^{-1}\cdot\text{s}^{-1}) = 20.4 - 1049 \cdot (T^{-1}/\text{K}^{-1})$$

for 10 wt.% NaMAA in aqueous solution.

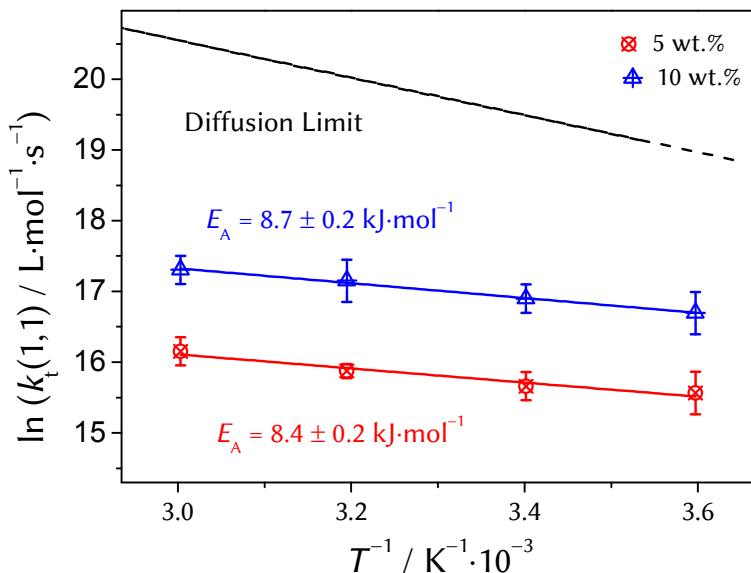


Figure 7.9: Arrhenius plot of $k_t(1,1)$ for 5 and 10 wt.% along with the Smoluchowski diffusion limit calculated on the basis of $k_t(1,1) = 1/3 \cdot R \cdot T \cdot \eta^{-1}$ via the separately measured activation energy of fluidity for 10 wt.%, $E_A(\eta^{-1}) = 20.3 \text{ kJ} \cdot \text{mol}^{-1}$.

The activation energies for both monomer concentrations are close to each other: $E_A(k_t(1,1)) = 8.7 \text{ kJ} \cdot \text{mol}^{-1}$ for 10 wt.% and $E_A(k_t(1,1)) = 8.4 \text{ kJ} \cdot \text{mol}^{-1}$ for 5 wt.%, which is well below the associated activation energies of fluidity, $E_A(\eta^{-1}) = 20.3 \text{ kJ} \cdot \text{mol}^{-1}$ and $E_A(\eta^{-1}) = 19.4 \text{ kJ} \cdot \text{mol}^{-1}$ at 10 and 5 wt.% NaMAA. The assumption that $E_A(\eta^{-1}) = E_A(k_t(1,1))$ which has been suggested to be a universal relationship for termination of non-ionized species in organic and aqueous phase (see Sections 4.4, 5.2 and 6.2.3) does not hold for NaMAA between 5 and 10 wt.%.¹⁰⁹ Moreover, the relatively low activation energies for both k_p and $k_t(1,1)$ give rise to the similarity of radical concentration vs time profiles from SP–PLP–EPR shown above. The absolute values of $k_t(1,1)$ for 5 and 10 wt.% demonstrate that the higher termination rate for the more viscous system, i.e., 10 wt.%, is not an artefact resulting from CLD k_t . The values for both concentrations differ in total by approximately a factor of 3 while fluidity varies by about 20 % in the opposite direction (see Appendices). In

comparison to non-ionized species, $k_t(1,1)$ of NaMAA is reduced by several orders of magnitude. In particular, compared to 10 wt.% of non-ionized MAA in aqueous solution, $k_t(1,1)$ of 10 wt.% NaMAA is lower by two orders of magnitude at 333 K while with "hindered" di(*n*-butyl) itaconate radicals in bulk DBI polymerization, $k_t(1,1)$ is higher by a factor of 17 (see Section 6.2.3). Note that $E_A(k_t(1,1))$ for DBI and MAA with around 20 kJ·mol⁻¹ are far higher than for NaMAA. Thus the differences in $k_t(1,1)$ between these monomers vary with temperature, but $k_t(1,1)$ of NaMAA stays in between these $k_t(1,1)$ values of the non-ionized species under typical polymerization temperatures.

Taking all these findings into account, one may conclude that termination of NaMAA radicals may not be easily understood in terms of "classical" diffusion control with respect to what is known from non-ionized radicals. Describing the low activation energies of monomeric radical termination, intermolecular electrostatic interactions should be considered as dominant. It goes without saying that termination between two equally charged species, i.e., the MAA⁻-radicals, has to be mediated by counter ions to ensure the encounter event and thus enable the termination process. It is assumed that in order to accomplish the mediating role, the ions have to be located in the immediate vicinity of the radicals.²⁰⁹ In aqueous solution the situation is complex in that a dynamic equilibrium of different types of ions may be assumed which can be described to some extent by the simplified scheme (Figure 7.10) containing three species, i.e., contact-ion pairs, solvent-separated and free ions.

The species differ in terms of ion distances and hence in the strength of electrostatic interactions. It is obvious that termination is more likely for the electronically neutral contact-ion pair than for the free ions which, in terms of the Smoluchowski equation (eq (2.31)), may be assigned to an enhanced capture radius and a lower hydrodynamic radius for the counter-ion pair. On the other hand, the free ions provide large electric conductivity. Thus, the equilibrium constant, K , according to Figure 7.10 may be determined by conductivity measurements. The experiments by P. Drawe for acrylic acid indicate that increasing temperature in the range from 5 to 60 °C favours the formation of free ions.^{107,209} As a consequence, the low $E_A(k_t(1,1))$ is the result of the competition between self-diffusion and the ion dissociation with a related activation energy and enthalpy of $E_A(\eta^{-1}) \approx 20$ kJ·mol⁻¹ and $\Delta H(K) = (15 \pm 3)$ kJ·mol⁻¹, respectively.¹⁰⁷ The addition of salt shifts the equilibrium toward the contact-ion pairs and thus enhances $k_t(1,1)$ which may in principle be experimentally tested. As mentioned above, the addition of small amounts of sodium chloride causes a break-down of critical coupling and thus impedes EPR measurements.

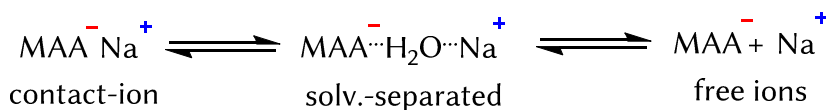


Figure 7.10: Illustration of the proposed dynamic equilibrium in aqueous solution of a weak electrolyte, e.g, NaMAA, between different species: contact-ion pairs, solvent-separated and free ions. For a more detailed description see text.

The addition of monomer, i.e., upon passing from 5 to 10 wt.% NaMAA, shifts the equilibrium, as additional sodium chloride does which is seen from the higher termination rate in 10 wt.% NaMAA polymerization. It might be interesting to see whether the observed effect of monomer concentration is also seen with strong electrolytes, e.g., 2-acrylamido-2-methylpropanesulfonic acid (AMPS), for which only a negligible fraction of counter-ion pairs are present.¹¹⁵

7.3 Diffusion-controlled Termination of fully-ionized Radicals

If *steric* effects are *absent*, the termination kinetics of radicals may be interpreted in the light of the Smoluchowski-Stokes-Einstein equation (eq (2.32)). The so-obtained expression for the diffusion limit defines the highest possible value for k_t since termination is assumed whenever two spherical radicals encounter. This expression may thus be valid for radical atoms which can be characterized by a radial-symmetric distribution of spin density.

$$k_t(1,1) = \frac{R \cdot T}{3 \cdot \eta} \quad (2.32)$$

Eq (2.32) highlights the discussed fundamental correlation between $k_t(1,1)$ and viscosity, i.e., $k_t(1,1) \cdot \eta \approx \text{const}$, meaning that viscosity determines the changes in $k_t(1,1)$, e.g., upon varying monomer content and temperature. The finding that $k_t(1,1)$ scales with η^{-1} and not with $T \cdot \eta^{-1}$ (see Figure 4.10) might be due to the fact that Stokes-Einstein equation is not strictly valid since the radius of the radical is not significantly higher than the radius of the solvent molecules.⁹³

For *substituted non-ionized* radicals, a shielding of the radical functionality is observed which reduces the probability for termination. As could be shown in Figure 4.7, Figure 6.15 and Table 5.3, the impact of side groups reduces $k_t(1,1)$ systematically by a constant factor, i.e., $k_t(1,1) \cdot \eta$ remains constant. Thus the impact of shielding is temperature independent and may be expressed by the ratio of capture radius and hydrodynamic radius, R_c/r_1 , taking into account that only a fraction of the hydrodynamic radius is effective for termination.

$$k_t(1,1) = \frac{R \cdot T}{6 \cdot \eta} \cdot \frac{R_c}{r_1} \quad (2.31)$$

For *fully-ionized* NaMAA radicals, lower $k_t(1,1)$ values are observed as with non-ionized species. In addition, the empirical $k_t(1,1) \cdot \eta$ relation breaks down, although the diffusion of fully-ionized radicals obeys the Stokes-Einstein relationship to the same extent as non-ionized species do.^{210,211} The observed deviation from the classic termination behavior, i.e., $E_A(k_t(1,1)) < E_A(\eta^{-1})$ and $k_t(1,1)$ (10 wt.%) $>$ $k_t(1,1)$ (5 wt.%), might be understood in terms of a modified Smoluchowski-Stokes-Einstein equation. Since R_c and r_1 may change simultaneously with temperature and monomer content in the fully-ionized case, R_c/r_1 should be replaced by a single quantity f being the *microfriction*^{78,93} of termination reaction which is 1 for the diffusion limit, e.g., for spherical radicals, yielding eq (2.32) and should be higher but still temperature independent for non-ionized species. For ionized species the electrostatic interactions are captured by $f \gg 1$ with f being a function of the dielectric constant of the solvent, ϵ_{sol} , the charge of the radical and of the counter ion, z_{rad} and z_{Cl} , and for weak electrolytes of the equilibrium constant, K . Thus f is a temperature dependent for fully-ionized radical species (eq (7.1)).

$$k_t(1,1) = \frac{R \cdot T}{3 \cdot \eta} \cdot \frac{1}{f(\epsilon_{\text{sol}}, z_{\text{rad}}, z_{\text{Cl}}, K)} \quad (7.1)$$

For 5 and 10 wt.% NaMAA, the following expressions for f are obtained from the difference between the measured and the diffusion-limited values (eq (2.32)):

$$\ln(f) = 10.0 - 1646 \cdot (T^{-1}/K^{-1}) \quad (5 \text{ wt.}\% \text{ NaMAA})$$

$$\ln(f) = 7.8 - 1492 \cdot (T^{-1}/K^{-1}) \quad (10 \text{ wt.}\% \text{ NaMAA})$$

In the light of the discussion in Section 7.3 it comes as no surprise that the associated activation energies, i.e., $E_A(f) = 13.7 \text{ kJ}\cdot\text{mol}^{-1}$ for 5 wt.% NaMAA and $E_A(f) = 13.2 \text{ kJ}\cdot\text{mol}^{-1}$ for 10 wt.% NaMAA, are close to $\Delta H(K) = (15 \pm 3) \text{ kJ}\cdot\text{mol}^{-1}$. It is obvious that a similar behavior, i.e., $E_A(k_t(1,1)) \neq E_A(\eta^{-1})$, should be observed with other weak electrolytes. In case of MCRs being present, f should be lower for MCRs than with SPRs.

The direct comparison of $k_t(1,1)$ data between different types of radicals, e.g., between acrylate and methacrylate radicals, allows in principle for investigating the impact of radical structure on termination. However, such a comparison is only expedient if the compared systems exhibit similar viscosities. Since η may change significantly within a homologous series of monomers, it is advisable to use the presented quantity $k_t(1,1)\cdot\eta$, as long as the precondition $E_A(k_t(1,1)) \approx E_A(\eta^{-1})$ holds. The description in terms of microfriction is considered to be universally applicable, i.e., for fully-ionized species with $E_A(k_t(1,1)) \neq E_A(\eta^{-1})$ as well as for the non-ionized case. The analysis of $k_t(1,1)$ data via eq (7.1) in further studies of fully-ionized species may facilitate the systematic discussion of steric effects in termination processes and may thus allow for the estimate of $k_t(1,1)$ on the basis of easily accessible viscosity data.

Propagation, Termination and Transfer Kinetics of TMAEA

The beauty and power of the SP-PLP-EPR technique in radical polymerization rests on the ability of monitoring the active species, i.e., the radicals, with high time resolution. It comes as no surprise that in principle all information being necessary for a comprehensive description of polymerization kinetics is included in the recorded concentration vs time profiles. Within this thesis, the full spectrum of SP-PLP-EPR applications, i.e., chain-length dependent termination, transfer and for the first time also propagation kinetics, are demonstrated. So far, the investigation into transfer kinetics was restricted to systems with k_p data being known. It is obvious that the deduction of the entire set of rate coefficients including k_p^s from EPR data is the next step. It is the aim of this section to provide the rate coefficients of termination, backbiting, MCR and SPR propagation for aqueous-solution polymerization of TMAEA (20 wt.%) between 0 °C and 90 °C. The impact of monomer concentration on polymerization kinetics will be investigated by measurements of 10 wt.% TMAEA in aqueous solution at 50 °C. The k_p determination by the novel SP-PLP-EPR approach was restricted to systems with only one radical species being present. The assignment of monomer-to-polymer conversion which is necessary for deducing k_p is however difficult if two propagating radical

species coexist, as is the case for TMAEA polymerization. The problem may be overcome by analyzing the data with PREDICI®.

Although of industrial importance, e.g., for co-polymerizations with acrylamide,²¹² no rate coefficients are available for TMAEA homo-polymerization which may be due to the low terminations rate and intramolecular transfer (backbiting) impeding PLP-SEC investigations so far.

8.1 The EPR Spectrum in TMAEA Polymerization

Figure 8.1 shows the EPR spectra for TMAEA polymerization (20 wt.%) in aqueous solution at 21 and 95 °C recorded under pseudo-stationary conditions with a p.r.r. of 20 Hz which allows for an easy labeling of magnetic field positions assigned to fast terminating end-chain radicals (SPRs) and slowly terminating mid-chain radicals (MCRs). Bands due to SPRs at 21 °C (Figure 8.1, l.h.s.) reflect the applied p.r.r. as highlighted in the framed area due to the laser-induced oscillation in SPR concentration whereas the termination rate of MCRs is usually too small for a significant decay in MCR concentration within the time scale between two subsequent laser pulses. The effect of oscillating SPR concentration is less pronounced at lower SPR fractions, e.g., at higher temperatures, as illustrated by the spectrum for 95 °C (Figure 8.1, r.h.s.) where the SPR contribution to the spectrum is negligible. The positions assigned to SPRs correlate with a quartet hfc pattern of $a(3H) = 20.6$ G. In order to ensure an accurate determination of molar MCR fractions, x_{MCR} , the experiments were carried out under stationary UV irradiation. Two experimental spectra including the associated simulations are given for 0 and 80 °C in Figure 8.2. The simulations reveal a significant contribution of mid-chain radicals even at low temperatures. In agreement with polymerizations of TMAEMA in aqueous solution, a remarkably high S/N quality is achieved which is due to the very high overall radical concentration of $1.38 \cdot 10^{-4}$ mol·L⁻¹ (0 °C) and $1.93 \cdot 10^{-4}$ mol·L⁻¹ (80 °C), respectively. The experimental determination of monomer-to-polymer conversion which relates to the applied sweep time of 5.12 s turned out to be difficult due to the long life-time of TMAEA radicals (see below). Estimates based on an effective rate coefficient of propagation according to eq (2.7) yield numbers for monomer-to-polymer conversion of 60 % and 45 % for the lowest and the highest temperature under investigation, respectively. EPR spectra recorded with either a lower monomer concentration, i.e., 10 wt.%, or a higher sweep time, i.e., yielding higher conversion, but under otherwise identical experimental conditions, did not show any variation in hfc pattern or composition of the spectra.

Thus the impact of conversion on the EPR spectra can be considered as negligible for the presented spectra. The detailed understanding of EPR spectra is essential for systems with two or more species coexisting during polymerizations in order to ensure a correct band assignment due to a complicate band overlap.

8.1.1 Simulation of EPR Spectra in the Presence of MCRs

The simulations of experimental spectra were successful under the assumption of two MCR conformers yielding different hfc patterns (Table 8.1). One MCR conformer, in what follows denoted as MCR3, is a common species in acrylate MCR spectra and results in a triplet hfc pattern.^{165,167–169}

The fraction of MCR3 which decreases from 0.15 at $-5\text{ }^{\circ}\text{C}$ to 0.07 at $95\text{ }^{\circ}\text{C}$ turned out to be well below the fractions reported for butyl acrylate (in bulk and toluene) or for non-ionized acrylic acid polymerizations in aqueous solution.^{39,165,167–169,206}

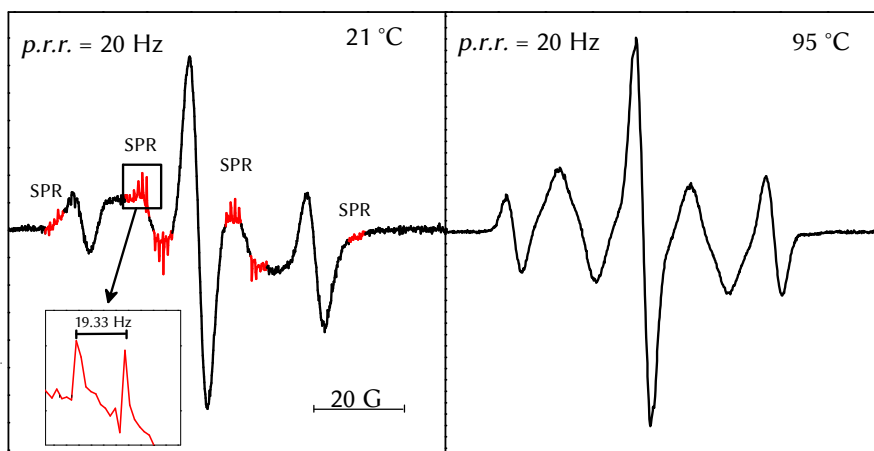


Figure 8.1: EPR spectra recorded during aqueous-solution polymerization of TMAEA (20 wt.%) at 21 and 95 °C under pseudo-stationary conditions with a p.r.r. of 20 Hz and with Darocur[®] ($1.9 \cdot 10^{-2} \text{ mol} \cdot \text{L}^{-1}$) acting as the photoinitiator. The magnetic field positions dominated by SPRs (red, l.h.s.) reflect the applied p.r.r. (framed area) which is not observed at lower SPR fractions, e.g., at 95 °C (r.h.s.). The underlying quartet SPR spectrum refers to $a(3\text{H}) = 20.6 \text{ G}$.

The second MCR conformer (MCR5) exhibits a strong temperature dependence of the hfcc (Table 8.1) which has not been observed with the MCR3 conformer. While at lower temperatures, the MCR5 spectrum is adequately assigned to a hfc of four non-equivalent β -methylene-protons yielding a 16 line hfc pattern, the MCR spectrum at higher temperatures is assigned to two pairs of non-equivalent β -methylene-protons (9 lines) indicating that, according to Heller-McConnel equation (eq (5.1)), the dihedral angles in the MCR5 conformer change significantly with temperature. For the simulation, line broadening has to be taken into account which reduces the hfc patterns of the MCR5 species to a phenotypical quintet as shown in Figure 8.4 below. Although the co-existence of two MCR conformers has also been reported for other acrylate polymerizations^{165,167-169}, the situation for TMAEA is different in that the MCR5 conformer at low temperature has not been observed with acrylate polymerization in organic and aqueous solution so far while, toward higher temperature, the MCR hfc pattern becomes similar the one reported for BA (1.5 M in toluene) between $-40\text{ }^{\circ}\text{C}$ and $60\text{ }^{\circ}\text{C}$.¹²¹ The temperature dependence of the hfcc indicates a significant change in MCR conformation of TMAEA which is perhaps due to the charged side group and to the associated intra- and intermolecular interactions.

Table 8.1: Hyperfine coupling constants (hfcc), $a(\text{H})$, for end-chain (SPR) and mid-chain radicals (MCR) deduced from fitting of experimental overall EPR spectra recorded during TMAEA (20 wt.%) polymerization in aqueous solution at the denoted temperatures. Two different MCR conformers, MCR3 and MCR5, are necessary for an adequate fitting (see text). The hfcc are identical for aqueous-solution polymerization of 10 wt.% TMAEA.

radical	$\theta/^{\circ}\text{C}$	$a(\text{H}) / \text{G}$	
SPR	-5 to +95	20.6 (3H, α -H)	
MCR3	-5 to +95	27.4 (2H, β -H)	
MCR5	-5	24.0 (1H, β -H)	3.5 (1H, β -H)
		15.8 (1H, β -H)	8.2 (1H, β -H)
MCR5	95	16.6 (2H, β -H)	11.0 (2H, β -H)

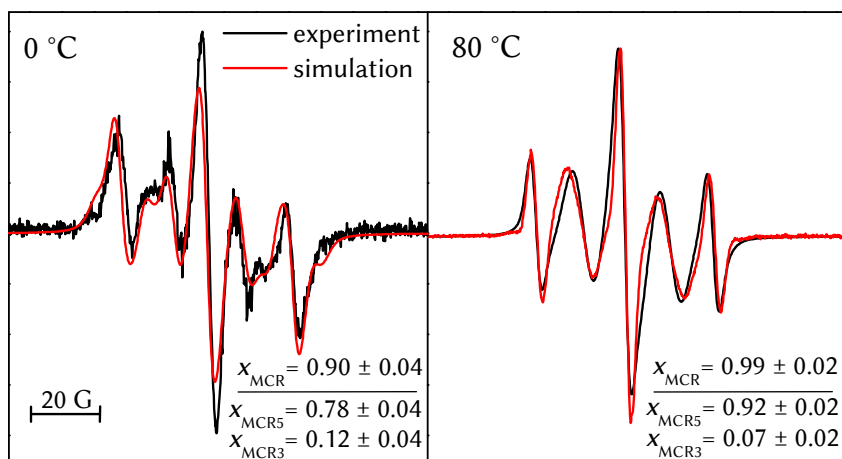


Figure 8.2: EPR spectra recorded during aqueous-solution polymerization of TMAEA (20 wt.%) at 0 and 80 °C. The spectra refer to a sweep time of 5.12 s and stationary UV irradiation with Darocur[®] ($1.9 \cdot 10^{-2} \text{ mol} \cdot \text{L}^{-1}$) acting as the photoinitiator. The simulations represented by the red lines reveal a high overall MCR fraction, x_{MCR} , and the co-existence of two MCR conformers denoted as MCR3 and MCR5.

Under the assumption that according to Heller-McConnel equation (eq (5.1)) $A(\beta\text{-H}) = 2 \cdot a(\alpha\text{-H})$, dihedral angles of $\Theta = 35.2^\circ$ for the MCR3 species and $\Theta = 40.2^\circ$ ($a(\beta\text{-H}) = 24.0 \text{ G}$), $\Theta = 72.9^\circ$ ($a(\beta\text{-H}) = 3.5 \text{ G}$), $\Theta = 51.7^\circ$ ($a(\beta\text{-H}) = 15.8 \text{ G}$) as well as $\Theta = 63.5^\circ$ ($a(\beta\text{-H}) = 8.2 \text{ G}$) result for the MCR5 species at -5°C whereas at 95°C numbers of $\Theta = 50.5^\circ$ ($a(\beta\text{-H}) = 16.6 \text{ G}$) and $\Theta = 58.8^\circ$ ($a(\beta\text{-H}) = 11.0 \text{ G}$) are obtained.

8.1.2 Fraction of Mid-chain Radicals under Stationary Conditions

The molar fractions of MCRs, x_{MCR} , which were deduced by fitting the experimental EPR spectra are shown from -5 to $+95$ °C in Figure 8.3. The numbers of x_{MCR} for TMAEA (20 wt.%) are significantly higher than with BA and AAm. This finding in conjunction with the high absolute radical concentration indicates that MCR propagation rather than termination is the dominant degradation pathway for MCRs in TMAEA polymerizations even at low temperatures and high radical concentrations. The x_{MCR} values should be adequately reproduced by eq (2.12).

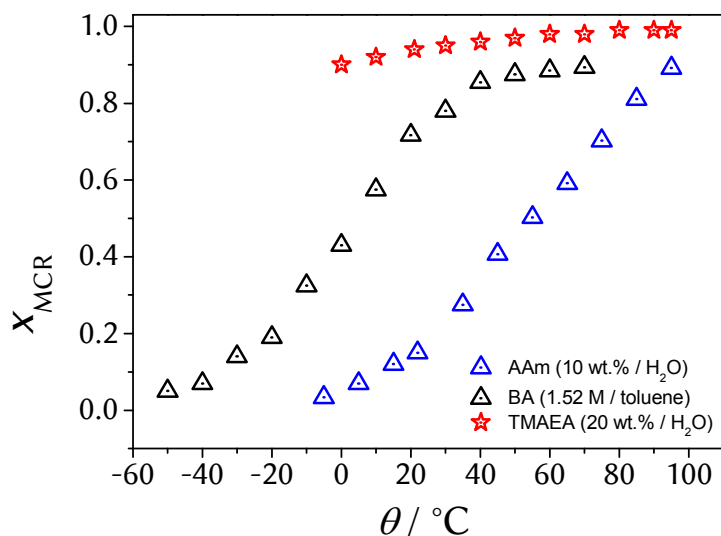


Figure 8.3: Molar fraction of mid-chain radicals, x_{MCR} , deduced from fitting the experimental EPR spectra recorded during polymerization of TMAEA (20 wt.%) in aqueous solution between -5 and $+95$ °C. The values of x_{MCR} are identical for solutions containing 10 wt.% TMAEA. For comparison, reported experimental values of x_{MCR} for BA polymerization (1.52 M in toluene)¹²¹ and AAm (10 wt.%) are included.

8.1.3 Band Assignment used with the SP–PLP–EPR Experiment

In contrast to investigations into the termination and transfer kinetics of AAm (Section 5), the overlap of individual signal bands allows for simultaneously monitoring both SPRs and MCRs as illustrated for the two MCR5 hfc patterns in Figure 8.4. The magnetic field position for the SPR monitoring in both spectra is identical which ensures an accurate determination of SPR concentration irrespective of variations in the MCR5 spectrum with changing temperature. It goes without saying that the magnetic field positions used for SPR monitoring in Figure 8.4 agrees with the positions related to the oscillation of SPR concentration shown in Figure 8.1.

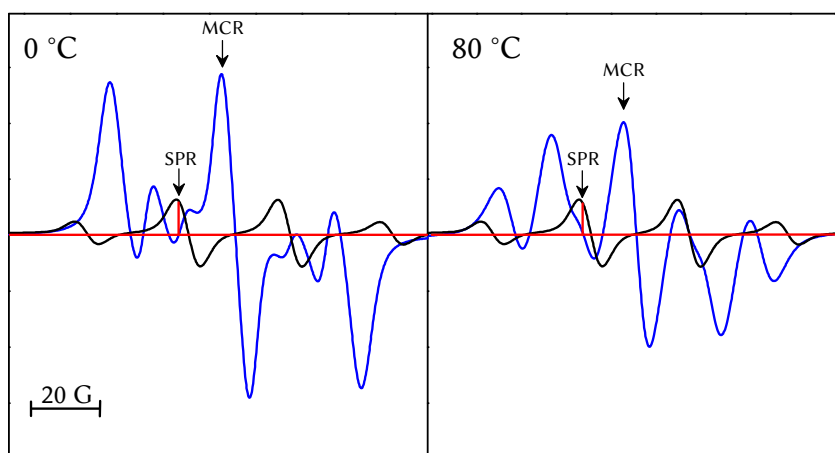


Figure 8.4: Simulated SPR and MCR5 spectra for 0 and 80 °C as deduced from fitting of experimental spectra shown in Figure 8.2 and according to the hfc is listed in Table 8.1. The positions used for SPR and MCR monitoring are labelled. The baseline included as the red horizontal line in order to illustrate the negligible contribution of MCR band intensity at magnetic field positions used for SPR monitoring in SP–PLP–EPR investigations.

8.2 Basic Strategy and Data Analysis

The analysis of SPR and MCR concentration vs time profiles for TMAEA polymerization rests on the PREDICI[®] model introduced for AAm polymerizations in Section 5.2.2 with the single but important difference that no data for k_p^s is available. The knowledge of k_p^s however is essential for an accurate determination of termination, i.e., in the light of chain-length dependency, and also for MCR propagation. The determination of k_p from SP-PLP-EPR was introduced in Section 6. The presented method which rests on the correlation of integrated radical concentration with monomer-to-polymer conversion is easily applied if only one radical species is present. In case of high concentrations of MCRs as in TMAEA polymerization, the strategy presented in this section is advisable since the conversion which relates to the MCR propagation is taken into account.

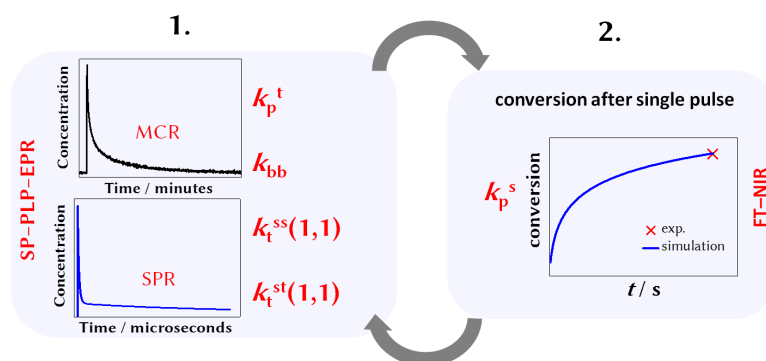


Figure 8.5: Illustration of the basic strategy for data analysis applied for TMAEA polymerization (see text). The fitting of radical concentration vs time profiles (l.h.s.) by PREDICI[®] allows for an accurate determination of $k_t^{ss}(1,1)$, $k_t^{st}(1,1)$, k_{bb} , and k_p^t but requires a reliable k_p^s value which may be determined from monomer-to-polymer conversion by the FT-NIR technique (r.h.s). The iterative fitting of radical concentration vs time profiles and monomer-to-polymer conversion provides a consistent set of rate coefficients.

In order to determine reliable rate coefficients, an iterative two-step procedure was applied (Figure 8.5). Starting from an estimated k_p^s value of $240,000 \text{ L}\cdot\text{mol}^{-1}\cdot\text{s}^{-1}$, the radical concentration vs time profiles were fitted yielding $k_t^{ss}(1,1)$, $k_t^{st}(1,1)$, k_{bb} and k_p^t as the only fitting parameters. As with investigations into the polymerization of AAm, $k_t^{ss}(1,1)$ and $k_t^{st}(1,1)$ refer to

an identical set of composite-model parameters, i.e., $\alpha_s = 0.65 \pm 0.09$, $\alpha_1 = 0.18 \pm 0.03$ and $i_c = 45 \pm 25$ which were adopted from TMAEMA polymerization (Section 6). The composite-model parameters were treated as temperature independent. Variation within the reported limits of uncertainty did not show any significant impact on the determined rate coefficients, i.e., $k_t^{ss}(1,1)$, $k_t^{st}(1,1)$, k_{bb} , and k_p^t . In the second step, the measured monomer-to-polymer conversion per single laser pulse was used to adjust k_p^s via the PREDICI[®] modelling. The conversion was determined directly after the SP-PLP-EPR experiment as illustrated in Section 3.3. The so-obtained new number for k_p^s was re-implemented into the PREDICI[®] model and the next generation of $k_t^{ss}(1,1)$, $k_t^{st}(1,1)$, k_{bb} and k_p^t values was determined followed by another estimation of k_p^s . The procedure was repeated until a consistent set of all five rate coefficients was achieved. The monomer-to-polymer conversion induced by the MCR propagation is considered within the PREDICI[®] model.

8.3 Results from PREDICI Fitting

The SP-PLP-EPR investigations were performed with a 20 wt.% solution of TMAEA in D₂O between 0 °C and 90 °C. The lifetime of MCRs and SPRs is orders of magnitude above the ones known from SP-PLP-EPR investigations into acrylate and AAm polymerizations (see Section 5.2). Moreover, the SPR concentration (Figure 8.6, l.h.s.) approaches a (quasi-) stationary concentration at high delay times which is highlighted by the dashed baseline and may be understood as a permanent "regeneration" of SPRs by MCR propagation indicating that cross-termination is less important for MCR degradation in TMAEA polymerization than with acrylate and AAm polymerizations. This conclusion is further supported by Figure 8.7 which illustrates the impact of monomer-to-polymer conversion on MCR concentration vs time profiles. Toward higher conversion, i.e., lower monomer concentration, the rate of MCR propagation decreases until termination is the single remaining reaction pathway.

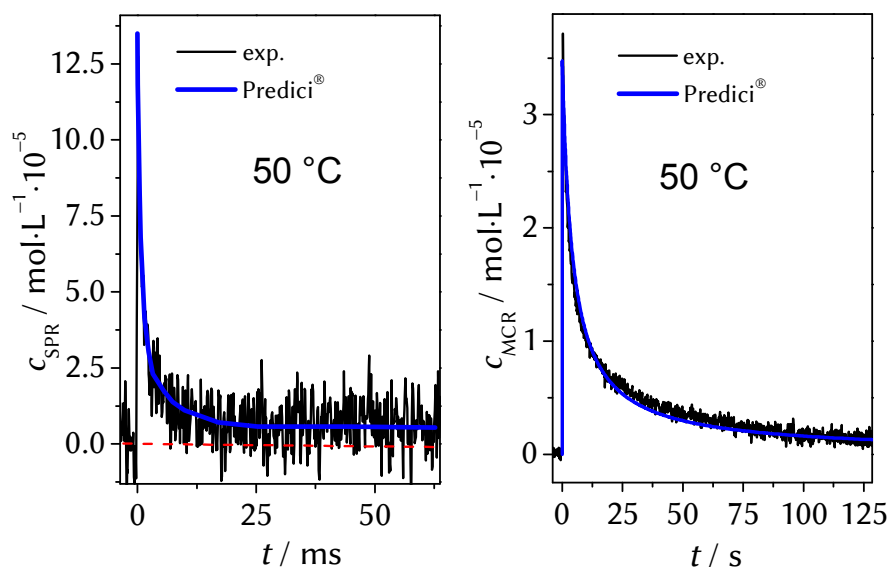


Figure 8.6: Measured and fitted SPR (l.h.s.) and MCR (r.h.s.) concentration vs time profiles after applying a single laser pulse at $t = 0$ during TMAEA polymerizations (20 wt.% / D_2O) at 50 °C. The baseline for the SPR trace is indicated by the dashed line.

The conversion dependence of the radical decay can be neglected with the SPR concentration vs time profiles in TMAEA polymerization and was not observed with MCR traces in BA, AA and AAm polymerizations, i.e., with polymerizations in which cross-termination is definitely of high importance. The rapidly decreasing monomer concentration within the first laser pulse, which was used for data analysis, is (automatically) taken into account by the PREDICI® model via the adjusted k_p^s value (see above). Unfortunately, analysis of the MCR traces for high conversion, which in principle allow for determination of $k_t^{tt}(1,1)$, are not trivial since the calibration of the EPR signal setup breaks down when polarity changes with conversion. If the calibration used for the first MCR trace is applied and only termination is considered for the MCR decay a chain-length averaged $\langle k_t^{tt} \rangle = 9.3 \cdot 10^2 \text{ L} \cdot \text{mol}^{-1} \cdot \text{s}^{-1}$ is obtained which is significantly lower than corresponding numbers for cross-termination being around $\langle k_t^{st} \rangle = 2.1 \cdot 10^4 \text{ L} \cdot \text{mol}^{-1} \cdot \text{s}^{-1}$ at 50 °C (see below). The extremely low $\langle k_t^{tt} \rangle$ is of high uncertainty, because the generation of MCRs by H-abstraction from dead macromolecular chains by primary photoinitiator-derived radicals cannot be excluded at high conversion.

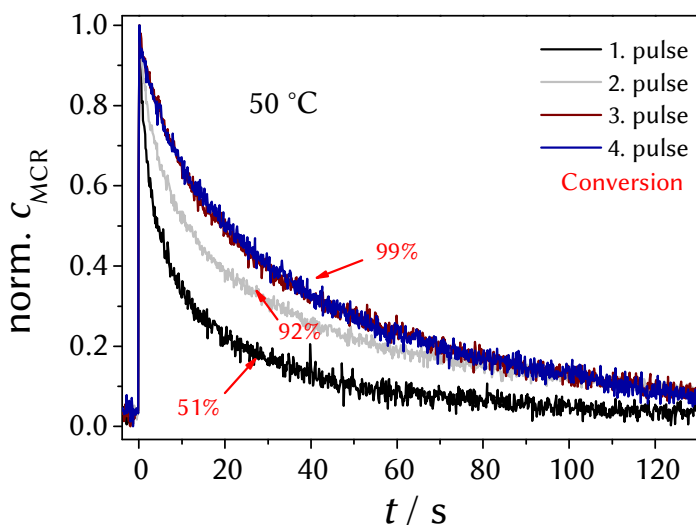


Figure 8.7: Normalized MCR traces measured upon applying several laser pulses and hence reaching different degrees of monomer-to-polymer conversion in TMAEA polymerization (20 wt.% / D₂O). The numbers refer to conversion after complete decay of the radical concentration. The illustrated impact of conversion was not observed with SPRs traces and may be indicative of the dominating role of MCR propagation for the MCR decay in aqueous-solution polymerization of TMAEA.

Nevertheless, the MCR homo-termination rate might be seen as very low even in the initial polymerization period. It comes as no surprise that MCR homo-termination is negligible in SP-PLP-EPR investigations into TMAEA polymerizations. Moreover, no indications for β -scission and depropagation were found.

8.3.1 Termination and Transfer Kinetics of TMAEA Radicals

The numbers for k_{bb} deduced from the SPR and MCR concentration vs time profiles between 0 and 90 °C are shown in the Arrhenius plot in Figure 8.8. No significant variation of k_{bb} with monomer content between 10 and 20 wt.% TMAEA is observed at 50 °C. The numbers for 20 wt.% are adequately represented by the relationship

$$k_{bb} / \text{s}^{-1} = 7.1 \cdot 10^9 \cdot \exp(-5846 \cdot (T^{-1}/\text{K}^{-1})) \quad (\text{for } 20 \text{ wt.}\%),$$

which is associated with an activation energy of $E_A(k_{bb}) = (48 \pm 2) \text{ kJ}\cdot\text{mol}^{-1}$ and a pre-exponential factor of $A(k_{bb}) = (7.1 \pm 0.5) \cdot 10^9 \text{ s}^{-1}$ being close to the corresponding Arrhenius parameters of AAm polymerization (Table 8.2). Although $A(k_{bb})$ of TMAEA is higher than with other acrylates, a similar k_{bb} at 50 °C is obtained due to the higher $E_A(k_{bb})$. Compared to non-ionized acrylic acid (AA), $A(k_{bb})$ of TMAEA is higher by a factor of seven and be even more than two orders of magnitude higher compared to fully-ionized AA (NaAA). Taking AA as a reference, $E_A(k_{bb})$ differs by approximately $10 \text{ kJ}\cdot\text{mol}^{-1}$ for TMAEA and NaAA in reported directions. An detailed interpretation of TMAEA k_{bb} data on the basis of the listed parameters in Table 8.2 turns out to be difficult due to the large structural differences between TMAEA and the tabulated monomers.

Table 8.2: Comparison of the rate coefficients for backbiting, k_{bb} , at 50 °C and related Arrhenius parameters of various monomers in aqueous or in organic solution.

k_{bb}	$E_A(k_{bb})/$ $\text{kJ}\cdot\text{mol}^{-1}$	$A(k_{bb})/$ $10^8 \cdot \text{s}^{-1}$	$k_{bb}(50 \text{ }^\circ\text{C})$ $/ \text{s}^{-1}$	Ref.
AAm (10 wt.%, 20 wt.% / H₂O)	(49 ± 2)	(37 ± 7)	44	this work
TMAEA (20 wt.% / D₂O)	(48 ± 2)	(71 ± 5)	99	this work
AA (20 wt.% / H₂O)	(38 ± 3)	(10 ± 2)	705 ^{a)}	176
NaAA (20 wt.% / H₂O)	(26 ± 2)	(0.22 ± 0.09)	160	39
BA (1.5 M / toluene)	(35 ± 2)	(0.48 ± 0.07)	393	37

a) determined by ¹³C-NMR technique. Italicized numbers are of higher uncertainty.

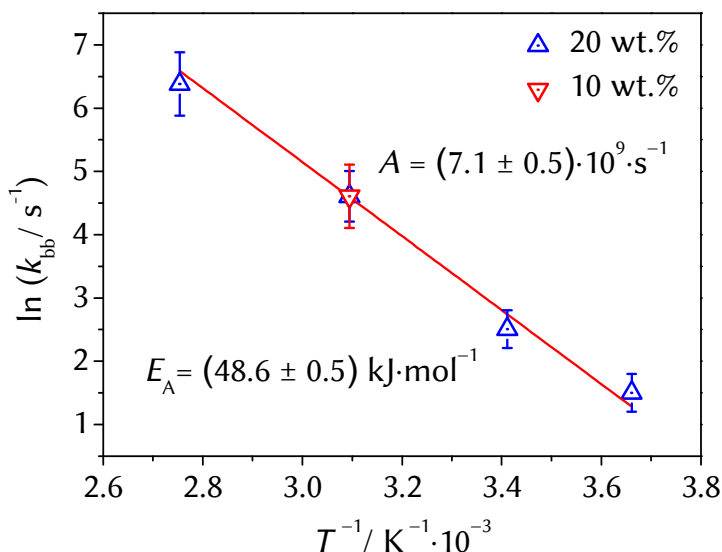


Figure 8.8: Arrhenius plot of the backbiting rate coefficient, k_{bb} , for 20 wt.% TMAEA between 0 and 90 °C as well as k_{bb} for 10 wt.% at 50 °C. The rate coefficients were determined by PREDICI[®] fitting of SPR and MCR concentration vs time profiles. A single regression line is applied to the data of 20 wt.% TMAEA.

As with other rate coefficients, e.g., k_t (Section 7) and k_p ,^{s 35,72} the dominant role of ionic interactions is obvious but difficult to quantify. On the one hand, the electrostatic repulsion may lead to a higher ring strain in the six-membered TS structure and hence to a higher activation energy of backbiting. On the other hand, it is seen from the EPR spectra recorded during TMAEA polymerization that the conformers of the MCR species differ from those reported for acrylates. The conformation may play a role for the entropy penalty during formation of the TS structure. This impact of conformation may also favour the entropy-driven pre-exponential factor.

The second quantity deduced from the radical concentration vs time profiles is the rate coefficient of MCR propagation, k_p^t . As seen from Figure 8.9, no impact of monomer conversion is observed. The data is represented by

$$k_p^t / (\text{L} \cdot \text{mol}^{-1} \cdot \text{s}^{-1}) = 6.8 \cdot 10^4 \cdot \exp(-3127 \cdot (T^{-1} / \text{K}^{-1})) \quad (20 \text{ wt.}\%)$$

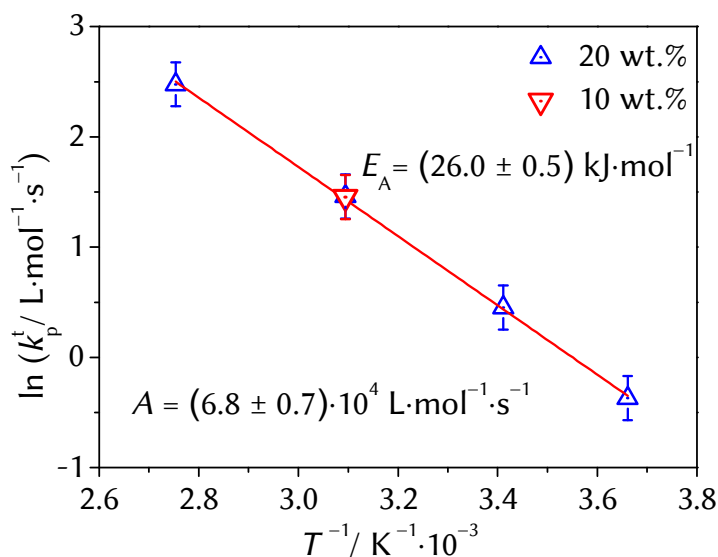


Figure 8.9: Arrhenius plot of the rate coefficients for MCR propagation, k_p^t , of 20 wt.% TMAEA in D_2O between 0 °C and 90 °C as well as the k_p^t value of 10 wt.% TMAEA for 50 °C. The full red line represents the fit for 20 wt.%.

Table 8.3: Comparison of the rate coefficients for MCR propagation, k_p^t , at 50 °C and of the Arrhenius parameters for various monomers in aqueous and in organic phase.

k_p^t	$E_A(k_p^t) / \text{kJ}\cdot\text{mol}^{-1}$	$A(k_p^t) / 10^6 \text{ s}^{-1}$	$k_p^t(50\text{ °C}) / \text{L mol}^{-1} \text{ s}^{-1}$	Ref.
AAm (10 wt.%, 20 wt.% / H_2O)	(30 ± 2)	(1.4 ± 0.2)	20	this work
TMAEA (20 wt.% /D_2O)	(26 ± 2)	(0.068 ± 0.02)	4	this work
NaAA (20 wt.% / H_2O)	(23 ± 3)	(0.06 ± 0.01)	14	39
BA (1.5 M / toluene)	(28 ± 2)	(0.9 ± 0.2)	25	37

Italicized numbers are of higher uncertainty.

The corresponding activation energy of 20 wt.% TMAEA, i.e., $E_A(k_p^{\ddagger}) = (26.0 \pm 0.5) \text{ kJ}\cdot\text{mol}^{-1}$, is close the reported numbers for acrylates and even to AAm in aqueous solution, while the pre-exponential factor, i.e., $A(k_p^{\ddagger}) = (6.8 \pm 0.7)\cdot 10^4 \text{ L}\cdot\text{mol}^{-1}\cdot\text{s}^{-1}$, is lower than with non-ionized monomers, but similar to $A(k_p^{\ddagger})$ of NaAA (Table 8.3).

This finding may be interpreted in terms of a reduced internal mobility in the TS structure of MCR propagation which is induced by electrostatic repulsion due to the charged side group. The close agreement of absolute numbers for $A(k_p^{\ddagger})$ of NaAA and TMAEA indicates a very similar extent of hindrance. The absolute values for k_p^{\ddagger} , however, differ for NaAA and TMAEA at 50 °C due to a higher $E_A(k_p^{\ddagger})$ for TMAEA.

The remaining parameters to be deduced from the SP–PLP–EPR traces are the rate coefficients of SPR homo-termination and of SPR-MCR cross-termination for radicals of chain length unity, $k_t^{ss}(1,1)$ and $k_t^{st}(1,1)$ (Figure 8.10).

In contrast to NaMAA (Section 7), no significant difference of k_t with monomer concentration is observed for $k_t^{ss}(1,1)$ and $k_t^{st}(1,1)$ at 10 and 20 wt.% TMAEA (Table 8.4).

The temperature dependence according to the Arrhenius fits in Figure 8.10 is given by the relations:

$$k_t^{ss}(1,1) / (\text{L}\cdot\text{mol}^{-1}\cdot\text{s}^{-1}) = 2.6\cdot 10^8 \cdot \exp(-998\cdot(T^{-1}/\text{K}^{-1}))$$

for 20 wt.% TMAEA

$$k_t^{st}(1,1) / (\text{L}\cdot\text{mol}^{-1}\cdot\text{s}^{-1}) = 3.8\cdot 10^7 \cdot \exp(-1276\cdot(T^{-1}/\text{K}^{-1}))$$

for 20 wt.% TMAEA.

The associated activation energies, i.e., $E_A(k_t^{ss}(1,1)) = (8.3 \pm 0.9) \text{ kJ}\cdot\text{mol}^{-1}$ and $E_A(k_t^{st}(1,1)) = (10.6 \pm 0.8) \text{ kJ}\cdot\text{mol}^{-1}$, are close to each other, but are significantly below $E_A(\eta^{-1}) = (16.98 \pm 0.05) \text{ kJ}\cdot\text{mol}^{-1}$, i.e., the activation energy of fluidity for 20 wt.% TMAEA in D₂O, which was used for estimating the diffusion limiting behaviour illustrated in Figure 8.10. As with NaMAA, the small numbers for $E_A(k_t)$ may be interpreted in terms of counter-ion mediation which is lowered toward higher temperature as is the case with weak electrolytes such as TMAEA (see Section 7).¹⁰⁷

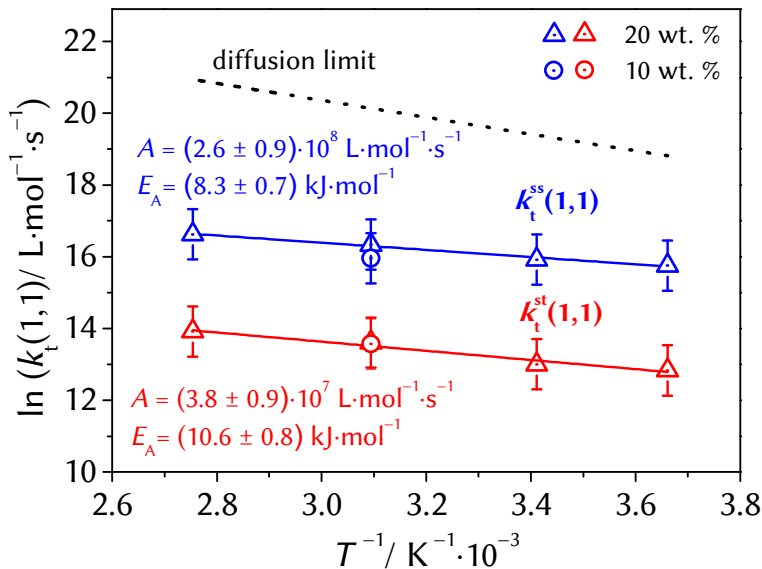


Figure 8.10: Arrhenius plot of the rate coefficients for SPR homo-termination and for MCR-SPR cross-termination, $k_t^{ss}(1,1)$ and $k_t^{st}(1,1)$, at 20 wt.% TMAEA in D_2O between 0 and 90 °C as well as $k_t^{ss}(1,1)$ and $k_t^{st}(1,1)$ for 10 wt.% at 50 °C. The rate coefficients were determined by PREDICI[®] fitting of the SPR and MCR concentration vs time traces from SP-PLP-EPR experiments. The dashed line represents the diffusion limit as estimated via the separately measured viscosities, η , which are associated with an activation energy of fluidity: $E_A(\eta^{-1}) = (16.98 \pm 0.05) \text{ kJ}\cdot\text{mol}^{-1}$.

The absolute values are well below the diffusion limit due to shielding of radical functionality by electrostatic repulsion. Within the temperature range under investigation, the ratios of the SPR-MCR cross-termination to SPR homo-termination rate coefficients are found to be around $k_t^{st}(1,1)/k_t^{ss}(1,1) = 0.06 \pm 0.02$ for 20 wt.% and $k_t^{st}(1,1)/k_t^{ss}(1,1) = 0.09 \pm 0.04$ for 10 wt.% TMAEA at 50 °C. The ratios are lower than with AAm polymerizations ($k_t^{st}(1,1)/k_t^{ss}(1,1) = 0.25 \pm 0.05$).

Table 8.4: Rate coefficients of SPR homo-termination, $k_t^{ss}(1,1)$, and of SPR-MCR cross-termination, $k_t^{st}(1,1)$, for 10 and 20 wt.% TMAEA in D₂O at 50 °C.

50 °C	$k_t^{ss}(1,1) /$ L mol ⁻¹ ·s ⁻¹ ·10 ⁵	$k_t^{st}(1,1)/$ L mol ⁻¹ ·s ⁻¹ ·10 ⁵
TMAEA (20 wt.%/D₂O)	(130 ± 25)	(8.4 ± 0.9)
TMAEA (10 wt.%/D₂O)	(84 ± 18)	(7.6 ± 0.8)

Table 8.5: Comparison of microfriction, f , according to eq (7.1) for the fully-ionized radicals of NaMAA and TMAEA in aqueous solution at 60 °C. If not stated otherwise, values refer to end-chain homo-termination, i.e., to $k_t^{ss}(1,1)$.

	f
NaMAA (5 wt.% / H₂O)	84.2
NaMAA (10 wt.% / H₂O)	21.8
TMAEA (20 wt.% / D₂O)	47.8
TMAEA (20 wt.% / D₂O, $k_t^{st}(1,1)$)	428
AAm (10 wt.% / H₂O)	1.7
AAm (10 wt.% / H₂O, $k_t^{st}(1,1)$)	2.4

Thus, $k_t^{st}(1,1)$ is reduced to a larger extent than $k_t^{ss}(1,1)$ with TMAEA which may be assigned to a higher microfriction, f , for MCRs (see Table 8.5) being described by the following expressions for 20 wt.% monomer content.

$$\ln(f) = 7.9 - 1345 \cdot (T^{-1} / K^{-1}) \quad \text{for } k_t^{ss}(1,1)$$

$$\ln(f) = 9.2 - 1071 \cdot (T^{-1} / K^{-1}) \quad \text{for } k_t^{st}(1,1)$$

The expressions represent the differences between the diffusion limit and the measured values in Figure 8.10. The associated activation energies,

i.e., $E_A(f) = 11.2 \text{ kJ}\cdot\text{mol}^{-1}$ for $k_t^{ss}(1,1)$ and $E_A(f) = 8.9 \text{ kJ}\cdot\text{mol}^{-1}$ for $k_t^{st}(1,1)$, are smaller than for NaMAA indicating a lower $\Delta H(K)$.

The direct comparison of the microfriction, f , between NaMAA, TMAEA and AAm (Table 8.5) shows that the deviation from the diffusion limit for both $k_t^{ss}(1,1)$ and $k_t^{st}(1,1)$ is more pronounced with the termination of fully-ionized radical species in the order $f(10 \text{ wt.}\% \text{ NaMAA}) < f(\text{TMAEA}) < f(5 \text{ wt.}\% \text{ NaMAA})$. While $k_t^{ss}(1,1)$ of non-ionized AAm radicals is only around 60 per cent below the number estimated via eq (2.32), the values for termination of ionized radicals are lowered by more than one order of magnitude. The polymerizations of 20 wt.% TMAEA and 10 wt.% NaMAA refer to almost the same molar concentrations (see Table 3.1). A direct comparison between these systems suggests that the longer side chain with TMAEA radicals provides an additional hindrance for termination. For 5 wt.% NaMAA the lower counter-ion concentration impedes the termination event by a preferred free-ion formation as expected from the proposed equilibrium in Section 7.3. In agreement with the mentioned $k_t^{st}(1,1)/k_t^{ss}(1,1)$ values, the ratios of $f(k_t^{st}(1,1))/f(k_t^{ss}(1,1))$, i.e., 8.9 for TMAEA and 1.4 for AAm, is higher for TMAEMA as compared with AAm. This finding indicates that the impact of electrostatic repulsion is more pronounced with MCRs for which the radical functionality is "screened" by two charged side groups moieties rather than by one as with SPRs.

Table 8.6: Comparison of the termination rate coefficients $k_t(1,1)$ for selected monomers in organic and in aqueous solution at 60 °C. The rate coefficients exclusively refer to chain-end radicals.

60 °C	$k_t(1,1) / 10^7 \cdot \text{L}\cdot\text{mol}^{-1}\cdot\text{s}^{-1}$	Ref.
TMAEMA (20 wt.% in D₂O)	1.2	this work
TMAEA (20 wt.% in D₂O)	1.3	this work
NaMAA (10 wt.% in H₂O)	3.1	this work
NaMAA (5 wt.% in H₂O)	1.0	this work
AAm (10 wt.% in H₂O)	63	this work
Sty (bulk)	69	this work
VAc (bulk)	123	42
MMA (bulk)	90	117
BA (1.5 M in toluene)	62	37

As the diffusion limits for TMAEA (20 wt.%) and NaMAA (10 wt.%) radicals are similar, the higher friction opposing termination in TMAEA polymerization yields an absolute number of $k_t^{st}(1,1)$ of TMAEA at 60 °C which is below the one with NaMAA and close to the number for TMAEMA (Table 8.6).

Table 8.7: Cross-termination rate coefficients, $k_t^{st}(1,1)$, for several monomers at 50 °C.

60 °C	$k_t^{st}(1,1) / \text{L}\cdot\text{mol}^{-1}\cdot\text{s}^{-1}\cdot 10^7$	Ref.
AAm (10 wt.% / H₂O)	14	this work
AAm (20 wt.% / H₂O)	9	this work
BA (1.5 M / toluene)	3.8	37
TMAEA (20 wt.% / D₂O)	0.085	this work

The entire set of values from Table 8.6 for fully-ionized species are by at least one order of magnitude below the reported numbers for non-ionized monomers in organic and aqueous solution which highlights the significant impact of ionization on termination rate.

Also the absolute number for $k_t^{st}(1,1)$ in 20 wt.% TMAEA (Table 8.7) is by up to two orders of magnitude below the associated numbers for AAm and BA polymerization which supports the assumption that cross-termination is of minor importance in aqueous solution polymerization of 20 wt.% TMAEA. The obtained rate coefficients for aqueous-solution polymerization of 20 wt.% TMAEA allow for the calculation of molar MCR fractions (red line in Figure 8.11) which were obtained from fitting of the stationary EPR spectra. According to eq (2.12), the rate coefficient of cross-termination, even though of minor importance for x_{MCR} , was implemented as chain-length averaged quantity, $\langle k_t^{st} \rangle$. The related value was estimated on the basis of the composite-model parameters for $k_t^{st}(1,1)$ and a chain length of $i = 1000$. The end-chain radical concentration, c_{SPR} , was set to $1.5 \cdot 10^{-3} \text{ mol}\cdot\text{L}^{-1}$ for all temperatures according to the very small temperature dependence of overall radical concentrations mentioned above.

$$x_{\text{MCR}} = \frac{k_{\text{bb}}}{k_{\text{bb}} + k_{\text{p}}^t \cdot c_{\text{M}} + \langle k_t^{st} \rangle \cdot c_{\text{SPR}}} \quad (2.12)$$

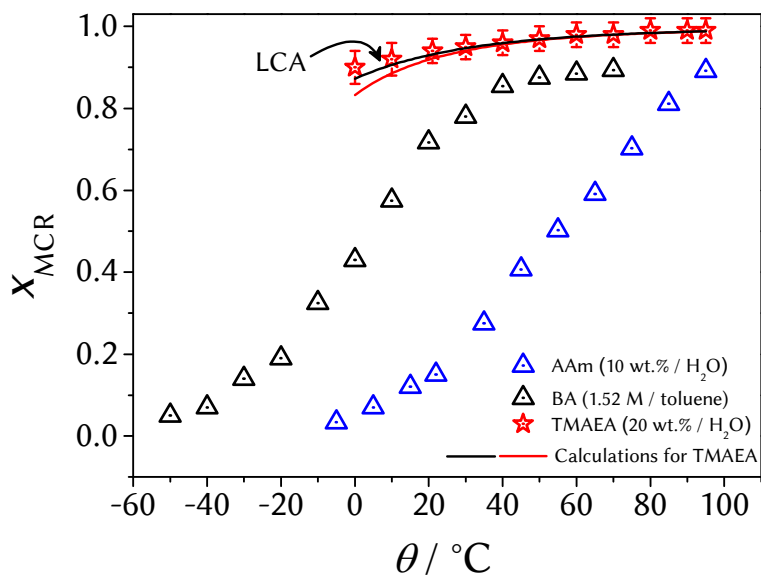


Figure 8.11: Molar fractions of mid-chain radicals, x_{MCR} , deduced from fitting of the experimental EPR spectra recorded during polymerization of TMAEA (20 wt.%) in aqueous solution between -5 and $+95$ °C. For comparison, reported experimental values of x_{MCR} for BA polymerization (1.52 M in toluene)¹²¹ and AAm (10 wt.%) are included. The calculation for TMAEA refers to eq (2.12) taking cross-termination into account. LCA = long-chain approximation (see text).

The satisfying agreement between experimental and calculated numbers underlines the quality of the data obtained so far. The agreement at low temperatures is even better if cross-termination is neglected, i.e., eq (2.11) for the so-called long-chain approximation (LCA) is used instead of eq (2.12).

8.3.2 Interplay of Backbiting, MCR Propagation and Termination in TMAEA, AAm and BA Polymerizations

The relevant rate coefficients for the transfer kinetics (see eq (2.12)) of TMAEA, AAm and BA polymerization in organic and aqueous solution, respectively, are given in Table 8.8 for 50 °C. As shown in Figure 8.11 the

numbers for x_{MCR} of BA are in between the values found with AAm and TMAEA. Compared to AAm, the higher x_{MCR} (TMAEA) cannot exclusively be explained with the higher k_{bb} value of TMAEA. Moreover, x_{MCR} (TMAEA) is even higher than with BA although BA exhibits the highest k_{bb} among these three monomers. The reason behind this effect is the large discrepancy in the MCR degradation rate. The values for k_{p}^{t} (TMAEA) and $k_{\text{t}}^{\text{st}}(1,1)$ (TMAEA) are clearly below the corresponding ones of AAm and BA resulting in a higher x_{MCR} for TMAEA.

The k_{p}^{t} and $k_{\text{t}}^{\text{st}}(1,1)$ values for AAm and BA are similar. As a consequence, x_{MCR} (BA) exceeds x_{MCR} (AAm) due to the higher value of k_{bb} (BA).

Table 8.8: Comparison of rate coefficients of backbiting, k_{bb} , MCR propagation, k_{p}^{t} , and SPR-MCR cross-termination, $k_{\text{t}}^{\text{st}}(1,1)$, at 50 °C between TMAEA, AAm and BA in aqueous and organic-solution, respectively.

50 °C	$k_{\text{bb}} / \text{s}^{-1}$	$k_{\text{p}}^{\text{t}} / \text{L mol}^{-1} \text{s}^{-1}$	$k_{\text{t}}^{\text{st}}(1,1) / 10^8 \text{ L mol}^{-1} \text{s}^{-1}$
TMAEA (20 wt.% /D₂O)	98	4.2	0.007
AAm (10 wt.% /H₂O)	44	22	1.2
BA (1.5 M / toluene)	394	25	3.6

8.3.3 Propagation Kinetics of End-chain Radicals in TMAEA Polymerization

The numbers for the monomer-to-polymer conversion, X , determined after applying a single laser pulse are listed in Table 8.9 and were implemented into the PREDICI[®] for estimating k_{p}^{s} being the only variable in this step (see Section 8.2). It has carefully been checked by the EPR data that the radical concentration has completely decayed before X has been measured. According to this procedure, k_{p}^{s} is the final coefficient within an iterative turn being fitted. As a consequence, experimental uncertainties may be accumulated in k_{p}^{s} . The obtained values for k_{p}^{s} are considered to be accurate within a factor of two.

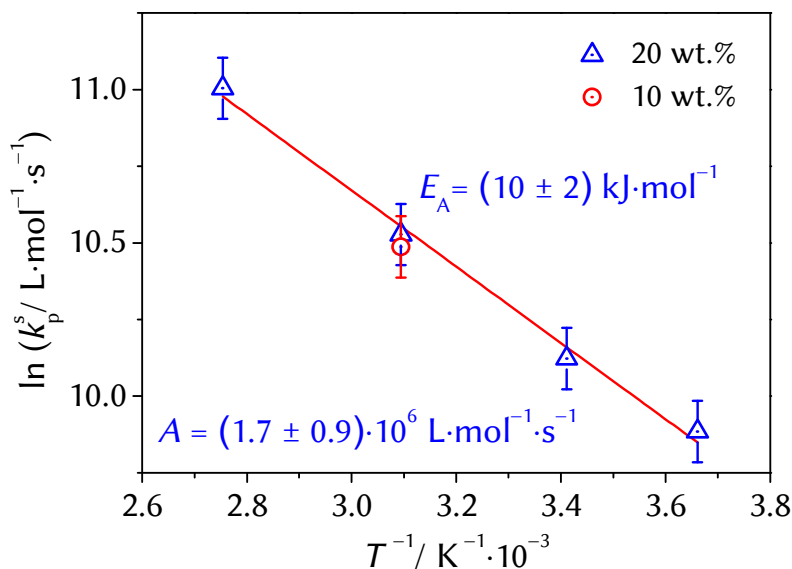


Figure 8.12: Arrhenius fit of the propagation rate coefficient for end-chain TMAEA radicals, k_p^s , at 20 wt.% monomer content between 0 °C and 90 °C as well as the k_p^s value for 10 wt.% at 50 °C. The regression refers to 20 wt.% TMAEA in aqueous solution.

Table 8.9: Fractional monomer-to-polymer conversion, X , and rate coefficients for SPR propagation, k_p^s , for 20 wt.% TMAEA in D_2O as well as for 10 wt.% TMAEA at 50 °C from PREDICI® fitting (see text).

T / K	X	$k_p^s / 10^4 \cdot \text{L}\cdot\text{mol}^{-1}\cdot\text{s}^{-1}$
20 wt.%		
273	0.42 ± 0.05	1.8 ± 0.4
293	0.44 ± 0.07	2.5 ± 0.3
323	0.51 ± 0.04	3.7 ± 0.2
363	0.60 ± 0.02	5.7 ± 0.3
10 wt.%		
323	0.41 ± 0.05	3.5 ± 0.2

The values for k_p^s of 20 wt.% TMAEA are given in an Arrhenius plot in Figure 8.12 and can be described by the relationship

$$k_p^s / (\text{L}\cdot\text{mol}^{-1}\cdot\text{s}^{-1}) = 1.7\cdot 10^6 \cdot \exp(-1239\cdot(T^{-1}/\text{K}^{-1}))$$

for 20 wt.% TMAEA

Using this expression, a value of $k_p^s = 42,500 \text{ L}\cdot\text{mol}^{-1}\cdot\text{s}^{-1}$ is obtained for 60 °C which is significantly higher than the corresponding number for TMAEMA, i.e., $k_p^s = 3500 \text{ L}\cdot\text{mol}^{-1}\cdot\text{s}^{-1}$, at the same temperature and monomer weight percentage. An identical trend between a methylated and non-methylated derivate is reported for MAA and AA (Table 8.10) which is due to a higher activation energy and an enhanced entropy penalty for TS formation since the methyl group induces a reduced internal mobility in TS structure. In terms of the activation energy for k_p^s , $E_A(k_p^s)$, TMAEA is quite close to AA and NaMAA, similar to MAA but smaller than $E_A(k_p^s)$ of AAm. The tabulated monomers in Table 8.10 differ in their pre-exponential factors with BA, AA and AAm exhibiting the highest values for $A(k_p^s)$.

Table 8.10: Comparison of the rate coefficients for propagation of end-chain radicals, k_p^s , at 50 °C and of Arrhenius parameters for various monomers in aqueous solution.

k_p^s	$E_A(k_p^s)/$ $\text{kJ}\cdot\text{mol}^{-1}$	$A(k_p^s)/10^7\cdot$ $\text{L}\cdot\text{mol}^{-1}\cdot\text{s}^{-1}$	$k_p^s(50\text{ °C})/10^3$ $\text{L}\cdot\text{mol}^{-1}\cdot\text{s}^{-1}$	Ref.
TMAEA (20 wt.% / D_2O)	(10 ± 2)	(0.17 ± 0.09)	37	this work
NaMAA (20 wt.% / H_2O)	(12.4 ± 0.6)	(0.02 ± 0.01)	1.9	35
MAA (20 wt.% / H_2O)	(14.1 ± 0.3)	(0.9 ± 0.2)	4.8	35
AAm (10 wt.% / H_2O)	(17.4 ± 0.5)	(5.8 ± 0.3)	81	29
AA (20 wt.% / H_2O)	(11.9 ± 0.9)	(1.2 ± 0.6)	140	23
BA (1.5 M / toluene)	(17.4 ± 0.8)	(1.8 ± 0.5)	27	19

The value for TMAEA is larger than $A(k_p^s)$ for NaMAA but smaller than $A(k_p^s)$ of MAA in aqueous solution indicating an increasing internal mobility for the TS in the order NaMAA, TMAEA, MAA, AA and AAm.

The k_p^s values for 10 wt.% and 20 wt.% at 50 °C (Table 8.9) are very close to each other. The strong variation of k_p^s with monomer concentration for non-ionized monomers as described in Section 5.2.2 is not seen for fully-ionized species.^{35,72} For the aqueous-solution polymerization of NaMAA, the reported numbers for k_p^s increase by a factor of two upon passing from 5 to 10 wt.% monomer and reach a plateau of higher concentrations.³⁵ No reason is seen why SPR and MCR propagation should not behave the same way. Since no significant variation in k_p^t for TMAEA has been observed toward higher monomer concentration, no variation is expected for k_p^s as well.

The k_p^t/k_p^s ratio for TMAEA at 50 °C, i.e., $1.1 \cdot 10^{-4}$, is not that different from $3.5 \cdot 10^{-4}$ found for 10 wt.% and 20 wt.% AAm but smaller than with BA (1.5 M/toluene), $k_p^t/k_p^s = 9.1 \cdot 10^{-4}$.^{19,22,29} The discrepancy between k_p^s (BA) and k_p^s (TMAEA) is mainly due to the activation energies. The ratio of the pre-exponential factors for TMAEA, i.e., $A(k_p^t)/A(k_p^s) = 0.04$, is very close to the corresponding number for BA, i.e., $A(k_p^t)/A(k_p^s) = 0.05$, and above the mean-value of AAm, i.e., $A(k_p^t)/A(k_p^s) = 0.02$.

8.3.4 Simulation of Steady-state Polymerizations of TMAEA

The obtained set of rate coefficients which comprises propagation, termination and transfer kinetics allows for the simulation of conversion vs time profiles, recorded under stationary conditions for 20 wt.% TMAEA at 50 and 70 °C shown in Figure 8.13.¹⁰⁷ The measured conversion vs time trace is compared to the data simulated by the PREDICI[®] program on the basis of the determined rate coefficients from SP-PLP-EPR. For this simulation, ideal polymerization kinetics was assumed to be applicable. The effective rate coefficient of initiator decomposition for VA-86 was taken from literature.^{200,201} The close agreement between simulation and experiment underlines the quality of the determined rate coefficients and supports the experimental strategy of deducing the entire set of rate coefficients from a single SP-PLP-EPR with the related monomer-to-polymer conversion being accurately known.

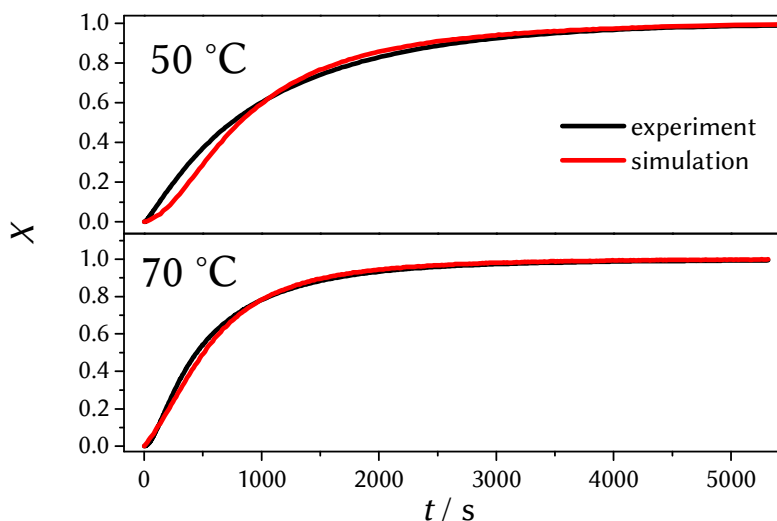


Figure 8.13: Comparison of experimental and simulated conversion, X , vs time traces for chemically initiated TMAEA (20 wt.% in D_2O) polymerization at 50 and 70 °C with VA-086, $c_{VA-86} = 2.9 \text{ mmol}\cdot\text{L}^{-1}$ and $c_{VA-86} = 1.2 \text{ mmol}\cdot\text{L}^{-1}$, respectively, acting as the thermally decomposing initiator. The simulation is based on ideal polymerization kinetics with the rate coefficients taken from the SP-PLP-EPR experiment presented above. The experiment for chemically initiated TMAEA polymerizations were performed by Patrick Drawe.¹⁰⁷

Open Questions and Remaining Challenges^{iv}

Despite the success reached so far, an enormous amount of work remains to be done, e.g., into the detailed homopolymerization kinetics of various types of monomers, including partially and fully ionized monomers with different counter ions, as well as into systems at moderate and high degrees of monomer conversion, not to talk about copolymerization and the kinetics of short-living species, i.e., primary radicals.

9.1 CLDT up to High Conversion

So far, reliable data of CLDT is only available for the initial period of radical polymerizations. As technical processes are carried out up to much higher conversions, it appears to be a matter of priority to extend the method into the region of medium and high degrees of monomer conversion. Moreover, a significant fundamental interest focuses on termination under conditions of extreme diffusion control. The viscosity of bulk polymerizations at high conversion may exceed the one of the initial monomer system by several orders of magnitude.⁴⁴ The qualitative change

^{iv} Reproduced in parts with permission from Buback, M.; Schroeder, H; Kattner, H. *Macromolecules* **2016**, 49, 3193–3213, Copyright 2016, American Chemical Society

of chain-length-averaged k_t , $\langle k_t \rangle$, as a function of monomer-to-polymer conversion, X , has been presented in Ref.⁸² for MMA bulk polymerization. An initial range of segmental diffusion control is followed by a region where translational diffusion controls $\langle k_t \rangle$. Toward even higher conversion, reaction diffusion may operate. Depending on the monomer under investigation, the individual modes of control may extend over quite different ranges of monomer conversion thus giving rise to a wide pattern of $\langle k_t \rangle$ vs X correlations.

Some data on CLDT for higher X have been measured via RAFT-CLD-T.²¹³ The results indicate an increase of the power-law exponent with X .^{95,141,214} The data, however, is restricted to high temperatures and suffers from the restriction that in RAFT-CLD-T the conversion and the chain length increase simultaneously thus reaching large chain lengths only at very high degrees of monomer conversion. The impact of conversion and chain length on termination rate may thus not be investigated independently. Along the same lines, no information about the termination rate coefficient of short radicals at high conversion is accessible from RAFT-CLD-T. This information is however required, as small-size are expected to occur at high conversion due to the increase in radical concentration by the gel-effect and the lower monomer concentrations. Moreover, the numbers of $k_t(i,i)$ for RAFT-CLD-T are estimated indirectly from polymerization rate which may be affected by the RAFT kinetics.²¹⁵

To carry out SP-PLP-EPR experiments at high monomer conversions, this region may be approached by two strategies: (1) A thermally initiated polymerization which does not affect the photoinitiator may be carried out first followed by the SP-PLP-EPR experiment at high polymer content. (2) A significant amount of polymer is added to a mixture of monomer and photoinitiator. The advantage of this second procedure relates to the fact that detailed termination kinetics may be measured for different types of polymeric background material being added. Problems may arise from the significant changes in the polarity of the system making the EPR signal intensity a function of conversion which is particularly challenging with respect to the calibration procedure. Thus the experiments should be conducted for styrene polymerization²¹⁶⁻²¹⁸ since the EPR intensity remains constant up to high conversion whereas a threefold intensity increase was observed for MMA bulk polymerization.¹²⁴

9.2 DP-PLP-EPR-Experiments

The SP-PLP-EPR experiments illustrated so far deliver rate coefficients for termination of two radicals of more or less identical size. Thus the question arises whether and how the so-obtained coefficients may be used in conventional polymerization. The termination rate coefficients from SP-PLP-EPR are directly applicable toward reversible deactivation polymerizations, which are characterized by a very narrow distribution of radicals, but in conventional polymerization and thus in most of the technical processes, termination occurs between radicals of different size. The rate coefficient, $k_t(i,j)$, for termination of two radicals, of chain length i and j , (cross-termination) therefore needs to be known for simulation of the majority of polymerization processes. Three models have been used to estimate $k_t(i,j)$ from known coefficients for termination of two radicals of identical size, $k_t(i,i)$ and $k_t(i,i)$: the geometric-mean model (gm), the diffusion-mean model (dm) and the harmonic-mean model (hm) (see Section 2).¹⁰¹ To decide which model is best suited, double-pulse experiments (DP-PLP-EPR) should be carried out, in which a second laser pulse is applied at a pre-selected delay time. For fully-ionized methacrylic acid (5 wt.% in H₂O), taken as an example, a DP-PLP-EPR measurement has been performed at 60 °C (Figure 9.1). On the basis of the reported rate coefficients and composite-model parameters from Section 7.2.2, the program package PREDICI[®] was used to estimate $k_t(i,j)$. The underlying PREDICI[®] model differs from the one applied to TMAEMA polymerization only by $k_t(i,j)$ being implemented according to the above-mentioned mean values. The second laser pulse generating an enhanced concentration of the species with chain length j was applied at a delay time of $t_{\text{sec}} = 16$ ms resulting in a difference in chain length between the two distributions of $\Delta i,j = 7$, i.e., $i = j+7$. The comparison between the experiment (black line) and the simulation without cross-termination (red line) demonstrates the important role of cross-termination. The differences between the three models are, however, less pronounced which is due to the low k_p/k_t ratio of NaMAA radicals. The simulations indicate that a higher $\Delta i,j$ (i.e., for a high k_p , and a higher concentration of radicals from the first pulse at t_{sec} (i.e., for low k_t) enlarges the differences between the three models and may allow for model discrimination. TMAEMA with k_p being four times higher than $k_p(\text{NaMAA}, 5 \text{ wt.}\%)$ should be a suitable candidate to answer the question for the best model approach.

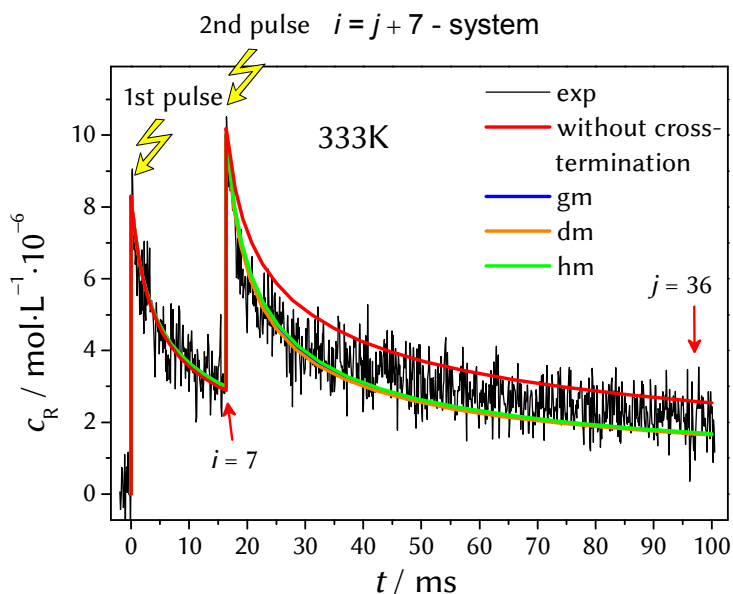


Figure 9.1: Radical concentration vs time traces for double-pulse experiments (DP-PLP-EPR) of fully-ionized methacrylic acid (NaMAA, 5 wt.% in H₂O) at 60 °C. The simulations are based on the known rate parameters from Section 7.2.2 adopting the harmonic mean (hm), geometric mean (gm) and the diffusion mean (dm) models for cross-termination of radicals. The discrepancies between the models become more pronounced toward higher k_p and lower k_t .

9.3 Polymerization Kinetics of Ionic Monomers

The present study provides access to the propagation, termination and transfer kinetics of ionic monomers by SP-PLP-EPR. Nevertheless a large amount of research remains to be done. Drawe *et. al.*²¹⁹ reported a strong impact of counter ions on the polymerization rate of acrylic acid. The role of counter ions might be investigated for different cationic and anionic monomers, e.g., sulfonic acids and ammonium salts, with respect to concentration and to the type of the counter ion, e.g., Na⁺, Li⁺, Cl⁻ or SO₄²⁻, respectively. In this context, the trapping of cations by cryptands and crown ethers for anionic monomers promises further insight into the mechanisms of propagation, termination and backbiting. Because of the

complex kinetics in systems with MCRs, the special effects of the type and concentration of counter ions should first be studied on methacrylates.

9.4 Termination Kinetics in Radical Copolymerization

The SP-PLP-EPR results presented so far refer exclusively to homopolymerizations. First time-resolved EPR experiments were performed by L. Riemann for the copolymerization of methyl methacrylate (MMA) with styrene in bulk at 333 K.²²⁰ The results indicate that the rate coefficient for termination between a monomeric styryl and a MMA radical, $k_t^{\text{cross}}(1,1)$, is clearly above the corresponding homotermination coefficients, $k_t^{\text{sty}}(1,1)$ and $k_t^{\text{MMA}}(1,1)$, see (Figure 9.2). The PREDICI[®] model needed for the analysis of time-resolved EPR data is of high complexity, as penultimate-unit effects were included.²²¹ Until now, no explanations is at hand for the high $k_t^{\text{cross}}(1,1)$ and thus further investigations are required.

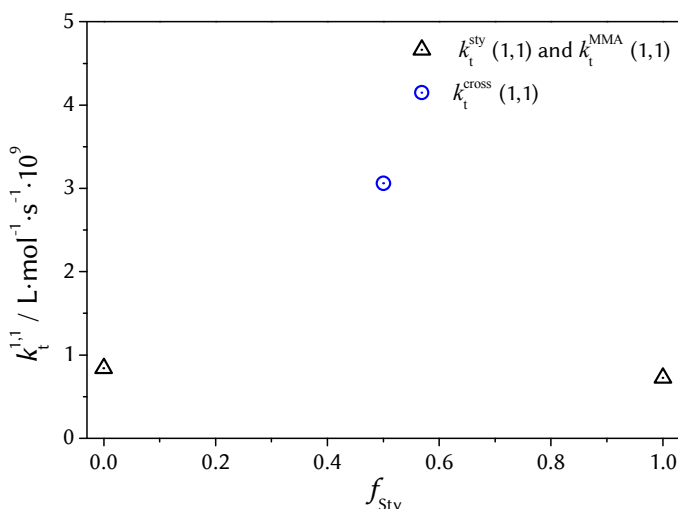


Figure 9.2: Monomeric rate coefficient of termination for homopolymerizations of styrene ($f_{\text{sty}} = 1$) and MMA ($f_{\text{sty}} = 0$) in bulk as well as for the associated copolymerization ($f_{\text{sty}} = 0.5$) at 333 K with DCP ($9 \cdot 10^{-2} \text{ mol} \cdot \text{L}^{-1}$) acting as the photoinitiator. f_{sty} is the molar fraction of styrene. Data taken with permission from Ref.²²⁰

9.5 Transient EPR Spectroscopy

The investigations presented here rest on continuous-wave (CW-) EPR spectroscopy which requires magnetic field modulation (MFM) to obtain a high signal quality. With a modulation frequency of 100 kHz three and up to four modulation cycles of the magnetic field have usually to be passed for a single data point of EPR intensity.²²² It comes thus as no surprise that the EPR time resolution is significantly reduced by the MFM which however is an integral part of CW-EPR spectroscopy. The employed state-of-the-art microwave bridge and digitizer provide a theoretical time resolution of 1 ns which is diminished to 10 μ s. The time resolution is sufficiently high for resolving reaction steps, e.g., termination and backbiting, which occur on a millisecond time scale and are sufficient for reactions on a microsecond time-scale, such as propagation. The CW-EPR spectroscopy thus allows for a detailed investigation into CLDT. The investigation of very fast reaction steps, e.g., of initiation processes, are currently beyond reach.

The modulation-free transient EPR (trEPR) spectroscopy provides time resolution from the microsecond scale to 10 ns. Here, the decay of the chemically induced dynamic electron spin polarization (CIDEP) is measured. The related non-equilibrium spin states result from the photochemical generation of transient paramagnetic species. For a detailed discussion about CIDEP mechanisms see Ref.^{223,224} The induced polarization is by orders of magnitude larger than the "Boltzmann" signal. Nevertheless, a series of signals have to be co-added to yield a signal quality as with CW-EPR spectroscopy. The relaxation time into the Boltzmann equilibrium has to be considered for kinetic data analysis but is usually on the microsecond time scale and thus sufficiently high for investigations into very fast reaction steps which might be: 1) initiation, i.e, the addition of primary, photoinitiator-derived radicals to monomer molecules, 2) propagation of monomeric radicals providing information about k_p^1 and insight into the chain-length dependency of propagation, 3) transfer processes in the initial period of reversible-deactivation radical polymerization, e.g., in the pre-RAFT-equilibrium, 4) retardation and inhibition processes. Since the CIDEP decay is measured at constant magnetic field, several experiments have to be conducted at different field positions in order to record an entire trEPR spectrum. Using a flow-system, e.g., AquaX[®], ensures identical and reproducible experimental conditions.

The CW-EPR setup used within this thesis meets all requirements for trEPR, e.g., contains a transient-recorder. The time-resolution may however be limited to 300 ns due to the applied SHQE cavity. It should be

checked whether a MD5(FT) model with a resolution below 1 ns can be used instead. Both cavities are compatible with the AquaX system which is already available in the EPR laboratory.

Appendices

Appendix A

Density and Fluidity Data

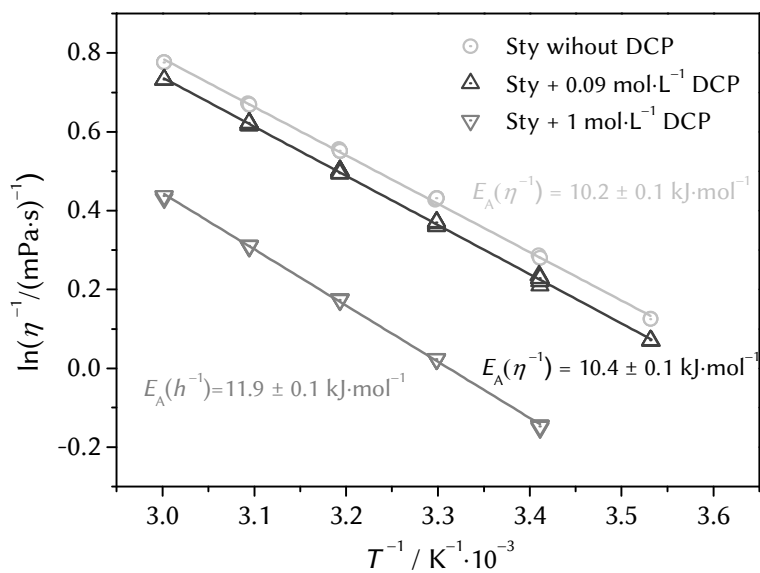


Figure A 1: Arrhenius plots of fluidity for Sty-H8 (bulk) containing different amounts of DCP. Within the SP-PLP-EPR experiments, a concentration of 0.09 mol·L⁻¹ DCP was used.

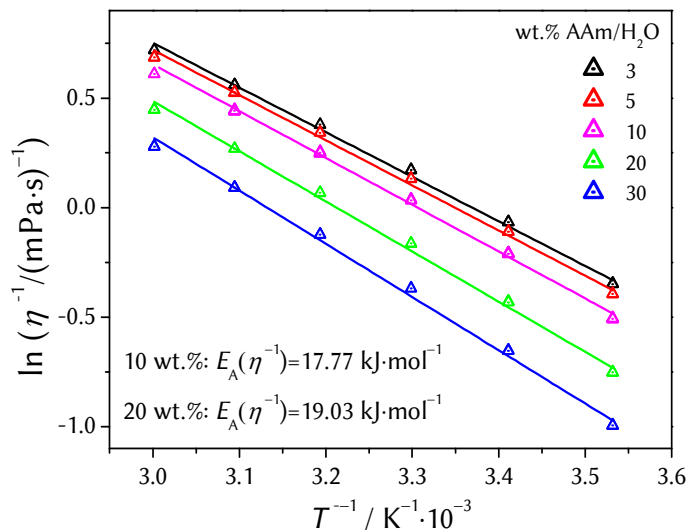


Figure A 2: Temperature dependence of fluidity (i.e., inverse viscosity) for different AAm concentrations in aqueous solution between 20 and 60 °C. The relevant activation energies are noted in the figure.

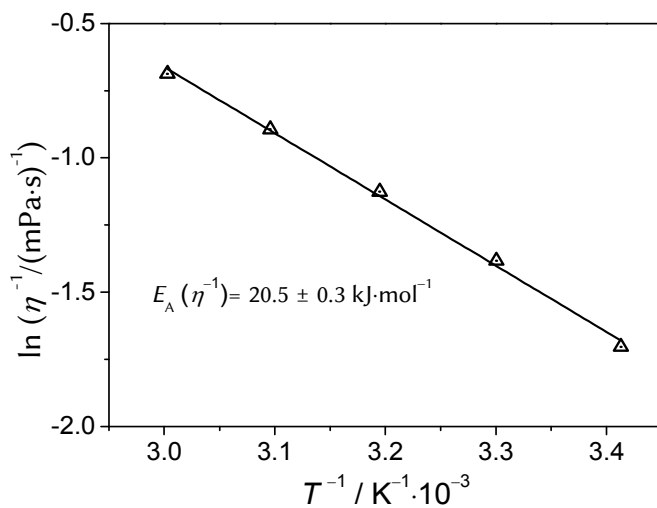


Figure A 3: Temperature dependence of fluidity for bulk DBI between 20 and 60 °C.

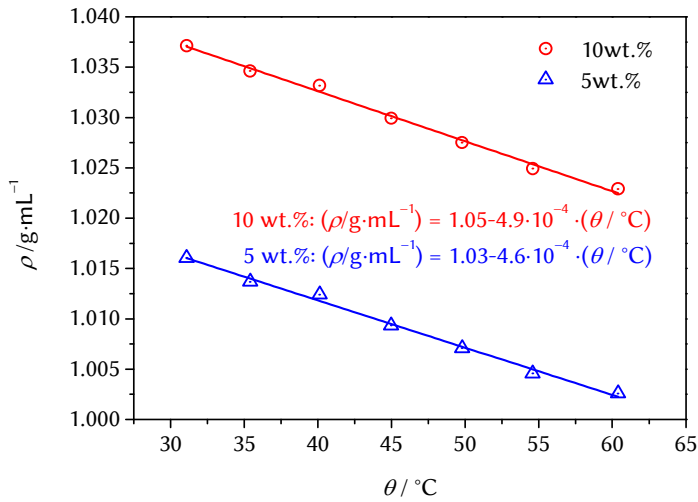


Figure A 4: Temperature dependence of density for the aqueous solutions of 5 and 10 wt.% fully-ionized methacrylic acid (NaMAA) between 31 and 62 °C.

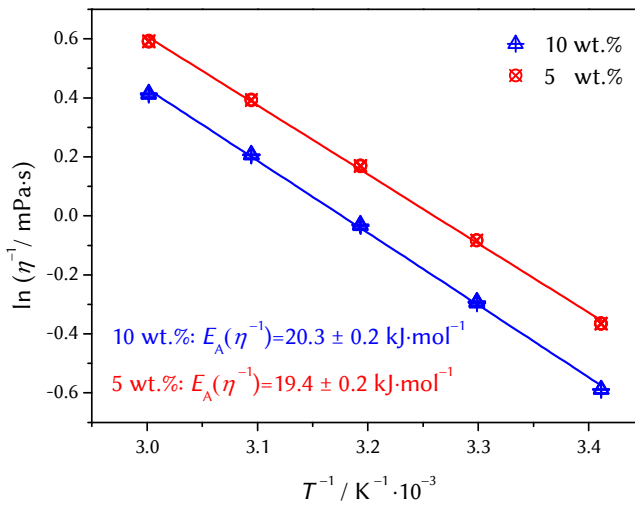


Figure A 5: Temperature dependence of fluidity for the aqueous solutions of 5 and 10 wt.% NaMAA between 20 and 60 °C. The related activation energies are noted.

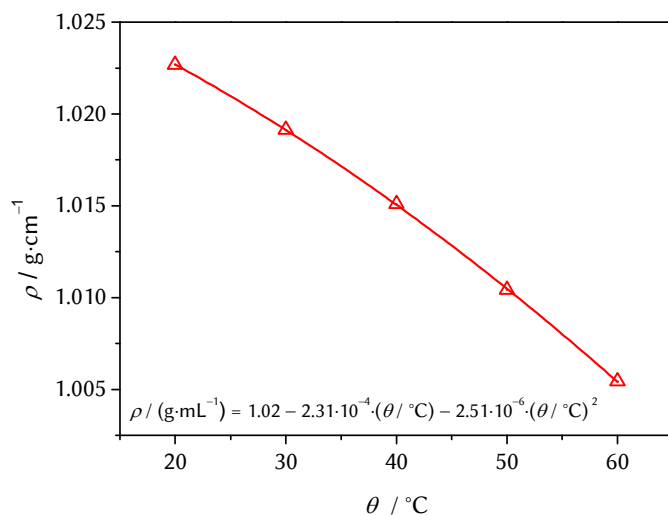


Figure A 6: Temperature dependence of density for the aqueous solution of 20 wt.% TMAEMA between 22 and 61 °C.

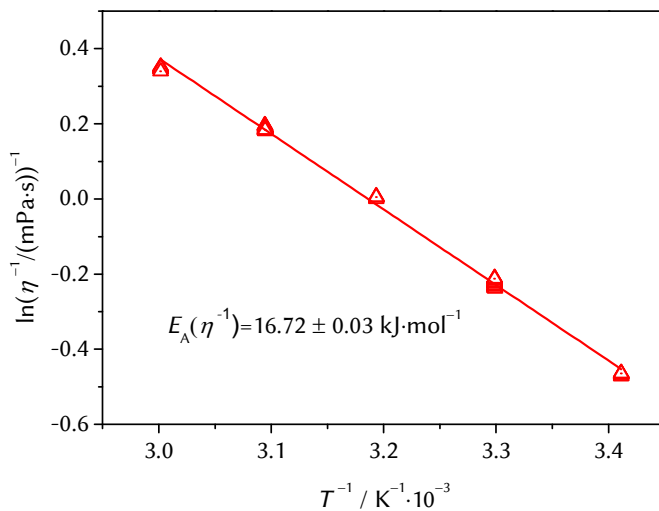


Figure A 7: Temperature dependence of fluidity for the aqueous solution of 20 wt.% TMAEMA between 30 and 60 °C.

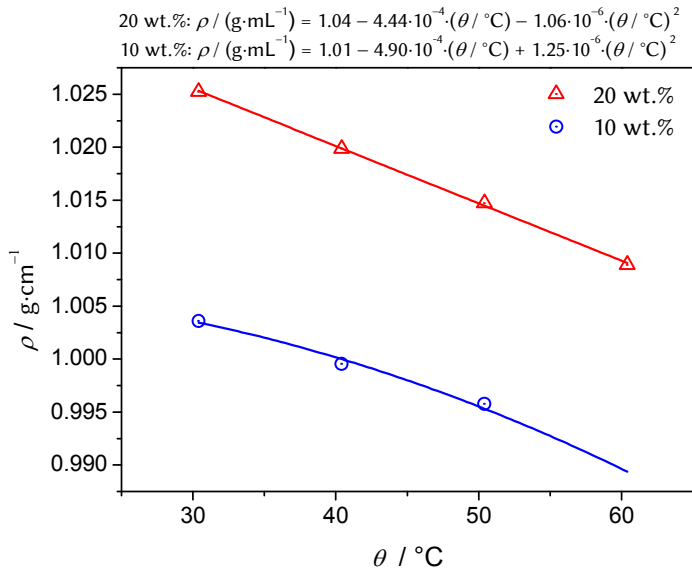


Figure A 8: Temperature dependence of density for the aqueous solutions of 10 and 20 wt.% TMAEA between 31 and 62 °C.

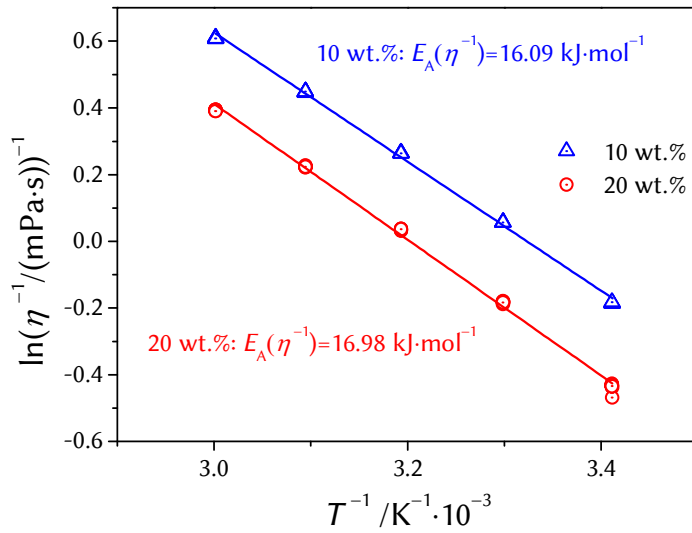


Figure A 9: Temperature dependence of fluidity for aqueous solutions of 10 and 20 wt.% TMAEA between 20 and 60 °C.

Temperature Dependent Crossover Chain Length

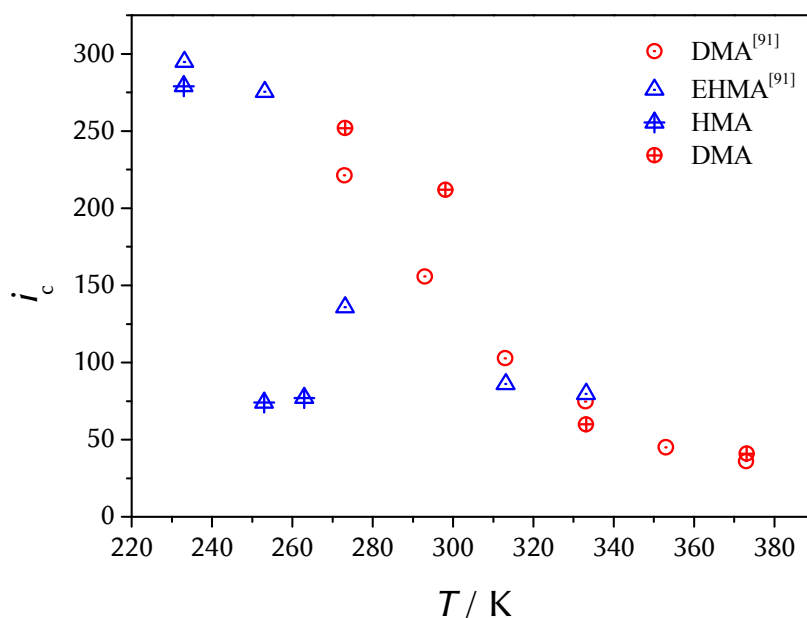


Figure A 10: Crossover chain-length, i_c , for bulk polymerizations of dodecyl methacrylate (DMA), ethylhexyl methacrylate (EHMA) and hexyl methacrylate (HMA) deduced from SP-PLP-EPR experiments with MMMP as the photoinitiator (27 mM). The measurements were performed in cooperation with Lara Riemann and served the purpose of verifying the temperature dependence of i_c as observed for methacrylates by N. Sørensen.⁹¹

PREDICI[®] Simulation of Styrene and AAm Polymerization

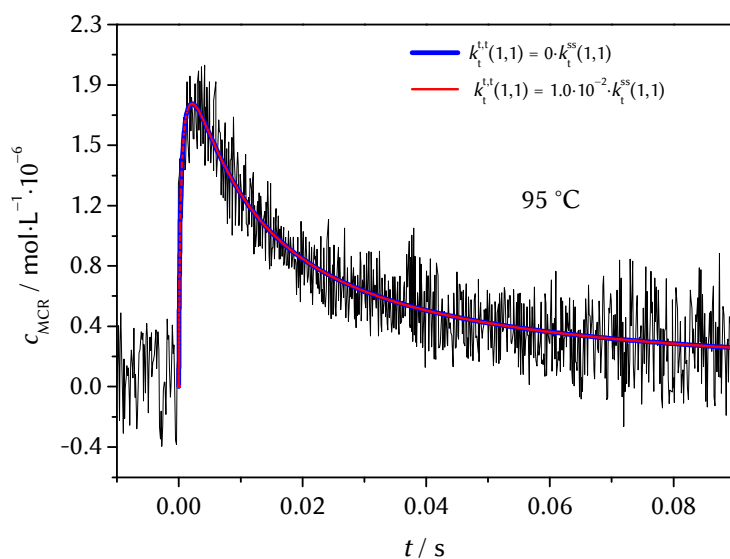


Figure A 11: PREDICI[®] fitting of the MCR concentration vs time profile deduced from an SP-PLP-EPR measurement at 95 °C and 10 wt.% AAm (in aqueous solution) assuming the rate coefficient of MCR-MCR termination, $k_t^{tt}(1,1)$, to be either zero or $0.01 \cdot k_t^{ss}(1,1)$. The figure serves the propose of illustrating that MCR-MCR termination does not contribute to the measured decay of c_{MCR} vs t .

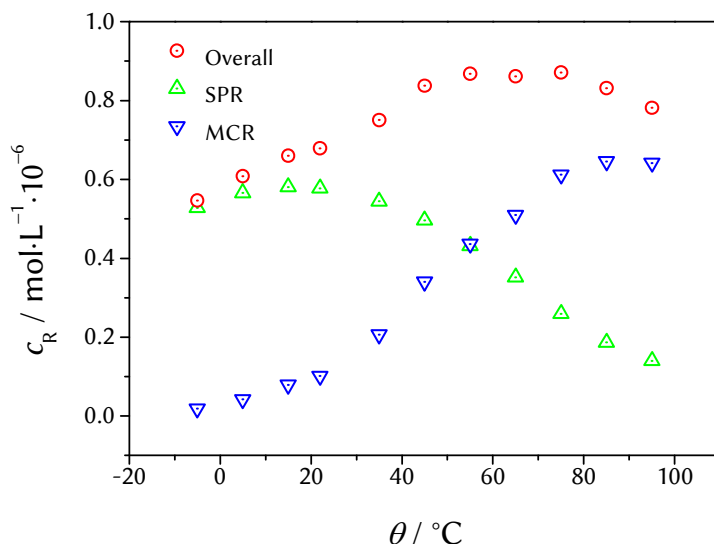


Figure A 12: Overall and individual radical concentrations during AAm homopolymerization (10 wt.%) in aqueous solution under stationary conditions between -5 and $+95$ °C. The data has been deduced from experimental EPR spectra by double-integration and calibration against TEMPOL solutions. The individual SPR and MCR concentrations were used for the calculation of x_{MCR} .

PREDICI Simulation and Fitting Procedure with Styrene Polymerization

For styrene homopolymerization at low degrees of monomer conversion, chain-length-dependent rate coefficients of termination, $k_t(i,i)$, were transferred into the associated chain-length-averaged $\langle k_t \rangle$ values by PREDICI fitting carried out in two steps: Based upon the data for initiation, propagation and for the concentrations applied in Ref.¹²⁰, $k_t(i,i)$ was estimated via the so-called *Combination/Disproportionation* reaction step by .fun-file using the composite-model parameters reported in the text. The resulting macroradical concentration vs t profiles were re-fitted in a second step by a modified model using the *parameter estimation* mode. Thereby, termination was treated as being chain-length independent within the *Combination/Disproportionation* reaction step

Appendix B

Simulation and Fitting of EPR Spectra

Matlab Scriptum using Easyspin (TMAEA 353 K)

```
clc
clear all
close all
easyspin
```

%% Import data from text file.

% Script for importing data from the following text file:

```
%C:\Users\HK\Documents\Uni\Promotion\ESR-
  Auswertung\FA1Quat\20140124\FA1Quat_353K.txt
```

%% To extend the code to different selected data or a different text file,
% generate a function instead of a script.

% Auto-generated by MATLAB on 2014/06/17 10:55:09

%% Initialize variables.

```
filename='C:\Users\HK\Documents\Uni\Promotion\ESR-
  Auswertung\FA1Quat\20140124\FA1Quat_353K.txt';
```

```
delimiter = '\t';
```

%% Format string for each line of text:

% column1: double (%f)

% column2: double (%f)

% For more information, see the TEXTSCAN documentation.

```
formatSpec = '%f%f%[\n\r]';
```

```
%% Open the text file.
```

```
fileID = fopen(filename,'r');
```

```
%% Read columns of data according to format string.
```

```
% This call is based on the structure of the file used to generate this  
% code. If an error occurs for a different file, try regenerating the code  
% from the Import Tool.
```

```
dataArray = textscan(fileID, formatSpec, 'Delimiter', delimiter, 'ReturnOnError', false);
```

```
%% Close the text file.
```

```
fclose(fileID);
```

```
%% Post processing for unimportable data.
```

```
% No unimportable data rules were applied during the import, so no  
% post  
% processing code is included. To generate code which works for  
% unimportable data, select unimportable cells in a file and regenerate  
% the script.
```

```
%% Allocate imported array to column variable names
```

```
VarName1 = dataArray{:, 1};
```

```
VarName2 = dataArray{:, 2};
```

```
%% Clear temporary variables
```

```
clearvars filename delimiter formatSpec fileID dataArray ans;
```

```
B=VarName1;
```

```
spc=VarName2;
```

```
plot(B,spc)
```

```
%Definition of Systems%
```

```
Sys1.g = 1.9962088285294222; %http://www.easypin.org/%
```

```

A1 =2.0682;
A2 =1.8537;
A1= mt2mhz(A1,2.0023193043617);
A2= mt2mhz(A2,2.0023193043617);
Sys1.Nucs = '1H,1H';
Sys1.A = [A1 A2];
Sys1.n = [1 2];
Exp.ModAmp = 0.3;
Exp.mwFreq = 9.410;
Exp.Range = [329.3 344.285352];
Sys1.lw = [0.44 0.4];
Vary1.g = [0.01];
Vary1.A = [1 1];
Vary1.lw = [0.45 0.3];

Sys2.g = 1.99755; %http://www.easyspin.org/%
A3 = 1.6524;
A4 = 1.1066;
A3= mt2mhz(A3,2.0023193043617);
A4= mt2mhz(A4,2.0023193043617);
Sys2.Nucs = '1H,1H';
Sys2.A = [A3 A4];
Sys2.n = [2 2];
Sys2.lw = [0.503059853110559 0.543816986043898];

Sys3.g = 1.99755;%http://www.easyspin.org/%
A7 =2.7459;
A7= mt2mhz(A7,2.0023193043617);
Sys3.Nucs = '1H';
Sys3.A = [A7];
Sys3.n = [2];
Sys3.lw = [0.315254443018229 -0.00102242059933400];

```

%Variation of Parameters%

```
Vary1.g = [0.01];  
Vary1.A = [1 1];  
Vary1.lw = [0.1 0.1];  
Vary2.g = [0.01];  
Vary2.A = [10 10];  
Vary2.lw = [0.3 0.3];  
Vary3.g = [0.01];  
Vary3.A = [10];  
Vary3.lw = [0.3 0.3];
```

%Fractions%

```
Sys1.weight = 0.0;  
Sys2.weight = 0.308233064633229;  
Sys3.weight = 0.0233490769353011;
```

```
MCR3fraction = (Sys3.weight)/(Sys2.weight+Sys3.weight)  
Vary1.weight = 0.9;  
Vary2.weight = 0.9;  
Vary3.weight = 0.1;
```

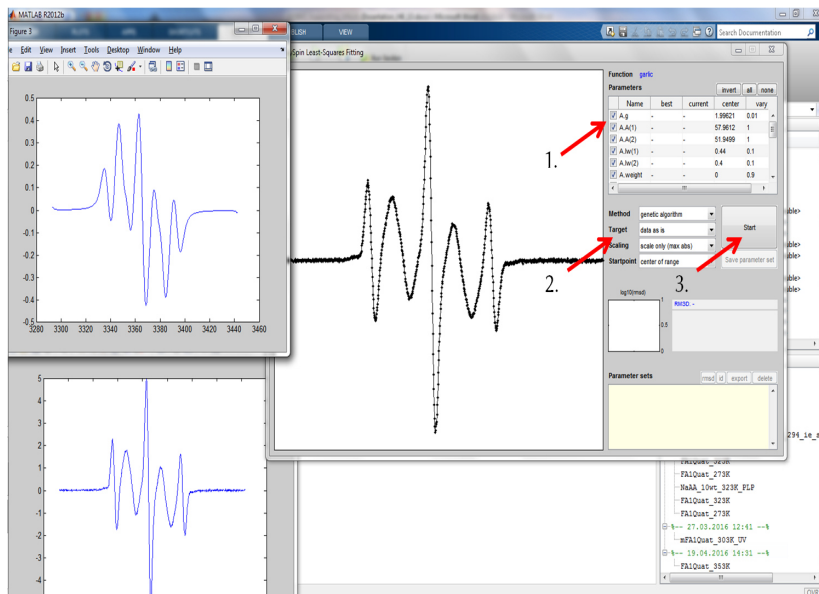
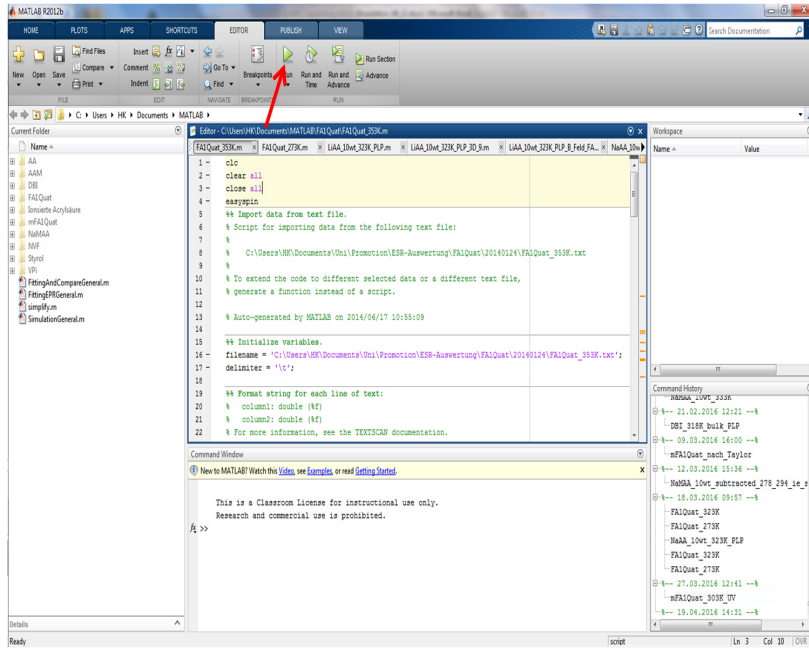
%Fitting%

```
SimOpt.Method = 'perturb';  
FitOpt.Method = 'genetic fcn';  
FitOpt.Scaling = 'maxabs';  
esfit('garlic',spc,{Sys1,Sys2,Sys3},{Vary1,Vary2,Vary3},Exp,SimOpt,FitO  
pt);
```

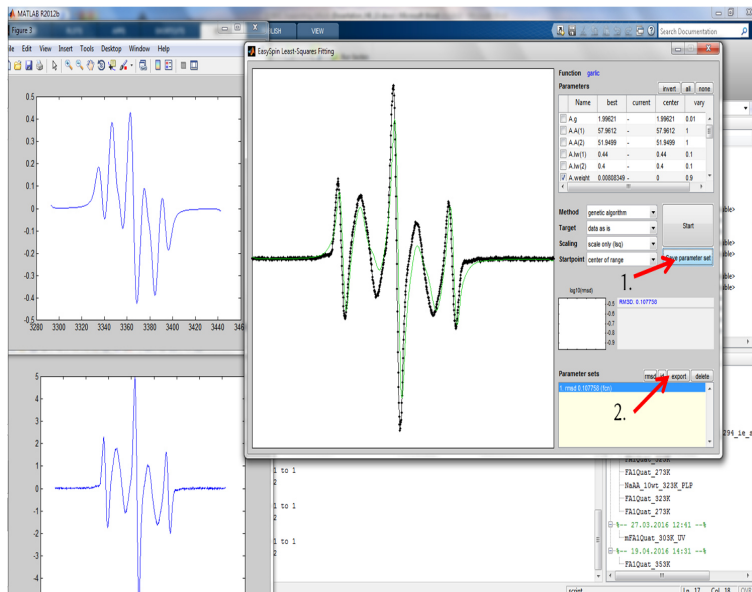
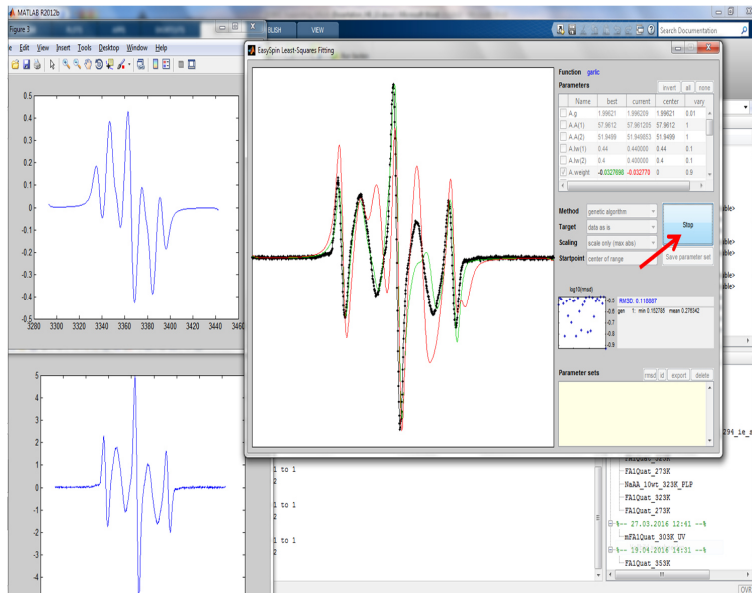
%Extraction of Individual Spectra:

```
MCR1=garlic(Sys2,Exp);  
MCRscale1=MCR1*Sys2.weight;  
MCR2=garlic(Sys3,Exp);  
MCRscale2=MCR2*Sys3.weight;  
plot(B,MCRscale1)
```

Using the Graphical User Interface



Appendix B: Simulation and Fitting of EPR Spectra



Appendix C

Abbreviations

Abbreviations and Acronyms

AA	acrylic acid (non-ionized)
AAM	acrylamide (monomer)
A(H)	proportional factor for Heller-McConnel Equation
$a(H)$	hyperfine coupling constant for an H-atom
$A(k_x)$	(Arrhenius) pre-exponential factor of the rate coefficient k_x
α	power-law exponent describing the chain-length
α_l	α in the long chain-length regime
AMPS	2-acrylamido-2-methylpropane sulfonic acid
α_s	α in the short chain-length regime
BA	butyl acrylate
B_x	magnetic field position
CI	chemically initiated
CLD	chain-length dependent
CLDP	chain-length dependent propagation
CLDT	chain-length dependent termination
C_{RD}	reaction diffusion constant
CRP	conventional radical polymerization
c_{SPR}	concentration of end-chain macroradicals
CTA	chain-transfer agent
c_x	concentration of substance x
c_x^0	initial concentration of substance x

Appendix C: Abbreviations

DA	dodecyl acrylate
DBI	di(<i>n</i> -butyl) itaconate
DCP	dicumyl peroxide
DMA	dodecyl methacrylate
DMPA	2,2-dimethoxy-2-phenyl acetophenone
D	self-diffusion coefficient
$E_A(k_x)$	activation energy of coefficient k_x
EPR	electron paramagnetic resonance
eq	equation
f	initiator efficiency or microfriction
FT	Fourier transformation
η	dynamic viscosity
hfc	hyperfine coupling
hfcc	hyperfine coupling constant
ΔH	change of enthalpy
h_1, h_2	calibration constants in SP-PLP-ESR
η_r	relative viscosity
I	EPR signal intensity
I^0	initial EPR signal
i, j	radical chain length
i_c	cross-over chain length according to the Composite Model
k_b	Boltzmann constant
k_{bb}	backbiting rate coefficient
k_d	initiator decomposition rate coefficient
K	equilibrium constant
k_i	rate coefficient of monomer addition to initiator-derived primary radicals
k_p	propagation rate coefficient
k_p^0	propagation rate coefficient without the contribution of diffusion
k_p^s	propagation rate coefficient of secondary propagating radicals
k_p^t	propagation rate of midchain radicals
k_p^{eff}	effective propagation rate coefficient
k_{SD}	rate coefficient of segmental diffusion
k_t	termination rate coefficient
$\langle kt \rangle$	chain-length-averaged termination rate coefficient
k_t^0	termination rate coefficient of (hypothetical) coiled

	monomeric radicals
$k_t(1,1)$	termination rate coefficient of radicals of chain length unity
k_{tc}	rate coefficient for termination by combination
k_{TD}	rate coefficient of translational diffusion
k_{td}	rate coefficient for termination by disproportionation
k_t^{eff}	effective termination rate coefficient
$k_t(i,i)$	termination rate coefficient of radicals of identical chain length i
$k_t(i,j)$	termination rate coefficient of radicals of size i and j
k_{RD}	reaction diffusion controlled termination rate coefficient
$k_t^{ss}(1,1)$	termination rate coefficient of two monomeric secondary propagating radicals
$k_t^{st}(1,1)$	termination rate coefficient of a monomeric secondary propagating radical and hypothetical monomeric midchain radical
k_t^{tt}	termination rate coefficient of a two hypothetic monomeric midchain radicals
LC	regime long contact regime
M	molecular mass
MA	methyl acrylate
MAA	methacrylic acid
MEHQ	hydroquinone monomethyl ether
MMD	Molar mass distribution
MMMP	2-methyl-4-(methylthio)-2-morpholino-propiophenone
N_A	Avogadro's number
NaAA	fully-ionized acrylic acid
NaMAA	fully-ionized methacrylic acid
NIR	near infrared
NMR	nuclear magnetic resonance
ω	reaction order in monomer concentration
p.r.r.	pulse repetition rate
NVP	<i>N</i> -vinyl pyrrolidone
PLP	pulsed laser polymerization
R_C	capture radius according to Smoluchowski equation
RD	reaction diffusion

Appendix C: Abbreviations

r_1	hydrodynamic radius of a monomeric radical
R_p	rate of polymerization
SD	segmental diffusion
SEC	size exclusion chromatography
S/N	signal-to-noise ratio
SP	single pulsed
Sty	styrene
T	absolute temperature (in Kelvin)
t	time
Θ	dihedral angle (see Heller-McConnel Equation)
θ	temperature in degrees centigrade ($^{\circ}\text{C}$)
t_p	propagation time
TD	translational diffusion
TEMPO	2,2,6,6-tetramethyl-1-piperidinyloxy
TMAEA	Trimethylaminoethyl acrylate chloride (monomer)
TMAEMA	Trimethylaminoethyl methacrylate chloride (monomer)
TS	transition state
TST	transition state theory
UV	ultra violet
VAc	vinyl acetate
VPi	vinyl pivalate
V50	2,2'-Azobis (2-methylpropionamidine) dihydrochloride (initiator)
V86	2,2'-Azobis[2-methyl- <i>N</i> -(2-hydroxyethyl)propionamide] (initiator)
wt.%	weight percent with respect to the monomer-solvent mixture
X	monomer-to-polymer conversion
x_i	molar fraction of species i

Bibliography

- (1) *Plastics – the Facts 2015 - An analysis of European plastics production, demand and waste data*; Plastics Europe, EuPC, EuPR, 2015.
- (2) Baekeland, L. H. *Chemiker-Zeitung* **1909**, *33*, 317–318.
- (3) Staudinger, H. *Ber. dtsh. Chem. Ges.* **1920**, *53*, 1073–1085.
- (4) Staudinger, H.; Fritsch, J. *Helv. Chim. Acta* **1922**, *5*, 785–806.
- (5) Elias, H.-G. *Makromoleküle – Industrielle Polymere und Synthesen*; Vol. 3, 6th edition.; WILEY-VCH, Weinheim, 2001.
- (6) Yunkai, L.; Tingwu, X.; Zhiyun, O.; Xiongcai, L.; Honglu, L.; Zhongyong, H.; Peiling, Y. *J. Appl. Polym. Sci.* **2009**, *113*, 3510–3519.
- (7) Wypych, G. In *Handbook of Polymers*; Wypych, G., ChemTec Publishing, Toronto, 2012.
- (8) Akbari, M.; Fazaelpoor, M. H.; Goharizi, A. S. *Biotechnol. Bioprocess Eng.* **2011**, *16*, 407–412.
- (9) Aktay, L.; Johnson, A. F.; Holzapfel, M. *Comp. Mater. Sci.* **2005**, 252–260.
- (10) Candau, F.; Buchert, P. *Colloids and Surfaces* **1990**, *48*, 107–122.
- (11) Losada, R.; Wandrey, C. *Macromol. Rapid Commun.* **2008**, *29*, 252–257.
- (12) Losada, R.; Wandrey, C. *Macromolecules* **2009**, *42*, 3285–3293.
- (13) Matyjaszewski, K.; Davis, T. P. *Handbook of Radical Polymerization*; John Wiley and Sons, Inc., Hoboken, 2002.
- (14) Barner-Kowollik, C.; Buback, M.; Egorov, M.; Fukuda, T.; Goto, A.; Olaj, O. F.; Russell, G. T.; Vana, P.; Yamada, B.; Zetterlund, P. B. *Prog. Polym. Sci.* **2005**, *30*, 605–643.
- (15) Olaj, O. F.; Bitai, I.; Hinkelmann, F. *Makromol. Chem.* **1987**, *188*, 1689–1702.
- (16) Olaj, O. F.; Schnöll-Bitai, I. *Eur. Polym. J.* **1989**, *25*, 635–641.

- (17) Buback, M.; Gilbert, R. G.; Russell, G. T.; Hill, D. J. T.; Moad, G.; O'Driscoll, K. F.; Shen, J.; Winnik, M. A. *J. Polym. Sci. Part A Polym. Chem.* **1992**, *30*, 851–863.
- (18) Beuermann, S.; Buback, M.; Hesse, P.; Kuchta, F.-D.; Lacík, I.; van Herk, A. M. *Pure Appl. Chem.* **2007**, *79*, 1463–1469.
- (19) Beuermann, S.; Buback, M. *Prog. Polym. Sci.* **2002**, *27*, 191–254.
- (20) Kuchta, F. D.; van Herk, A. M.; German, A. L. *Macromolecules* **2000**, *33*, 3641–3649.
- (21) Buback, M.; Hesse, P.; Lacík, I. *Macromol. Rapid Commun.* **2007**, *28*, 2049–2054.
- (22) Lacík, I.; Beuermann, S.; Buback, M. *Macromolecules* **2003**, *36*, 9355–9363.
- (23) Lacík, I.; Beuermann, S.; Buback, M. *Macromolecules* **2001**, *34*, 6224–6228.
- (24) Beuermann, S.; Buback, M.; Hesse, P.; Kukučková, S.; Lacík, I. *Macromol. Symp.* **2007**, *248*, 23–32.
- (25) Beuermann, S.; Buback, M.; Hesse, P.; Lacík, I. *Macromolecules* **2006**, *39*, 184–193.
- (26) Beuermann, S.; Buback, M.; Hesse, P.; Kukučková, S.; Lacík, I. *Macromol. Symp.* **2007**, *248*, 41–49.
- (27) Pascal, P.; Napper, D.; Gilbert, R. *Macromolecules* **1990**, *23*, 5161–5163.
- (28) Seabrook, S. A.; Tonge, M. P.; Gilbert, R. G. *J. Polym. Sci. Part A Polym. Chem.* **2005**, *43*, 1357–1368.
- (29) Lacík, I.; Chovancová, A.; Uhelská, L.; Preusser, C.; Hutchinson, R. A.; Buback, M. *Macromolecules* **2016**, *49*, 3244–3253.
- (30) Ganachaud, F.; Balic, R.; Monteiro, M. J.; Gilbert, R. G. *Macromolecules* **2000**, *33*, 8589–8596.
- (31) Schrooten, J.; Lacík, I.; Stach, M.; Hesse, P.; Buback, M. *Macromol. Chem. Phys.* **2013**, *214*, 2283–2294.
- (32) Schrooten, J.; Buback, M.; Hesse, P.; Hutchinson, R. A.; Lacík, I. *Macromol. Chem. Phys.* **2011**, *212*, 1400–1409.
- (33) Stach, M.; Lacík, I.; Kasák, P.; Chorvát, D.; Saunders, A. J.; Santanakrishnan, S.; Hutchinson, R. A. *Macromol. Chem. Phys.* **2010**, *211*, 580–593.
- (34) Lacík, I.; Sobolčiak, P.; Stach, M.; Chorvát Jr., D.; Kasák, P. *Polymer* **2016**, *87*, 38–49.
- (35) Lacík, I.; Učňová, L.; Kukučková, S.; Buback, M.; Hesse, P.; Beuermann, S. *Macromolecules* **2009**, *42*, 7753–7761.

-
- (36) Drawe, P.; Buback, M. *Macromol. Theory Simul.* **2015**, *25*, 74–84.
- (37) Barth, J.; Buback, M.; Hesse, P.; Sergeeva, T. *Macromolecules* **2010**, *43*, 4023–4031.
- (38) Barth, J.; Meiser, W.; Buback, M. *Macromolecules* **2012**, *45*, 1339–1345.
- (39) Barth, J.; Buback, M. *Macromolecules* **2012**, *45*, 4152–4157.
- (40) Buback, M.; K ulpmann, A. *Macromol. Chem. Phys.* **2003**, *204*, 632–637.
- (41) Barth, J.; Buback, M.; Russell, G. T.; Smolne, S. *Macromol. Chem. Phys.* **2011**, *212*, 1366–1378.
- (42) Kattner, H.; Buback, M. *Macromol. Chem. Phys.* **2014**, *215*, 1180–1191.
- (43) Kattner, H.; Buback, M. *Macromol. Symp.* **2013**, *333*, 11–23.
- (44) Barth, J.; Buback, M. *Macromolecules* **2011**, *44*, 1292–1297.
- (45) Buback, M.; Russell, G. T. In *Encyclopedia of Radicals in Chemistry, Biology and Materials*; John Wiley & Sons, Ltd, 2012; pp. 1737–1784.
- (46) Achilias, D. S. *Macromol. Theory Simul.* **2007**, *16*, 319–347.
- (47) Fischer, H.; Radom, L. *Angew. Chem. Int. Ed.* **2001**, *40*, 1340–1371.
- (48) Szymanski, R. *Macromol. Theory Simul.* **2011**, *20*, 8–12.
- (49) Junkers, T.; Barner-Kowollik, C. *J. Polym. Sci. Part A Polym. Chem.* **2008**, *46*, 7585–7605.
- (50) Roedel, M. J. *J. Am. Chem. Soc.* **1953**, *75*, 6110–6112.
- (51) Yu, X.; Broadbelt, L. J. *Macromol. Theory Simul.* **2012**, *21*, 461–469.
- (52) Campbell, J. D.; Teymour, F.; Morbidelli, M. *Macromolecules* **2003**, *36*, 5491–5501.
- (53) Campbell, J. D.; Teymour, F.; Morbidelli, M. *Macromolecules* **2003**, *36*, 5502–5515.
- (54) Cuccato, D.; Mavroudakos, E.; Dossi, M.; Moscatelli, D. *Macromol. Theory Simul.* **2013**, *22*, 127–135.
- (55) Kajiwara, A.; Nanda, A. K.; Matyjaszewski, K. *Macromolecules* **2004**, *37*, 1378–1385.
- (56) Kajiwara, A. *Macromol. Symp.* **2007**, *248*, 50–59.
- (57) Scott, G. E.; Senogles, E. *J. Macromol. Sci. Part A - Chem.* **1970**, *4*, 1105–1117.
- (58) Scott, G. E.; Senogles, E. *J. Macromol. Sci. Part C Polym. Rev.* **1973**, *9*, 49–69.
- (59) Scott, G. E.; Senogles, E. *J. Macromol. Sci. Part A - Chem.* **1974**, *8*, 753–773.

- (60) Wunderlich, W. *Makromol. Chem.* **1976**, *177*, 973–989.
- (61) Madruga, E. L.; Fernández-García, M. *Macromol. Chem. Phys.* **1996**, *197*, 3743–3755.
- (62) Kaszás, G.; Földes-Bereznich, T.; Tüdös, F. *Eur. Polym. J.* **1983**, *19*, 469–473.
- (63) McKenna, T. F.; Villanueva, A.; Santos, A. M. *J. Polym. Sci. Part A Polym. Chem.* **1999**, *37*, 571–588.
- (64) Nikitin, A. N.; Hutchinson, R. A. *Macromol. Theory Simul.* **2006**, *15*, 128–136.
- (65) Nikitin, A. N.; Hutchinson, R. A.; Kalfas, G. A.; Richards, J. R.; Bruni, C. *Macromol. Theory Simul.* **2009**, *18*, 247–258.
- (66) Nikitin, A. N.; Hutchinson, R. A. *Macromolecules* **2005**, *38*, 1581–1590.
- (67) Nikitin, A. N.; Hutchinson, R. A. *Macromol. Rapid Commun.* **2009**, *30*, 1981–1988.
- (68) Nikitin, A. N.; Hutchinson, R. A.; Wang, W.; Kalfas, G. A.; Richards, J. R.; Bruni, C. *Macromol. React. Eng.* **2010**, *4*, 691–706.
- (69) Nikitin, A. N.; Hutchinson, R. A.; Buback, M.; Hesse, P. *Macromolecules* **2007**, *40*, 8631–8641.
- (70) Barth, J.; Buback, M.; Barner-Kowollik, C.; Junkers, T.; Russell, G. T. *J. Polym. Sci. Part A Polym. Chem.* **2012**, *50*, 4740–4748.
- (71) Lin, C. Y.; Izgorodina, E. I.; Coote, M. L. *Macromolecules* **2010**, *43*, 553–560.
- (72) Lacík, I.; Beuermann, S.; Buback, M. *Macromol. Chem. Phys.* **2004**, *205*, 1080–1087.
- (73) Degirmenci, I.; Ozaltın, T. F.; Karahan, O.; Van Speybroeck, V.; Waroquier, M.; Aviyente, V. *J. Polym. Sci. Part A Polym. Chem.* **2013**, *51*, 2024–2034.
- (74) Wang, W.; Nikitin, A. N.; Hutchinson, R. A. *Macromol. Rapid Commun.* **2009**, *30*, 2022–2027.
- (75) Smoluchowski, M. *Z. phys. Chem.* **1917**, *XXXVII*, 129–168.
- (76) Fischer, H.; Schuh, H.-H. *Helv. Chim. Acta* **1978**, *61*, 2130–2164.
- (77) Fischer, H. *J. Polym. Sci. Part B Polym. Lett.* **1964**, *2*, 529–532.
- (78) Schuh, H.; Fischer, H. *Int. J. Chem. Kinet.* **1976**, *VIII*, 341–356.
- (79) Benson, S. W.; North, A. M. *J. Am. Chem. Soc.* **1962**, *84*, 935–940.
- (80) Benson, S. W.; North, A. M. *J. Am. Chem. Soc.* **1959**, *81*, 1339–1345.
- (81) Buback, M.; Huckestein, B.; Russell, G. T. *Macromol. Chem. Phys.* **1994**, *195*, 539–554.

-
- (82) Buback, M. *Makromol. Chem.* **1990**, *191*, 1575–1587.
- (83) Andrzejewska, E. *Prog. Polym. Sci.* **2001**, *26*, 605–665.
- (84) Heuts, J. P. A.; Gilbert, R. G.; Radom, L. *Macromolecules* **1995**, *28*, 8771–8781.
- (85) Olaj, O. F.; Vana, P.; Zoder, M.; Kornherr, A.; Zifferer, G. *Macromol. Rapid Commun.* **2000**, *21*, 913–920.
- (86) Olaj, O. F.; Vana, P.; Zoder, M. *Macromolecules* **2002**, *35*, 1208–1214.
- (87) Heuts, J. P. A.; Russell, G. T. *Eur. Polym. J.* **2006**, *42*, 3–20.
- (88) Degirmenci, I.; Avci, D.; Aviyente, V.; Cauter, K. Van; Speybroeck, V. Van; Waroquier, M. *Macromolecules* **2007**, *40*, 9590–9602.
- (89) Barner-Kowollik, C.; Russell, G. T. *Prog. Polym. Sci.* **2009**, *34*, 1211–1259.
- (90) Smith, G. B.; Russell, G. T.; Heuts, J. P. A. *Macromol. Theory Simul.* **2003**, *12*, 299–314.
- (91) Sörensen, N. *Kinetics and Mechanism of Cu-Catalyzed Atom Transfer Radical Polymerization*, PhD Thesis, Georg-August-Universität Göttingen, 2015.
- (92) Johnston-Hall, G.; Theis, A.; Monteiro, M. J.; Davis, T. P.; Stenzel, M. H.; Barner-Kowollik, C. *Macromol. Chem. Phys.* **2005**, *206*, 2047–2053.
- (93) Fischer, H.; Paul, H. *Acc. Chem. Res.* **1987**, 200–206.
- (94) Kirkwood, J. G.; Riseman, J. *J. Chem. Phys.* **1948**, *16*, 565–573.
- (95) Johnston-Hall, G.; Monteiro, M. J. *J. Macromol. Sci. Part A Polym. Chem.* **2008**, *46*, 3155–3173.
- (96) Friedman, B.; O’Shaughnessy, B. *Macromolecules* **1993**, *26*, 5726–5739.
- (97) Khokhlov, A. R. *Makromol. Chem., Rapid Commun.* **1981**, *2*, 633–636.
- (98) Olaj, O. F.; Zifferer, G. *Macromolecules* **1987**, *20*, 850–861.
- (99) Fröhlich, M. G.; Vana, P.; Zifferer, G. *J. Chem. Phys.* **2007**, *127*, 164906.
- (100) Kattner, H.; Buback, M. *Macromolecules* **2015**, *48*, 309–315.
- (101) Olaj, O. F.; Kornherr, A.; Zifferer, G. *Macromol. Theory Simul.* **1998**, *7*, 501–508.
- (102) Russell, G. T. *Aust. J. Chem.* **2002**, *55*, 399–414.
- (103) Smith, G. B.; Russell, G. T. *Z. Phys. Chem.* **2005**, *219*, 295–323.
- (104) Buback, M.; Müller, E.; Russell, G. T. *J. Phys. Chem. A* **2006**, *110*, 3222–3230.
- (105) Vana, P.; Davis, T. P.; Barner-Kowollik, C. *Aust. J. Chem.* **2002**, *55*, 315–318.

- (106) Kattner, H. *Untersuchung der radikalischen Polymerisation von Vinylacetat durch Pulsaserexperimente in Verbindung mit EPR und SEC*, Master Thesis, Georg-August University Göttingen, 2012.
- (107) Drawe, P. PhD Thesis, Göttingen, 2016.
- (108) Kattner, H.; Drawe, P.; Buback, M. *Macromol. Chem. Phys.* **2015**, *216*, 1737–1745.
- (109) Kattner, H.; Buback, M. *Macromolecules* **2015**, *48*, 7410–7419.
- (110) *User Service Training Course*, Chapter 5: EPR Resonators, Bruker Biospin, 1–26.
- (111) Eaton, G.; Eaton, S.; Barr, D.; Weber, R. *Quantitative EPR*; Springer: Wien, 2010.
- (112) Nesmelov, Y. E.; Gopinath, A.; Thomas, D. D. *J. Magn. Reson.* **2004**, *167*, 138–146.
- (113) Malmberg, C. G.; Maryott, A. A. *J. Res. Natl. Bur. Stand. (1934)*. **1956**, *56*, 1–8.
- (114) Kattner, H.; Buback, M. *Macromolecules* **2016**, *49*, 3716–3722.
- (115) Beuermann, S.; Buback, M.; Hesse, P.; Junkers, T.; Lacík, I. *Macromolecules* **2006**, *39*, 509–516.
- (116) Buback, M.; Egorov, M.; Junkers, T.; Panchenko, E. *Macromol. Chem. Phys.* **2005**, *206*, 333–341.
- (117) Barth, J.; Buback, M. *Macromol. Rapid Commun.* **2009**, *30*, 1805–1811.
- (118) Barth, J.; Buback, M.; Hesse, P.; Sergeeva, T. *Macromolecules* **2009**, *42*, 481–488.
- (119) Beuermann, S.; Buback, M.; Hesse, P.; Hutchinson, R. A.; Kukučková, S.; Lacík, I. *Macromolecules* **2008**, *41*, 3513–3520.
- (120) Taylor, D. R.; van Berkel, K. Y.; Alghamdi, M. M.; Russell, G. T. *Macromol. Chem. Phys.* **2010**, *211*, 563–579.
- (121) Barth, J.; Buback, M.; Hesse, P.; Sergeeva, T. *Macromol. Rapid Commun.* **2009**, *30*, 1969–1974.
- (122) Kamachi, M. *J. Polym. Sci. Part A Polym. Chem.* **2002**, *40*, 269–285.
- (123) Kamachi, M.; Kuwae, Y.; Kohno, M.; Nozakura, S. *Polym. J.* **1985**, *17*, 541–543.
- (124) Kubota, N.; Kajiwara, A.; Zetterlund, P. B.; Kamachi, M.; Treurnicht, J.; Tonge, M. P.; Gilbert, R. G.; Yamada, B. *Macromol. Chem. Phys.* **2007**, *208*, 2403–2411.
- (125) Yamada, B.; Kageoka, M.; Otsu, T. *Macromolecules* **1992**, *25*, 4828–4831.

-
- (126) Yamada, B.; Tagashira, S.; Sakamoto, K.; Nagano, Y.; Miura, Y. *Polym. Bull.* **1997**, *346*, 339–346.
- (127) Fairhurst, S. A.; Pilkington, R. S.; Sutcliffe, L. H. *J. Chem. Soc., Faraday Trans. 1* **1983**, *79*, 925–940.
- (128) Holz, M.; Mao, X.; Seiferling, D.; Sacco, A. *J. Chem. Phys.* **1996**, *104*, 669–679.
- (129) Gilbert, R. G. *Pure Appl. Chem.* **1996**, *68*, 1491–1494.
- (130) Buback, M.; Gilbert, R. G.; Hutchinson, R. A.; Klumperman, B.; Kuchta, F.-D.; Manders, B. G.; O’Driscoll, K. F.; Russell, G. T.; Schweer, J. *Macromol. Chem. Phys.* **1995**, *196*, 3267–3280.
- (131) Asua, J. M.; Beuermann, S.; Buback, M.; Castignolles, P.; Charleux, B.; Gilbert, R. G.; Hutchinson, R. A.; Leiza, J. R.; Nikitin, A. N.; Vairon, J. P.; Van Herk, A. M. *Macromol. Chem. Phys.* **2004**, *205*, 2151–2160.
- (132) Lyons, R. A.; Hutovic, J.; Piton, M. C.; Christie, D. I.; Clay, P. A.; Manders, B. G.; Kable, S. H.; Gilbert, R. G. *Macromolecules* **1996**, *29*, 1918–1927.
- (133) Buback, M.; Kurz, C. H.; Schmaltz, C. *Macromol. Chem. Phys.* **1998**, *199*, 1721–1727.
- (134) Beuermann, S.; Buback, M.; Davis, T. P.; Gilbert, R. G.; Hutchinson, R. A.; Olaj, O. F.; Russell, G. T.; Schweer, J.; van Herk, A. M. *Macromol. Chem. Phys.* **1997**, *198*, 1545–1560.
- (135) Beuermann, S.; Buback, M.; Davis, T. P.; Gilbert, R. G.; Hutchinson, R. A.; Kajiwara, A.; Klumperman, B.; Russell, G. T. *Macromol. Chem. Phys.* **2000**, *201*, 1355–1364.
- (136) Junkers, T.; Voll, D.; Barner-Kowollik, C. *e-Polymers* **2009**, *076*, 1–8.
- (137) Monyatsi, O.; Hutchinson, R. A. *Macromol. Chem. Phys.* **2016**, *217*, 51–58.
- (138) Russell, G. T. *Macromol. Theory Simul.* **1995**, *4*, 549–576.
- (139) Matheson, M. S.; Auer, E. E.; Bevilacqua, E. B.; Hart, E. J. *J. Am. Chem. Soc.* **1951**, *73*, 1700–1706.
- (140) Clouet, G.; Chaffanjon, P. *J. Macromol. Sci. Part A - Chem.* **1990**, *27*, 193–212.
- (141) Johnston-Hall, G.; Monteiro, M. J. *Macromolecules* **2008**, *41*, 727–736.
- (142) Friedman, B.; O’Shaughnessy, B. *Macromolecules* **1993**, *26*, 4888–4898.
- (143) Piton, M. C.; Gilbert, R. G.; Kuchel, P. W. *Macromolecules* **1993**, *26*, 4472–4477.
- (144) Buback, M.; Kowollik, C. *Macromol. Chem. Phys.* **2000**, *201*, 464–469.
- (145) Buback, M.; Kowollik, C. *Macromolecules* **1998**, *31*, 3211–3215.

- (146) Mahabadi, H. K. *Macromolecules* **1985**, *18*, 1319–1324.
- (147) Olaj, O. F.; Zifferer, G.; Gleixner, G. *Macromolecules* **1987**, *20*, 839–850.
- (148) Olaj, O. F.; Zifferer, G.; Gleixner, G. G. *Makromol. Chem., Rapid Commun.* **1985**, *6*, 773–784.
- (149) Fan, W.; Zhou, Q.; Sun, J.; Zhang, S. *J. Chem. Eng. Data* **2009**, *54*, 2307–2311.
- (150) Buback, M.; Junkers, T. *Macromol. Chem. Phys.* **2006**, *207*, 1640–1650.
- (151) Bune, Y. V.; Zhuravleva, I. L.; Sheinker, A. P.; Bogachev, Y. S.; Teleshov, E. N. *Polym. Sci. U.S.S.R.* **1986**, *28*, 1427–1433.
- (152) De Sterck, B.; Vaneerdeweg, R.; Du Prez, F.; Waroquier, M.; Van Speybroeck, V. *Macromolecules* **2010**, *43*, 827–836.
- (153) Hunkeler, D. *Macromolecules* **1991**, *24*, 2160–2171.
- (154) Husain, M. M.; Misra, S. N.; Gupta, A. *Makromol. Chem.* **1976**, *177*, 2919–2926.
- (155) Ishige, T.; Hamielec, A. E. *J. Appl. Polym. Sci.* **1973**, *17*, 1479–1506.
- (156) Seabrook, S. A.; Gilbert, R. G. *Polymer* **2007**, *48*, 4733–4741.
- (157) Seabrook, S. A.; Pascal, P.; Tonge, M. P.; Gilbert, R. G. *Polymer* **2005**, *46*, 9562–9573.
- (158) Theis, A.; Davis, T. P.; Stenzel, M. H.; Barner-Kowollik, C. *Polymer* **2006**, *47*, 999–1010.
- (159) Pascal, P.; Winnik, M. A.; Napper, D. H.; Gilbert, R. G. *Macromolecules* **1993**, *26*, 4572–4576.
- (160) Preusser, C. *Kinetics and Modeling of Free Radical Aqueous Phase Polymerization of Acrylamide with Acrylic Acid at Varying Degrees of Ionization*, PhD Thesis, Queen's University, Kingston, 2015.
- (161) Preusser, C.; Chovancová, A.; Lacík, I.; Hutchinson, R. A. *Macromol. React. Eng.* **2016**, DOI:10.1002/mren.201500076.
- (162) Pierik, S. C. J.; van Herk, A. M.; Plessis, C.; van Steenis, J. H.; Loonen, T.; Bombeek, A. *Eur. Polym. J.* **2005**, *41*, 1212–1218.
- (163) Castignolles, P.; Nikitin, A. N.; Couvreur, L.; Mouraret, G.; Charleux, B.; Vairon, J.-P. *Macromol. Chem. Phys.* **2006**, *207*, 81–89.
- (164) Hermosilla, L.; Calle, P.; Sieiro, C.; García, N.; Tiemblo, P.; Guzmán, J. *Chem. Phys.* **2007**, *340*, 237–244.
- (165) Willemse, R. X. E.; van Herk, A. M.; Panchenko, E.; Junkers, T.; Buback, M. *Macromolecules* **2005**, *38*, 5098–5103.

- (166) Buback, M.; Hesse, P.; Junkers, T.; Sergeeva, T.; Theis, T. *Macromolecules* **2008**, *41*, 288–291.
- (167) Kajiwara, A.; Kamachi, M. In *Advances in Controlled/Living Radical Polymerization*; ACS Symposium Series; American Chemical Society, Washington DC, 2006, Vol. 854, pp. 86–100.
- (168) Kajiwara, A. In *Controlled/Living Radical Polymerization*; ACS Symposium Series; American Chemical Society Washington DC, 2006; Vol. 944, pp. 111–124.
- (169) Sato, E.; Emoto, T.; Zetterlund, P. B.; Yamada, B. *Macromol. Chem. Phys.* **2004**, *205*, 1829–1839.
- (170) Azukizawa, M.; Yamada, B.; Hill, D. J. T.; Pomery, P. J. *Macromol. Chem. Phys.* **2000**, *201*, 774–781.
- (171) Yamada, B.; Azukizawa, M.; Yamazoe, H.; Hill, D. J. T.; Pomery, P. J. *Polymer* **2000**, *41*, 5611–5618.
- (172) Dai, S. *J. Chem. Educ.* **1991**, *68*, 894–895.
- (173) Hesse, P. *Radical Polymerization Kinetics in Aqueous Solution and in Systems with Secondary and Tertiary Radicals Studied by Novel Pulsed-Laser Techniques*, PhD Thesis, Universität Göttingen, Cuvillier Verlag, Göttingen, 2008.
- (174) Kattner, H.; Buback, M. *Macromol. Rapid Commun.* **2015**, *36*, 2186–2191.
- (175) Karatekin, E.; O’Shaughnessy, B.; Turro, N. J. *Macromol. Symp.* **2002**, *182*, 81–101.
- (176) Wittenberg, N. F. G.; Preusser, C.; Kattner, H.; Stach, M.; Lacík, I.; Hutchinson, R. A.; Buback, M. *Macromol. React. Eng.* **2015**, *10*, 95–107.
- (177) Achilias, D. S.; Kiparissides, C. *Polymer* **1994**, *35*, 1714–1721.
- (178) Achilias, D. S.; Kiparissides, C. *Macromolecules* **1992**, *25*, 3739–3750.
- (179) Fischer, H.; Baer, R.; Hany, R.; Verhoolen, I.; Walbiner, M. *J. Chem. Soc., Perkin Trans. 2* **1990**, 787–798.
- (180) Zytowski, T.; Fischer, H. *J. Am. Chem. Soc.* **1996**, *118*, 437–439.
- (181) Kirby, C. F.; McHugh, M. A. *Chem. Rev.* **1999**, *99*, 565–602.
- (182) Santanakrishnan, S.; Hutchinson, R. A.; Učňová, L.; Stach, M.; Lacík, I.; Buback, M. *Macromol. Symp.* **2011**, *302*, 216–223.
- (183) Beuermann, S. *Macromol. Rapid Commun.* **2009**, *30*, 1066–1088.
- (184) Beuermann, S.; García, N. *Macromolecules* **2004**, *37*, 3018–3025.
- (185) Yamada, B.; Westmoreland, D. G.; Kobatake, S.; Konosu, O. *Prog. Polym. Sci.* **1999**, *24*, 565–630.

- (186) Wayne Garrett, R.; Hill, D. J. T.; O'Donnell, J. H.; Pomery, P. J.; Winzor, C. L. *Polym. Bull.* **1989**, *22*, 611–616.
- (187) Carswell, T. G.; Hill, D. J. T.; Hunter, D. S.; Pomery, P. J.; O'Donnell, J. H.; Winzor, C. L. *Eur. Polym. J.* **1990**, *26*, 541–544.
- (188) Tian, Y.; Zhu, S.; Hamielec, A. E.; Fulton, D. B.; Eaton, D. R. *Polymer* **1992**, *33*, 384–390.
- (189) Iwasaki, M.; Sakai, Y. *J. Polym. Sci. Part A-1 Polym. Chem.* **1969**, *7*, 1537–1547.
- (190) Kamachi, M.; Kuwae, Y.; Nozakura, S.; Hatada, K.; Yuki, H. *Polym. J.* **1981**, *13*, 919–925.
- (191) Kajiwara, A.; Maeda, K.; Kubo, N.; Kamachi, M. *Macromolecules* **2003**, *36*, 526–528.
- (192) Best, M. E.; Kasai, P. H. *Macromolecules* **1989**, *22*, 2622–2627.
- (193) Kamachi, M.; Kohno, M.; Liaw, D. J.; Katsuki, S. *Polym. J.* **1978**, *10*, 69–75.
- (194) Hutchinson, R.; Richards, J.; Aronson, M. *Macromolecules* **1994**, *27*, 4530–4537.
- (195) Barudio, I.; Févotte, G.; McKenna, T. F. *Eur. Polym. J.* **1999**, *35*, 775–780.
- (196) Liang, K.; Hutchinson, R. A. *Macromol. Rapid Commun.* **2011**, *32*, 1090–1095.
- (197) Dossi, M.; Storti, G.; Moscatelli, D. *Macromol. Symp.* **2010**, *289*, 119–123.
- (198) Liu, S.; Srinivasan, S.; Grady, M. C.; Soroush, M.; Rappe, A. M. *Int. J. Quantum Chem.* **2014**, *114*, 345–360.
- (199) Buback, M. *Macromol. Symp.* **2009**, *275-276*, 90–101.
- (200) Wittenberg, N. F. G. *Kinetics and Modeling of the Radical Polymerization of Acrylic Acid and of Methacrylic Acid in Aqueous Solution*, PhD Thesis, Georg-August University Göttingen, 2013.
- (201) Torii, H.; Fujimoto, K.; Kawaguchi, H. *J. Polym. Sci. Part A Polym. Chem.* **1996**, *34*, 1237–1243.
- (202) Wolpers, A.; Russell, G. T.; Vana, P. *Macromol. Theory Simul.* **2011**, *20*, 667–674.
- (203) Sato, T.; Hirose, Y.; Seno, M.; Tanaka, H.; Uchiumi, N.; Matsumoto, M. *J. Polym. Sci. Part A Polym. Chem.* **1987**, *25*, 637–652.
- (204) Szablan, Z.; Stenzel, M. H.; Davis, T. P.; Barner, L.; Barner-Kowollik, C. *Macromolecules* **2005**, *38*, 5944–5954.
- (205) Sakai, Y.; Iwasaki, M. *J. Polym. Sci. Part A-1 Polym. Chem.* **1969**, *7*, 1749–1764.

- (206) Gilbert, B. C.; Smith, J. R. L.; Milne, E. C.; Whitwood, A. C.; Taylor, P. J. *Chem. Soc. Perkin Trans. 2* **1994**, 1759–1769.
- (207) Barth, J.; Siegmann, R.; Beuermann, S.; Russell, G. T.; Buback, M. *Macromol. Chem. Phys.* **2012**, *213*, 19–28.
- (208) Wittenberg, N. F. G.; Buback, M.; Hutchinson, R. A. *Macromol. React. Eng.* **2013**, *7*, 267–276.
- (209) Kabanov, V. A.; Topchiev, D. A.; Karaputadze, T. M. *J. Polym. Sci. Polym. Symp.* **1973**, 173–183.
- (210) Okamoto, K.; Hirota, N.; Terazima, M. *J. Chem. Soc. Faraday Trans.* **1998**, *94*, 185–194.
- (211) Wedler, G.; Freund, H. J. *Lehrbuch der Physikalischen Chemie*; 6. Ausgabe.; Wiley-VCH Verlag GmbH & Co. KG, Weinheim, 2012.
- (212) Cuccato, D.; Storti, G.; Morbidelli, M. *Macromolecules* **2015**, *48*, 5076–5087.
- (213) Johnston-Hall, G.; Barner-Kowollik, C.; Monteiro, M. J. *Macromol. Theory Simul.* **2008**, *17*, 460–469.
- (214) Griffiths, M. C.; Strauch, J.; Monteiro, M. J.; Gilbert, R. G. *Macromolecules* **1998**, *31*, 7835–7844.
- (215) Meiser, W.; Barth, J.; Buback, M.; Kattner, H.; Vana, P. *Macromolecules* **2011**, *44*, 2474–2480.
- (216) Zetterlund, P. B.; Yamazoe, H.; Yamada, B.; Hill, D. J. T.; Pomery, P. J. *Macromolecules* **2001**, *34*, 7686–7691.
- (217) Yamazoe, H.; Zetterlund, P. B.; Yamada, B.; Hill, D. J. T.; Pomery, P. J. *Macromol. Chem. Phys.* **2001**, *202*, 824–829.
- (218) Buback, M.; Huckestein, B.; Ludwig, B. *Die Makromol. Chem., Rapid Commun.* **1992**, *13*, 1–7.
- (219) Drawe, P.; Buback, M.; Lacík, I. *Macromol. Chem. Phys.* **2015**, *216*, 1333–1340.
- (220) Riemann, L. *Untersuchung der Terminierungskinetik von radikalischen Copolymerisationen mittels zeitaufgelöster ESR-Spektroskopie*, Master Thesis, Georg-August-University Göttingen, 2016.
- (221) Heuts, J. P. A.; Gilbert, R. G.; Maxwell, I. A. *Macromolecules* **1997**, *30*, 726–736.
- (222) Forbes, M. D. E. *Photochem. Photobiol.* **1997**, *65*, 73–81.
- (223) McLauchlan, K. A. *Chem. Soc. Rev.* **1993**, *22*, 325–328.
- (224) McLauchlan, K. A.; Simpson, N. J. K. *J. Chem. Soc. Perkin Trans. 2* **1990**, *8*, 1371–1377.

Acknowledgements

Ein paar Worte des Dankes in eigener Sprache.

Mein besonderer und herzlicher Dank gilt Herrn Prof. Dr. Michael Buback für seine Motivation sowie für die wertvollen Gespräche und Diskussionen. Ich bin dankbar für das mir entgegengebrachte Vertrauen und für seine stete Unterstützung bei meiner fachlichen und persönlichen Weiterentwicklung.

Ich danke Herrn Prof. Dr. Philipp Vana nicht nur für die Übernahme des Korreferats, sondern auch für die interessanten und motivierenden Diskussionen.

Ich möchte Herrn Prof. Dr. Burkhard Geil, Herrn Prof. Dr. Ricardo Mata, Herrn PD Dr. Thomas Zeuch und Herrn Dr. Florian Ehlers für die Teilnahme an meinem Prüfungskomitee danken.

Ich bin froh, während meiner Promotion Menschen getroffen zu haben, die ich fachlich und menschlich sehr schätze und für deren Zusammenarbeit ich ihnen danke. Ich möchte mich besonders bei Dr. Igor Lacík (Polymer Institut, Bratislava, Slowakei), Prof. Dr. Atsushi Kajiwara (Universität Nara, Japan), Prof. Dr. Sabine Beuermann (TU Clausthal), Dr. Calista Preusser (BASF SE, USA) und Prof. Dr. Robin A. Hutchinson (Universität Queen's, Kingston, Kanada) bedanken.

Des Weiteren gilt mein Dank Prof. Dr. Giuseppe Storti, Dr. Danilo Cuccato (beide ETH Zürich) und Dr. Hugo Vale (BASF SE, Ludwigshafen) für den Austausch inspirierender Ideen und für eine wertvolle Kooperation. In diesem Zusammenhang möchte ich der BASF SE sowie der Deutschen Forschungsgemeinschaft (DFG) für die finanzielle Unterstützung danken.

Ich schätze mich glücklich, mit talentierten Kolleginnen und Kollegen in einer herzlichen und kooperativen Atmosphäre zusammenarbeiten zu dürfen. Es war mir eine Freude, Lara Riemann während ihrer Masterarbeit zu begleiten und ich möchte mich bei allen Mitgliedern der Arbeitsgruppen "Buback" und "Vana" für die schönen Momente bedanken. Mein besonderer Dank gilt Dr. Hendrik Schröder, Dennis Hübner,

Sebastian Smolne, Patrick Drawe, Christian Roßner, Dr. Arne Wolpers, Dr. Bastian Ebeling, Dr. Nils Wittenberg, Dr. Jens Schrooten und Shinsuke Kokubo für die vielen interessanten und leidenschaftlichen Diskussionen. Ich danke Dr. Florian Ehlers für seine Unterstützung beim ESR und meinen Bürokolleginnen Dr. Cathrin Conrad, Dr. Katharina Tietz und Vanessa Koch für ihre mütterliche Fürsorge. Sandra Lotze, Heike Rohmann und Dr. Hans-Peter Vögele möchte ich für ihre Hilfe bei der Bewältigung der Herausforderungen des Laboralltags danken.

Eine Promotion ist ohne eine Familie, die unterstützt und Mut zuspricht, undenkbar. Von ganzem Herzen danke ich meinen Eltern. Ohne euch wäre ich nicht so weit gekommen. Ich danke meinem Bruder Phil, der wesentlich zu meinem sportlichen Ausgleich beigetragen hat und mich mit seinem Humor stets zum Lachen bringt. Mein tiefer Dank gilt auch dir, Franzi. Ich bin glücklich, dich in meinem Leben zu haben.

About the Author

Hendrik Kattner, *July 11, 1987, Duderstadt, German citizen.

Curriculum vitae

- 2004** *Improved primary-school examination* (with distinction), Heinz-Sielmann-Realschule, Duderstadt, final grade: 1.3.
- 2007** *Abitur (final secondary-school examination)*, Eichsfeld-Gymnasium, Duderstadt, (with distinctions in Chemistry and Physics), final grade: 1.4.
- 2007-2010** *Bachelor of Science*, Georg-August-University Göttingen, final grade: 1.3 ("*with distinction*"), Bachelor Thesis: "Kinetische Untersuchung der Ditihiobenzoat-vermittelten Butylacrylat-Polymerisation mittels ESR" in the group of Prof. Dr. Michael Buback.
- 2010-2012** *Master of Science*, Georg-August-University Göttingen, final grade: 1.1 ("*with distinction*"), Master Thesis: "Untersuchung der radikalischen Polymerisation von Vinylacetat durch Pulslaserexperimente in Verbindung mit EPR und SEC" in the group of Prof. Dr. Michael Buback.
- 2012-2016** *Doctoral Studies*, Georg-August-University Göttingen, supervisor: Prof. Dr. M. Buback
- 2012-2015** Cooperation with the BASF SE: "Kinetics of water soluble monomers"
- since 2015** Task group member of the IUPAC project: *Critically evaluated EPR spectra of important polymerization-related radicals.*

Publications

- "EPR Measurement of Fragmentation Kinetics in Dithiobenzoate-Mediated RAFT Polymerization"
W. Meiser, J. Barth, M. Buback, H. Kattner, P. Vana
Macromolecules **2011**, *44*, 2474–2480.
- "Detailed Investigations into Radical Polymerization Kinetics by Highly Time-Resolved SP–PLP–EPR"
H. Kattner, M. Buback *Macromol. Symp.* **2013**, *333*, 11–23.
- "Chain-Length-Dependent Termination of Vinyl Acetate and Vinyl Pivalate Bulk Homopolymerizations Studied by SP–PLP–EPR"
H. Kattner, M. Buback *Macromol. Chem. Phys.* **2014**, *215*, 1180–1191.
- "Chain-Length-Dependent Termination of Styrene Bulk Homopolymerization Studied by SP–PLP–EPR"
H. Kattner, M. Buback *Macromolecules* **2015**, *48*, 309–315.
- "Modeling Acrylic Acid Radical Polymerization in Aqueous Solution"
N. F. G. Wittenberg, C. Preusser, H. Kattner, M. Stach, I. Lacík, R. A. Hutchinson, M. Buback. *Macromol. React. Eng.* **2015**, *10*, 95–107.
- "Termination and Transfer Kinetics of Acrylamide Homopolymerization in Aqueous Solution"
H. Kattner, M. Buback *Macromolecules* **2015**, *48*, 7410–7419.
- "EPR Study of Backbiting in the Aqueous-Solution Polymerization of Acrylamide"
H. Kattner, M. Buback *Macromol. Rapid Commun.* **2015**, *36*, 2186.

- "Novel Access to Propagation Rate Coefficients of Radical Polymerization by the SP–PLP–EPR Method"
H. Kattner, P. Drawe, M. Buback *Macromol. Chem. Phys.* **2015**, *216*, 1737–1745.
- "Detailed Kinetic and Mechanistic Insight into Radical Polymerization by Spectroscopic Techniques"
M. Buback, H. Schroeder, H. Kattner, *Macromolecules* **2016**, *49*, 3193–3213.
- "Propagation and Chain-Length-Dependent Termination Rate Coefficients Deduced from a Single SP–PLP–EPR Experiment"
H. Kattner, M. Buback, *Macromolecules* **2016**, *49*, 3716–3722.
- "Chain-length-dependent Termination of Sodium Methacrylate Polymerization in Aqueous Solution Studied by SP–PLP–EPR"
H. Kattner, P. Drawe, M. Buback, *in preparation*.

Contributions to Conferences

- "Termination and Transfer Kinetics of Vinyl Acetate studied by SP–PLP–EPR"
Poster, JungChemikerForum, Göttingen, **June 2013**.
- "Termination and Transfer Kinetics of Vinyl Acetate and Styrene studied by SP–PLP–EPR"
Poster, 3rd Controlled / Living Polymerization Symposium "CLP'14", Antalya, Turkey, **Mai 2014**.
- "Kinetics of Radical Polymerization in Organic and Aqueous Solution studied via SP–PLP–EPR experiments"
Oral, "Pacifichem" 2015, Honolulu, Hawaii, **December 2015**

Awards

- 2010** Scholarship of Lower Saxony
"Landesstipendium Niedersachsen"
- 2012** Bunsen Book Award for the master thesis: *Untersuchung der radikalischen Polymerisation von Vinylacetat durch Puls laserexperimente in Verbindung mit EPR und SEC*
- 2012** "Gustav-Tammann-Preis" of the Faculty for Chemistry, Georg-August-University Göttingen, for the best master thesis.